Geochemical variations in magmatic rocks from southern Costa Rica as a consequence of Cocos Ridge subduction and uplift of the Cordillera de Talamanca

DISSERTATION

zur
Erlangung des Doktorgrades
der Mathematisch-Naturwissenschaftlichen Fakultäten
der Georg-August-Universität zu Göttingen

vorgelegt von

MICHAEL ABRATIS
aus Oldenburg/Holstein

Göttingen 1998

D7

Referent: Prof. Dr. Gerhard Wörner
Korreferent: Prof. Dr. Bent Hansen

Tag der mündlichen Prüfung: 4. November 1998

Pour ma femme Catherine

LE SANG DE LA TERRE
COULE DANS LES VEINES DU VOLCAN.
Katia et Maurice Krafft

Abstract

The Cordillera de Talamanca, which constitutes the magmatic arc in SE Costa Rica, its related forearc (Fila Costeña) and backarc region (Limon Basin) are a segment of the Central American arc system.

To describe and explain the Neogene to Quaternary magmatic evolution of this segment of the Central American arc system, I investigated the geochemical and isotopic (Sr, Nd, Pb) composition of magmatic rocks. The results indicate various magma sources for the igneous rocks in this region. The evolution of the magmatic system is temporally and genetically related to the ridge-trench collision of Cocos Ridge and Central America.

With increasing arc maturity, magmatic products change from arc-tholeiitic to calc-alkaline magma compositions in Costa Rica. These changes take place during the Miocene.
Prior to collision of the Cocos Ridge and SE Costa Rica, erupted magmas had their source in the mantle wedge. This is in accordance with generally accepted models for arc magmatism. Derivation from a depleted, sediment and fluid modified mantle source is documented by the isotopic and trace element signature (Nb/Zr: 0.03-0.09, Ba/La: 20-134, $^{87}Sr/^{86}Sr$: 0.7036-0.7042, $^{143}Nd/^{144}Nd$: 0.51300-0.51304, $^{206}Pb/^{204}Pb$: 18.72-18.87).
When the Cocos Ridge collided with SE Costa Rica, this “normal” arc magmatism ended and a gap formed in the chain of arc volcanoes.

Simultaneously with the collision event, alkaline magmas started to erupt in the backarc region. Their composition is geochemically and isotopically distinct from the former arc magmatic products (Nb/Zr: 0.17-0.46, Ba/La: 13-19, $^{87}Sr/^{86}Sr$: 0.7035-0.7036, $^{143}Nd/^{144}Nd$: 0.51297-0.51298, $^{206}Pb/^{204}Pb$: 19.06-19.12), indicating derivation from decompressional melting of new upwelling sub-slab mantle material. Tapping of this new magma source occurred when the subducting plate ruptured and opened a slab window in response to ridge-trench collision. A temporal and spatial association of alkalic backarc magmatism with the slab window formation can be shown by $^{40}Ar/^{39}Ar$ dating. From this it has to be concluded that the slab window opened in a north-westward direction, consistent also with the direction of decreasing sub-Costa Rican mantle wedge contamination by enriched Galapagos plume mantle.

Shortly after collision and backarc activity, minor volumes of calc-alkaline lavas erupted in the Fila Costeña (inner forearc), very close to the trench.

Adakites erupted as the latest phase of magmatic activity at the location of previously voluminous calc-alkaline arc magmatism. Adakites are considered to be products of partial melting of hydrated oceanic crust which could have formed when hot upwelling sub-slab asthenosphere came in contact with subducted oceanic crust at the slab window margins. Under these rare circumstances of slab window opening, adakites could be formed even in a fast converging subduction zone.

Kurzfassung

Plattengrenzen sind üblicherweise die Orte auf der Erde, an denen eine hohe vulkanische Aktivität herrscht. So ist auch Mittelamerika, bedingt durch die Subduktion der Cocos Platte unter die Karibische Platte, vulkanisch eine der aktivsten Regionen weltweit. Im südlichen Costa Rica allerdings, sind im Gegensatz zu den benachbarten Gebieten derzeit keine aktiven Vulkane zu finden.

Das betroffene und in dieser Arbeit untersuchte Segment des Mittelamerikanischen Arcs umfaßt die Cordillera de Talamanca als Hauptmagmatischen Rücken, sowie die Fila Costeña als assoziierten Forearc und das Limon Becken als Backarc Bereich.

Mit geochemischen, isotopengeologischen und geochronologischen Methoden wurde die Abfolge der Magmatite aus dieser Region untersucht. Eine Entwicklung des Magmatismus sollte Rückschlüsse auf mögliche Veränderungen in der Magmenbildungszone ermöglichen.

Die Ergebnisse dokumentieren ein sehr vielfältiges Magmen Inventar in Südost Costa Rica, was nicht mit der Herkunft aus einer einzigen Magmenquelle zu erklären ist. Die Evolution des Magmatismus in der jüngeren Zeit ist zeitlich und offensichtlich auch genetisch mit der Kollision und Subduktion des Cocos Rückens unter diesen Abschnitt des Mittelamerikanischen Arcs verknüpft.

Die Entwicklung des Magmatismus im Miozän belegt das Heranreifen des Südost Costa Ricanischen Arc-Segments: Arc-tholeiitische Magmen werden zunehmend von Kalk-alkalischen Magmen abgelöst. Letztere geben deutliche Hinweise auf eine sich aufbauende, verdickende Arc-Kruste, in der sie in Magmenkammern in hohem Maß Kristalle fraktionieren und Nebengestein assimilieren.

Diese Magmen, die vor der Kollision des Cocos Rückens mit dem Arc gefördert werden, sowohl die Arc-tholeiitischen als auch die Kalk-alkalischen Magmen, haben ihre Quelle im Mantelkeil über der subduzierenden Platte. Der Mantelkeil ist heute als der primäre Ort für die Bildung von Magmen an Subduktionszonen anerkannt. Die Herkunft der Magmen aus einer durch Schmelzbildungen relativ verarmten, aber mit Sedimenten und Fluiden von der subduzierenden Platte modifizierten Mantelquelle dokumentiert sich in ihrer Spurenelement-Signatur und Isotopie (Nb/Zr: 0.03-0.09, Ba/La: 20-134, $^{87}Sr/^{86}Sr$: 0.7036-0.7042, $^{143}Nd/^{144}Nd$: 0.51300-0.51304, $^{206}Pb/^{204}Pb$: 18.72-18.87).

Als der Cocos Rücken mit Südost Costa Rica kollidierte, endete dieser “normale” Arc-Magmatismus und es bildete sich eine Lücke in der Kette der Vulkane Mittelamerikas.

Gleichzeitig mit dem Kollisionsereignis eruptieren und intrudieren alkalische Magmen im Backarc Bereich. Ihre Zusammensetzung ist geochemisch und isotopisch sehr verschieden von den vorangehenden magmatischen Produkten des Arcs (Nb/Zr: 0.17-0.46, Ba/La: 13-19, $^{87}Sr/^{86}Sr$: 0.7035-0.7036, $^{143}Nd/^{144}Nd$: 0.51297-0.51298, $^{206}Pb/^{204}Pb$: 19.06-19.12). Sie zeigen nur geringfügig die Signaturen der Subduktionszone und scheinen aus neuem, aufsteigenden Mantelmaterial zu stammen, welches bei der Dekompression zu schmelzen beginnt. Aufgrund der geochemischen und isotopischen Ähnlichkeit zu Magmen, die vom Galapagos Hot Spot produziert wurden, kann angenommen werden, daß sie aus eben diesem Mantelmaterial gebildet werden, welches durch ein Fenster in der subduzierenden Platte in den Mantelkeil aufsteigt. Das Fenster hat sich wahrscheinlich in Folge der Cocos-Rücken Kollision gebildet, wobei die subduzierende Platte entlang von Transformstörungen aufriß, die in diesem Gebiet sehr zahlreich sind. Der Zusammenhang zwischen Fensterbildung und Rückenkollision ergibt sich aus dem zeitlichen und räumlichen Bezug von Kollisionsereignis und Auftreten von Backarc Magmatismus als magmatischem Fensterindiz. Mit Hilfe der $^{40}Ar/^{39}Ar$

Geochronologie an den Backarc Magmatiten kann die Erweiterung des Fensters in nordwestliche Richtung abgelesenen werden. In eben diese Richtung verbreitet sich auch die Kontamination des Mittelamerikanischen Mantelkeils mit Galapagos Plume Material, wie es sich in der Reihe der aktiven Vulkane in Costa Rica und Nicaragua dokumentiert.

Magmatische Aktivität, die lokal und zeitlich beschränkt in der Fila Costeña, nahe am Trench auftritt, markiert offenbar den Wiedereinsatz der Subduktion in der Region. Durch die dann sehr flach verlaufende Subduktion dieses Teilstücks der Cocos Platte bleibt späterer Arc-Magmatismus aus.

Adakite eruptieren in der letzten Phase magmatischer Aktivität in Südost Costa Rica dort, wo zuvor voluminöser Kalk-alkalischer Arc-Magmatismus geherrscht hat. Diese partiellen Schmelzprodukte aus hydratisierter, subduzierter, basaltischer Kruste, haben sich in diesem Fall gebildet, als heiße, aufsteigende Asthenosphäre die Ränder des Fensters in der subduzierenden Platte, d.h. den sich nunmehr unterschiebenden Cocos Rücken, aufschmolz. Unter diesen besonderen Umständen mit Bildung eines Fensters in der subduzierenden Platte konnten sich Adakite bilden, wo ansonsten aufgrund der hohen Konvergenzraten der geothermische Gradient ein Aufschmelzen der Kruste nicht ermöglicht hätte.

CONTENTS

FIGURES

TABLES

Abbreviations

AFC-Process	Assimilation, Fractional Crystallisation: process during magma genesis
Amph	Amphibole
Arc	Volcanic arc above a convergent margin
Bio	Biotite
Cc	Calcite
Cpx	Clinopyroxene
EPR	East Pacific Rise
GI	Galapagos Islands
Hbl	Hornblende
Grt	Garnet
GSC	Galapagos Spreading Centre
HFSE	High Field Strength Elements: Incompatible Elements of high ionic potential (cationic charge/ cationic radius > 2), e.g. Ti, Nb, Ta, Zr and Hf
HIMU	High ratio of 238U/ 204Pb
HREE	Heavy Rare Earth Elements
ICP-MS	Inductively- coupled Plasma- Mass-spectrometry
Kfsp	Alkalifeldspar
LILE	Large Ion Lithophile elements
LREE	Light Rare Earth elements
MAT	Middle America Trench
MOR	Mid Ocean Ridge
MORB	Mid Ocean Ridge Basalt
Mt	Magnetite
Ne	Nephelinite
ODP	Ocean Drilling Program
OIB	Ocean Island Basalts
Ol	Olivine
Opx	Orthopyroxene
PFZ	Panama Fracture Zone
Plag	Plagioclase
PM	Partial Melting
P-T	Pressure – Temperature (path)
Qz	Quartz
Spl	Spinel
XRF	X-ray fluorescence analysis

1 Introduction

1.1 Objectives

Southern Costa Rica shows a distinct evolution within the Central American Arc during its younger geological history.
In respect of many geological aspects, this area differs from the adjacent areas in the arc. These features are for example deformation, rapid uplift and the lack of active strato-volcanoes [Kolarsky et al., 1995] in midst of one of the volcanically most active arcs world-wide [Carr & Stoiber, 1990].

Several geological and geophysical studies of the deformation and uplift history came to the conclusion that indentation and shallow subduction of the buoyant, aseismic Cocos Ridge is responsible for the distinct evolution in this arc segment [e.g. Kolarsky et al., 1995]. The causal relationship is evident when one recognises that the extension of the geologically modified arc section correlates with the width and location of the ridge entering the convergence zone and that the modification correlates also in time with the indentation and subduction event. Very similar geological features at other sites of ridge subduction support the hypothesis [e.g. Vogt et al., 1976; Kelleher & McCann, 1976; Chung & Kanamori, 1978; McGeary et al., 1985; Adamek et al., 1987].

The aim of the present study is to test if the observed geochemical and magmatic changes in time and space within the area of the Cordillera de Talamanca could also be related to Cocos Ridge subduction.

Volcanism along convergent plate margins is generally related to mantle wedge melting, induced by fluid transfer from the subducting slab [Gill, 1981].
Thus, if major changes in the volcanic activity of arcs occur, this could indicate important changes in the convergence zone parameters (subduction zone geometry), affecting the normal process of melt generation.

McGeary et al. [1985] conclude that shallow subduction of the Cocos Ridge and displacement of the asthenospheric mantle wedge inhibit magma generation. Protti et al. [1995] attribute the absence of subduction-related volcanic activity primarily to a lack of dehydration of the slab which did not reach the appropriate depths.
In contrast, de Boer et al. [1995] suggest low magma production in the source region, the inability of those magmas to rise through the thickened crust, and/or lateral escape of magmas to adjacent arc segments.
However, Johnston & Thorkelson [1997] find an alternative hypothesis and propose the development of a slab window as reason for the absence of normal arc volcanism and the occurrence of a magmatic anomaly, rejecting a causal relationship to the Cocos Ridge itself.

These hypotheses have been tested in the present study.
To solve this task, geochemical and isotope analyses are used to characterise the magmatic rocks of the southern Costa Rican arc segment, and to identify their melt sources and subsequent magmatic evolution. Dating of the rocks helps to constrain the time frame for the occurrence of specific magmatic features.

Besides the description of the geochemical evolution in the Cordillera de Talamanca, the thesis aims to answer the following questions:

- Does a mantle wedge exist underneath the Cordillera de Talamanca?
- What is the depth of the subducting plate in that region?
- Can we get new insights in the Late Neogene-Quaternary plate tectonic evolution in southern Central America?
- How do slab windows and slab break-offs form and are they important for subduction zones world-wide and through earth-history?
- How do adakites (i.e. slab melting products) form, are they bound to distinct plate tectonic configurations like slab windows, what is the proportion and importance of adakitic magmas for crustal formation processes through earth-evolution?
- What are the driving forces for the evolution of orogenic belts and mountain building processes?

1.2 Geological setting

1.2.1 Magmatic geological history of Costa Rica

Costa Rica is a part of the Central American Arc system that evolved on the western margin of the Caribbean Plate (Fig.1). The Caribbean Plate is a product of oceanic volcanism within a complex interplate realm [Pindell & Barrett, 1990]. Its evolution is mainly governed by relative plate motions of North and South America.
The formation of the Caribbean started when South America moved rapidly away from North America after the Late Triassic-Jurassic break-up of Pangaea [Donnelly et al., 1990]. Oceanic crust produced during that event is proven in the Venezuelan Basin and also by ophiolitic assemblages in Venezuela and Costa Rica (Santa Elena) [Diebold et al., 1981; Ghosh et al., 1984].

When plate motions slowed in the Caribbean upon concurrent South Atlantic Ocean opening, flood basalts covered the area. Samples of this Caribbean Large Igneous Province (CLIP) [Hauff, 1998] or Jurassic-Cretaceous Basalt Province [Donnelly et al., 1990] are found as ophiolitic complexes throughout the Caribbean and along the Pacific coast of South America as far south as Ecuador (Fig. 3, Fig. 8) [Donnelly et al., 1990; Alvarado et al., 1997; Hauff et al., 1997]. Exposures in Costa Rica are bound to the Pacific coast and their rocks date back to the Jurassic to Cretaceous [e.g. Astorga, 1997; Tournon & Alvarado, 1997]. These flood basalts show the characteristics of MORB and OIB [Donnelly et al., 1990; Hauff, 1998]. In Costa Rica and western Panama (Chorotega Block), the basaltic ophiolitic complex has been named the Nicoya complex [Dengo, 1962].

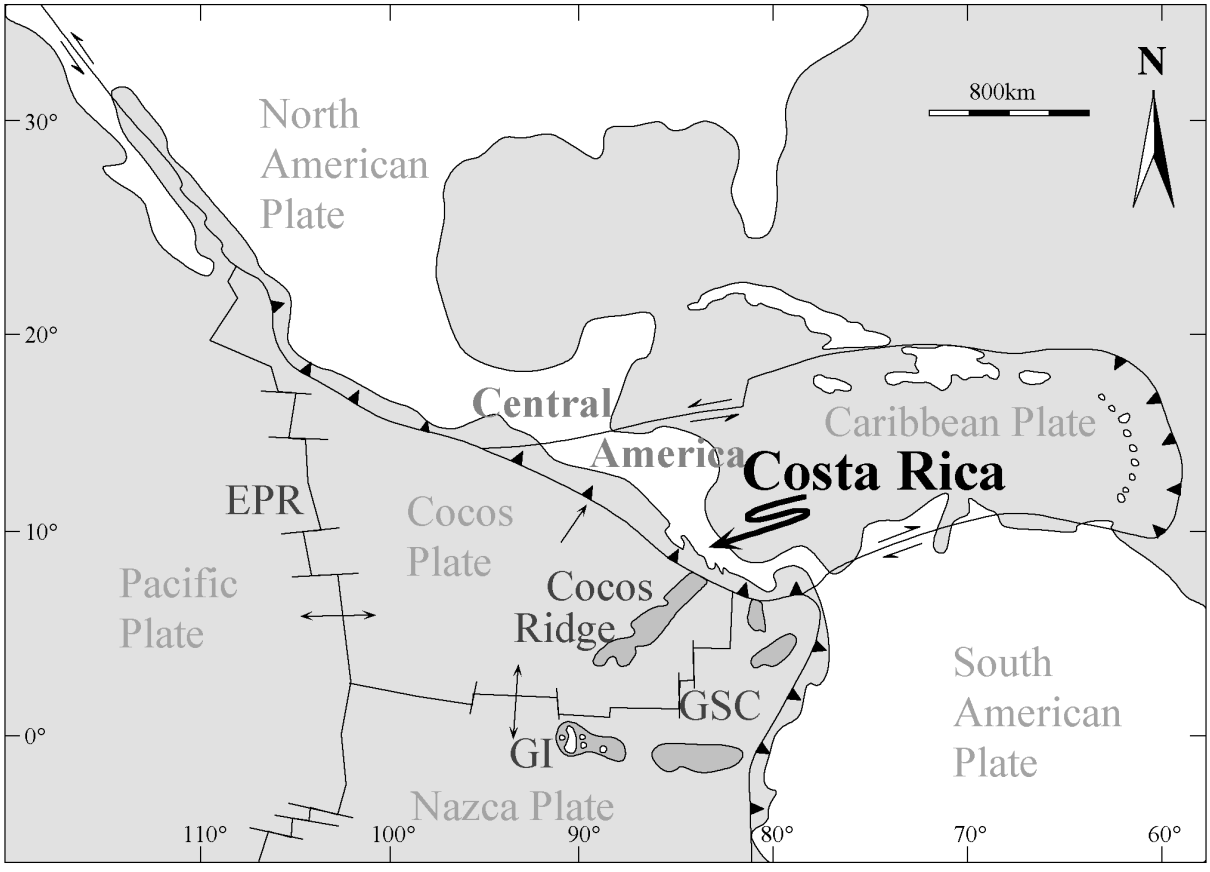

Figure 1: *Plate tectonic environment of the East Pacific and Caribbean region (simplified after Mann & Burke, 1984), and the location of Costa Rica in southern Central America.*

Central America emerged above sea-level primarily as a consequence of subduction related volcanism. Formation of the western convergent margin of the Caribbean and appearance of the first arc magmatism during the Upper Cretaceous is related to north-eastward movement of South America, causing a compressional tectonic environment in Central America [Donnelly et al., 1990]. Subduction of the Farallon Plate underneath the Caribbean Plate resulted then in the first occurrence of the Central American Arc.
In northern Costa Rica (Santa Elena, Nicoya Peninsula) as well as in western Panama, first incidences of arc volcanism date back to the Campanian-Maastrichtian [Fisher & Pessagno, 1965; Kuijpers, 1979; Weyl, 1980; Tournon, 1984; Sick, 1989; Lundberg, 1991]. Andesitic clasts of calc-alkaline character are intercalated in submarine sediments and give indirect evidence for the existence of mature arcs. Under debate are findings of even older andesitic (calc-alkaline) volcanic clasts within Albian-Campanian sedimentary successions on the Nicoya Peninsula [Calvo & Bolz, 1994]. At that time, the area of the Cordillera de Talamanca was still covered by submarine tholeiitic basaltic massive and pillowed flows and hyaloclastites [Tournon & Alvarado, 1997].
In the Middle to Upper Eocene, the sedimentary sequences of northern and southern Costa Rica contain more evidence of andesitic volcanism [Tournon & Alvarado, 1997]. Some volcaniclastic sediments are also deposited in the Talamanca area at Río Chirripó Atlanticó and Río Lari [Fisher & Pessagno, 1965; Tournon, 1984].
There are only a few rock samples radiometrically testifying for an age of the Talamanca arc as old as Oligocene (at Río Lari, and near Division) [Saenz, 1982; Appel et al., 1992; de Boer et al., 1995]. Rocks of that period are arc-tholeiitic [de Boer et al., 1995].
Thus, there is less evidence for an Upper Cretaceous to Lower Tertiary arc within the area of the Cordillera de Talamanca than in northern Costa Rica and western Panama [Tournon & Alvarado, 1997].

The Miocene was a period of high volcanic activity throughout Central America, resulting from a general plate tectonic reorganisation in the Pacific. Fragmentation of the Farallon Plate in the Cocos and Nazca plates occurred at about 26 Ma (Oligocene/Miocene boundary) [Handschuhmacher, 1976] and had an important effect on the intensity of magmatism in Central America.
Large volumes of ignimbrites erupted in Guatemala, Honduras, Nicaragua, north-western Costa Rica, and central Panama during the Miocene [Weyl, 1961].
Neogene northwest-southeast regional compression which meant a change from oblique to near-orthogonal convergence at the Middle America Trench [Donnelly et al., 1990] led to the production of massive volumes of mantle-wedge-derived magma also in southern Central America [de Boer et al., 1995].
Since the Miocene, the geochronological record of arc magmatism becomes more continuous in Costa Rica. The majority of primary arc volcanic formations in Costa Rica that could be dated directly and reliably with radiometric methods date back to the Miocene [Tournon, 1984; Alvarado et al., 1992; Appel et al., 1994] and document a vivid arc magmatic activity also in the Talamanca area: Arc volcanic rocks found in the Cordillera de Talamanca are of Middle to Upper Miocene age, intrusive rocks are mostly of Upper Miocene age [Berrange & Whittaker, 1977; Bellon & Tournon, 1978; Bergoeing, 1982; Alvarado et al., 1992; Defant et al., 1992; Appel et al., 1994; Drummond et al., 1995].

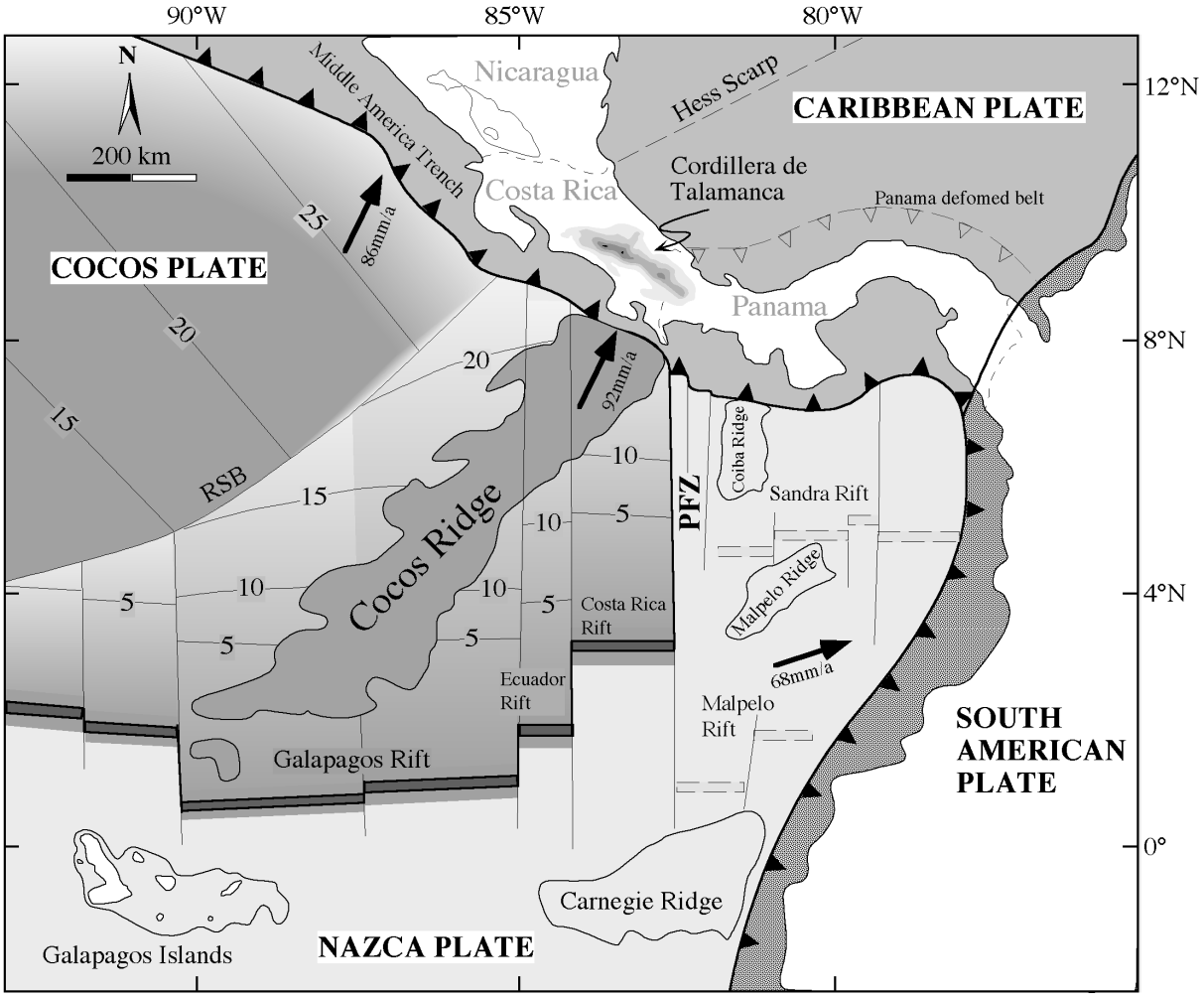

Figure 2: *Plate-tectonic map of southern Central America and the Galapagos area after Hey [1977]. The four lithospheric plates are separated by transform faults, subduction zones and spreading centres. Segments of the Cocos-Nazca spreading centre are labelled with their names. The Cocos Plate can be separated by the Rough-Smooth-Boundary (RSB, Hey et al., 1977) into a smooth north-western part which was produced by the East-Pacific-Rise and a rough south-eastern part which was produced by the Cocos-Nazca spreading centre. Plate ages of the Cocos Plate are given at the respective iso-lines. PFZ is the Panama fracture zone, a prominent transform fault between the Cocos and Nazca Plate. The outlines of the Cocos Ridge and the other submarine highs are given by the 2000 m below sea-level-depth-contours.*

Subduction of the Cocos and Nazca plates (Fig. 2) continues along the entire length of Central America until today. Presently, convergence rates of the Cocos Plate vary from about 60 mm/yr. off southern Mexico to about 90 mm/yr. off Costa Rica and for the obliquely subducting Nazca Plate, the orthogonal component of subduction off Panama is estimated to be between 15 and 40 mm/yr. [de Boer et al., 1988; de Boer et al., 1991].

Volcanic activity in northern and central Costa Rica is intense from upper Miocene to present [Carr & Stoiber, 1990; Donnelly et al., 1990; Alvarado et al., 1994]. Widespread Pliocene and Quaternary ignimbrites (Cordillera de Guanacaste, Cordillera Central) are succeeded by a chain of strato-volcanoes from northern to central Costa Rica in the Lower Pleistocene (Fig. 3), producing andesitic lavas and dacitic to rhyolitic pyroclastic flows.

From the Upper Pleistocene to present, spacing of strato-volcanoes which produce calc-alkaline volcanics gets less dense. Nevertheless, the remaining active volcanoes are the most productive within the Central American chain [Stoiber & Carr, 1973; Leemann & Carr, 1995].

Closure of the isthmus between the Americas took place during the Pliocene [e.g., Keigwin, 1982; Tiedemann et al., 1998] and is reflected in marine fauna differentiation into Pacific and Caribbean associations as well as intermingling of North and South American terrestrial fauna species. This closure documents the last step in the evolution of Central America from an archipelago to a peninsula, an isthmus and finally the present land bridge.

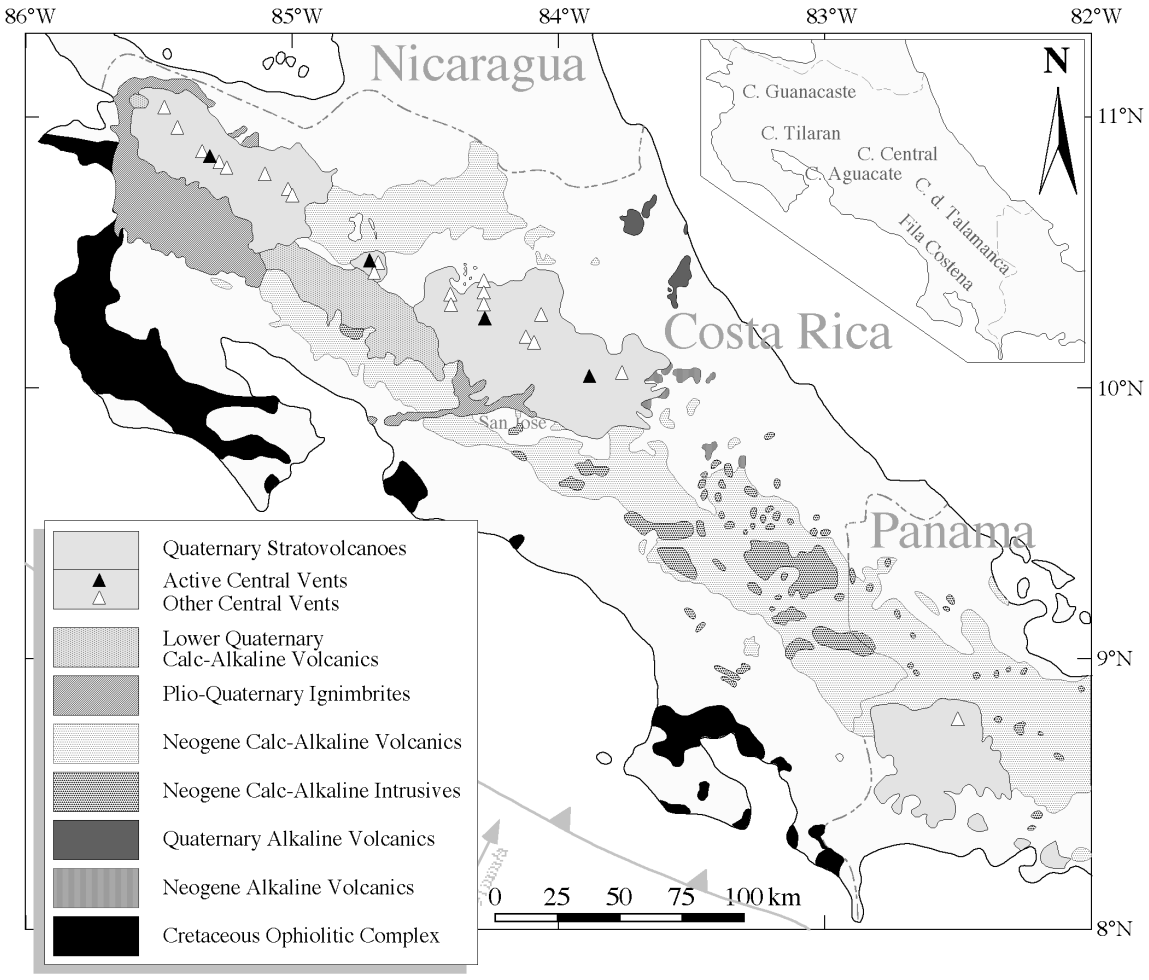

Figure 3: *Geological sketch map of Costa Rica and western Panama after Kussmaul et al. [1994] showing the distribution of Neogene and Quaternary igneous rocks.*

1.2.2 Geology of the Cordillera de Talamanca

1.2.2.1 Magmatic succession

The geological sketch map of Costa Rica (Fig. 3) shows that, with respect to magmatic rocks, the Cordillera de Talamanca is mainly made up of Neogene volcanics and Neogene intrusives. Whereas Neogene volcanics are exposed all along the Costa Rican and western Panamanian part of the Central American Arc, the massive occurrence of intrusive bodies is a particularity of the Cordillera de Talamanca.
Intrusive rocks of the Cordillera de Talamanca, intruding sedimentary and volcanic series as batholiths and stocks of granitoids are pervasive in this magmatic arc, but predominantly found in the axial zone (Fig. 3) [e.g., Dengo, 1962]. These intrusions are generally differentiated and comprise quartz-diorites and monzonites. Granites and gabbros are subordinate [Weyl, 1957; Kussmaul, 1987; Drummond et al., 1995].
As in the older series of Montes del Aguacate [Kussmaul et al., 1994], an evolution from arc tholeiitic to calc-alkaline series can be observed for the Talamanca magmatism, for volcanics as well as intrusives.

Since the Pliocene, calc-alkaline arc volcanism is absent in the central Cordillera de Talamanca. Instead, Pliocene calc-alkaline volcanism occurs in the tectonised and uplifted Fila Costeña (inner forearc) [Henningsen, 1966; Kesel, 1978; Bergoing et al., 1978; de Boer et al., 1995].

Alkaline magmatic rocks emplaced on the Caribbean side of Costa Rica date from the uppermost Miocene in the SE to sub-recent in the NW [Bellon & Tournon, 1978; Robin & Tournon, 1978; Tournon, 1984; this thesis]. A climax of alkaline magmatism around 4Ma is evidenced by intrusive (teschenites, alkaline syenites) and volcanic (nephelinites, alkali basalts, basanites, ankaramites) alkaline rocks near Guayacan (Fig, 3) [Tournon, 1972; Azambre & Tournon, 1977; Tournon, 1984; Tournon & Alvarado, 1997].

During Upper Pliocene and Lower Pleistocene times, adakitic magmatism (genetic term indicating slab melting) occurs in the central and southern Cordillera de Talamanca. The products are andesitic to dacitic domes and related breccias [Ballmann, 1976; Tournon, 1984; Defant et al., 1992; Drummond et al., 1995; de Boer et al., 1995; this thesis].

1.2.2.2 Volcanic gap

Active volcanoes in Central America are predominantly aligned as a well defined belt which parallels the Middle America trench and coastline (Fig. 4). This volcanic front represents one of the most active circum-Pacific volcanic belts with one of the highest densities of active volcanic centres among convergent plate margins world wide [Carr & Stoiber, 1990].
However, a 175km wide gap in the chain of closely spaced Quaternary stratovolcanoes is found in the Central American volcanic front between the volcanoes Irazú/Turrialba and Tisingal/El Barú about the projected onshore extension of the Cocos Ridge (Fig. 4). The width of the gap correlates approximately with the width of the Cocos Ridge and corresponds precisely to the topographic elevation of the Cordillera de Talamanca.
Some Pliocene and Plio-Pleistocene volcanics, petrologically and geochemically distinct from normal arc volcanics, occur within the former active arc (i.e. the gap) and in particular within the fore arc and back arc region [Ballmann, 1976; Tournon, 1984; Defant et al., 1991; Drummond et al., 1995; de Boer et al., 1995].

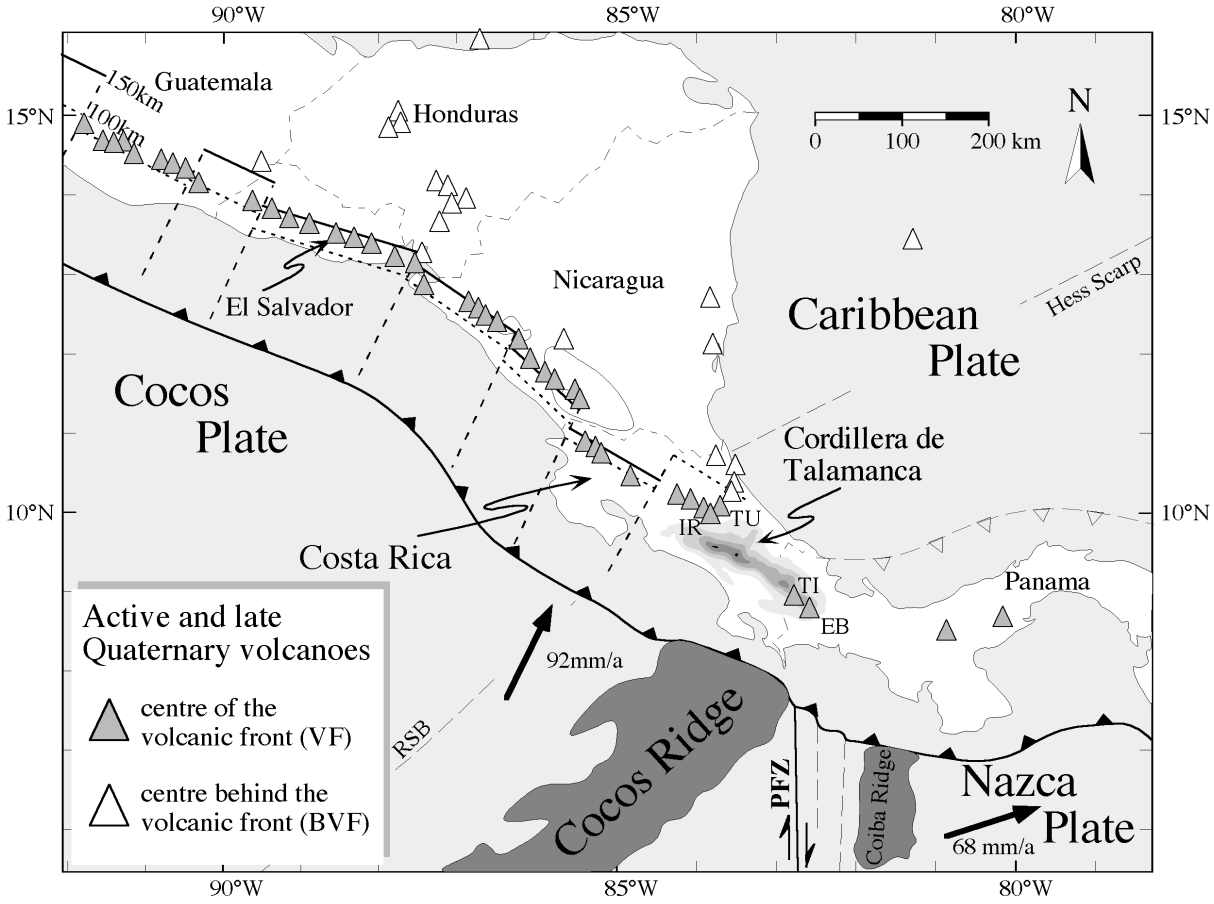

Figure 4: *Map of active and inactive late Quaternary volcanic centres in Central America after Carr et al. [1979]. The Cordillera de Talamanca is a volcanic gap between the volcanoes Irazú (IR) / Turrialba (TU) in southern Costa Rica and Tisingal (TI) / El Barú (EB) in western Panama. A distinction was made between volcanic centres aligned in the volcanic front and those from fields behind the front.*

1.2.2.3 Topographic uplift and exhumation

Topographic elevation of the central segment of the Chorotega arc (the Cordillera de Talamanca) to heights over 3500 m is conspicuous within the Central American Arc (Fig. 5A). The maximum elevation of 3819 m at Cerro Chirripó is prominent and the general topographic elevation of the area above 2000 m is unique in Central America [Kolarsky et al., 1995]. Thus, Costa Rica is higher than any other part of Central America, excluding continent-based Guatemala. The surrounding areas of the Cordillera de Talamanca in Costa Rica and Panama are affected by topographic uplift, reflected in the enormous height of the neighbouring volcanoes and a decrease of volcanic heights from central to northernmost Costa Rica (Volcán Irazú 3432 m to Volcán Miravalles 2028 m) [Weyl, 1980].
Uplift has probably occurred differentially with periods of rapid uplift followed by periods of relative quiescence [Kruckow, 1974]. From marine Miocene deposits of the Valle Central he calculated uplift rates between 0.040 and 0.095 mm/yr. Alt et al. [1980] have proposed an extremely high uplift rate of 25 mm/yr for the Coastal Range and Miyamura [1975] calculated a present rate of uplift for the central mountain range of Costa Rica at 1 to 2 mm/yr and Collins et al. [1995] report net rates of emergence of 1000 m/m.y. for the Pacific coast and 156 m/m.y. for the Caribbean coast. Recent estimates using mineral closing ages of samples

from Cerro Chirripó gave uplift rates of 1.4 ±0.5 km/Ma with a start of exhumation at 3.5 Ma [Graefe et al. 1998]. The presence of flat lying sedimentary and volcanic successions on Cerro Chirripó indicates vertical uplift [Tournon & Alvarado, 1997].
Cocos Ridge collision and subsequent shallow subduction is also affecting the forearc (Fila Costeña) and backarc (Limón basin) region [e.g., Klitgord et al., 1978; Corrigan et al., 1990; Gardner et al., 1992; Collins et al., 1995]. The forearc and backarc basins are volcanically active, structurally inverted and topographically uplifted in the contact area of the Cocos Ridge [cf. Kolarsky et al., 1995]. Along strike in Nicaragua, the inverted backarc basin changes rapidly to an extensional graben structure that is much lower in elevation (Fig. 5C).
Rapid crustal uplift of the overriding plate, associated faulting and erosion exposed the remains of volcanic arcs predating the Quaternary volcanic arc to the north and south of that area. Exhumation brought Miocene sub-volcanic rocks such as batholiths and granitoid stocks to the surface and high elevations (Fig. 3). Kesel & Lowe [in Gardner et al., 1987], showed that along the present crest of the Cordillera de Talamanca upper Miocene rocks were raised from about 400 to 900 m to elevations in excess of 3000 m.

Exhumation of southern Costa Rica and western Panama, building up the orogen of the Cordillera de Talamanca takes place since the Pliocene [Dengo, 1962; Graefe, 1998] and is ascribed to indentation and shallow subduction of the Cocos Ridge [Kolarsky et al., 1995]. Plio-Quaternary tectonic events are documented from the forearc to the backarc as for example by conglomerates, and thrusting and folding of Eocene to Miocene sedimentary sequences in the Limon Basin [Rivier, 1985; Collins et al., 1995].

Since the Cordillera de Talamanca, the area of topographic uplift and exhumation is placed directly opposite to the locus of Cocos Ridge subduction, a causal relation is obvious.

1.2.2.4 Neotectonic fault pattern

Both, convergent and divergent structures related to isostatic uplift and sub-horizontal island arc shortening are described for southern Costa Rica and western Panama by Corrigan et al. [1990]. The pattern of faulting in Neogene sediments in Costa Rica appears to reflect predominantly horizontal shortening perpendicular to the trench and is consistent with the width of the subducting Cocos Ridge [Heywood, 1984]. Major Neogene faults are typically reverse faults that strike parallel to the arc and dip steeply to the north-east (Fig. 5B) [Rivier, 1985; Mann et al., 1990].
Maximum horizontal compressive stress directions trend N-S and N-E, respectively, in the central and south-eastern Costa Rican inner arc area, overthrusts are nearly perpendicular to that direction [Montero, 1994]. Montero [1994] deduced Costa Rican neotectonics and related stresses from collision of the oceanic Cocos Ridge with southern Costa Rica, whereby the Cocos Ridge behaves as a rigid indenter and the region of central and southern Costa Rica as a rigid-plastic material. The regional stress field of Costa Rica inferred by Kolarsky et al. [1995] from P and T axes of earthquake focal mechanisms describe a radial pattern about the subducting Cocos Ridge.
Forearc indentation of the Pacific margin of Costa Rica as a typical feature of aseismic ridge or oceanic plateau collision with an island arc was described by Montero [1994] and Kolarsky et al. [1995].

1.2.2.5 Shallow dipping of Benioff Zone and seismicity

Burbach et al. [1984], Guendel [1986] and Protti et al. [1995] point out that the dip of the subducted Cocos Plate decreases significantly beneath central Costa Rica (from about 60° dip between Mexico and northern Costa Rica to 35-40° dip beneath central Costa Rica and Panama). For the depth interval of 25 to 250 km Guendel [1986] documents shallowing in subduction angle and in the 200- and 250-km isodepth contours he indicates an eastward deflection to the top of the Benioff Zone (Fig. 7). Protti et al. [1995] emphasise the abrupt termination of Benioff Zone seismicity deeper than 50 km southeast of Punta Uvita (83°55'W), indicating a tear or contortion in the downgoing slab beneath Costa Rica.
Historical large earthquakes (Ms > 7) reported from the area of the Osa peninsula support the hypothesis of shallow ridge subduction by documenting the high compressive stress regime on the upper plate [Protti et al., 1995; Tajima & Kikuchi, 1995].
Noticeable is the abrupt decrease in seismicity below 75km [Guendel, 1986], characterising a zone of relative seismic quiescence or a seismic gap.

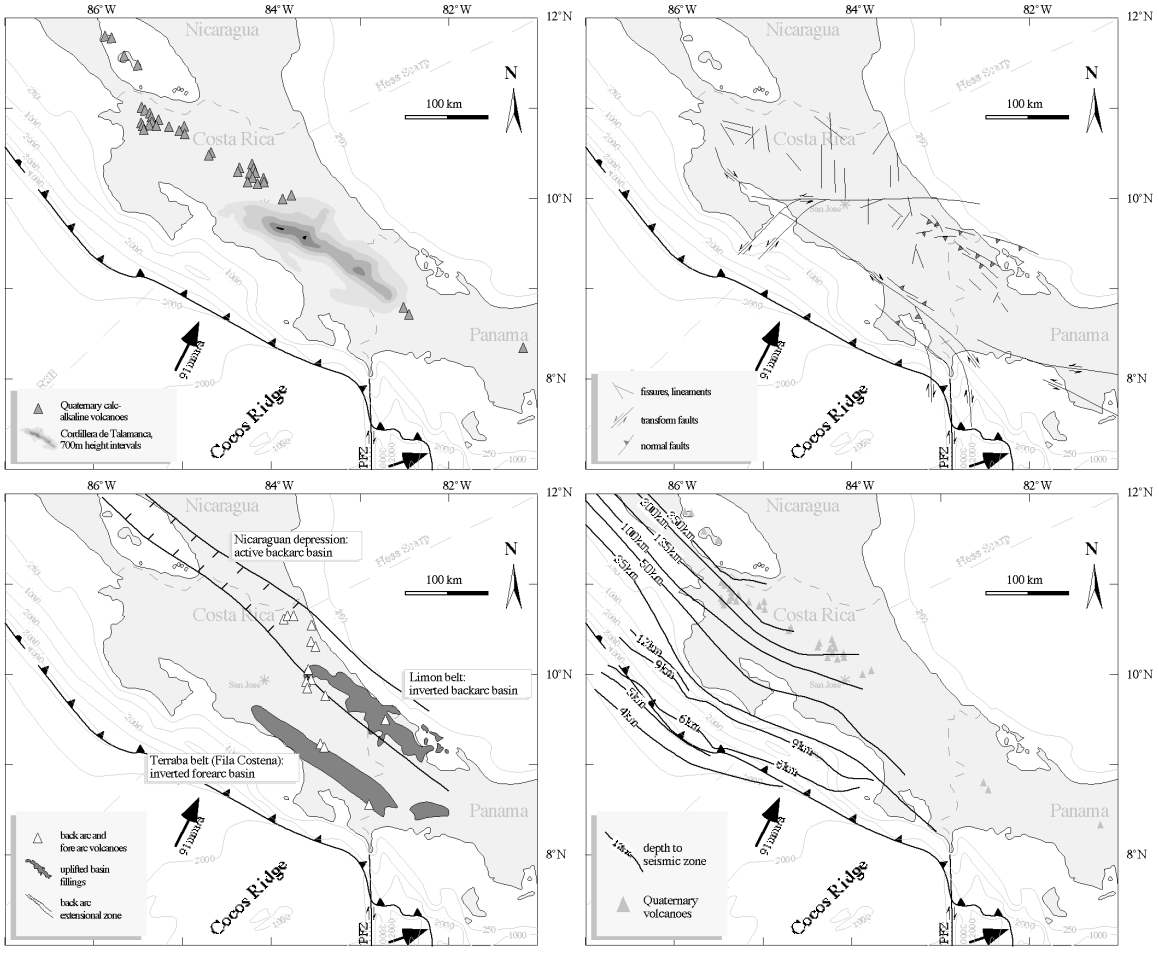

Figure 5: *Geological characteristics of the Cordillera de Talamanca. After Kolarsky et al. [1995].*
A: Topographic elevation of the Cordillera de Talamanca indicated by 700m height intervals.
B: Fault-pattern in Costa Rica characterises southern Costa Rica as an area of sub-horizontal shortening and uplift.
C: Basin inversion occurs on either side of the Cordillera de Talamanca.
D: Shallowing of the subduction zone beneath the Cordillera de Talamanca is indicated by bending of the plate-depth isolines.

The area of the Cordillera de Talamanca displays thus a section of the arc that is unequivocally strongly modified in comparison to a simple subduction zone. All the described phenomena are ascribed to indentation and shallow subduction of the aseismic, buoyant Cocos Ridge. The resultant effects of crustal shortening upon compressive stresses and isostatic uplift of the low density mass find expression in the geologic evolution observed in the Cordillera de Talamanca.
Modifications as they are present in the Central American Arc at southern Costa Rica and western Panama are world-wide observable as common complications arising from subduction of anomalous bathymetric features [e.g., Vogt et al., 1976; Kelleher & McCann, 1976; Chung & Kanamori, 1978; McGeary et al., 1985; Adamek et al., 1987].

1.2.3 Talamanca crust and subducting Cocos Plate

1.2.3.1 Talamanca crust

Geological and geophysical investigations in the Caribbean region [Case and MacDonald, 1990] show that the crust of the Talamanca area is of an accretionary type (Fig. 6), formed by subduction in oceanic environment. In contrast to the northern end of the Central American Arc, no continental crust fragments are indicated.

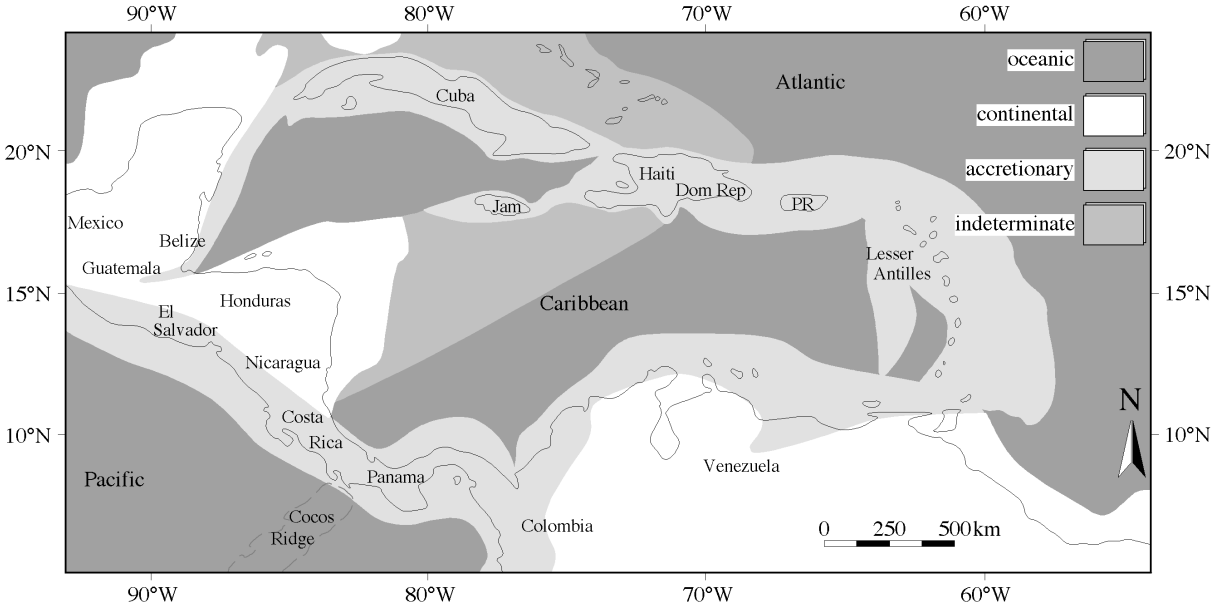

Figure 6: *Genetically distinct types of crust within the Caribbean as characterised by Case et al. [1990]. Indicated are oceanic, continental and accretionary crust types as well as crust where no data is currently present. The map shows that southern Central America (Costa Rica and Panama) is made up of accretionary crust and northern Central America is underlain by continental crust.*

1.2.3.1.1 Crustal Thickness

Costa Rican crust is intermediate between continental and oceanic (Fig. 7). It is not as thick, old and layered as continental crust but thickened compared to oceanic crust. Crustal thickness in Costa Rica is locally as much as 40 km. Matumoto et al. [1977] found 43±7 km for the northern part of the country, the recent most seismic investigations in northern Costa Rica documented 40 km [Goedde et al., 1998]. Crustal thickness in southern Costa Rica seems to be less (Fig. 7). Stavenhagen et al. [1997] found a thickness of only 20 km. Although the topography of the Talamanca mountain range stands well above the surrounding area, the total crustal thickness is not as much as that of the less elevated northern Costa Rica and Nicaragua. This implies a mass deficiency in the lower crust and thus isostatic disequilibrium for that particular region [Case et al., 1990], and characterises the Talamanca as a region of very young and rapid uplift (chapter 1.2.2.3). Reduced crustal thickness in southern Costa Rica may result from the late establishment of arc magmatism in that region compared to northern Costa Rica [Tournon & Alvarado, 1997], (chapter 1.2.1), from a locally reduced thickness of the pre-arc crust, from much higher erosion rates, or from thermal erosion of the lower crust.

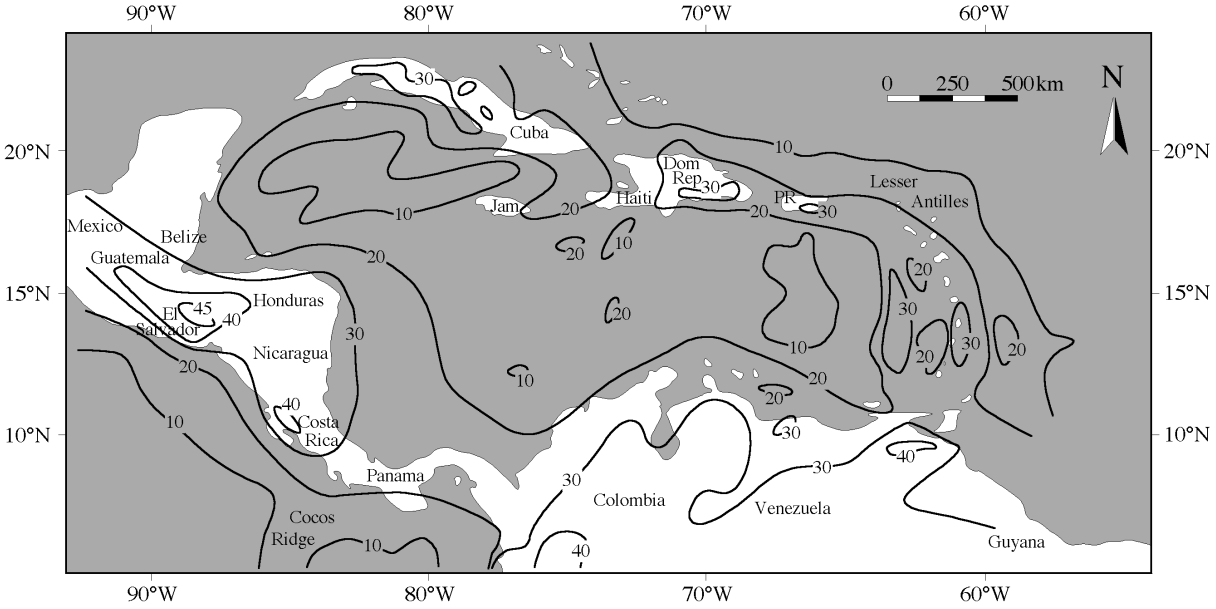

Figure 7: *Map of the Caribbean depicting the crustal thickness (from Case and MacDonald, 1990). Contour lines are 10 km intervals. This map shows that the crust underneath the Cordillera de Talamanca is less than 30 km in thickness.*

1.2.3.1.2 Crustal composition

Continental basement is unknown for Costa Rica and Panama [e.g., Tournon & Alvarado, 1997]. No continental basement xenoliths or outcrops of such basement are presently known.
Seismic refraction patterns lack the appropriate layering typical of continental crust [Goedde, 1998]. From seismic investigation it was concluded that the crust in Costa Rica consists of a thick section of basaltic composition comparable to the Ontong Java Plateau [TICOSECT, 1998].
Sr-Nd isotope variation diagrams for volcanics of the active arc show no contamination by old continental crust for Costa Rica opposed to Guatemala where old continental crust is evident

by the distinct pattern of Sr-Nd isotope enrichment along the mantle array [Carr & Feigenson, 1986]. Using Sr isotopic compositions of Costa Rican volcanic rocks, Thorpe et al. [1979] exclude the presence of sialic crust older than about 80 m.y.

1.2.3.2 Subducting plate

The subduction zone off the Cordillera de Talamanca in southern Costa Rica and western Panama is complex because it is the location of a triple junction. Two oceanic plates, the Cocos and the Nazca plate, subducting underneath the Caribbean plate at different rates and angles, meet in this area. Furthermore, this convergence zone is modified by the subduction of the aseismic Cocos Ridge riding on the Cocos Plate.

1.2.3.2.1 Cocos Plate

The oceanic plate subducting underneath southern Costa Rica is currently the Cocos Plate. This plate subducts along the entire Central American Arc except for Panama. The Cocos Plate terminated by the Galapagos Spreading Centre (GSC; also called Cocos-Nazca-Spreading-Centre) in the south and by the East Pacific Rise (EPR) in its west.
Lithology and geochemical compositions are probed by DSDP and ODP drillings off Guatemala (Leg 495), near the Galapagos Rift (Site 504), and recently near Nicoya, Costa Rica (Leg 170).
The south-eastern part of the Cocos Plate may be separated from the remainder by the rough-smooth-boundary (RSB) after Hey [1977] and is characterised by the presence of abundant seamounts and the aseismic Cocos Ridge.
At its subducting end, the Cocos Plate is still very young. Within the segment between the RSB and Panama-fracture-zone (PFZ), it dates to only about 15 Ma (Fig. 2) [Hey, 1977].
Very high heat flow values above 3 HFU are remarkable for the north-eastern end of the Cocos Plate near the triple junction as well as for the neighbouring Nazca Plate [Bowin, 1976].

1.2.3.2.2 Cocos Ridge

The Cocos Ridge, located on the Cocos Plate south of Central America extends from southern Costa Rica to the Galapagos Archipelago (Fig. 10). It is a broad, shallow, bathymetric feature that rises 2 to 2.5 km above the surrounding ocean floor. Marine refraction studies indicate a crustal thickness of 15 km [Bentley, 1974] to 25 km [TICOSECT, 1998] beneath the Cocos Ridge. This is significantly thicker than surrounding normal oceanic crust of the Cocos and Nazca plates.

Today it is well established that the Cocos Ridge is a product of hot spot volcanism from the Galapagos hotspot [e.g., Duncan & Hargraves, 1984; Larson & Olsen, 1991; Hauff et al., 1997].
Earlier two alternative hypotheses about the origin of the Cocos Ridge were discussed: (1) a hot spot hypothesis and (2) an ancestral-ridge hypothesis.
In the ancestral-ridge hypothesis [van Andel et al., 1971; Malfait & Dinkelman, 1972; Heath & van Andel, 1973; Rea & Malfait, 1974; Meschede et al., 1998], the Cocos Ridge would be a former active spreading centre.

However, in most recent studies, the Cocos Ridge is believed to be a trace from the Galapagos hot spot, produced by intense plume magmatism during relative movement of that plume to the oceanic plate (Cocos Plate). This hypothesis was put forth by Wilson [1963] and Morgan [1971] and elaborated by Hey et al. [1977]. Lack of seismic activity as well as lack of parallel magnetic anomaly stripes are indicators for the hotspot origin and arguments against an explanation as a spreading ridge [e.g., Hey, 1977].
A combined model of a former spreading ridge with superimposed hot spot volcanism is proposed by [Lonsdale & Klitgord, 1978] and [Meschede et al., 1998]. In that case, the vast volcanic edifice of the Cocos Ridge would be a result of temporary ridge-hot spot interaction as can be observed today in Iceland.

In either of the above models, the Cocos Ridge must be even younger than the rather young Cocos Plate.
Ages of the Cocos Ridge are mostly concluded from plate-tectonic reconstructions and are therefore quite different for the above mentioned hypotheses. Meschede et al. [1998] calculate an age of 24 to 15 Ma for the Cocos Ridge in their spreading ridge model. Hey [1977] gives an age of about 20 Ma at its north-eastern end and Lonsdale & Klitgord [1978] deduce an age of middle to late Miocene (~10-15 Ma?). Protti et al. [1995] calculate an age of 13-17 Ma for the Cocos Plate at the trench near the Cocos Ridge, so that the superimposed hot spot trace must be younger than that.
New direct Ar/Ar age determinations on Cocos Ridge samples give an age of 13 to 14 Ma for the Ridge at its end near the MAT [v.d.Bogaard & Werner, 1998].
However, very recent activity along the ridge is documented by the Cocos Islands revealing an age of 1.91 ± 0.1 Ma [Bellon et al., 1983; Alvarado et al., 1992].

The bulk chemistry of the Cocos Ridge is tholeiitic similar to the chemistry found on the Galapagos Islands [Castillo, 1984; Castillo et al., 1988]. New analyses by Werner [1998] support this and indicate a trace element signature of MORB and Sr/Nd isotopic signatures of mixed MORB – Plume sources as described by White [1993] for the Galapagos Islands. The radiogenic isotopic composition of the Cocos Ridge matches that of the Galapagos Islands and is distinct from that of the Cocos Plate [Werner, 1997]. This geochemical evidence points to a connection of the Cocos Ridge and the Galapagos hot spot.
Seamounts on and adjacent to the Cocos Ridge are predominantly alkalic in composition and display OIB signatures [Werner, 1998].

About 5 Ma ago the Cocos Ridge collided with the Central American trench. Since parts of the ridge were possibly cut in an en echelon manner along transform faults on the Cocos Plate [Malfait & Dinkelman, 1972], precursors could have been subducted below Panama prior to the actual Cocos Ridge collision. The Malpelo Ridge is thought to be such a cut off fragment of the Cocos Ridge [Lonsdale and Klitgord, 1978; Gardner et al., 1992; Meschede et al., 1998].
The exact timing of the collisional event depends on the respective model of plate tectonic evolution or type and location of studies. However, all current research points to a date earlier than former assumptions. Studies on emergence rates in the back arc of Costa Rica and Panama [Collins et al., 1995] point to 3.6 Ma, palaeotectonic reconstruction models for the Cocos plate [Meschede et al., 1998] point to 4 Ma, evolution of local volcanism points to 5 Ma [de Boer et al., 1995] and investigations on exhumation rates at Cerro Chirripó reveal 5.4 Ma [Graefe, 1998] for the beginning of Cocos Ridge subduction.
These new results are older than the ages of Lonsdale and Klitgord [1978], Corrigan et al. [1990], and Gardner et al. [1992], who proposed a date around 1 to 2 Ma for the collision.

It is convincingly shown that the buoyant ridge did not stall or pivot when it encountered the trench but was instead subducted beneath Central America. Direct observations of currently occurring underthrusting were made with studies using submersibles [Heezen and Rawson, 1977], and numerous studies documented the Cocos Ridge subduction indirectly by its effect on the arc (chapter 1.2.2).
When subduction ceased at a ridge-trench encounter, the buoyant parts of the subducting plate broke up into non-subducting micro-plates [Atwater & Severinghaus, 1989].
Bathymetric and tectonic investigations have documented a westward shift of the transform plate boundary between the Nazca and the Cocos Plate next to the Cocos Ridge [Moore & Sender, 1995]. This westward jump of the plate boundary may well be induced by sequential indentation of the Cocos Ridge precursors and the Cocos Ridge itself, occurring upon temporarily reduced convergence rates in the respective area.
However, there is no direct observation of disruption of the subducting Cocos Plate or Cocos Ridge as a consequence of collision with the Central American trench.

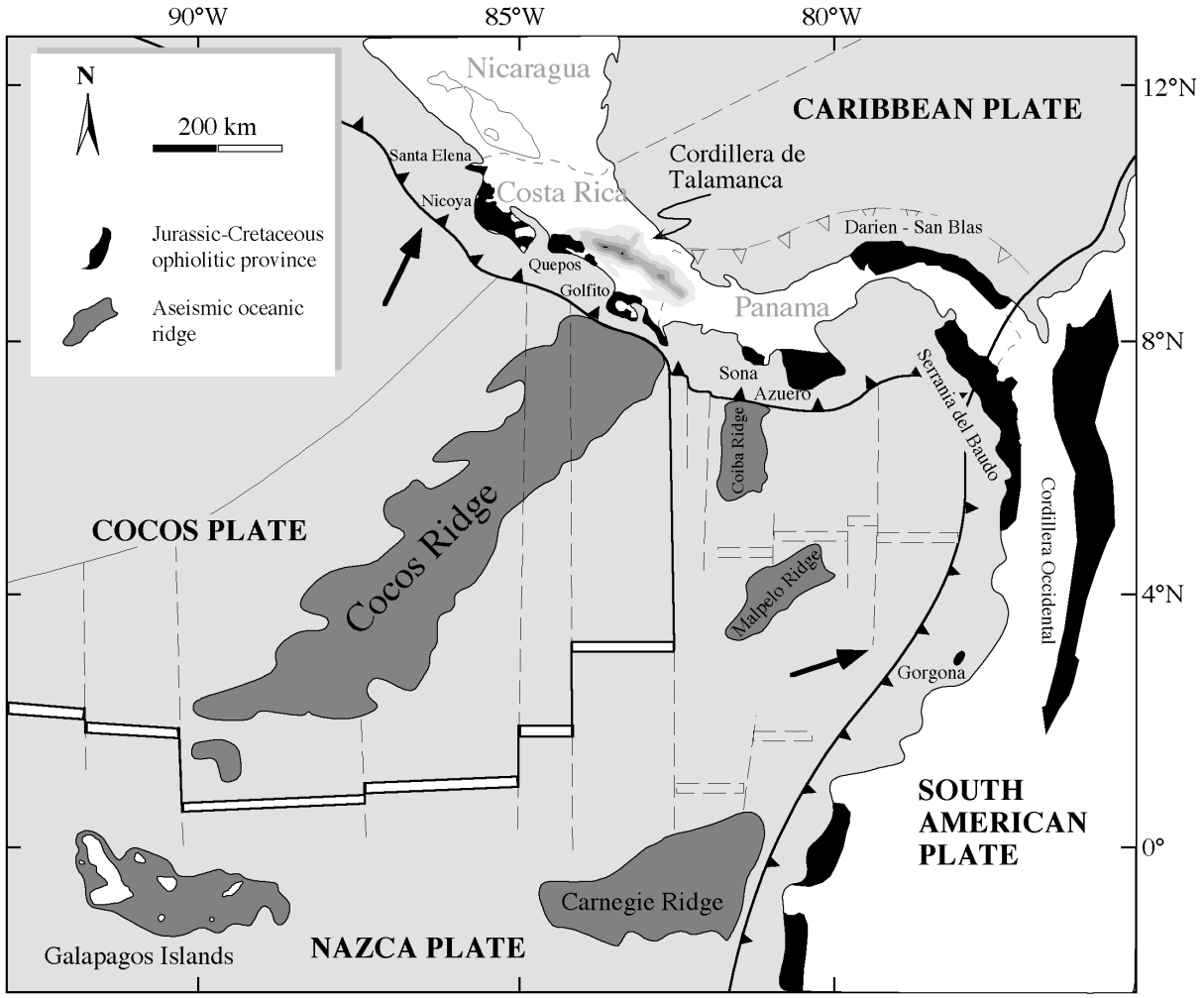

Figure 8: *Tectonic map of southern Central America and the Galapagos area showing locations of oceanic, aseismic ridges and exposures of ophiolites after Donnelly et al. [1990] and Hauff et al. [1997]. The ophiolites are of Cretaceous age and assumed to be parts of the Caribbean (Super-) Plume-event which shows compositional similarity to the present Galapagos hot spot. The aseismic ridges are produced by the hot-spot during a later period of activity.*

1.2.3.2.3 Sediment cover

The sedimentary cover on the Cocos Plate, a potential candidate to subduction, is probed by the drillings of ODP Leg 170 off Costa Rica and by DSDP Leg 67 Site 495 off Guatemala. Lithological and especially geochemical composition of the sediment is well documented for the Guatemala Site and available at GERM [1998].
New detailed information about the lithology of the subducting sediment section off Costa Rica is gained from reference Site 1039 of Leg 170 off the Nicoya peninsula, very close to the trench [Shipboard Sci. Party Leg 170, 1997].
The sediment column can be subdivided into three lithostratigraphic units, comprising from top to bottom: a unit of diatomaceous ooze, a second one of silty clay and a third one of calcareous ooze. The lowermost sediments of the section are of early to middle Miocene age.
Carbonates are prevailing in the sediments currently being subducted in the Costa Rican subduction zone [Shipboard Sci. Party Leg 170, 1997].

For bulk geochemistry, the sedimentary column subducting beneath Costa Rica is broadly similar to that entering the trench off Guatemala. Slight exceptions exist with respect to a few incompatible elements: K and Rb contents of the bulk sediment section are slightly higher, Sr and Ba lower in the Costa Rican section as compared to the Guatemalan one. This is explained by higher proportions of hemipelagic sediments in the sediment column off Costa Rica, generally higher sedimentation rates and greater dilution of the marine barite contribution [Kimura et al., 1997].

Intercalated ash layers of the upper ¾ of the sediment column have trace element signatures (Zr/Nb) indicating their derivation from a volcanic arc, whereas ash layers in the lowermost part (early to middle Miocene age) show affinities to the Galapagos plume mantle [Kimura et al., 1997]. The shift in ash layer compositions traces the productivity of the respective volcanic systems but also the plate motion from its site of generation near the Galapagos islands towards its site of destruction at the Central American arc.

Seismic measurements across the Nicoya peninsula indicate that currently no sedimentary accretion takes place at the Costa Rican convergent margin [Goedde et al., 1997]. These findings were substantiated by constraints from trace element concentrations, testifying that sediments above the decollment are distinct from those on the incoming plate [Valentine et al., 1997].
Geophysical data point to active underplating in Costa Rica [Shipboard Sci. Party Leg 170, 1997], but the magnitude is not quantifiable by these methods. From comparisons of the ^{10}Be inventory of volcanics from Costa Rica and the sediment section, the amount was specified to $\geq$40% of incoming sediment that were removed by underplating [Valentine et al., 1997].
Effective separation of the upper hemipelagic sediment portion by underplating explains the absence of ^{10}Be reported by Morris et al. [1990] for the active volcanoes in Costa Rica.
Therefore, only about 60% or less of the incoming sediment section is reaching depths of magma generation. Evidently, this is the lower part of the column.

Rates of sediment subduction in southern Costa Rica are influenced by the Cocos Ridge subduction, which was reported to have deep, partly sediment filled grabens on its north-eastern end [Lonsdale & Klitgord, 1978].

1.3 Previous Works

Systematic regional geological investigations of Central America began in the later nineteenth century [cf. Draper & Dengo, 1990].
Due to its volcanic quiescence and inaccessibility, the area of the Cordillera de Talamanca was excluded from many research projects and reports [see e.g., v. Seebach, 1892, or Feigenson & Carr, 1986]. Nevertheless, there exist now several studies from the area describing the geology, petrology and in parts geochemistry or the effects of Cocos Ridge collision on this segment of the arc.
Primarily due to difficult accessibility of the Talamanca region, petrologic research has for long time been of a reconnaissance nature.

The first scientific reports on the geology of the Cordillera de Talamanca are from Gabb [1874a, b, 1875], who explored the mountain chain in 1873 and 1874. Several years later, after extensive research in Central America, Sapper [1937] summarised the existing geological knowledge in a book that also contains a schematic geological map of the Cordillera de Talamanca. He already noted rapid and high uplift of the mountain chain and rejects the opinion that the Talamanca completely lacks young volcanic structures.
Important systematic studies directly related to the Talamanca mountain chain are those from Weyl [1957, 1980] and Dengo [1962]. Their research provided fundamental knowledge of the petrography and stratigraphy from the Cordillera de Talamanca and a basis for the first complete geological maps and sections.
Interest in the Talamanca increased when mining companies started exploration for porphyry copper ores in the 1970s. Results of these campaigns are however not published but in parts referred to by Escalante [1990]. Ballmann's mapping work during an exploration campaign in a remote area in the central part of the Talamanca gave evidence for the existence of spots with relatively young volcanic activity within this mountain chain [Ballmann, 1976].
Tournon [1984] provided a comprehensive overview on magmatism in Costa Rica with an emphasis on geochemical and geochronological data, including detailed information about the respective sample locations. Sampling for my study profited mostly from that thesis.
A study of petrographic classification and major element geochemical comparison for intrusive rocks from the Cordillera de Talamanca and other locations in Costa Rica is published by Kussmaul [1987]. Alvarado et al. [1992] compiled a review of geochronology data for Costa Rican igneous rocks. This data set is expanded in respect of the Talamanca rocks by works of Defant et al. [1992], and de Boer et al. [1995].
The publications of de Boer et al. [1995] and Drummond et al. [1995] are so far the most elaborate geochronological and geochemical studies on igneous rocks from the Cordillera de Talamanca. Their work concentrated on the central mountain range but included the Panamanian part of the Talamanca. They define four distinct lithologic groupings of rocks (mid-Oligocene tholeiitic gabbros, mid-Oligocene El Barú plutonic rocks, Late Miocene calc-alkaline plutonic rocks, and a Pliocene-Pleistocene undifferentiated volcanic group), which overlap with groups of this study. Their study does not comprise igneous rocks from the forearc and backarc region.

Geochemical and geochronological work on backarc igneous rocks from the area around Guayacan was carried out by Azambre & Tournon [1977], Tournon & Bellon [1978], Stack [1991], Gargantini [1993], and Luoni [1993].

Igneous rocks in the inner forearc (Fila Costeña) are described in studies of Henningsen [1966], Mora [1979], Rivier [1985], Tournon, [1984], Kesel [1983], and Estrada & Alvarado

[1993]. Published geochemical data from these rocks exist only to a very limited extent [Kussmaul et al., 1994; deBoer et al., 1995].

The effects of Cocos Ridge collision and subduction on the southern segment of the Central American arc system (comprising SE Costa Rica and W Panama) has been the subject to numerous studies. Since this incident directly affects the investigated area and its magmatic evolution, these publications should also be listed here. Lonsdale & Klitgord [1978] were the first to postulate a date for the ridge/arc collision from their plate tectonic reconstruction. Corrigan et al. [1990] and Gardner et al. [1992] have studied the effect of the Cocos Ridge subduction by investigating uplift rates in the forearc region. Collins et al. [1995] did comparable studies in the backarc region. A relation of the gap in the chain of active volcanoes in SE Costa Rica to Cocos Ridge subduction was drawn by McGeary et al. [1985]. Kolarsky et al. [1995] presented a compilation of the known effects ascribed to Cocos Ridge subduction.

Johnston and Thorkelson [1997] postulated a slab window underneath SE Costa Rica and W Panama which they hold responsible for the occurrence of certain magmatic rocks in this arc segment. By plate-tectonic reconstruction they show that segments of the Cocos-Nazca spreading centre may have been subducted at this site resulting in the slab window formation.

Previous works on the geochemistry of the area are selective by investigating solely a single, restricted arc region (e.g., Talamanca sensu strictu in [Drummond et al., 1995]) or even only a certain magmatic suite (e.g., Guayacán sills in [Gargantini, 1993]). Thus, spatial and temporal evolutions within this segment of the Central American arc system could not be investigated comprehensively so far. The present study tries to fill in this gap by describing and explaining the evolution of this arc segment in its entirety and therefrom concluding to a consistent plate-tectonic model.

A new geological map including comprehensive explicative notes on the up-to-date knowledge of Costa Rican stratigraphy is provided by Tournon and Alvarado [1997].

2 Field relationships and petrography

Volcanic and plutonic samples were collected along the entire length of the magmatic arc in southern Costa Rica (Cordillera de Talamanca) as well as in the forearc (Fila Costeña) and backarc (Limón basin), with the highest density of sampling from rocks dating around the collisional event. Samples of magmatic rocks in southern Costa Rica were collected in a manner that those rocks would report the effects of Cocos Ridge collision as well as the characteristics of normal pre-collisional arc magmatism in that arc segment.
Based on age relations, geochemical and isotopic data, petrography and geographic distribution within the arc, five rock groups could to be distinguished: the pre-collisional arc-tholeiitic and calc-alkaline groups, and the syn- and post-collisional forearc calc-alkaline, backarc alkaline and adakite groups.
Sample locations for the five rock groups are compiled in the topographic map (Fig. 9) to give an overview on the distribution of the groups. For detailed information on sample locations refer to the geological maps of Fig. 10.

2.1 Arc tholeiite group – pre-collisional

2.1.1 Field relationships

Tholeiitic samples are exposed within the Cordillera de Talamanca (central magmatic arc) as well as within the Fila Costeña (forearc). In the fore arc they appear as dikes and small stocks in the lower sections, outcropping near Puerto Nuevo and Punta Uvita (Fig. 10.1). Dikes are also present within the central magmatic arc near Division where the Interamericana (Pan-American Highway) crosses the watershed of the Cordillera (Fig. 10.3). Volcanics of that group were found along the southern slopes of the Cordillera de Talamanca at Cerro Chirripó (Fig. 10.3) and Cerro Echandi near the Panamanian border (Fig. 10.5).

2.1.2 Lithology and petrography

The tholeiitic groups comprises basalts, basaltic andesites and andesites as well as gabbros. In hand specimen the volcanic rocks appear aphyric to porphyritic. The rocks are middle to dark grey and dense. Signs of alteration are noticeable by a greenish touch, but most samples appear fresh.
Porphyritic to glomerophyric texture is common for these rocks, some of the samples display a more intergranular, intersertal or serial texture. Principal minerals are pyroxene and plagioclase, the latter as phenocrysts and microphenocrysts, mostly euhedral, often sericitisated and sometimes with sieve texture. Olivine is sometimes found, but almost entirely corroded and recrystallized to secondary minerals. Opaque minerals, predominantly magnetite, are always present, as phenocrysts or groundmass component. Only one sample contains minor amounts of anhedral brown-green amphibole. Conspicuous is the alteration of the samples. The least altered contain only minor amounts of chlorite, the highly altered samples contain chlorite, epidote, quartz, hematite, and calcite.
Gabbros of the group are dark grey and massive. Their textures are more anhedral-granular than intergranular. Main minerals are plagioclase and pyroxene, the former are euhedral to subhedral, the latter more often anhedral. Olivine is present in almost all gabbro samples, but often corroded. Ore minerals are always present, some of the samples contain biotite. Alteration is shown by sericitization of plagioclase, corrosion of olivine and the presence of chlorite.

2.1.3 Interpretation:

The above described volcanics show the principal mineralogy of tholeiites comprising olivine, plagioclase and pyroxene for the basaltic samples and predominantly plagioclase for the andesites. The greenschist facies paragenesis of alteration minerals indicates the exposition to low-grade contact metamorphic conditions. These conditions were easily realised in the proximity to the intrusions and give a hint to their age as they have to be older than the intrusive phase within the Cordillera de Talamanca. Their lower age is confined by their appearance as massive subaerial lava flows, which requires the existence of an island arc, already emerged above sealevel.

Intrusive samples of this group are apparently less affected by alteration or low-grade metamorphic overprint than their volcanic equivalents. Thus, the original paragenesis of theses primitive island arc magmas is better preserved, facilitating estimations about the rocks chemistry. The generalised crystallisation sequence indicated by textural relationships in the gabbros is olivine followed by plagioclase, pyroxene, oxides, and finally biotite.

2.2 Calc-alkaline group – pre-collisional

2.2.1 Field relationships

This group comprises intermediate to silicic intrusive rocks and to a lesser amount volcanic rocks of calc-alkaline character. The samples were taken along the main magmatic arc, primarily in the crest region. Outcrops were found (from northwest to southeast) near the village Santa María de Dota (Fig. 10.2), along the Interamericana from the location Ojo de Agua down to the town San Isidro (Fig. 10.3), around Cerro Chirripó and Cerro Urán (Fig. 10.3), to the south of Cerro Durika (Fig. 10.4), and between Cerro Pando and Cerro Echandi at the Panamanian border (Fig. 10.5).

The volcanic rocks are exposed in the northwestern Cordillera de Talamanca, where the Interamericana (Pan-American Highway) intersects the mountain range.

2.2.2 Lithology and petrography

The plutonic rocks show granular fabrics in hand specimen, and vary in colour between gabbroic dark grey and tonalitic light grey. Two of the samples are aplite-granites and accordingly brightly coloured white to pinkish and fine-grained.

In thin sections, all these intrusives display granular textures, most often subhedral-granular. Plagioclase which is present throughout is often superseding other minerals in size and are commonly subhedral. Other major rock forming minerals of these Talamanca intrusive rocks are alkali feldspar (mostly orthoclase), quartz, pyroxene, amphibole, biotite and magnetite. Accessory minerals are apatite, zircon and sphene. At least one of the hydrous minerals amphibole or biotite is present in the rocks. Amphibole is always green in contrast to those from the adakitic samples. Alkali feldspar is commonly orthoclase and occurs interstitially in the more basic rocks and as large, anhedral crystals that ophitically enclose other minerals in the more acid samples. Granophyric intergrowths of alkali-feldspar and quartz are characteristic of the most highly differentiated rocks, the aplitic stocks. Secondary minerals like chlorite are present in minor amounts in some of the samples.

Volcanic rocks of that group are highly porphyritic andesites and dacites, containing plagioclase and pyroxene in a black glassy matrix.

The extremely porphyritic texture is characteristic of these samples. Large euhedral pyroxenes and plagioclases are embedded in a matrix of glass and tiny feldspar needles. All plagioclase phenocrysts display conspicuous sieve textures. Pyroxenes are both, clinopyroxenes and

orthopyroxenes. Further minerals are some large magnetite grains and accessory apatite. These volcanics appear quite fresh since non-devitrified glass is present.

2.2.3 Interpretation

In contrast to the related volcanics, amphibole is abundant in the intrusive rocks of the calc-alkaline group. This reflects most likely the increased stability of amphibole at depth. The overall abundance of hydrous minerals in these rocks may be indicative for the genesis of these calc-alkaline rocks, implying an essential contribution of hydrous phases from the subducting slab.
The textural appearance of the volcanic samples indicates their derivation from a rather hot, rapidly cooled magma. Preservation of the glassy texture is surprising since hydrothermal alteration was reported for most of the rocks in the immediate vicinity [Tournon & Alvarado, 1997]. Thus, low alteration grades suggest fairly young ages for the volcanics. Interpreting the mineral assemblage with its crystallisation sequence and the fabric points out to calc-alkaline composition.

2.3 Forearc calc-alkaline group – syn-collisional

2.3.1 Field relationships

Samples of this group are volcanics without exception. They were found in the central part of the Fila Costeña, either as clasts within the sediments of the Paso Real formation near the village of same name, as remnants of lava flows near Cerro Mano de Tigre or at newly encountered outcrops between the village Pejibaye and Río General (Fig. 10.1).

2.3.2 Lithology and petrography

This group comprises dark grey to black, porphyritic basalts and andesites.
Textural characteristics of these samples are predominantly porphyritic fabrics, sometimes porphyritic-aphanitic. In some of the samples, phenocrysts appear as aggregates, hence the rocks have a glomerophyric texture. Plagioclase and pyroxene, both as phenocrysts, microphenocrysts and groundmass component, make up the main mineral constituents of these samples. Plagioclase and pyroxene phenocrysts are large up to several mm in size and both are euhedral. In most of the samples, the plagioclases show a conspicuous sieve texture. Olivine is present in most if not in all of these samples, however, in some instances they are severely corroded, and detectable only by their contours. Ore minerals are present throughout and apatite was observed in some of the samples. Alteration other than olivine corrosion is confined to minor chlorite growth in some of the samples. Despite these incipient signs of alterations, the rocks have a quite fresh appearance.

2.3.3 Interpretation

Presence of pyroxene and plagioclase and their crystallisation relationship and the in most cases highly porphyritic nature point out to the calc-alkaline composition of these island arc basalts and andesites. Olivine corrosion and the sieve texture in plagioclase seem to signal disequilibrium in the magma, possibly related to mixing or assimilation processes. The overall fresh appearance suggests a rather young age of these rocks, hence they could not be related to the mafic intrusive rocks found in the forearc as well.

2.4 Adakite group – post-collisional

2.4.1 Field relationships

In SE Costa Rica, adakites are found in three separate locations. They occur either directly within the magmatic arc or at its southern end, whereby they seem to be extruded along major faults. A location within the Cordillera de Talamanca near Cerro Durika (Fig. 10.4) was described by Ballmann [1976]. Other outcrops, near the town San Vito at the villages Aguas Claras and San Bosco (Fig. 10.5) are described by Tournon [1984]. The latter occurrence is currently quarried for pavement purposes. Tournon provides chemical analysis and age data for the volcanics from these locations. A third location, about 20km NE from the San Vito quarry at Cerro Pelón and Cerro Chivo, was not examined so far, though it is of large extension. These newly described outcrops, together with already known centres of adakitic volcanism, point to a considerably broader area of this type of volcanism in southeast Costa Rica during Plio-Pleistocene times than recognised up to today.

2.4.2 Lithology and petrography

Samples of this group are blocky jointed or massive andesites and breccious dacites. The andesites are middle to dark grey whereas the dacites are pale grey and vesiculated. Conspicuous are large phenocrysts of white plagioclase and dark amphibole. Different is the appearance of two andesites which are black in colour and platy jointed, dense lava flows.
Porphyritic texture is common to all adakite samples. The main mineral components involve phenocrysts of euhedral to subhedral plagioclase and euhedral brown to green-brown amphibole. The former shows always strong zonation, the latter is generally opacitized except for the samples from the Durika area and a sample from the San Vito area. Euhedral to anhedral Pyroxene is also common. Pyroxene does not occur in the dacitic samples of the Durika area which contain instead anhedral biotite (xenocrysts?) and furthermore, well rounded, large quartz crystals. Euhedral to subhedral olivine is present only in three samples as xenocrysts where it is commonly strongly corroded. Titanomagnetite exists as phenocrysts and microphenocrsts, accessory minerals are zircon and apatite. Glomeroporphyritic xenoliths containing pyroxene, plagioclase and olivine are present within some of the samples. The groundmass is cryptocrystalline, probably formerly glassy, to microcrystalline. Alteration seems to be confined to the glassy groundmass that subsequently devitrified.

2.4.3 Interpretation:

The Durika samples contain a typical adakitic mineral assemblage (plag, mt, amph, bio, qz) as it is described by Defant et al. [1991] for the Panamanian samples. However, the pyroxene phyric, biotite and quartz free samples resemble adakites described for the southern Chile occurrences [Stern & Kilian, 1995].
Since all samples contain notable amounts of hydrous minerals (amphibole, biotite), they seem to be derived by lower degrees of melting than some of the Chilean or Kamchatka adakites that lack hydrous minerals [Stern & Kilian, 1995; Kepezhinskas et al., 1997]. Opacitization and strong corrosion of the amphibole phenocrysts suggests extensive water loss and reflects the increasing disequilibrium of the intratelluric amphiboles with the magma due to pressure reduction during uprise of the magma [e.g., Pichler & Schmitt-Riegraf, 1987]. No or only slight opacitization is present in the amphiboles from adakites of the Durika area, indicating faster uprise and cooling for these dacites.
Xenoliths and xenocrysts of clinopyroxene and olivine are most probably mantle derived and document the passage of these magmas through the mantle wedge. Contaminations of that kind rendered these adakites andesitic in composition and increased the Mg# (from about 40 to 70).

2.5 Backarc group – syn-collisional

2.5.1 Field relationships

Back arc magmas in Costa Rica erupted from several small centres along the entire length of the Caribbean coast (in the Limón basin). The back arc magmatism is exclusively of alkaline nature and the related volcanic and intrusive bodies are N-S aligned [Tournon, 1984]. The occurrence of the back arc magmatic features within only a few kilometres behind the active arc in Costa Rica is unusual for convergent margins [Milionis et al., 1986].
Three rock suites were found to represent the back arc group of this study, comprising all alkalic magmas.
One of these suites outcrops near the village Bribri at the Panamanian border (Fig. 10.7) and comprises alkaline extrusive rocks and a dike. These occurrences were not published so far. This rock suite consists of alkaline basalts.
The second suite was found near the village Guayacán between the cities Turrialba and Siquirres and the rivers Reventazón and Pacuare (Fig. 10.6). Some of the outcrops are near the young lava fields of volcano Turrialba. This suite is the most voluminous series of volcanic and intrusive alkaline rocks of a large compositional range in Costa Rica. It was already described in several studies [Azambre & Tournon, 1977; Tournon, 1984; Stack, 1991; Gargantini, 1993; Luoni, 1993].
The third suite is represented by a single sample, an amphibole bearing lamprophyr from Cerro Bola near the town Neily (Fig. 10.5). Though the lamprophyr outcrops in a fore arc location, it clearly belongs to the back arc group based on geochemical criteria. The link between fore arc and back arc and the geochemical similarity can be explained by plate-tectonic features discussed below. The outcrop is mentioned in Tournon & Alvarado [1997] as a dome of potassic dacite.

2.5.2 Lithology and petrography

Hand specimen of the Bribri suite can be described as middle grey to black and pyroxene porphyritic.
Textural characteristics are the porphyritic fabric with large euhedral augite phenocrysts in a crystalline matrix of plagioclase, pyroxene and opaque minerals. Olivine phenocrysts or microphenocrysts are present in all samples, except for a more differentiated sample. Brown, anhedral amphibole is found in two samples, where it appears very fresh despite opacitization at the rims. Biotite was found in two samples that also contain notable amounts of nepheline and sodalite. Minor chloritization occurs in some of the samples.

The Guayacán rock suite comprises alkaline basalts and basanites as well as teschenites (alkali gabbro) in dikes and sills. The former are pyroxene and olivine phyric, the latter appear fine-grained granular. An exception is one sample of light grey colour with abundant large, black, euhedral amphibole, obviously a late stage differentiate.
Glomerophyric texture is predominant in all these rocks, although in the intrusive samples increased size of groundmass crystals renders this texture slightly granular. The principal mineral assemblage of the rocks is olivine, calcic plagioclase, pyroxene, ore, and analcime. Olivine, occurring as large phenocrysts, is not present in the more differentiated rocks. Plagioclase is almost exclusively restricted to groundmass crystals. Euhedral pyroxene, most often in agglomerates of several individuals, is the dominating phenocryst, but also groundmass component. By its typical hourglass structure it can easily be identified as (ti-) augite. Opaque minerals are titano-magnetite, however in one case skeletal ilmenite was identified. Analcime is present in all samples as anhedral, isotrop component in the interstitial realm. Further feldspathoids, present in most of the samples are euhedral sodalite and anhedral nepheline. Biotite is always present in variable but minor amounts. Amphibole with

cores of augite was only found in a highly differentiated sample. Other components may be alkali feldspar, and relatively abundant apatite. Alteration is restricted to occasionally occurring slight corrosion of olivine along fractures with some patches of chlorite.

The lamprophyric sample from Neily is fine-grained, pale grey coloured and contains, beside crustal xenoliths, conspicuous megacrysts of biotite.
This impression is confirmed in thin sections as the rock has a porphyritic texture with pyroxene and biotite phenocrysts. Feldspar is present only as groundmass constituent. Further minerals are fine-grained opaque ore minerals, minor amphibole, abundant apatite, interstitial nepheline and euhedral sodalite.

2.5.3 Interpretation:

As it can be deduced from the development of crystal faces, size relations and intergrowths, the Limon backarc samples display a typical alkaline crystallisation sequence: olivine crystallising first is followed by augite and only thereafter crystallises plagioclase. This crystallisation sequence, the phenocryst assemblage, and of course the content of silica-undersaturated, alkali-rich minerals characterises these rocks as alkaline. Petrographically, they are quite distinct from samples of the other groups. The presence of hydrous primary minerals points out to low degrees of melting but also to the presence of some water in the magma source.
The sample from Neily is identified as a lamprophyr by its porphyritic character and the abundant, exclusively melanocratic phenocrysts. Silica undersaturation is a special characteristics of this lamprophyr. Being a typical dike rock, the occurrence of the lamprophyr may be bound to the landward projection of the PFZ, a major fracture zone that is traced to the overriding plate.

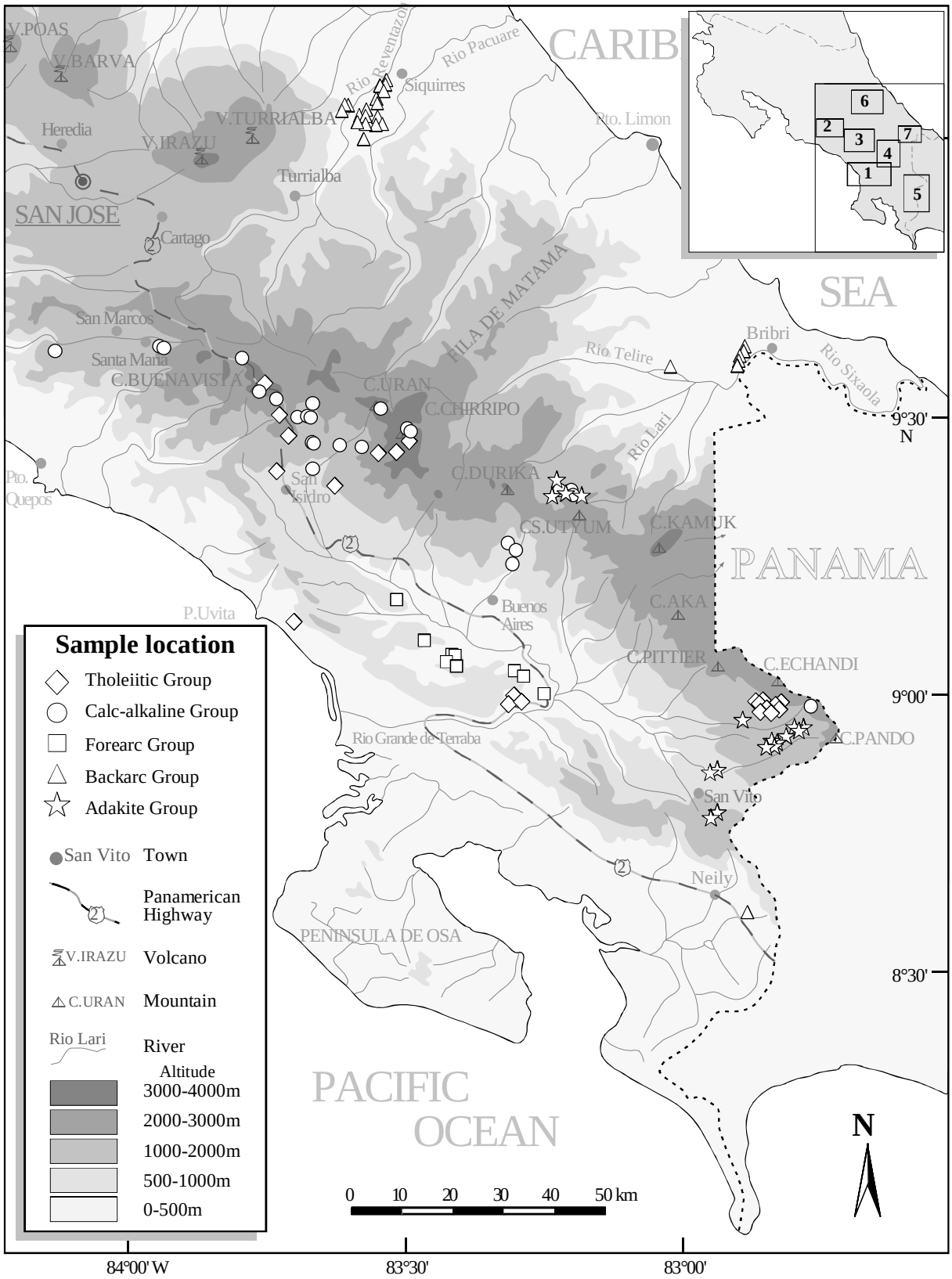

Figure 9: *Topographic map with sample localities in southern Costa Rica. The five sample groups are distinguished by different symbols. Location of the geological detail maps is indicated in the small inset.*

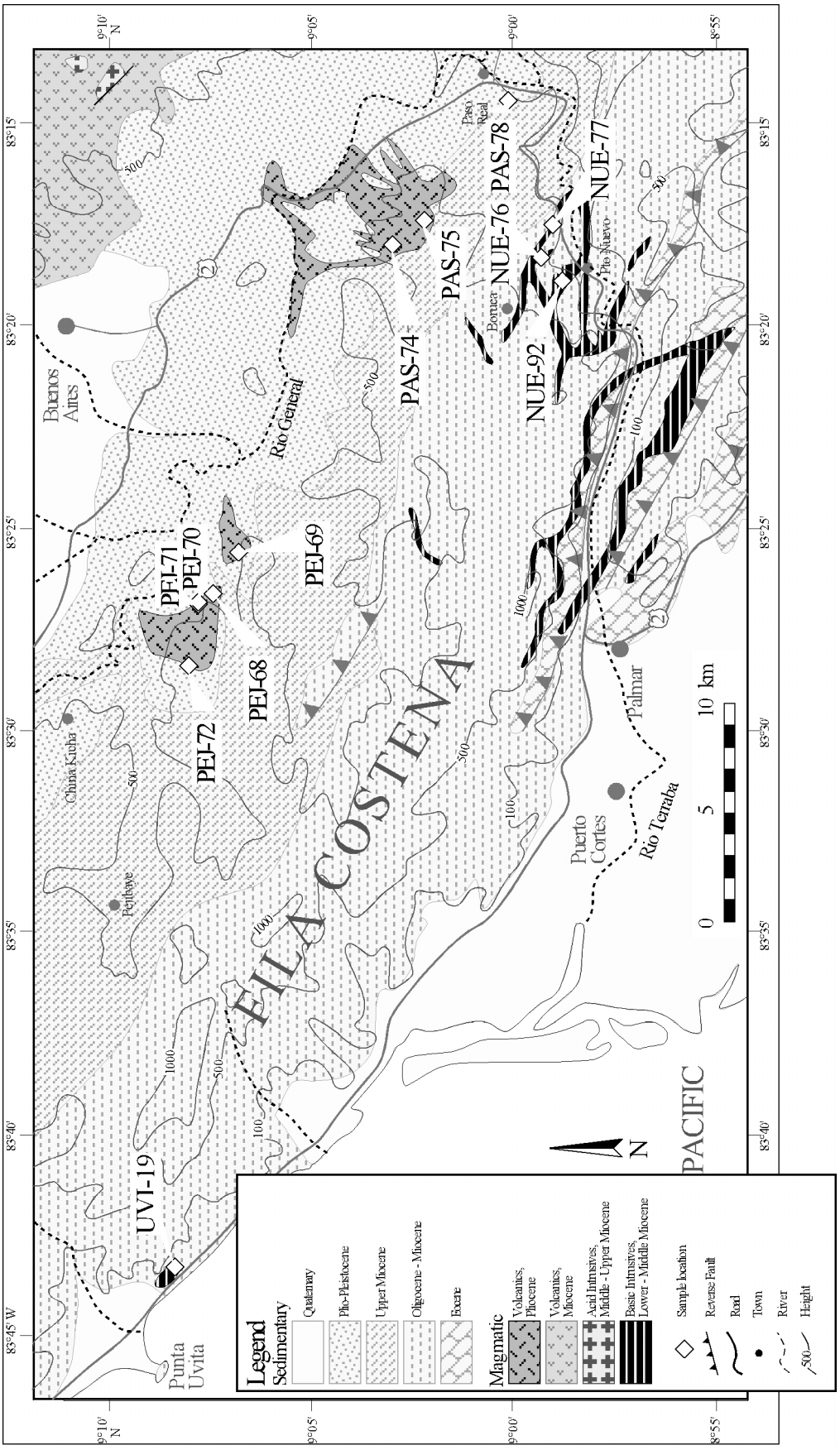

Figure 10.1*: Sample locations indicated in the geological map of the Fila Costeña between Paso Real and Punta Uvita. Map base from Tournon and Alvarado [1997].*

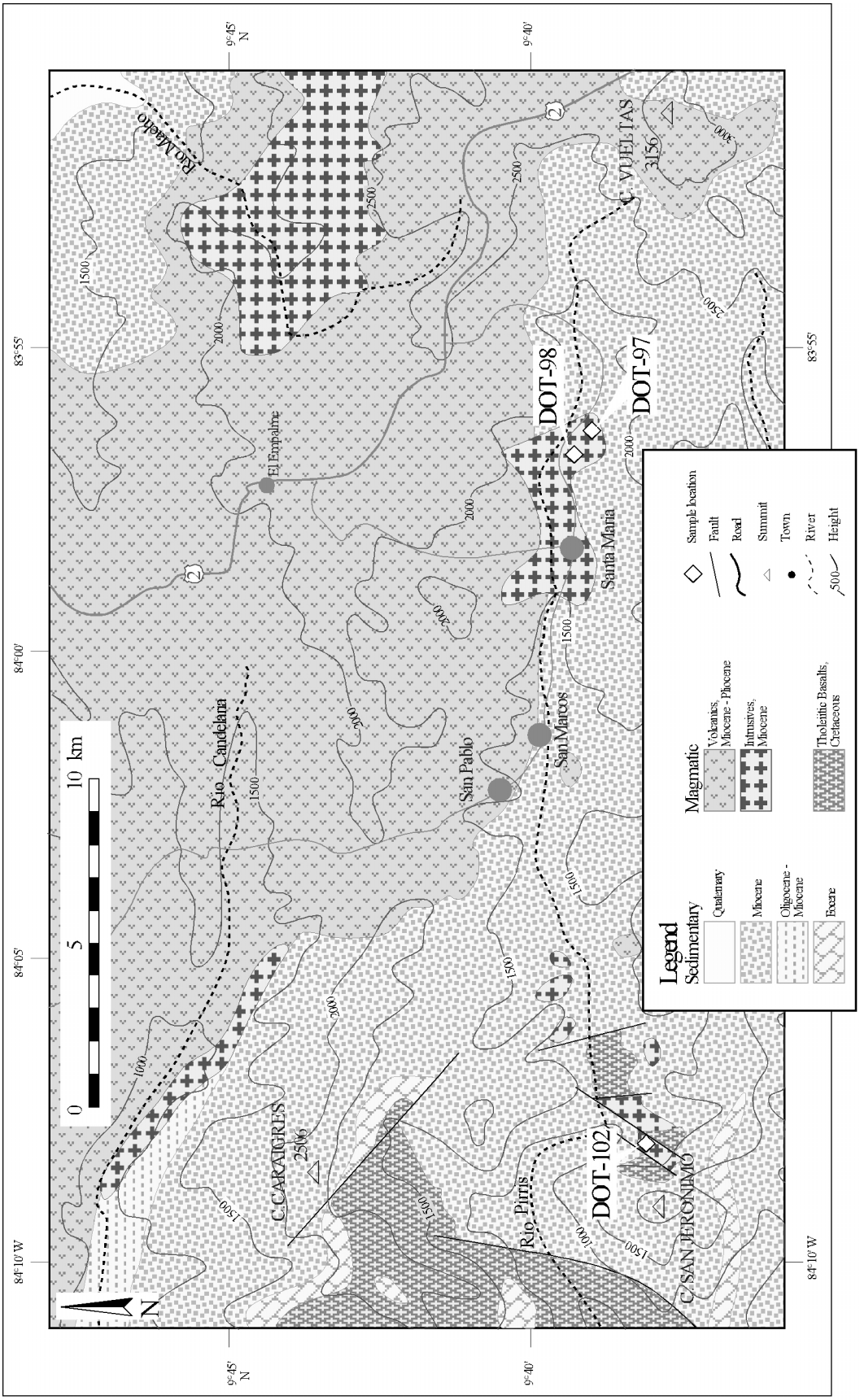

***Figure 10.2**: Sample locations indicated in the geological map of the north-western Cordillera de Talamanca around Santa Maria de Dota. Map base from Tournon and Alvarado [1997].*

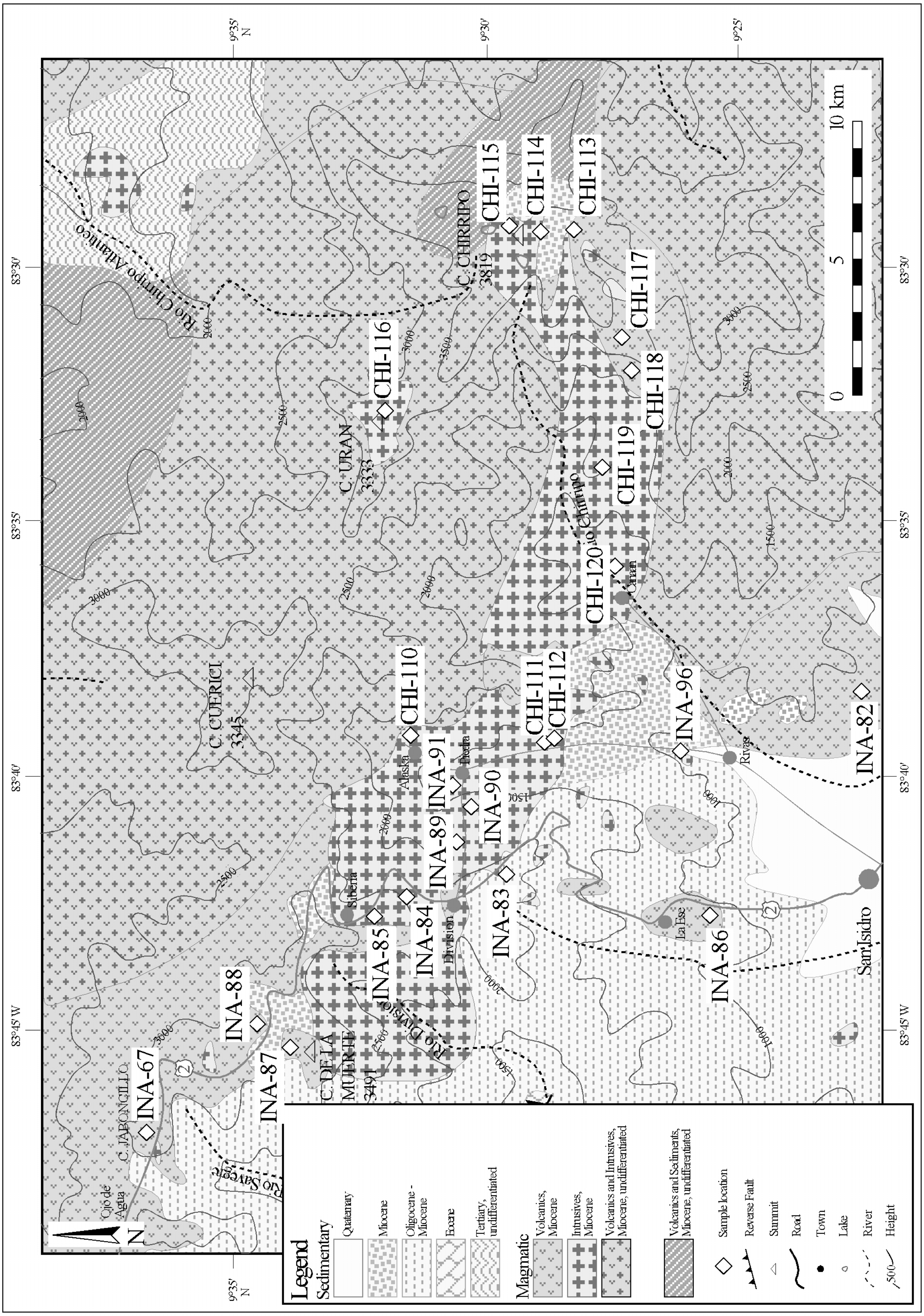

Figure 10.3*: Sample locations indicated in the geological map of the north-western Cordillera de Talamanca around the Pan-American Highway. Map base from Tournon and Alvarado [1997].*

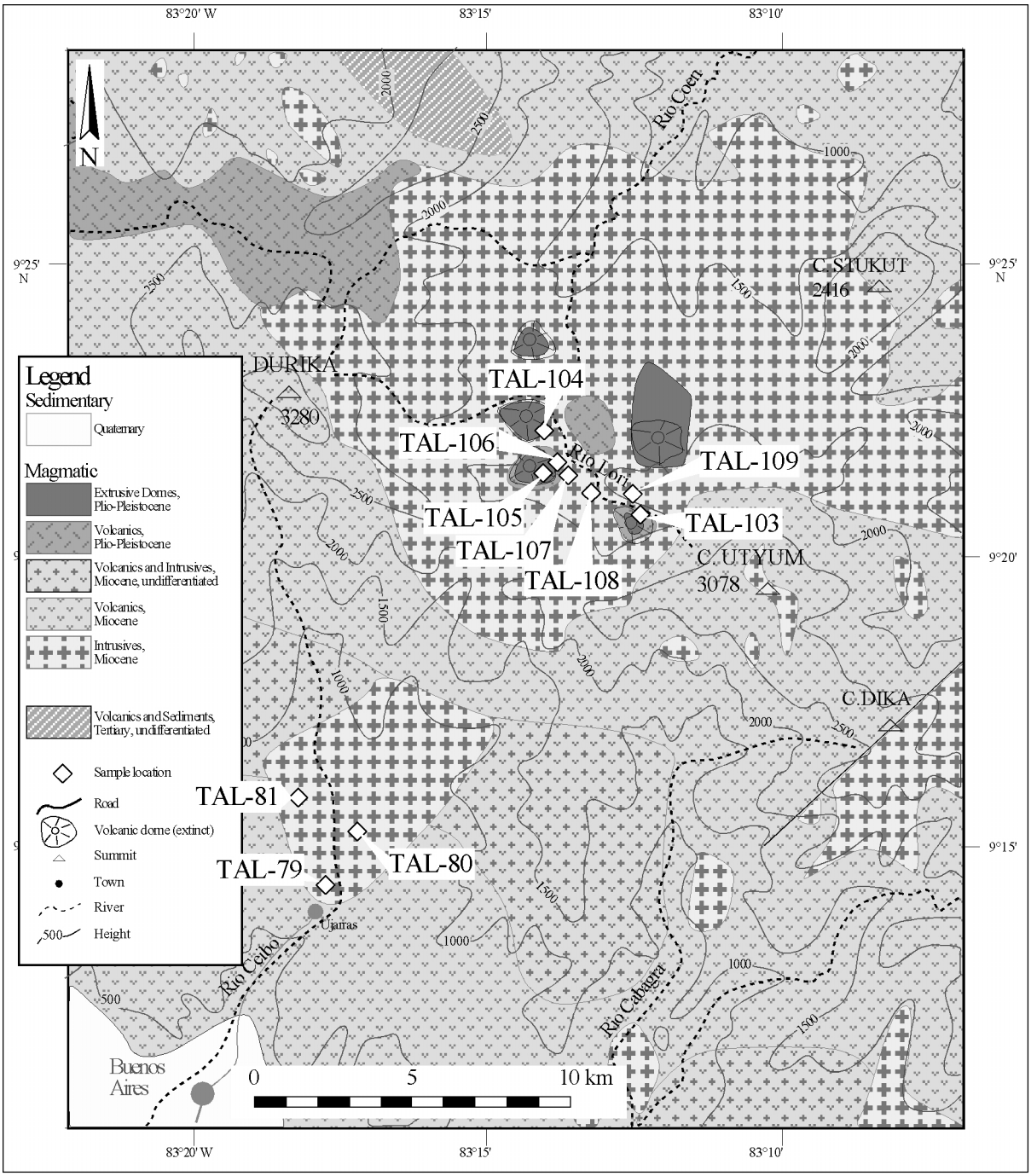

***Figure 10.4**: Sample locations indicated in the geological map of the central Cordillera de Talamanca around Cerro Durika. Map base from Tournon and Alvarado [1997].*

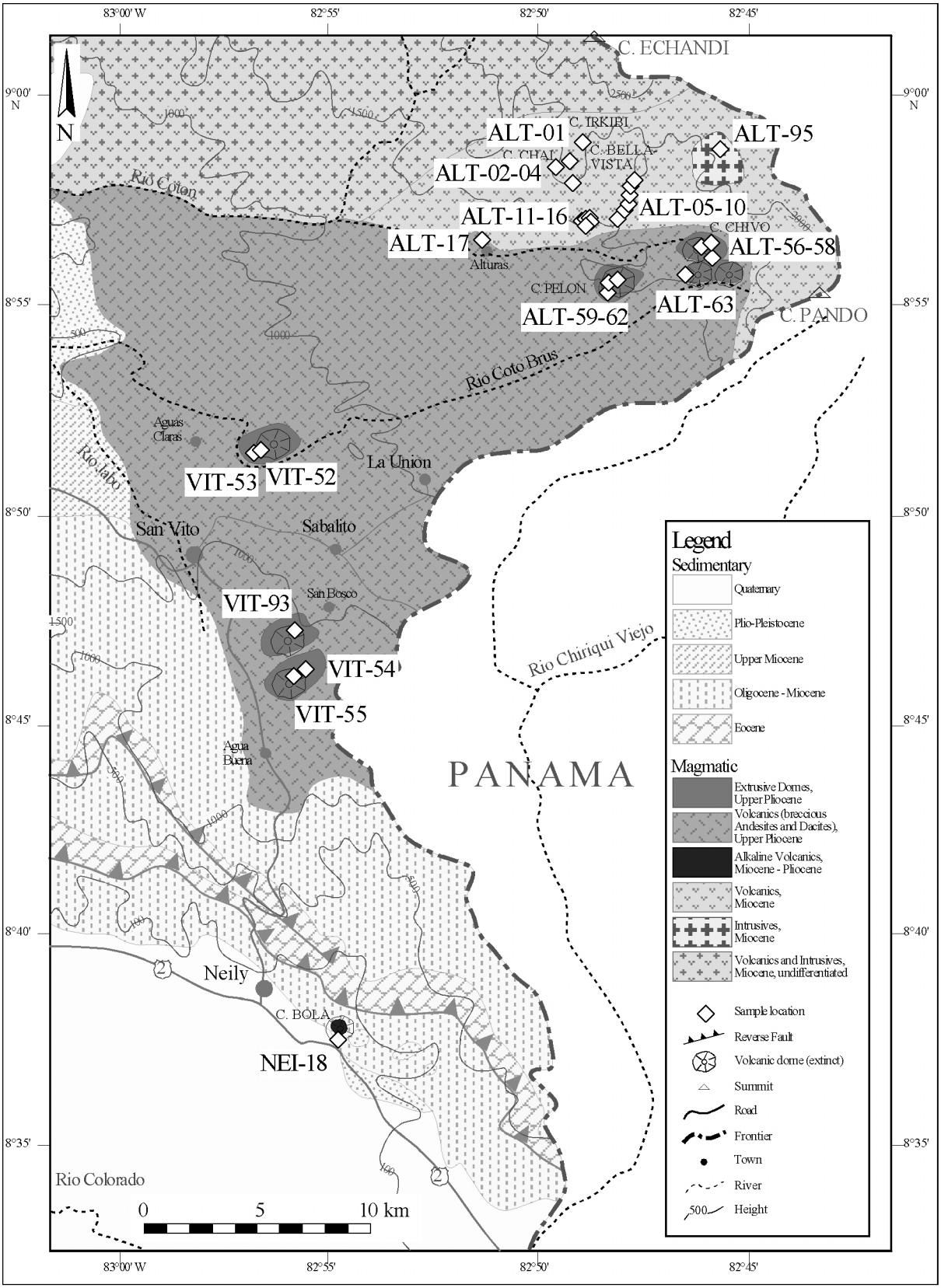

***Figure 10.5**: Sample locations indicated in the geological map of the south-eastern Cordillera de Talamanca and Fila Costeña around San Vito. Map base modified from Tournon and Alvarado [1997].*

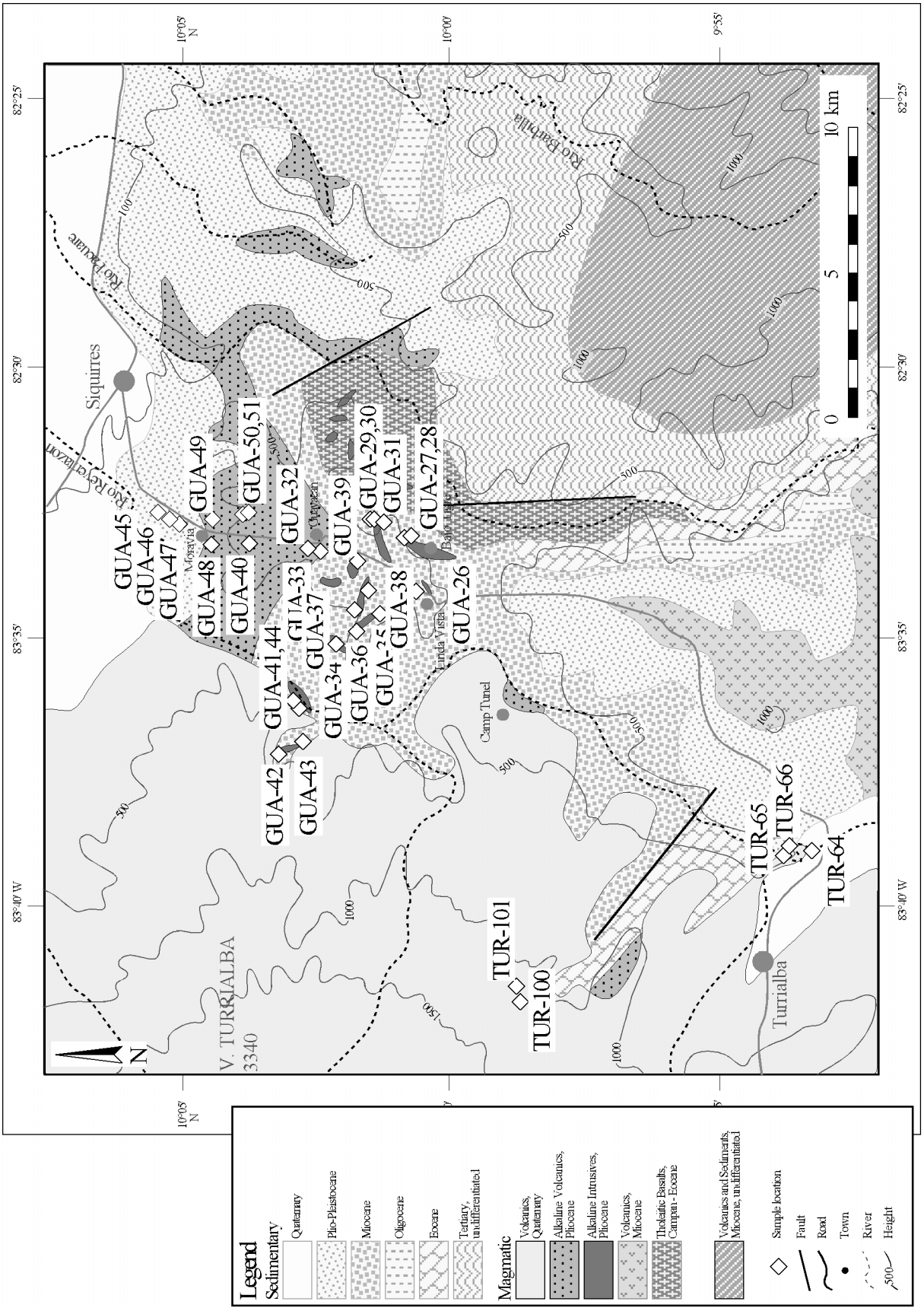

***Figure 10.6**: Sample locations indicated in the geological map of the north-eastern Limon Basin around Guayacan. Map base from Tournon and Alvarado [1997].*

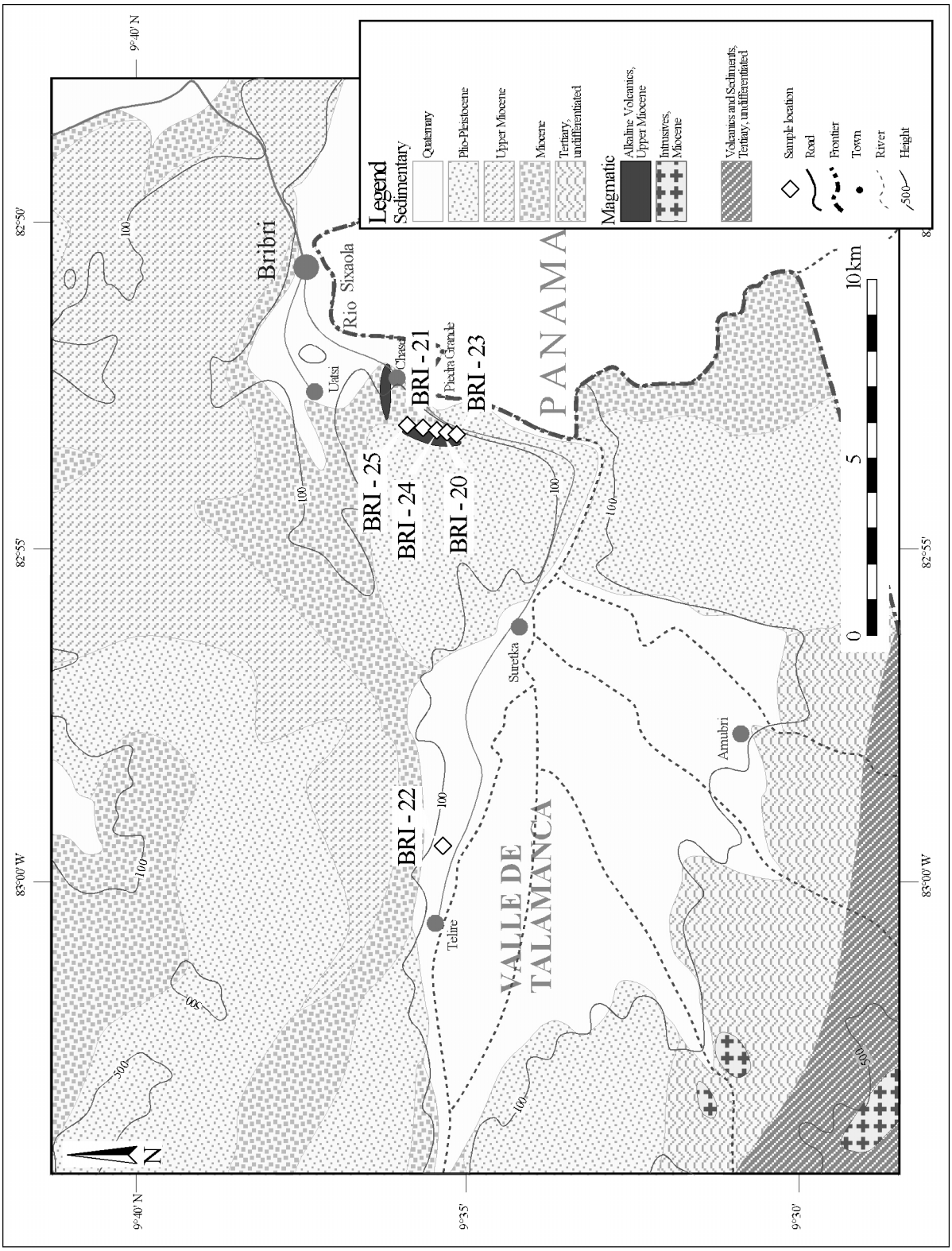

***Figure 10.7**: Sample locations indicated in the geological map of the north-eastern Limon Basin around Bribri. Map base modified from Tournon and Alvarado [1997].*

3 $^{40}Ar/^{39}Ar$ Age Analyses

Radiometric ages of samples from the area of the Cordillera de Talamanca were determined on amphibole separates by the Ar/Ar method.

The Ar/Ar method is a variant of the K-Ar isotopic dating method. Obtained ages reflect the time elapsed since cooling of the rock upon magmatic or metamorphic heating events below a critical temperature which is variable for different minerals. This temperature is referred to as the mineral closure temperature and falling below that temperature results in the prevention of Ar diffusion from the crystal.
In contrast to the K-Ar method, no direct determination of K_2O contents is necessary. Instead, Ar isotope ratios allow recalculation of the initial K_2O content. Thus, the method bears the advantage of reduced sample amounts, which in turn reduces time consuming and expensive separation work. Increased precision and reduced detection limits allow dating of very young samples up to Holocene ages.

Four samples, representative for their rock group, were selected for dating. These samples are an andesite from the Alturas suite of the Tholeiitic Group (ALT 16), a dacite from the Adakite Group (TAL 104), and a trachytic andesite and a teschenite from the Backarc Group (BRI 25, GUA 28). Petrographic examination shows them to be the least altered. Sample GUA 28 was selected in order to check consistency of the Ar/Ar ages with published K-Ar ages for this rock suite [Bellon & Tournon, 1978; Cassel, 1986]. The analysed samples, characteristics of the mineral separates, and the applied analytical technique are listed in Table 3-1.

Amphibole separates were dated rather than whole rocks, since mineral separates allow better control over alteration and metamorphic overprint. Low temperature alteration in the tropical environment leaches the soluble alkalis out of the rock's minerals and matrix to variable degrees [e.g., Nesbitt et al., 1980]. Furthermore, some of the rocks are highly susceptible to alteration due to their glassy and vesicular fabric. Age determination on whole rocks that have suffered K-loss due to alteration will result in erroneously high ages.
Though their K-content is not very high (see Table 3-1), hornblendes are very suitable minerals for the Ar/Ar dating method because of their excellent Ar retention properties [e.g., McDougall & Harrison, 1988]. Hornblende separates were obtained using standard separation techniques. Robust and euhedral grains of hornblende, free of visible secondary alteration effects, were selected for analysis.

Table 3-1: *STEP: Step-heating experiment with the resistance furnace; CTF: Conventional Total Fusion with the resistance furnace; LASER: Laser induced total fusion; LA-STEP: step-heating experiment with a laser. In brackets: method of minor importance for the respective sample.*

Sample	Group	Mineral Separate	Grain Size	Weight	K_2O (%)	Technique
ALT 16	Tholeiitic	Hornblende	125 - 315 µm	230 mg	0,25	STEP, (LASER)
BRI 25	Backarc	Hornblende	200 - 315 µm	210 mg	1,15	LASER, (CTF)
GUA 28	Backarc	Hornblende	200 - 315 µm	220 mg	1,06	STEP, (LASER)
TAL 104	Adakite	Hornblende	200 - 500 µm	820 mg	0,53	LASER, LA-STEP, (CTF)

Two different techniques of the Ar/Ar method were applied for dating:
1. the resistance furnace step-heating technique; and
2. the single crystal laser fusion technique

The step-heating technique is based on incremental heating of the sample material in a resistance furnace until total loss of gas. The released gas proportions are subsequently measured in a mass spectrometer.
The number of heating steps and their respective temperature has to be defined prior to measurement and is restricted by:
- sensitivity of the mass spectrometer
- sample weight
- radiogen Ar content

The radiogen Ar content depends on the K content, age, and possibly Ar retentivity of the sample.

Results of the analysis are plotted in total Ar release diagrams that reflect the spatial distribution of Ar in the crystal lattice. Depending on its site within the crystal, Ar shows different diffusion properties during heating. Ar that is loosely bound in the mineral rim is released during the early, low temperature steps, whereas more tightly bound Ar is released in late steps. Thus, the step-heating technique provides a powerful tool to detect disturbances of the K-Ar system. Disturbances may either be caused by Ar-loss or introduction of an extraneous Ar component. Thermally induced Ar-loss could occur upon re-heating of the sample under metamorphic conditions and will result in younger ages for the dated rocks as compared with their geological age due to loss of the daughter nuclide from the K-Ar system. Release patterns of samples that underwent such a processes are typically curved with young apparent ages for the first, low temperature, steps. The higher temperature steps ideally have similar ages within 2σ variation, defining a so-called plateau-age. This plateau-age corresponds to the geological age of the sample.
Other possibilities of Ar loss are loss of ^{39}Ar during neutron irradiation of the sample. This effect, called recoil, is common for K-rich minerals of high surface/volume ratio and low Ar retentivity [e.g., McDougall & Harrison, 1988]. The consequential increase of the $^{40}Ar/^{39}Ar$ ratio in these minerals results in erroneously old ages. Neighbouring K-poor minerals, like pyroxenes, may be susceptible to incorporation of recoil ^{39}Ar [e.g., Faure, 1986], lowering their $^{40}Ar/^{39}Ar$ ratio and hence their apparent ages.

Extraneous Ar can be differentiated into:
- inherited Ar
- excess Ar

Inherited Ar is radiogenic ^{40}Ar ($^{40}Ar^*$), introduced into the sample's K-Ar system by physical contamination with older material, i.e. xenocrysts. Such impurities should be a minor problem in carefully examined mineral separates but they might nevertheless be present as minute inclusions or adhering phases. Increase of total $^{40}Ar^*$ results in shifting of the apparent ages to older values.

Excess ^{40}Ar is defined as "^{40}Ar incorporated in rocks and minerals by processes other than the in situ decay of ^{40}K" [Lanphere & Dalrymple, 1976]. The occurrence of excess ^{40}Ar results in anomalously old ages.
A process that might explain the incorporation of excess ^{40}Ar into metamorphic rocks and minerals is related to degassing of older rocks and migration of Ar via circulating fluids [c.f. Wartho et al., 1996], resulting in high ^{40}Ar partial pressures in fluid phases during igneous

and metamorphic processes [e.g., Lanphere & Dalrymple, 1971]. Those fluids may then be trapped in fluid inclusions of the metamorphosed rocks and minerals [v. Blanckenburg & Villa, 1988].
U-shaped release spectra are indicative of excess ^{40}Ar [Lanphere & Dalrymple, 1971, 1976]. Low and high temperature steps yield very little gas and are therefore very susceptible to disturbance of the Ar system. The excess ^{40}Ar component is thus most obvious in these steps.
Uptake of excess argon may occur in any mineral. However, it was recognised as a severe problem in pyroxenes, due to their low potassium content [Hart & Dodd, 1962].

The laser fusion technique uses an IR-laser to heat samples with the option of high local resolution. Very small samples like single crystals can be measured by total fusion, or by step-heating if the radiogenic Ar content is high enough. Dating of individual mineral grains allows a good control on the involvement of extraneous components. Statistically well defined ages can be obtained by analysing multiple minerals of the same sample.

Results of multiple grain analyses with the laser fusion technique can be displayed in a so-called inverse isochron correlation diagram [Turner, 1971; Roddick et al., 1980], where the $^{36}Ar/^{40}Ar$ ratio is plotted versus $^{39}Ar/^{40}Ar$ or $^{40}K/^{40}Ar$. The latter is not commonly used, but allows direct age determination without knowledge of the respective J-values. The age is given by the intercept on the $^{40}K/^{40}Ar$ axis of a regression line through the data points. The upper intercept of the regression line gives the initial $^{40}Ar/^{36}Ar$ ratio of the sample, which corresponds to the isotopic composition of the trapped, non-radiogenic component in the sample.
Thus, the isochron analysis allows direct control on the composition of the non-radiogenic component, as opposed to other methods of age calculation that have to rely on the assumption that the trapped argon is of atmospheric composition ($^{40}Ar/^{36}Ar$=295.5). The non-radiogenic component has to be subtracted from the total argon when calculating the age. Since the ratio of radiogenic to non-radiogenic argon is lower in younger samples than in older, error propagation from inaccurately determined non-radiogenic argon results in poorly defined ages especially for the younger samples. Trapped Ar, with a $^{40}Ar/^{36}Ar$ ratio significantly higher than the atmospheric value of 295.5 signals excess Ar incorporation.

Goodness of fit of the data points to their regression, i.e. the isochron, can be measured by the mean square weighted deviate (MSWD). The MSWD is the sum of the squares of the weighted deviations from the best fit isochron, divided by the degrees of freedom, n-2, where n is the number of data points [McIntyre, 1966]. The expected value is 1 where the data fit the straight line to within experimental error. A MSWD > 2.5 would indicate that the simple isochron model is not appropriate for a particular data set [McDougall & Harrison, 1988].

Sometimes, data points of a single sample lie in a wedge shaped area rather than on a single isochron in the argon isotope correlation diagram. Chen et al. [1996] proposed the name sphenochron for this “wedge of time”. The upper boundary of this sphenochron, characterising the youngest material found in the sample, is thought to indicate the time of eruption. Crystals which plot significantly below this upper isochron of eruption must either be older than the eruption (containing inherited argon in respect to whole rock’s K-Ar system), or must appear older as a result of selective excess ^{40}Ar incorporation during their formation. These crystals are most likely xenocrysts if the sphenochron shows dispersion in ages with no evidence for a non-atmospheric initial ratio. Excess ^{40}Ar in these crystals would instead be indicated by a $^{40}Ar/^{36}Ar$ ratio of the trapped argon significantly higher than 295.5. This would not match the definition of a sphenochron as a “wedge of time”. Confining

isochrons of the sphenochron are constrained to pass through the $^{36}Ar/^{40}Ar$ ratio of modern atmosphere (1/295.5).

3.1 Chemical composition of the amphiboles

Electron microprobe analyses were carried out to determine the K-content of the amphiboles of the four samples that were selected for dating. The K-content of the amphiboles defines the amount of sample material necessary for the dating procedure and gives restrictions to the applicable dating methods (see above). Average K_2O contents of the amphiboles are presented in Table 3-1, the detailed analytical results are listed in Table xx in the Appendix.
Formula calculation of the hornblendes and adjusting of the ferrous/ ferric ratio was done according the procedure outlined in Schumacher [1997]. Guidelines for the adequate nomenclature of the amphiboles are provided by Leake et al. [1997].

Hornblende grains from the four samples show an extremely wide range in chemical composition from pargasite to magnesiohastingsite, and to kaersutite (Fig. 11).
For all compositions involved, $(Ca + Na)_B$ is above 1.00, Na is between 0.50 and 1.50, Ca_B is above 1.50, and $(Na + K)_A$ is above 0.50, defining them as a group of calcic amphiboles. One of the samples is characterised by Ti above 0.50 (all numbers refer to the standard amphibole formula, which was taken to contain 8 tetrahedral sites and was calculated to 23 oxygens).
Compositions of the hornblendes from three of the samples are internally comparatively uniform and plot into the fields of either pargasite, magnesiohastingsite, or kaersutite.
Hornblendes of sample TAL 104 are however outstanding due to their large compositional variability ranging from pargasite to magnesiohastingsite.

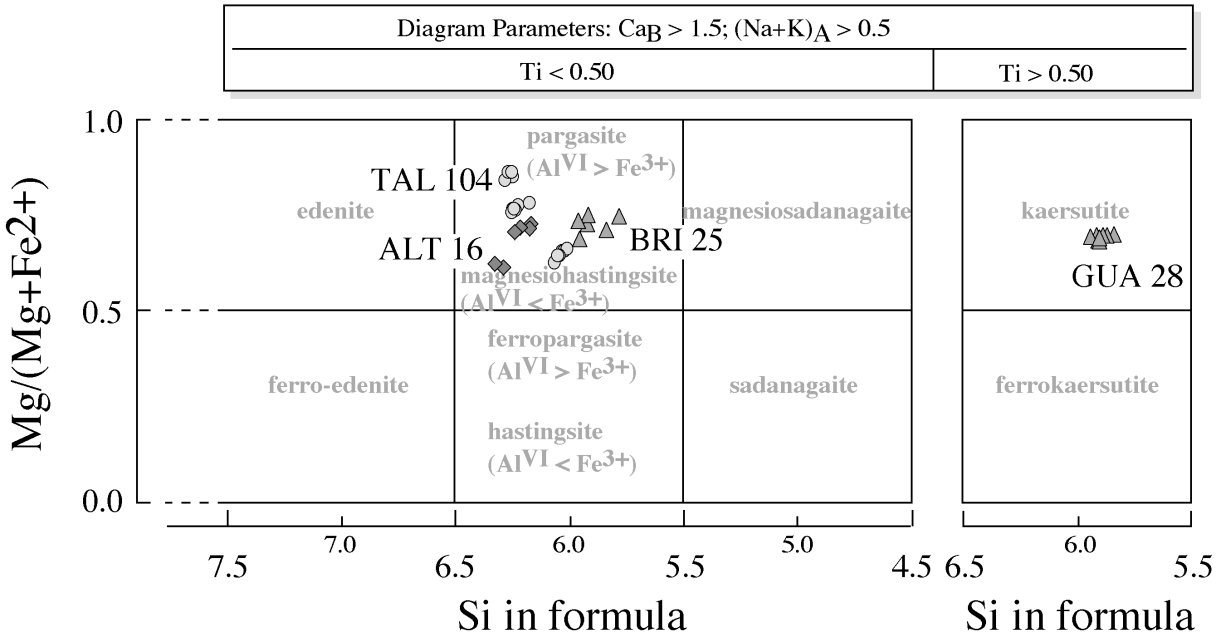

Figure 11: *Classification of amphiboles according to the recommendations of the International Mineralogical Association (IMA), published by Leake et al. [1997].*

The chemical variability of the amphiboles is displayed in diagrams of major element compositions (Fig. 12). These correlation diagrams allow a clear discrimination between two hornblende varieties in sample TAL 104. One of the hornblende varieties is enriched in Al and Fe relative to the second phase, which in turn has higher Si, Mg, and K concentrations. All samples exhibit distinct K2O variation over a relatively small CaO range, resulting in a considerable spread in the CaO/K2O ratio (Fig. 12). Note that the Al-Fe-rich hornblende is characterised by higher CaO/K2O ratios (~34-40) than the Si-Mg-K-rich hornblende (~17-20).

Electron microprobe analyses of hornblendes from sample TAL 104 thus point out their chemical heterogeneity with a mixture of two hornblende varieties. Pyroxene breakdown into Al-Fe-rich hornblende occurring within the oceanic crust during prograde metamorphism may have resulted in the generation of one of the end-members. The other end-member, Mg-Si-K-rich, could result from subsequent reactions of the silicic, adakitic melt with the mafic mantle wedge during ascent or from reactions with a second melt phase.

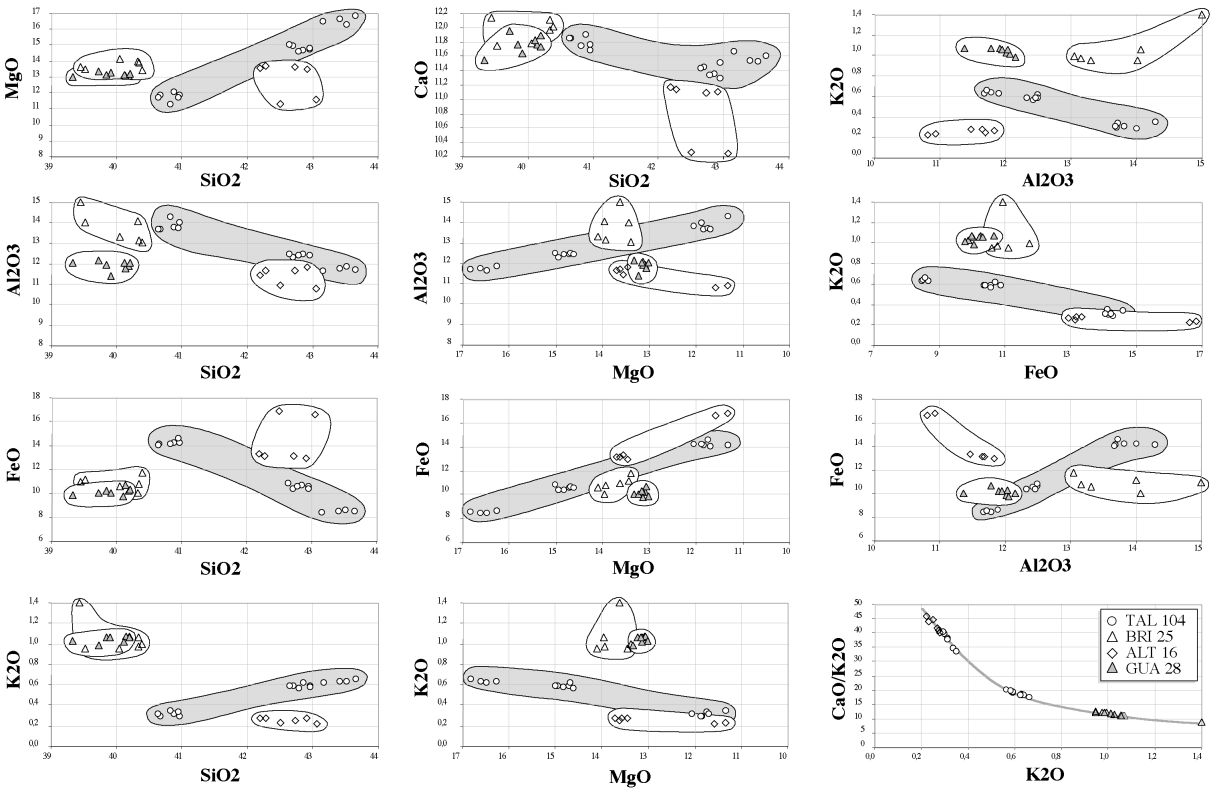

Figure 12: *Selection of diagrams illustrating the hornblende geochemical data acquired by microprobe analyses. The compositional variability displayed by hornblendes of sample TAL 104 (circles in grey field) are remarkably large.*

3.2 Step heating experiments

Two samples were measured with the step-heating technique: the tholeiitic andesite ALT 16 and the teschenite GUA 28. Results are plotted in a diagram of apparent age and Ca/K ratio against the fractional release of ^{39}Ar (Figs. 13, 14). The other two samples were fused in a single step (total fusion) within the resistance furnace apparatus, since they were expected to contain less argon.

3.2.1 ALT 16

Sample ALT 16 was measured in four steps, at 600°C, 1000°C, 1200°C, and 1550°C (Fig. 13). The third step, which yielded the largest amount of gas (90%), gave an age of 16.87 ±0.26 Ma. This is lower than the age obtained by integration of all fractions (the "total-gas" age of the sample: 18.33 ±0.39 Ma). The main release step is embraced by two steps of higher apparent ages. Thus, sample ALT 16 displays a saddle- or U-shaped release spectrum.
The 600°C step yields an age value with an extremely large error (2σ), due to the low amount of gas released (0.6% of total ^{39}Ar).

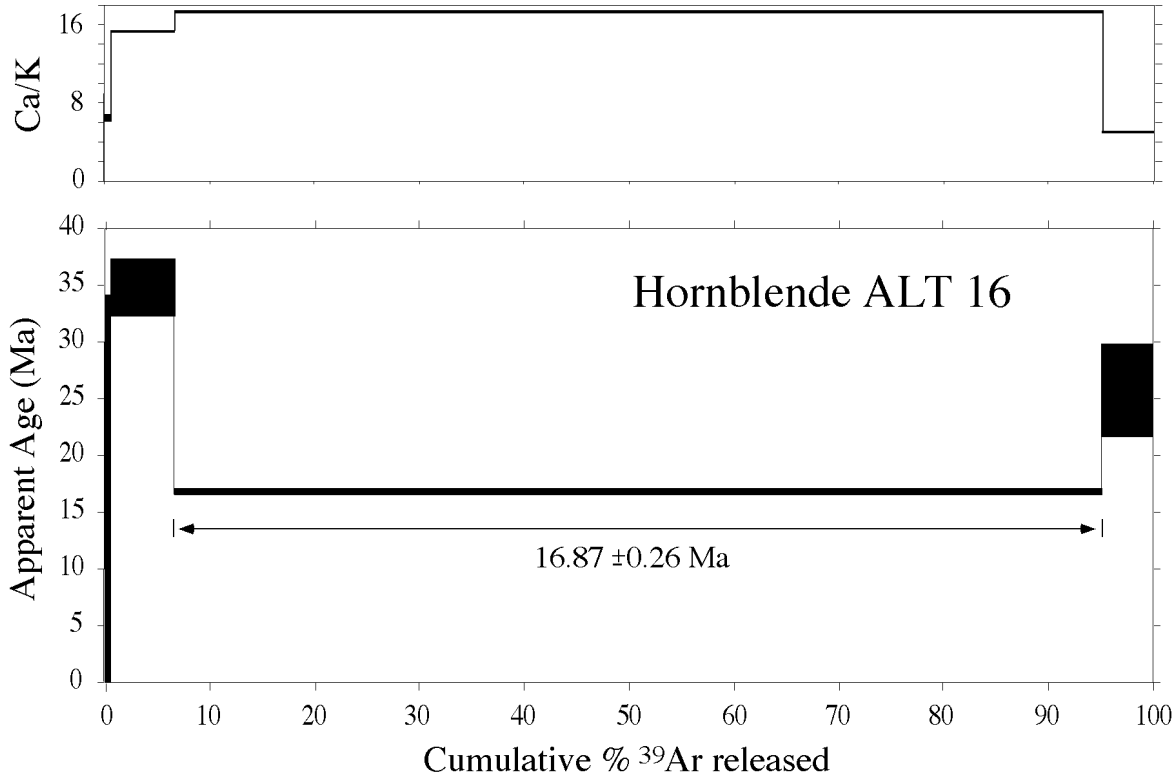

Figure 13: *Step heating experiment on sample ALT 16. The diagram shows the apparent age for each heating step versus the amount of ^{39}Ar released. A comparison with the Ca/K ratio received during the steps allows check for chemical disturbances.*

Small impurities may still be adhering to the hornblende grains, e.g. small matrix crystals or more or less altered glass. This material with low Ar-retentivity properties will release its Ar during the lowest temperature steps, as reflected by the Ca/K ratio. The groundmass is generally more K-rich than the hornblendes. Thus, in the earliest heating steps the Ca/K ratio is clearly lower than in the higher temperature steps. Even though the 600°C step gave an

essentially meaningless age, it got rid of “impure” Ar, thereby increasing the precision of the following steps as compared to the total fusion data.
The U-shaped release spectrum of sample ALT 16 indicates that excess ^{40}Ar was incorporated in this rock (see above). Therefore, the main release fraction, is closest to the eruption age of the tholeiitic sample, but defines a maximum age. This step that released almost 90% of the total Ar, may still contain an excess ^{40}Ar component.
Rocks of the tholeiitic group show petrographic evidence of a metamorphic overprint, most likely from nearby plutonic intrusions. Emplacement of these plutons in the Cordillera de Talamanca may have driven metamorphic fluids that carried excess argon.
Ar loss due to thermal affection of the rock could not be detected. A typical release spectrum from a sample that suffered Ar loss is differing from the observed one (see above).
The Ar degassing spectrum clearly shows that the K-Ar system of sample ALT 16 was (thermally) disturbed. K-Ar dating or total fusion dating could not have detected this disturbance, and would have given erroneous ages.

3.2.2 GUA 28

Sample GUA 28 was measured in three steps, at 600°, 1200°, and 1550°C (Fig. 14). The first step of the release spectrum is again virtually undetermined due to the low amount of gas released (1%). After degassing of matrix impurities by the first step, the following main step, characterised by a high Ca/K ratio, yields a reliable age. That temperature increment released about 95% of the total Ar and defines an age at 4.39 ±0.14 Ma. The apparent age in the last step is much higher. The simultaneously increased Ca/K ratio indicates that this increase results from a Ca rich component.

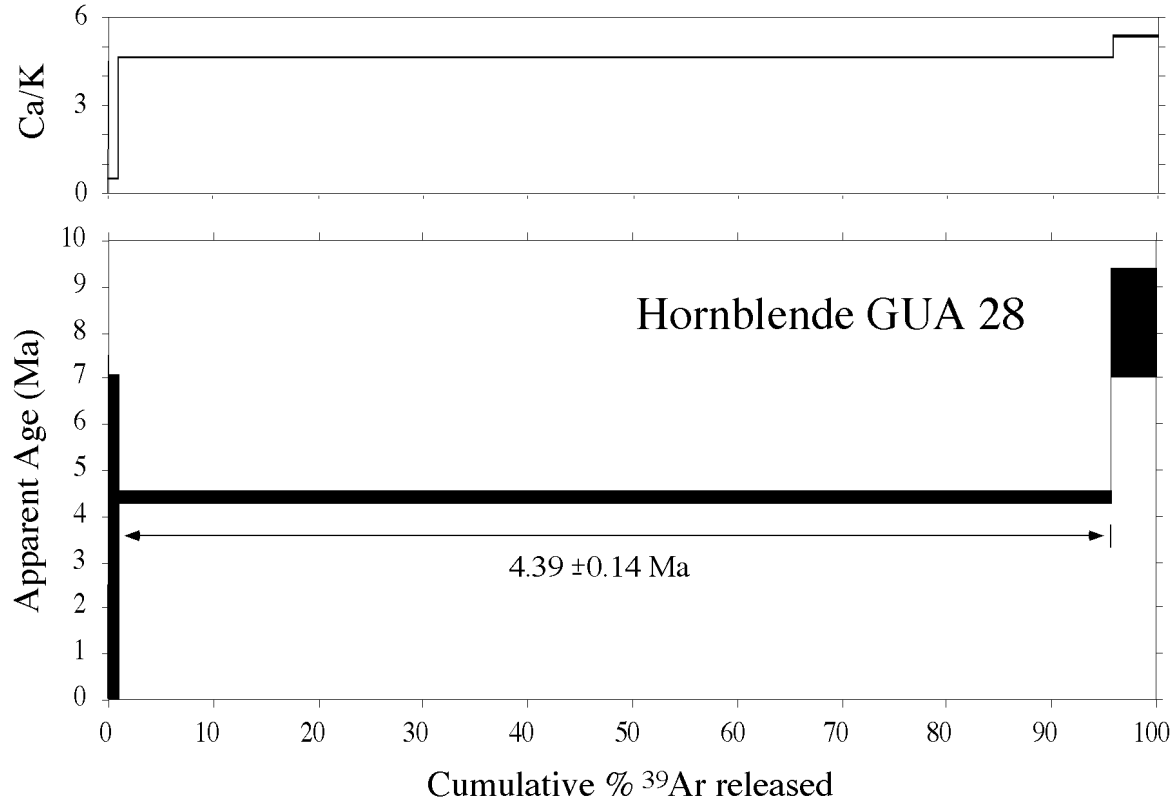

Figure 14: *Step heating experiment on sample GUA 28. The diagram shows the apparent age versus the amount of ^{39}Ar released and additionally the related Ca/K ratio received during the stepwise heating procedure.*

The Ar degassing spectrum of sample GUA 28 characterises a physically disturbed sample containing an extraneous component that displays higher apparent ages than the hornblende crystals. The most likely extraneous component in this case is pyroxene. Petrographic examination of the samples showed that the amphiboles frequently contain pyroxene cores (Chapter 2). A valid explanation for the release pattern is that these pyroxene cores contributed inherited Ar to the system. However, petrographic examination gives no hint that they might be xenocrysts. Another and very likely explanation for the higher $^{40}Ar/^{39}Ar$ ratio in these pyroxenes is the incorporation of excess ^{40}Ar. Due to their very low potassium content, pyroxenes are very sensitive to incorporation of excess argon. This is a common problem in pyroxenes.
Samples from this rock suite of Guayacan were dated earlier by Bellon & Tournon [1978] and Cassel [1986] with the K-Ar whole rock method. Ages provided by theses authors are identical to the total-gas age of sample GUA 28. The extraneous argon component in the rocks of the Guayacan suite was not detected by the K-Ar whole rock analyses, but appears to be insignificant in respect of the accuracy of the earlier age determinations.

3.3 Laser fusion experiments

The data acquired by laser fusion experiments on all dated samples are presented in Figure 15. Calculated ages are plotted versus R/R+A. Also shown are derived mean ages, weighted mean ages, and age of the main release fraction of the step-heating technique and total fusion age, respectively.

3.3.1 ALT 16; GUA 28

Few data points are available for the samples ALT 16 and GUA 28 (Figs 15 A, B). Since amphiboles of these samples were too small to yield measurable amounts of gas, three crystals were fused at once. Calculating a mean age from these few data results in a poorly defined value with large 2σ variations. The heterogeneous age distribution of sample ALT 16 hints again at disturbance of the K-Ar system of the hornblende, but could not decipher its nature.
Laser dates from sample GUA 28 give a lower mean age than the step-heating experiment. This may be because pyroxene inclusions were more carefully excluded from the laser separates. However, the crystals tend to give lower apparent ages with lower R/R+A. This could be explained by weathering of amphiboles or included glass phases.

3.3.2 BRI 25

Though individual data points show significant errors for sample BRI 25, the high number of multiple grain analyses defines a well constrained age with narrow 2σ confidence intervals (Fig. 15 C). Uncertainties in the individual measurements are a consequence of high proportions of atmospheric argon. These can be contributed to the distinctive opacitisation of the amphibole's rims. Ages derived from the laser fusion technique are considerably lower than those from total fusion in the resistance furnace. These higher ages may indicate contamination of the sample.
Hornblende sample BRI 25 defines a well constrained, meaningful age in the inverse isochron diagram (Fig. 16), with a MSWD value near 1. The isochron age of this sample is 5.88 +23/-22 Ma and the initial $^{40}Ar/^{36}Ar$ ratio is almost atmospheric in composition.
Both independent methods of weighted mean calculation from pooled age data of multiple measurements and the inverse isochron correlation diagram reveal a well defined age for sample BRI 25. The data set gives no hints to disturbance of the K-Ar system in this sample.

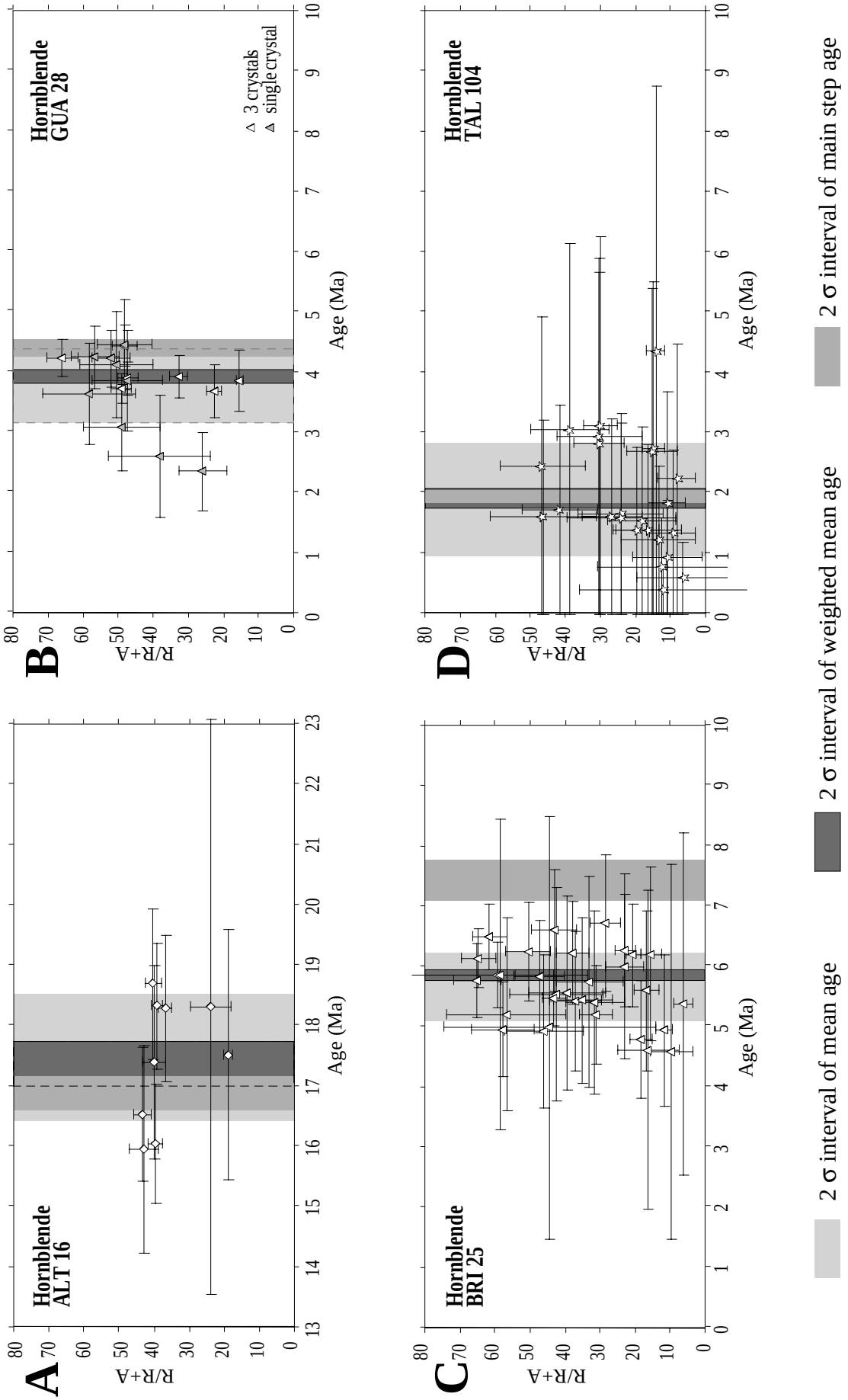

Figure 15: *^{40}Ar /^{39}Ar laser fusion experiments: Calculated single crystal ages versus R/R+A.*

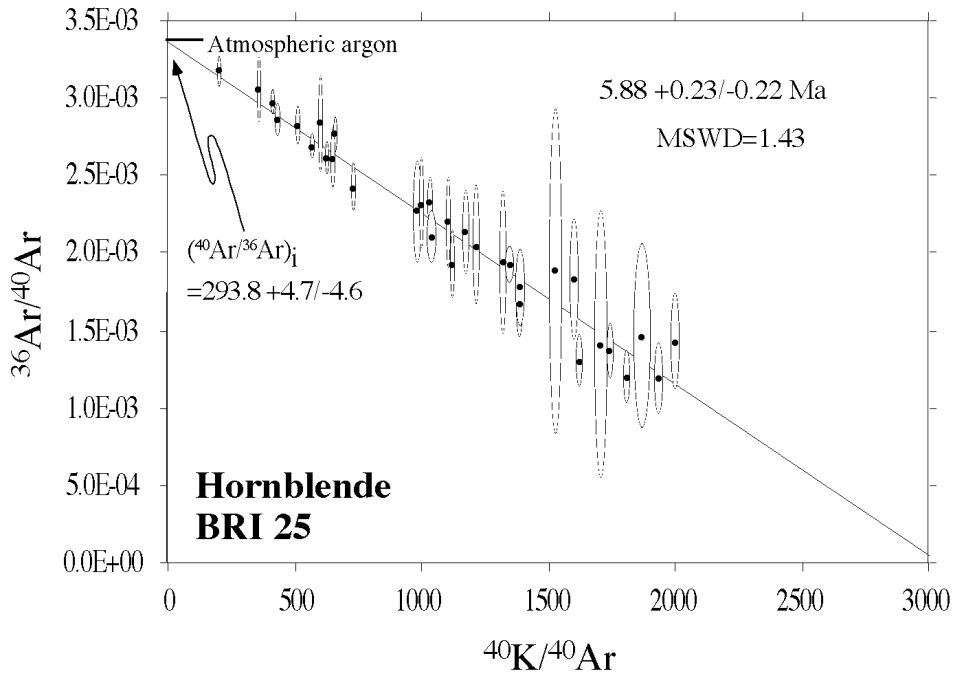

Figure 16: *Inverse isochron diagram ($^{36}Ar/^{40}Ar$ vs. $^{40}K/^{40}Ar$) for single grain laser fusion experiments on hornblende of sample BRI 25. Fit of the data to the isochron is very well as confirmed by the MSWD. Intersection on the abscissa gives the age, intersection on the ordinate the trapped argon composition of the rock.*

3.3.3 TAL 104

Hornblende crystals of sample TAL 104 display extremely variable ages with large errors (Fig. 15 D). This is more a result from sample heterogeneity than from low Ar yield (due to young ages and low potassium contents): These amphiboles were large and therefore contained appreciable amounts of Ar. Though, however, the proportion of trapped non-radiogenic argon was also large, as reflected in the R/R+A ratio.

In the argon isotope correlation diagram (Fig. 17), multiple crystal analyses of sample TAL 104 define a wedge shaped area, i.e. a sphenochron. The upper boundary of that sphenochron defines the eruption age of the volcanic rock at 1.34 ±x Ma. The lower boundary, passing through the oldest data found in that sample, gives an age of 3.49 ±x Ma.
There is no indication for excess ^{40}Ar incorporation in the sample. The sphenochron includes all data when passing through the atmospheric $^{40}Ar/^{36}Ar$ ratio (per definition).
Independent substantiation is coming from a laser step-heating experiment carried out on a large hornblende crystal. The derived isochron is almost identical to the lower boundary of the sphenochron, and the initial $^{40}Ar/^{36}Ar$ ratio of this sample is indistinguishable from atmospheric argon.
A meaningless isochron age derived from a regression through the entire heterogeneous data set gives a "mixing age" of 1.08 ±x Ma. That isochron would suggest the presence of extraneous argon in the sample.

Heterogeneity in the age of sample TAL 104 is also obvious in histograms of the calculated single grain laser fusion ages (Fig. 18). The presented histogram shows a peak (of high age probability) that can be to assigned to a juvenile component or the eruptive age besides other peaks derived from older components.

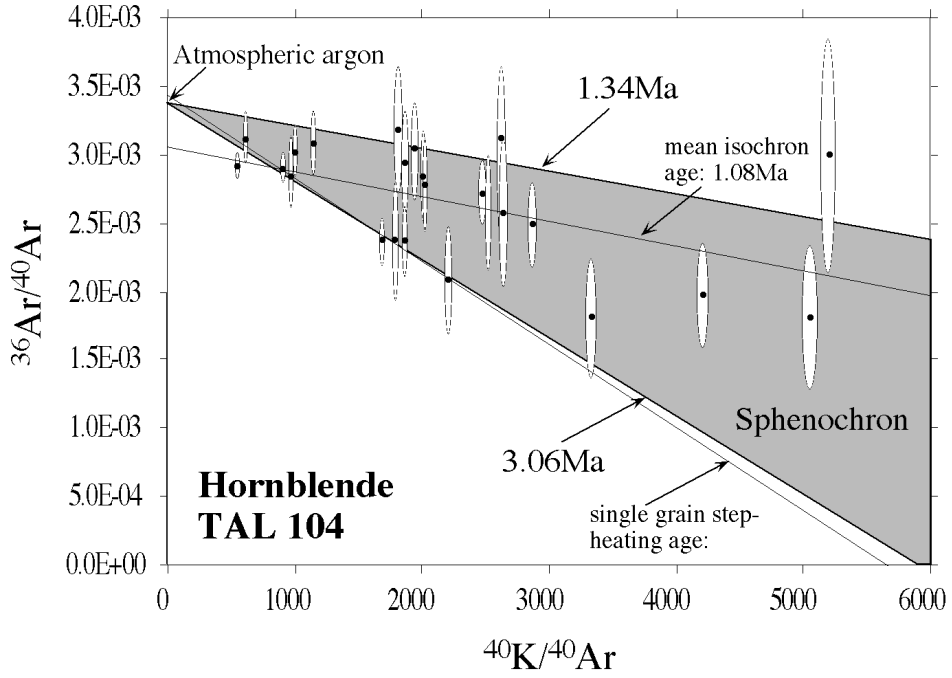

Figure 17: *Sphenochron diagram derived from single grain laser fusion experiments on hornblende of sample TAL 104. That sample gives heterogen age values, definitely not lying on a single isochron, and possibly documenting the preservation of two distinct age information within the sample.*

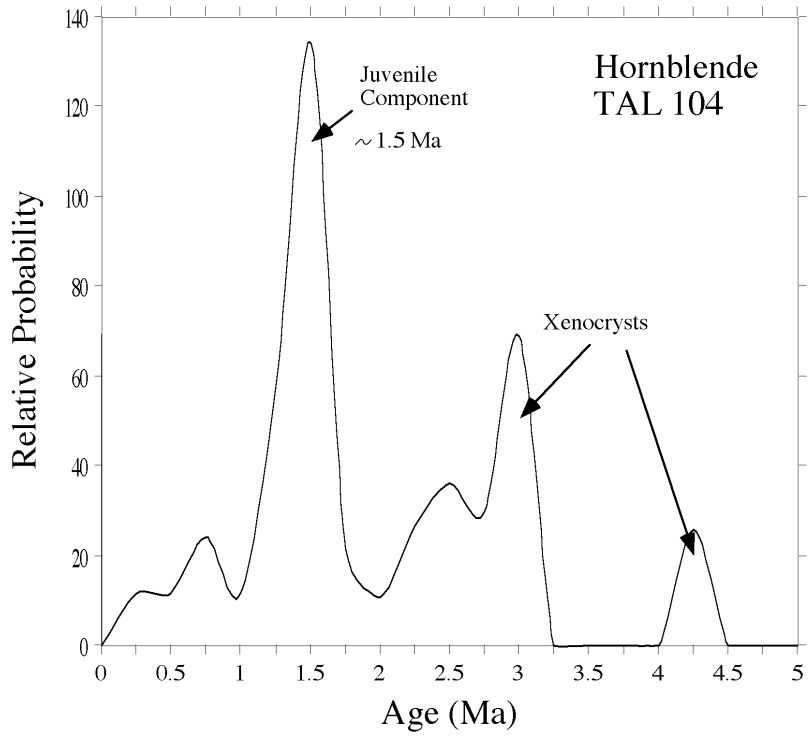

Figure 18: *Histogram of age data compiled from single grain laser fusion ages. It is shown to point out the heterogeneity of sample TAL 104 as well as to stress findings of data concentration around 1.5 and 3 Ma.*

Heterogeneity in the hornblende population of sample TAL 104 is reflected in its chemical composition as well. This can be shown in a plot of ^{37}Ar intensities versus ^{39}Ar intensities (Fig. 19). Intensities of these argon isotopes are proportional to the concentration of Ca and K, respectively, from which they are derived by neutron irradiation. All hornblende populations but those of sample TAL 104 show good correlation of ^{37}Ar and ^{39}Ar. Scatter of the data points of sample TAL 104 is conspicuous and is related neither to systematic potassium loss nor gain.
Further evidence of heterogeneity in chemical composition comes from microprobe analyses and was outlined above (Chapter 3.1).

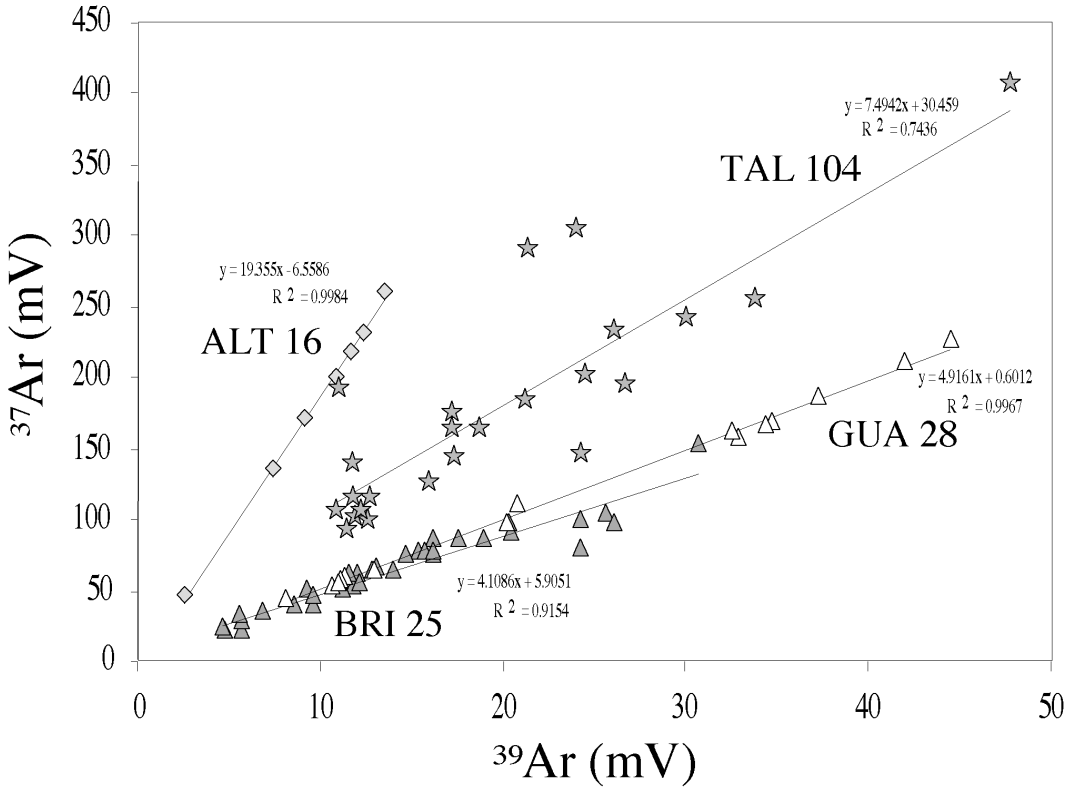

Figure 19: *Plot of ^{37}Ar versus ^{39}Ar takes as equivalents for K and Ca to present chemical variances of the four samples and to show the heterogeneity of the hornblende in sample TAL 104.*

Obviously, ages and chemical composition of hornblende grains from sample TAL 104 are very heterogeneous. The spread of ages is most likely related to variations between a young eruptive age and an older inherited component. The older component may reflect a signature inherited from the subducted slab that was partially molten to form these adakite samples. In that case, incomplete diffusive loss of the inherited argon during adakite formation would be responsible for the variable and older ages within some of the hornblende crystals. Since diffusion in the melt is depending on its temperature, it may be concluded that melting temperatures have been too low to get rid of the total amount of inherited argon by effective diffusion. Partial melting of the oceanic crust to form adakites starts already at temperatures little above 700°C [Defant], whereas loss of thermal stability in hornblendes occurs only beyond 600-800°C [Gaber et al., 1988]. Heterogeneity in age data detected in this sample may be a common problem in adakites due to their unusual generation by partial melting of amphibole bearing, metamorphosed oceanic crust at relatively low temperatures.

3.4 Ages of magmatic rocks from the Cordillera de Talamanca
Discussion of results from new $^{40}Ar/^{39}Ar$ age determinations and literature age data

New Ar/Ar ages on Talamanca magmatic rocks are reported in Table 3-2. Highlighted are those values that are considered as most reliable, following the explanations in the preceding chapter. These data, together with K-Ar whole rock ages from literature sources (listed in Table 3-3) are presented in Figure 20, versus their location in the arc profile. The five rock groups, defined on geochemical criteria, are to some extent also distinct by their ages.

***Table 3-2**: New Ar/Ar age determinations for magmatic rocks from the Cordillera de Talamanca area. Age differences result from different analytical methods and interpretation methods. Errors are 2σ of the mean. Highlighted are the most reliable age values.*

Sample	Furnace fusion	total	Furnace Step-	largest-	Laser mean age		Laser mean	weighted	Inverse Isochron	
ALT 16	18.33	+/- 0.40	**16.87**	**+/- 0.27**	17.46	+/- 1.05	17.36	+/- 0.37		
BRI 25	7.42	+/- 0.34	-		5.64	+/- 0.58	**5.82**	**+/- 0.09**	5.88	+/- 0.23
GUA 28	4.54	+/- 0.15	**4.39**	**+/- 0.14**	3.77	+/- 0.61	3.92	+/- 0.11		
TAL 104	1.92	+/- 0.10	-		1.89	+/- 0.93	1.90	+/- 0.17		

Arc-tholeiitic magmatism in the area of the Cordillera de Talamanca is documented by radiometric dating from about 32 to 11 Ma. The data point to increased arc-tholeiitic magmatic production during the Middle Miocene, with activity taking place within the Cordillera de Talamanca sensu strictu (ages between 17 and 11 Ma), as well as within the Fila Costeña (ages between 15 and 11 Ma).
These rocks are thus exclusively pre-collisional in respect of the Cocos Ridge arrival and represent products of subduction related volcanic activity in a young arc, and not products of an inserted tholeiitic phase in the volcanic cycle of a mature arc.

Samples of the calc-alkaline group are generally younger, but seem to overlap both, in time and space with the older tholeiitic group. Ages of these samples range predominantly from 12 to 8 Ma. Intrusive activity obviously continued for much longer in the northwestern end of the Cordillera de Talamanca than in the remainder areas of the Cordillera (7 to 2 Ma for the Escazu complex). In Panama, at El Baru (31 Ma), and in places east of it [de Boer et al., 1995], calc-alkaline intrusive activity was established earlier than in the Costa Rican part of the Cordillera de Talamanca.
Dated plutonic complexes from the Cordillera de Talamanca tend to decrease in age towards the northwestern end of this mountain chain. This trend is displayed in Figure 21 by the linear regression through the age data, which are plotted in a profile across the magmatic arc according to their outcrop locations. Northwestward younging of the intrusive rocks is inversely correlated with absolute heights in this mountain chain (see e.g., de Boer et al. [1988]), and may result from northwestward propagating uplift of the Cordillera de Talamanca. Prerequisites for this interpretation are however:

- Simultaneous intrusive activity along the entire length of the Cordillera de Talamanca
- Intrusions taking place at comparable crustal levels
- Intrusion ages decreasing upwards
- Almost constant erosion rates through time

If this holds true, those parts of the mountain chain that are uplifted earlier will have longer been subjected to erosion and hence been cut to deeper crustal levels, exposing older plutonic rocks.

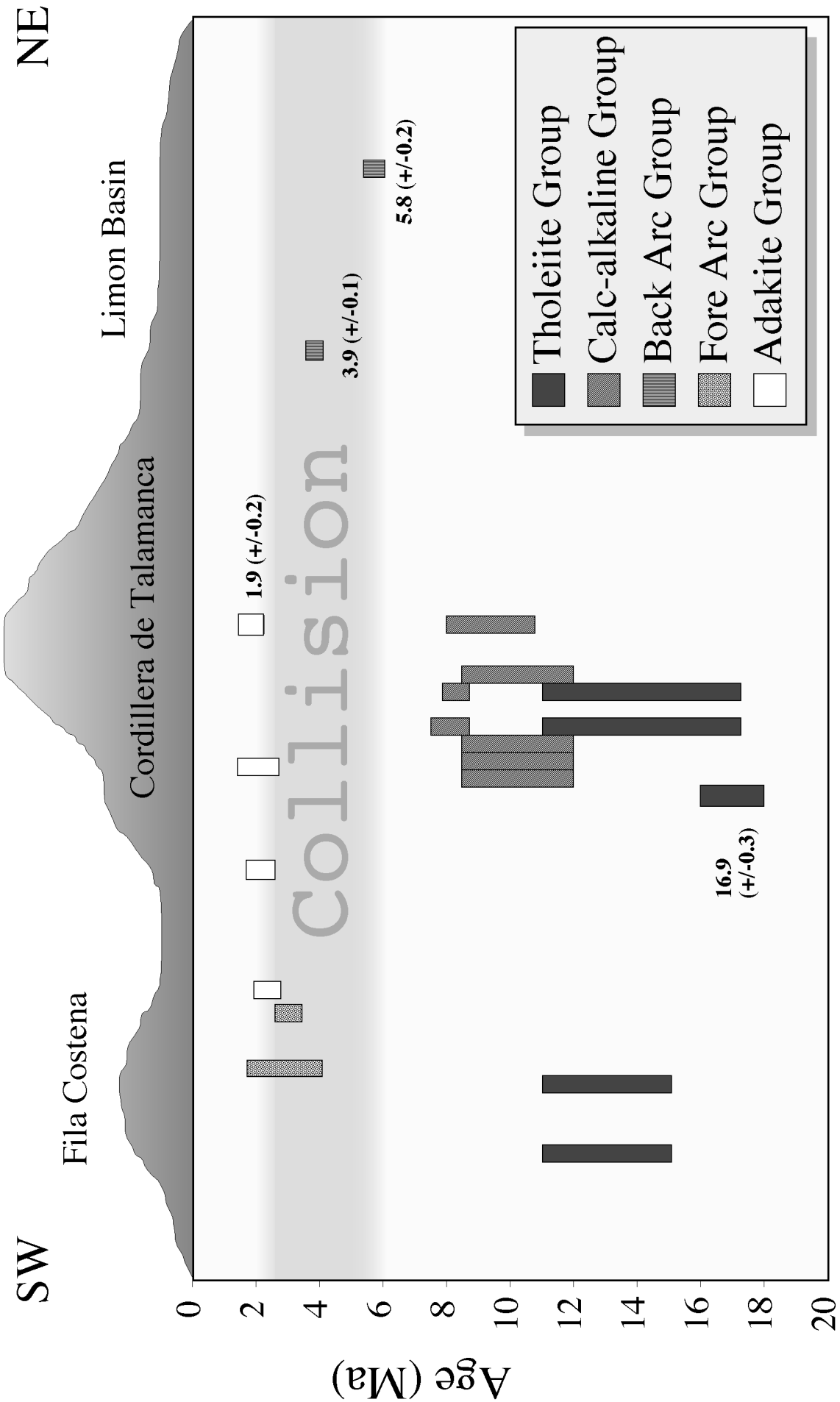

Figure 20: *Profile showing radiometric ages for the 5 rock groups. Numbers for new data.*

Calc-alkaline volcanics are generally younger than their intrusive counterparts. They outcrop only in the northern region of the Cordillera de Talamanca and range in age between 8 and 3 Ma. Other occurrences were probably effectively eroded. A radiometric age of about 17 Ma derived for a calc-alkaline volcanic sample [Bellon & Tournon, 1978] was seriously questioned by later investigations [Alvarado et al., 1992].
Calc-alkaline magmatic activity takes over the preceding tholeiitic activity during the Middle Miocene in southern Costa Rica. This change in arc magmatic composition characterises the increasing arc maturity. This kind of "normal" arc magmatism in the Cordillera de Talamanca sensu strictu is pre-collisional, and ended with the time of Cocos Ridge collision.

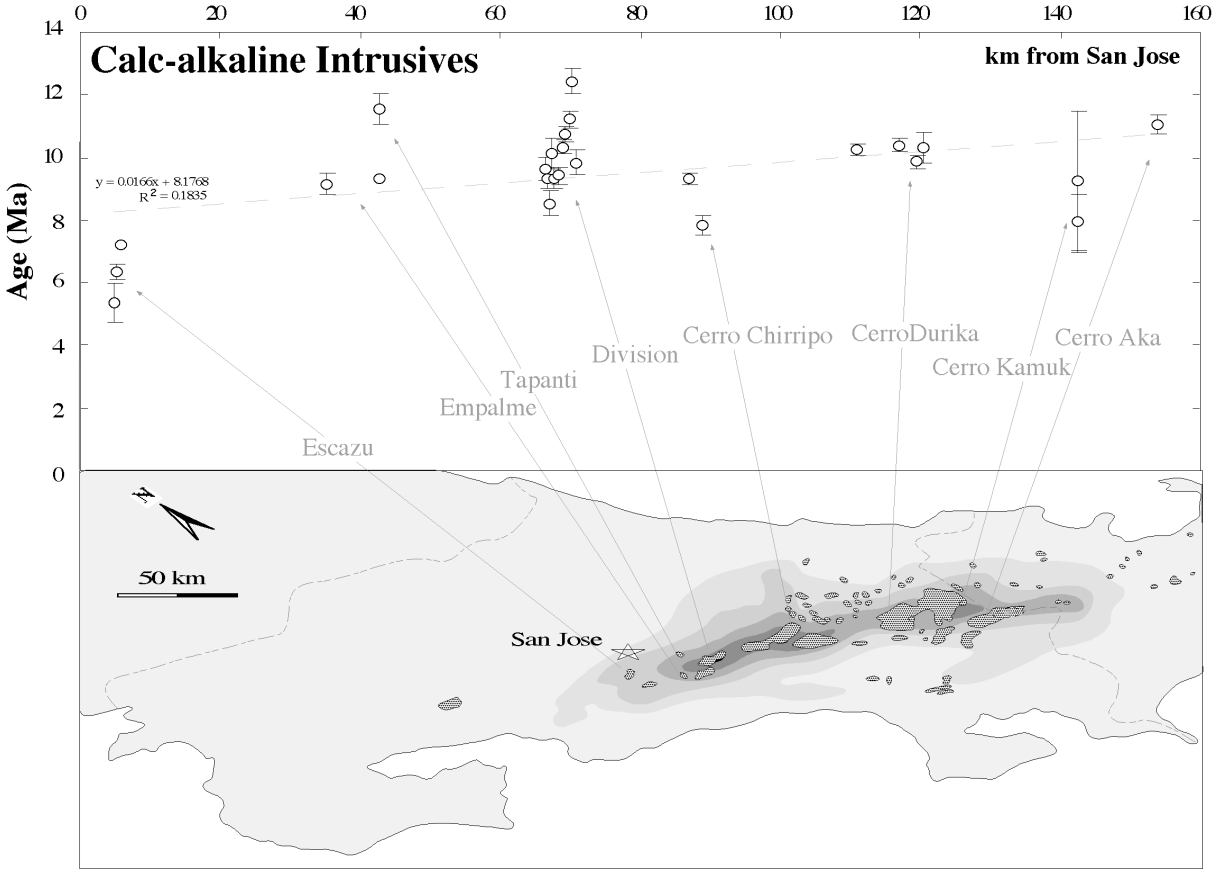

Figure 21: *Age data variations along the Cordillera de Talamanca compiled for samples of the calc-alkaline group. The diagram is based on radiogenic age data available from the literature (see table). As a result of the compilation it becomes evident that ages of dated plutonic complexes decrease to north-east within the Cordillera de Talamanca*

Backarc magmatism began during the uppermost Miocene and migrated in time towards northern Costa Rica. This trend of younging of backarc magmatic activity is evidenced by the rock suite of Bribri from near the Panamanian border dating to 5.8 Ma, the Guayacan suite in central Costa Rica of Pliocene age (4.4 to 4.6 Ma), and backarc suites off the investigated area to the north which are Pleistocene (1.2 Ma) to sub-recent.
A plot of age variations within alkalic rocks from locations along the backarc in Costa Rica (Fig. 22) presents the obvious younging trend of these complexes towards NW. This trend is emphasised by the linear regression through the available data points. Restricting assumptions that limit the interpretability of this trend are not necessary for these volcanic rocks in contrast to the intrusive rocks of the Calc-alkaline Group.

Alkaline backarc magmatic activity is simultaneous with the collision event of the Cocos Ridge with the Central American Arc. This activity occurs within restricted, relatively short-lived areas, that shift through time in a NW direction. The occurrence of these backarc magmatic rocks documents drastic changes in the melting regimes within this arc segment, that are related to major changes in plate configurations in southern Central America. The directed age trend for this kind of magmatism strongly suggests a northward or northwestward directed progression of these changes.

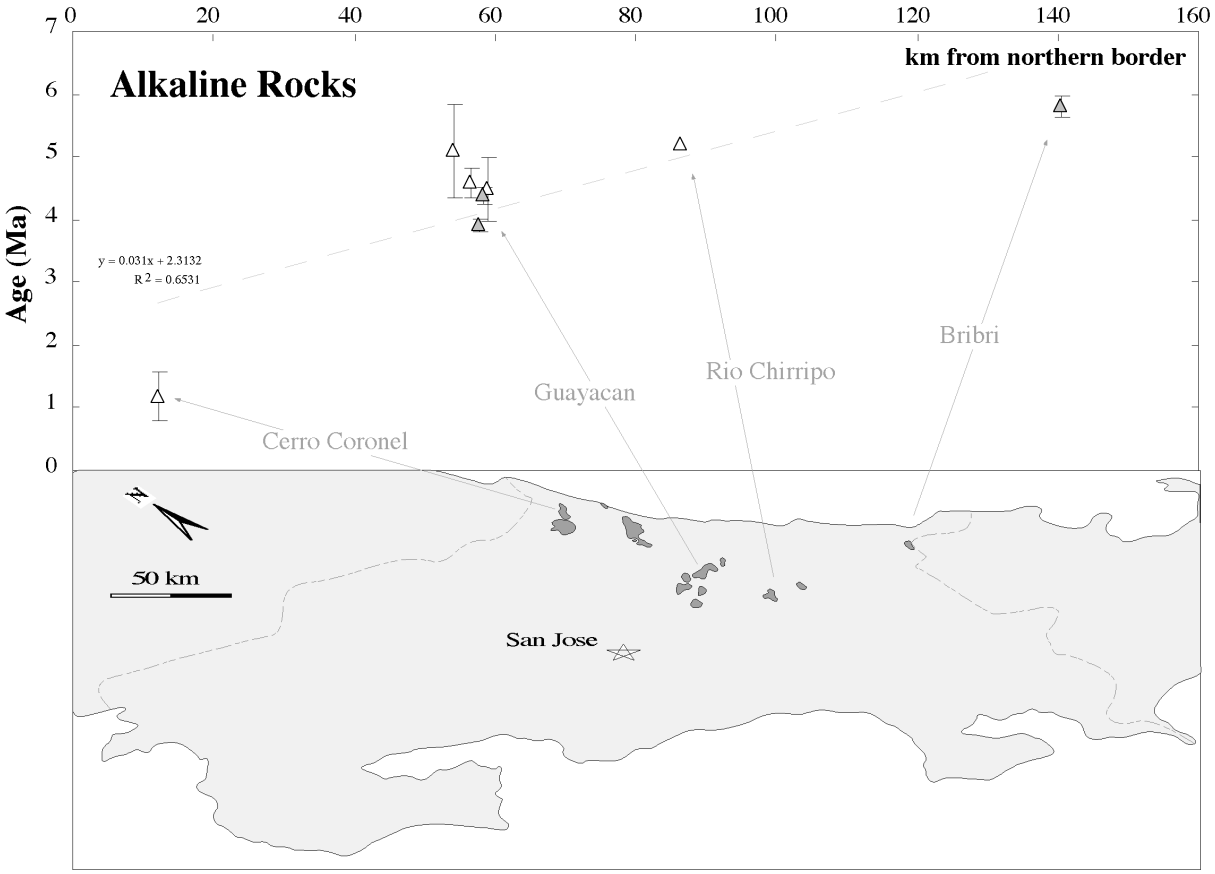

Figure 22: *A plot of age data variations for alkaline magmatic rocks along the Costa Rican back arc presents a distinctive younging towards NE. The diagram utilises radiogenic data available from literature as well as the new data provided by the present study for the backarc alkaline group.*

Calc-alkaline volcanic activity of the Fila Costeña is comparatively young. Samples are dated to the Plio-Pleistocene with most ages ranging from 4 to 1 Ma. Volcanism in this forearc area is localised and believed to be relatively short-lived, though the radiometric ages suggest repeated activity.
Calc-alkaline volcanic activity in the forearc area is post-collisional. From occurrence, extent, and ages it can be concluded that this activity may represent a relatively short phase of renewed arc volcanism offset to the trench, or the reflection of a thermal anomaly temporarily existing in the mantle underlying that area.

The adakitic samples are of Upper Pliocene to Pleistocene age. Maximal ages of 2.6 Ma and 2.8 Ma, respectively [Tournon, 1984; de Boer et al., 1995] are found in the southeastern Costa Rican outcrops as well as in the central Cordillera de Talamanca. Younger ages for the adakitic samples are also reported for both locations, ranging up to about 1Ma [de Boer et al.,

1995]. Thus, no systematic age variations are found for these locations of adakite eruptions. However, in the preceding chapter it was demonstrated that heterogeneity in ages may result from inherited components, which could stay undetected by use of an inadequate dating method. High susceptibility to alteration additionally limits the applicability of the K-Ar whole rock dating method for these rocks.

Further investigation of this rock group with the Ar/Ar method on separates of different minerals seems to be very promising to confine the problem of sample heterogeneity, and to determine the eruptive ages of adakites from different locations in southern Costa Rica. If this problem could be resolved, the possible establishment of an age sequence within the eruptions from the different locations would give new information on the relationship between adakite genesis and Cocos Ridge subduction.

Samples of the adakite group are post-collisional and restricted to a very short period of time. They are directly related to Cocos Ridge subduction, as they started erupting when the subduction process had been going on for some time and stopped erupting shortly after that, probably upon changes in the subduction zone geometry.

4 Geochemistry

This chapter discusses the compositional systematics of the magmatic rocks from the area of the Cordillera de Talamanca. After classification of the rocks, geochemical criteria for the distinction of the five rock groups are presented, differentiation trends of the magmatics are discussed, and source characteristics are presented.
Major and trace element data of the 80 analysed rock samples are listed in Appendix X, together with the description of analytical methods.

4.1 Major elements

4.1.1 Classification

Volcanic and intrusive rocks from the area of the Cordillera de Talamanca can be subdivided into members of two major magma series: alkalic and sub-alkalic. This distinction is presented in the Total Alkalis versus Silica (TAS) diagram, the dividing line after Irvine and Baragar [1971] separates the two series (Fig. 23). The alkalic series is represented by only one group: samples from backarc locations, the four remainder groups are all sub-alkaline.

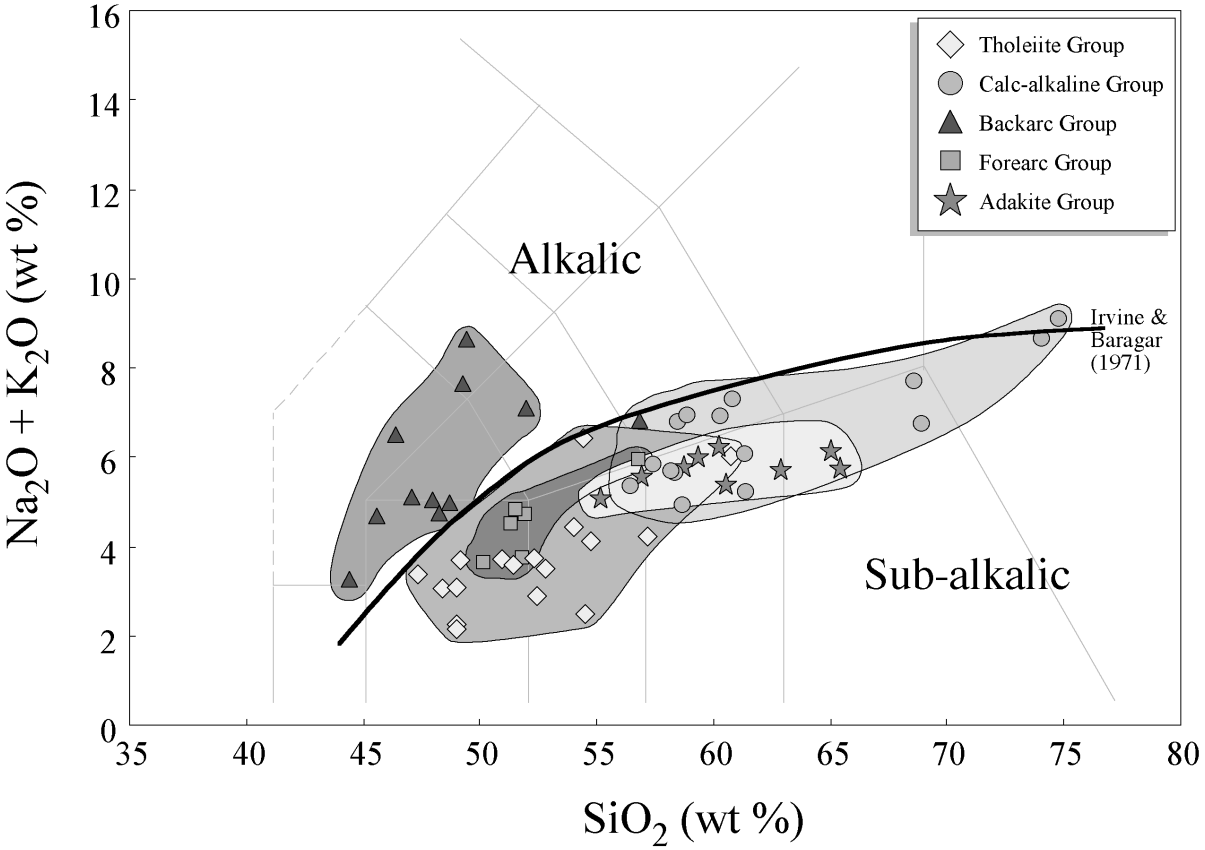

Figure 23: *Diagram of Na_2O+K_2O vs. SiO_2 (TAS diagram) for the distinction of the alkalic and sub-alkalic rock suites. The boundary is from Irvine & Baragar [1971].*

Sub-alkalic rocks can be further subdivided in a diagram of K_2O vs. SiO_2 (Fig. 24). This diagram shows subdivisions after Le Maître [1989] and Rickwood [1989], separating fields of low-K tholeiitic series, calc-alkaline series, high-K calc-alkaline series and shoshonite series. Magmatic rocks of southern Costa Rica display differentiation series that cross these subdivisions in a steep trend. Recognition of the four distinguished sub-alkalic groups from the area of the Cordillera de Talamanca is not feasible using this diagram. However, the "Tholeiitic Group" shows notable tendencies to low alkali contents, whereas the "Calc-

alkaline Group" samples have higher alkali contents and plot into the field of calc-alkaline to shoshonitic series. Overlap of these two groups is present. Samples of the Adakite Group and the Forearc Group plot within the central area of the diagram, varying between calc-alkaline series and high-K calc-alkaline series. The Forearc Group shows tendencies to the alkalic field.

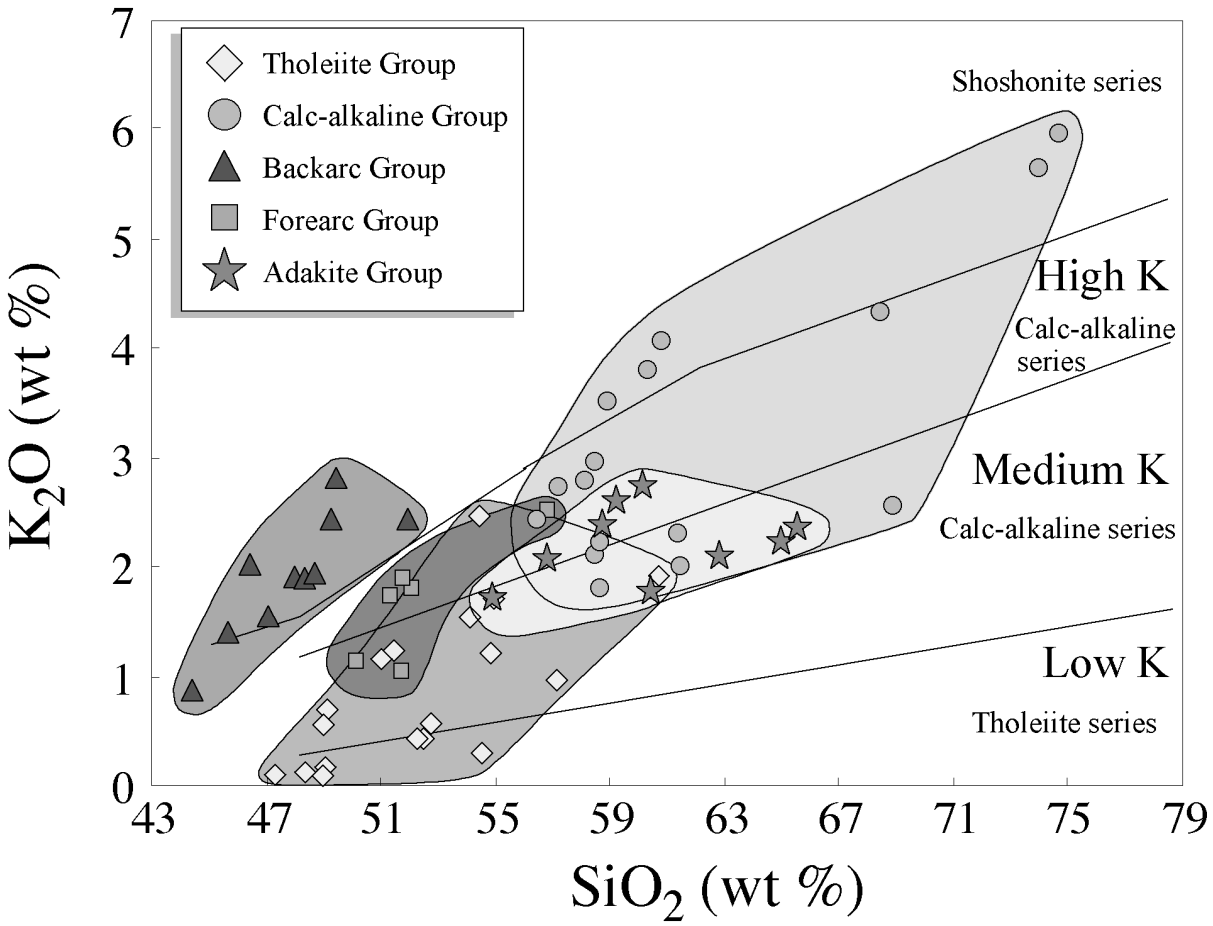

Figure 24: *Diagram of K_2O vs. SiO_2 [Pecerillo & Taylor, 1976] for the subdivision of sub-alkaline rocks. The four fields are outline according to Le Maître et al. [1989] and Rickwood [1989].*

In a TAS-diagram (Fig. 25), compositional classification of the magmatic samples was done according to the international nomenclature [Le Maître et al., 1989]. Intrusive rocks of the area are also plotted into the diagram, distinguished by pale colours from the bright coloured or black edged volcanic samples of the same group.
Backarc volcanic samples are basanites, a less alkalic suite of this group ranges from basalt to basaltic-trachyandesite. The intrusive equivalents to these alkalic volcanics are termed teschenite (i.e. alkali-gabbro). Samples of the Tholeiitic Group are either gabbros or basalts, basaltic andesites, and andesites. One sample plots into the basaltic-trachyandesite field. Calc-alkaline Group samples are predominantly intrusive, varying in composition between diorite, syeno-diorite, grano-diorite and alkali-granite. The few volcanic samples of this group are andesites or dacites. Forearc Group samples and Adakite Group samples are exclusively volcanic. The former range between basaltic to basaltic-trachyandesitic compositions, the latter plot into the field of basaltic andesites, andesites, and dacites.

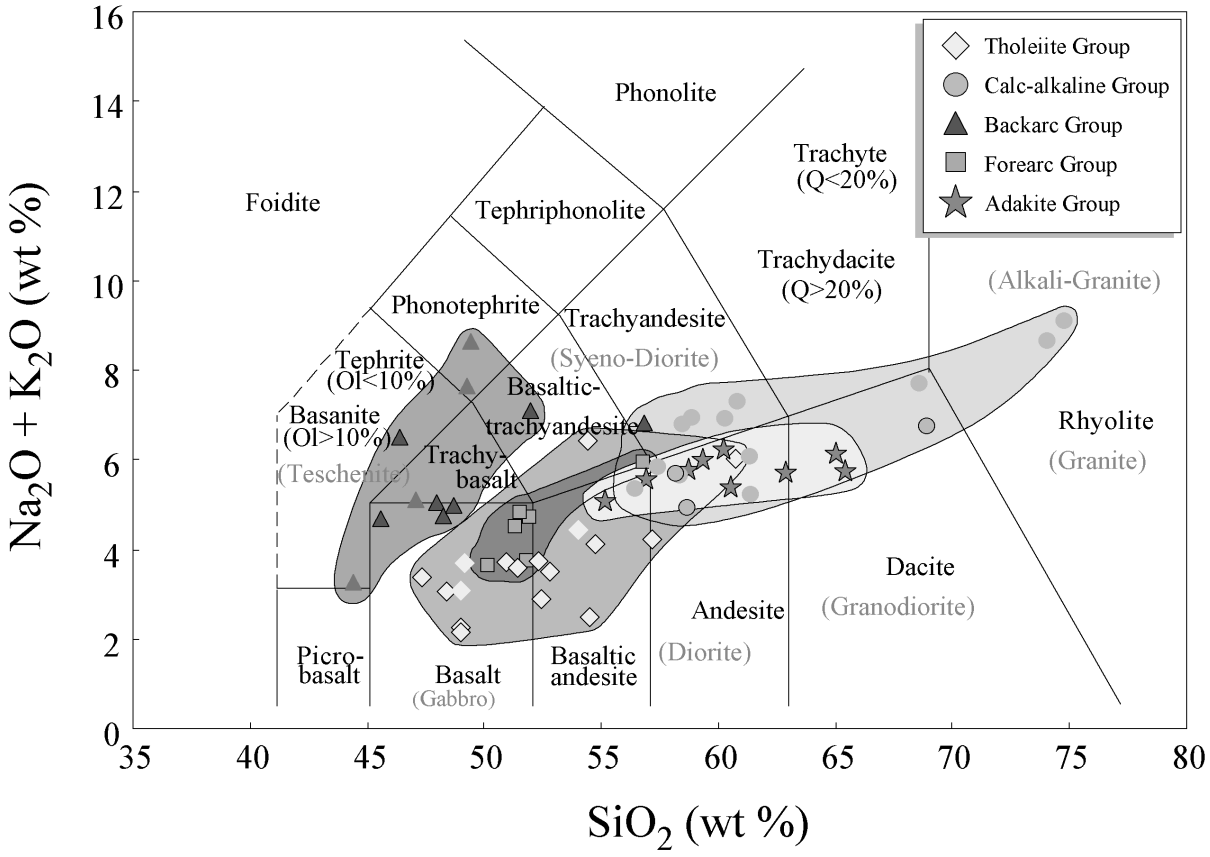

Figure 25: *TAS diagram after Le Maître et al. [1989] for the classification of igneous rocks.*

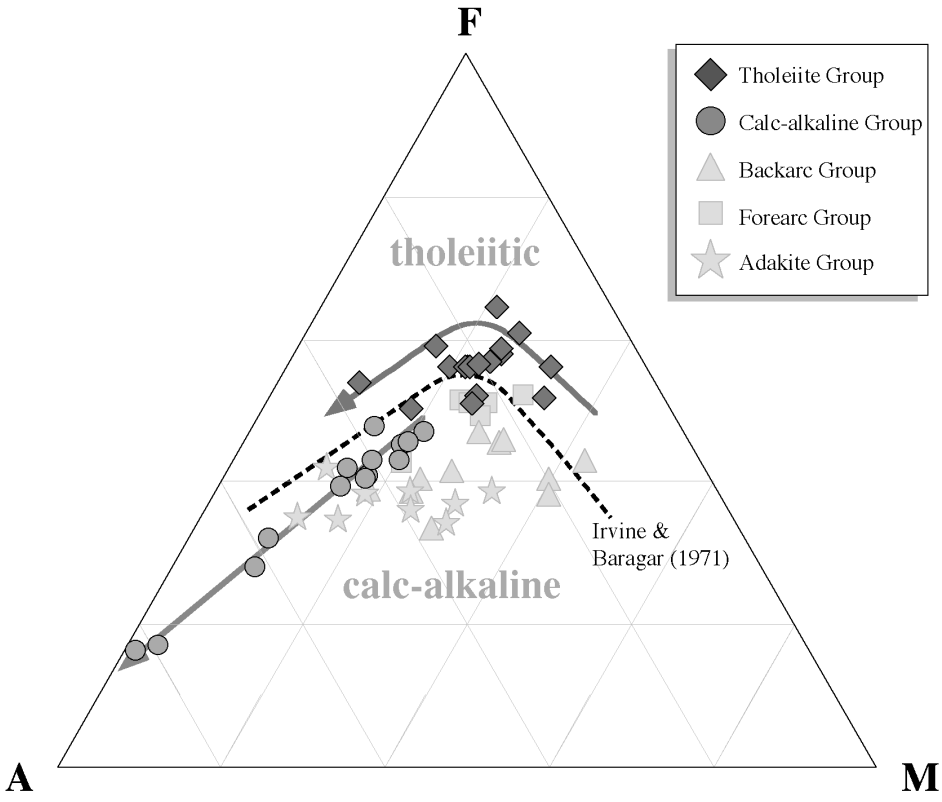

Figure 26: *AFM ternary for the differentiation of tholeiitic and calc-alkaline rock series. A stands for Na_2O+K_2O, F for total FeO, M for MgO. The dashed separation line is from Irvine & Baragar [1971].*

An AFM-diagram (Fig. 26), showing typical differentiation trends of Talamanca tholeiite and calc-alkaline rocks, can be used to stress the distinct character of these two groups. The Calc-alkaline Group displays a straight differentiation trend below the separation line after Irvine and Baragar [1971]. The trend of the tholeiite group is at higher FeO values and characterised by an additional ascending branch because of iron enrichment prior to a sudden start of stabilisation and fractionation of the ore minerals.

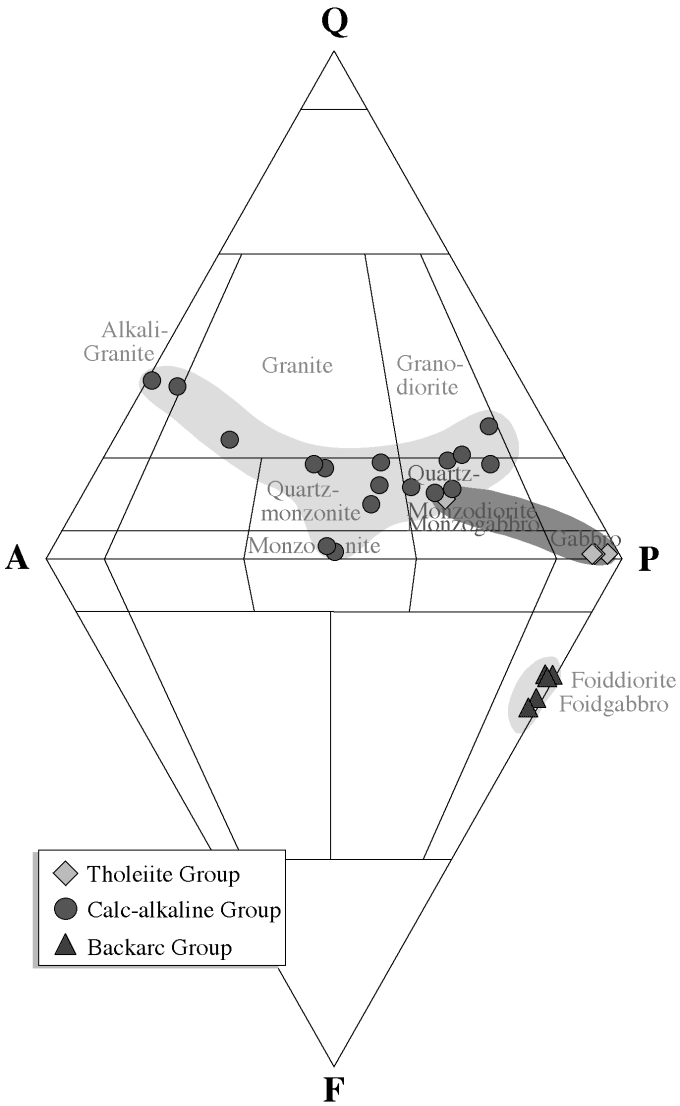

4.1.2 Classification of intrusives

In the following passages of this study, I will abandon a separate discussion of volcanic and plutonic rocks, since they are directly related and geochemically uniform.

However, for the sake of completeness, the intrusive rocks of the Talamanca area have to be classified in this chapter. Classification of intrusive rocks is best done in the QAPF diagram (Fig. 27) after Streckeisen [1976] and Le Maître et al. [1989] with recommendation by the IUGS Subcommission. This classification is fundamentally mineralogical but it may also be done by calculations based on the appropriate compositional analyses. For this purpose, the modal mineral content was calculated from the whole rock chemistry and typical mineral data of the respective plutonic rock type, using the least-square mass balance program Petmix after Le Maître [1979]. This method bears the advantage of being applicable also to more fine-grained varieties of intrusive rocks.

Calc-alkaline intrusives of SE Costa Rica are compositionally the most variable rock group, spreading in the diagram from quartz-monzodiorites over quartz-monzonites and granites to alkali-granites. Granodiorites and monzonites are also present. The tholeiite group comprises primarily gabbros but also a quartz-monzogabbro. The alkalic intrusives of the backarc group, which are known as teschenites, plot in the field of foidgabbros and foiddiorites.

The QAPF diagram contains some additional data points of rocks which had to be omitted from further investigation due to their alteration.

Figure 27: *QAPF diagram after Streckeisen [1976] and Le Maître et al. [1989] for classification of plutonic igneous rocks. The modal mineral content is calculated from whole rock and mineral compositions.*

4.1.3 Differentiation

Harker diagrams show the chemical differentiation trend of the Talamanca rock series in respect of the major elements (some plots with trace elements are added). Besides trends due to fractional crystallisation of different mineral phases, mixing lines are also apparent.

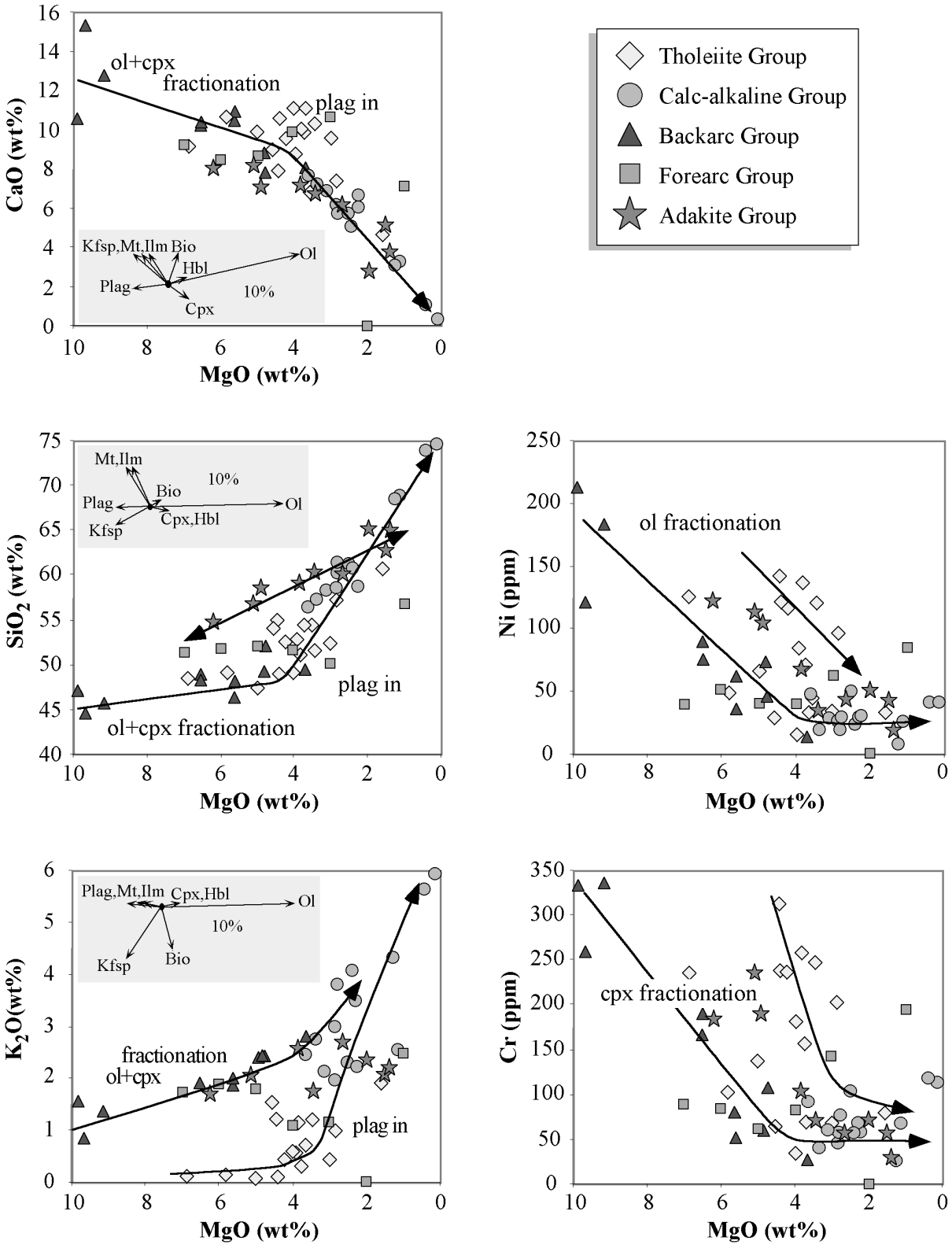

Figure 28: *Element variation diagrams for major and trace elements versus MgO. Kinks in the liquid lines of descent announce the start of crystal fractionation of a new mineral species.*

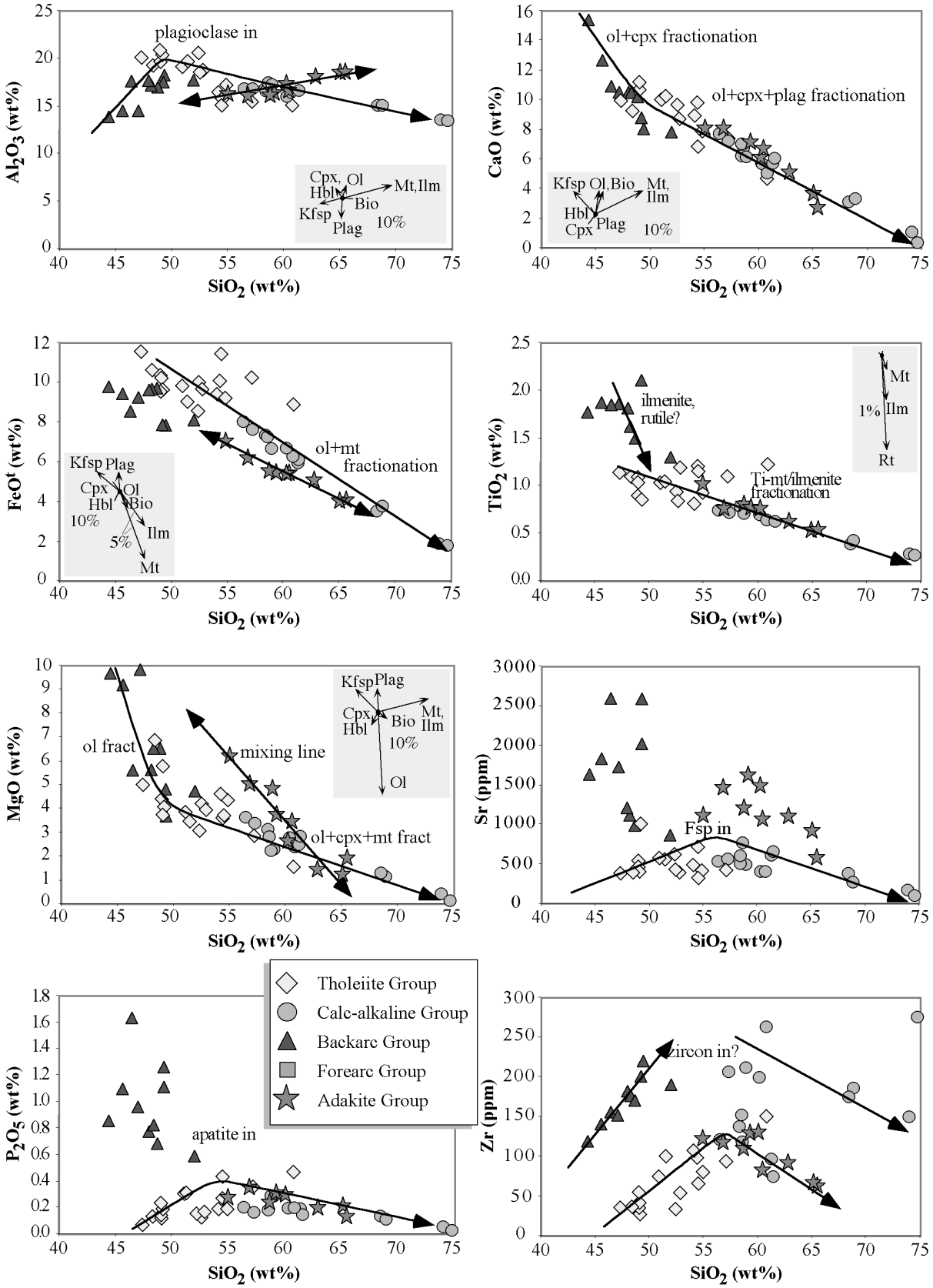

Figure 29: *Harker diagrams showing elemental variations of major elements and some trace elements versus SiO_2. The five rock groups of the Talamanca area display liquid lines of descent with clear evidence for fractionation and other straight lines due to mixing.*

Samples of the tholeiite group and those of the alkaline group are the most primitive of the Talamanca area, i.e. they have undergone the least crystal fractionation. This is obvious from the presented element variation diagrams. The alkaline rocks are only affected by some olivine and pyroxene fractionation. Samples of the calc-alkaline group are in contrast extremely differentiated by crystal fractionation. Fractionated to lesser degrees are the samples of the forearc group. The adakite group samples display however strong evidence for mixing. This mixing effect poses difficulties for the estimation of the role of fractionation for these rocks.

Plots of major and some trace elements versus MgO are the most suitable to show the chemical trend within the more mafic samples. Correlation of Ni with MgO and Cr with MgO are presented in Figure 28, lower right. The course of the liquid line of descent is at first mainly governed by Ol and Cpx fractionation. Backarc samples and tholeiitic samples show both considerable fractionation of these two minerals. For the samples of the Forearc Group and especially for those of the Calc-alkaline Group fractionation of these minerals has become negligible. However, the Adakite Group shows also co-variation of Ni and MgO as well as Cr and MgO.
Plots of CaO, SiO_2, and Al_2O_3 versus MgO present a marked inflection in the liquid line of descent that is related to plagioclase fractionation. At high MgO values only Ol and Cpx fractionation occurs, whereas around 4% MgO, plagioclase enters the fractionating assemblage. These diagrams point out that plagioclase is not a fractionating phase in the alkaline backarc samples.
Harker diagrams of major element oxides versus SiO_2 and some additional diagrams of trace elements versus SiO_2 (Fig. 29) characterise the major fractionating phases olivine, clinopyroxene, plagioclase, as well as alkali-feldspar, magnetite/ilmenite and the accessory phases like apatite and zircon. These geochemical findings are in accordance with the petrographical observations.
Whereas for most of the rock groups the trends are governed by fractional crystallisation, the trend of the Adakite group represents a mixing line. This is indicated by a straight line across the normal fractionation trend and is especially striking in diagrams of Al_2O_3 versus SiO_2 and MgO versus SiO_2. The high Al_2O_3- and SiO_2-endmember is represented by primary adakitic melts whereas the high Mg end-member reflects an admixed mafic component.

Extract calculations for several minerals are presented within the small insets in the variation diagrams. These calculations are useful to find out the principle fractionating minerals for the respective diagrams. Calculation was done after Cox et al. [1979] by starting from the most primitive rock of the data set and extracting 10% of the minerals.

4.2 Trace elements

4.2.1 Sample group distinction

A good means for the distinction of the five different groups of magmatic rocks from SE Costa Rica are REE plots (Fig. 30). The REE contents of the samples are normalised to primitive mantle concentrations after Sun & McDonough [1989]. For comparison, pattern of recent volcanics from central and northern Costa Rica are also shown in the diagrams.

The Forearc Group samples display a typical calc-alkaline pattern with enrichment of the LREE (Ce/Yb)n: 8-12).
The pattern of the Calc-alkaline Group is to some respect comparable but shows in most cases a negative Eu anomaly due to plagioclase fractionation, a lower ratio of La/Yb (Ce/Yb)n: 3-6) and for several samples higher HREE concentrations.
The REE pattern of the tholeiitic group is definitely distinct in that it shows a flat signature with almost no gradient from LREE to HREE (Ce/Yb)n: 1-4).
Completely contrary is the REE pattern of the Alkaline Group. That pattern is extremely steep (Ce/Yb)n: 15-33).
A similar gradient is seen in the REE pattern from samples of the Adakite Group (Ce/Yb)n: 15-33), however, it is shifted entirely to lower values with remarkably low HREE concentrations.

REE patterns of the rock samples from the area of the Cordillera de Talamanca reflect differing degrees of partial melting, fractionation, and source compositions.
Higher degrees of melting result in a flat pattern like that of the Tholeiitic Group, medium degrees give a pattern like that of the Forearc Group, and low degrees could be responsible for the pattern of the Alkaline Group samples. The pattern of the Calc-alkaline group is influenced by fractionation, not only obvious in the negative Eu-anomaly but also in the parallel shift of individual REE pattern to higher values. The pattern of the Adakite Group is governed by its source mineralogy. Low concentrations of HREE signal the presence of residual garnet (with high partition coefficients for HREE) in the source of these rocks and are an important characteristic of this rock group. Garnet becomes stable during prograde metamorphism of the subducted slab. As it is present during partial melting of the subducted, hydrated, oceanic crust, it imprints its signature to the adakites which are products of slab-melting (see chapter 4.2.2).

The REE pattern of samples from the active volcanoes in northern and central Costa Rica (data from Feigenson & Carr, 1993; Kussmaul et al., 1994) are different from all the magmatic rock groups of southern Costa Rica. These young volcanics display a generally steeper pattern, offset to higher concentrations also at the HREE, than volcanics from the former arc to the south. This fact points out, that the northern and central Costa Rican mantle source is actually more enriched than the older southern Costa Rican was. Only the backarc samples in SE Costa Rica show an REE pattern which is as steep or even steeper than that of the rocks from northern and central Costa Rica.

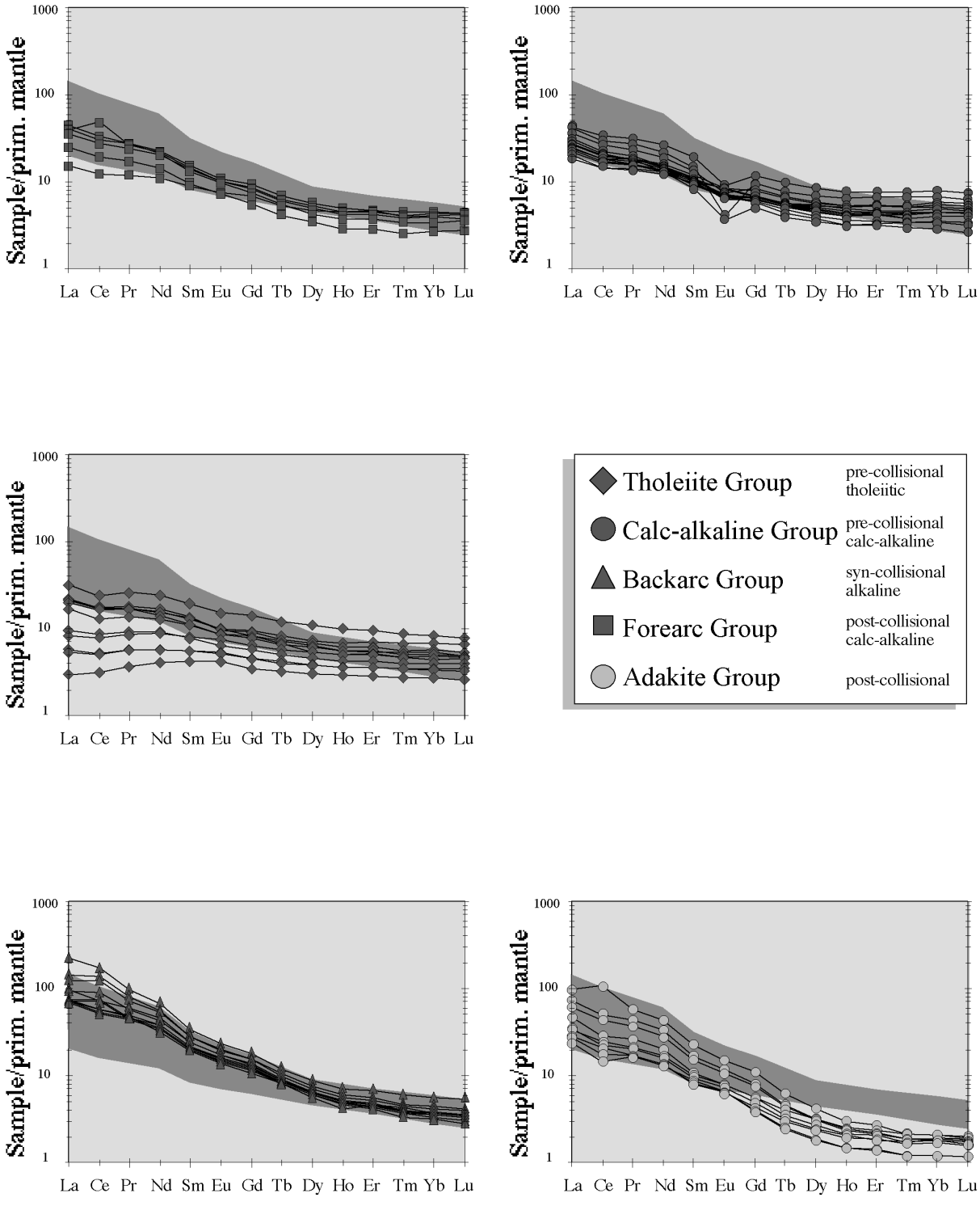

Figure 30: *REE diagrams for the Talamanca rocks. Inclination and shape of the pattern together with absolute REE concentrations are characteristics that help to separate the five rock groups. The shaded bar in the background displays the REE pattern of recent volcanics in northern and central Costa Rica.*

4.2.2 Characterisation of Adakites

Melt generation at subduction zones generally takes place within the mantle wedge above the dehydrating slab [Gill, 1981]. However, under certain circumstances some magmas at convergence zones can be generated by direct melting of the subducting oceanic crust [Defant & Drummond, 1990b]. Prerequisites for the formation of slab melts are 'hot' slab geotherms [Peacock, 1990; Rapp & Watson, 1995] like this is achieved by subduction of very young crust [Defant & Drummond], at subduction zones with low convergence velocities, high heat flow or high shear stress [Peacock et al., 1994]. Melting of the hydrated, subducting oceanic crust takes place during the breakdown of amphibole in the stability field of garnet. The resulting partial melts erupt as high Al_2O_3 andesites to dacites and are termed adakites [Defant & Drummond, 1990b].
Geochemically, adakites are characterised by high Sr, Low Y and HREE, consistent with an origin by partial melting of eclogite or garnet amphibolite [Defant & Drummond, 1990a,b].

A clear distinction of adakites from normal arc magmatic rocks can be made by their REE pattern with depletion in HREE (Figure 30) and by using a Sr/Y versus Y diagram (Fig. 31). In that diagram, adakites plot at high Sr/Y ratios and low Y contents due to their Y depletion and concomitant Sr enrichment. This geochemical signature is a consequence of their source features with garnet stability and plagioclase instability. Plotted in the diagram below are exclusively andesites, dacites, and the corresponding intrusive equivalents. Additionally represented are fields from adakites of localities in southern Chile [Kilian & Stern, 1994] and the type locality of Adak Island [Kay, 1978]. Mantle-wedge derived island-arc andesites and dacites plot within a field at low Sr/Y ratios and high Y concentrations.

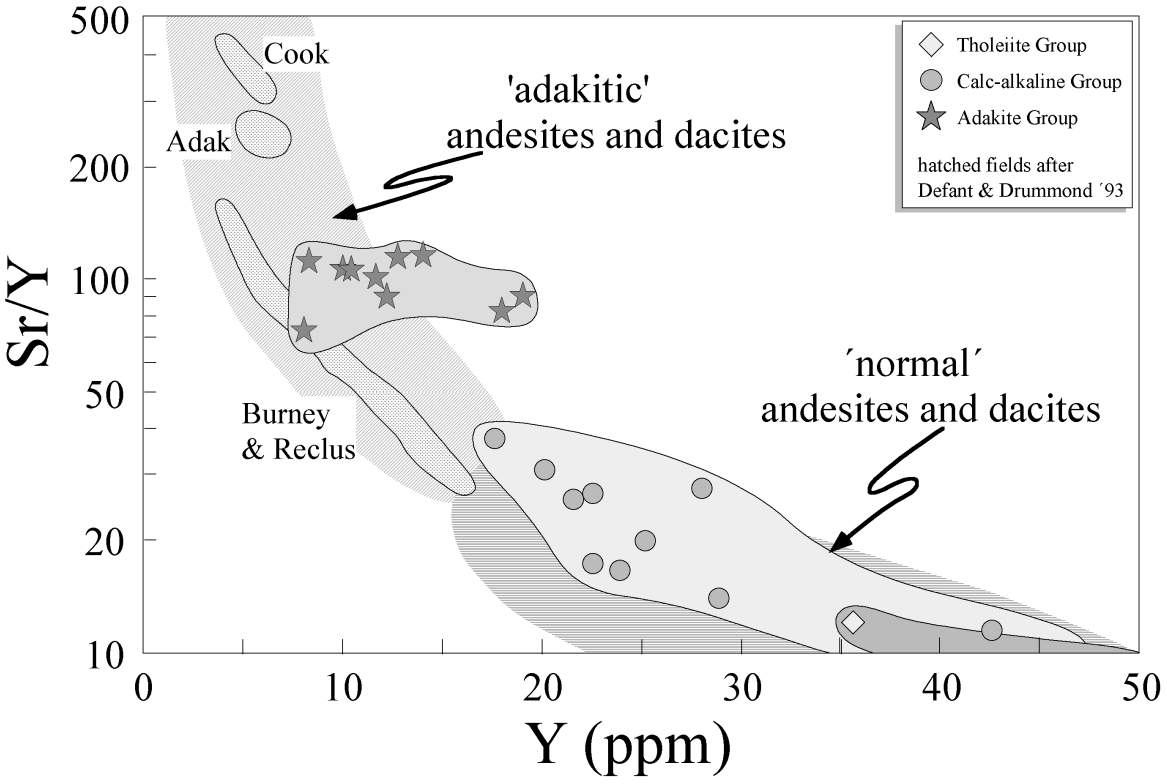

Figure 31: *Sr/Y versus Y diagram for the distinction of adakitic andesites and dacites from normal andesites and dacites after Defant & Drummond [1993] and Stern and Kilian [1996].*

4.2.3 Source Characteristics

Primitive-mantle-normalised [Sun & McDonough, 1989] multi-element diagrams (Fig. 32) show typical island arc signatures for almost all the samples. HFSE (Nb, Ta, Hf, Zr, Ti) depletion is a characteristic for this tectonic environment and most conspicuous with the Nb-Ta trough [Wilson, 1989]. This trough is clearly visible in samples from the Tholeiitic Group, Calc-alkaline Group, Forearc Group and Adakite Group. It is by far less evolved in the samples of the Backarc Group. Depletion of the entire suite of HFSE is seen throughout the rock groups with an exception of Zr that is enriched in samples of the Calc-alkaline Group.

Mobile elements like the LILE (Rb, Ba, K, Sr) are enriched in rocks of all groups but the Backarc Group. Enrichment of these elements is ascribed to fluids from subducted sediments or subducted basalts and hence a further characteristic for subduction related magmatic rocks. The pattern of the Backarc Group shows little similarities to magmatic rocks from subduction zones: Depletion of the HFSE is minor and enrichment of fluid-mobile elements in comparison with other elements is absent. Similarities of these rocks with intra-plate magmatic rocks is instead striking. This is demonstrated in the diagram by comparison to the pattern of a HIMU-OIB.

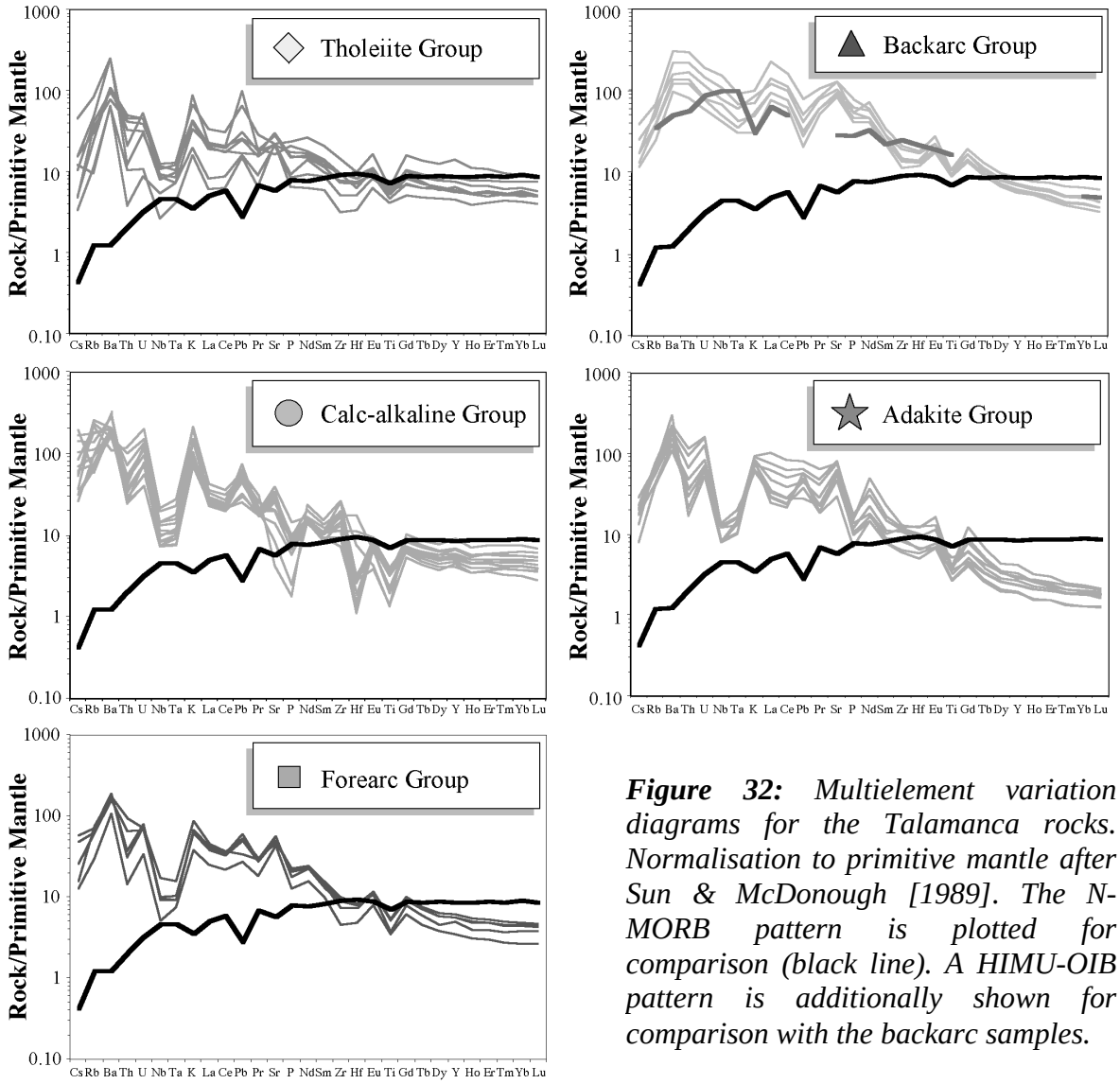

Figure 32: *Multielement variation diagrams for the Talamanca rocks. Normalisation to primitive mantle after Sun & McDonough [1989]. The N-MORB pattern is plotted for comparison (black line). A HIMU-OIB pattern is additionally shown for comparison with the backarc samples.*

4.2.3.1 Trace element ratios

Trace element ratio plots, presented in the following section, point to source characteristics of the five rock groups more easily than the multi-element diagrams.
Ratios of fluid mobile elements normalised to immobile elements like Ba/La [McCulloch & Gamble, 1991] or Ba/Th [e.g., Turner et al., 1997] can be a measure of subduction derived fluid (metasomatic fluid) or sediment subduction into the respective magma sources. Ba is present in high concentrations within subducting sediments off Costa Rica (Chapter 1.2.3.2.3). Thus, Ba is a very sensitive indicator for the involvement of sediment or fluids derived therefrom especially in this subduction zone [Leeman et al., 1994].
Ratios of immobile elements of differing ionic radii can be a measure of mantle source compositions. A low Nb/Zr ratio for example points to a depleted mantle portion due to previous melting events [Pearce & Norry, 1979].
Figure 33 displays variations of the Nb/Zr ratio versus Ba/Th ratio in the Talamanca rock samples. Virtually all rock groups but the Backarc Group show large (and variable) contributions of sediments or fluids to their mantle source. An influence of a fluid mobile slab component is absent for the Backarc Group samples. Instead they show less depletion of their mantle source in respect of the immobile elements.

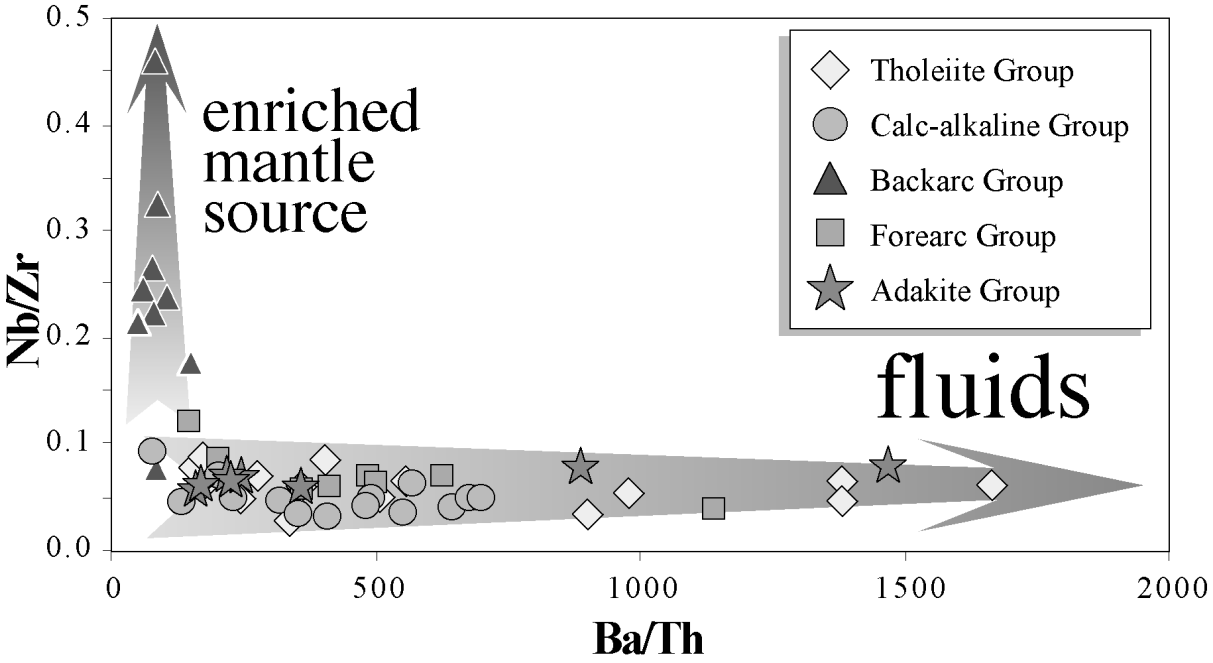

Figure 33: *Trace-element ratio plot of Nb/Zr vs. Ba/Th. The arc magmas show high but variable Ba/Th ratios indicating the contribution of slab fluids to the source. An exception is made by samples from the back arc. They vary instead in Nb/Zr ratio, a measure for the degree of source depletion by former melting events. Melting degrees have a minor influence on the ratio.*

A plot of (Gd/Yb)n versus Nb/Zr shows that the relative source enrichment in the backarc samples is not correlated with a present garnet signature. The high (Gd/Yb)n of the backarc samples means higher concentrations of garnet in the mantle source of these rocks as compared with the other mantle melts and thus a derivation from greater depths. Surprisingly, the forearc volcanic rocks display a garnet signature intermediate between the backarc rocks and the calc-alkaline rocks from the former central arc. The garnet signature is very prominent

for samples of the Adakite group, derived by melting from an eclogite residue. However, their signature does not correlate with Nb/Zr ratios.

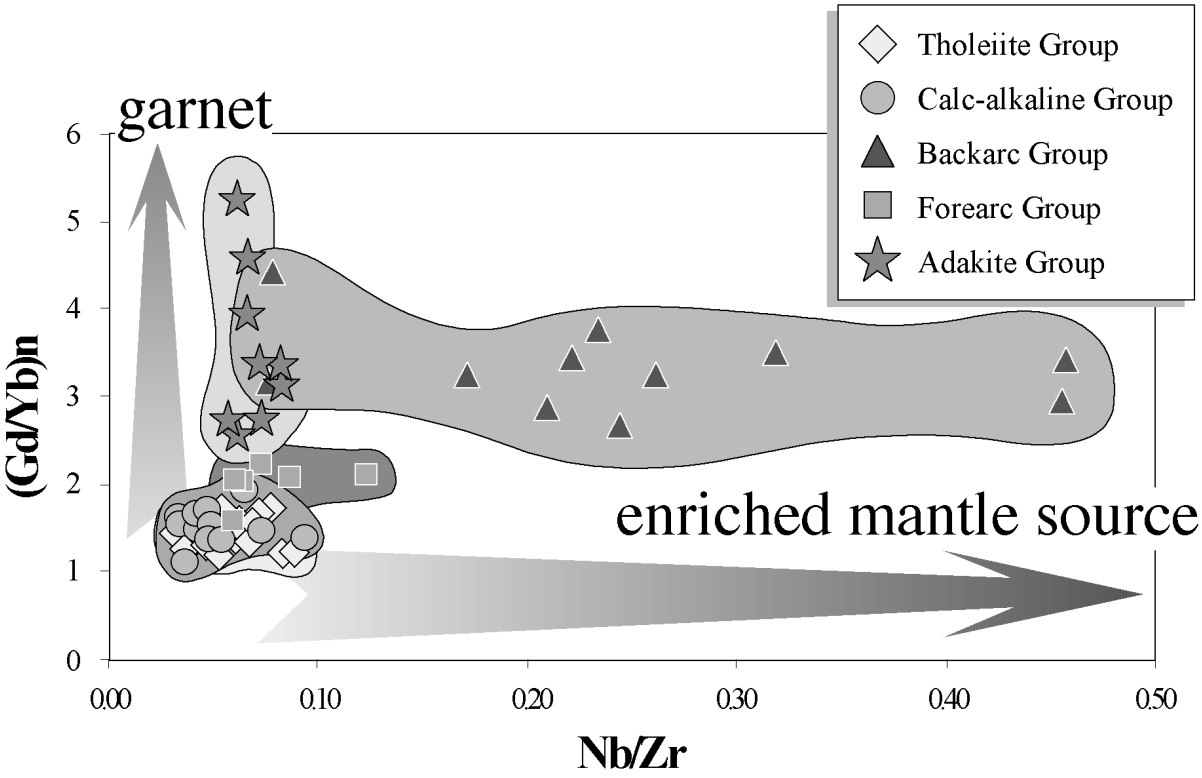

Figure 34: *Plot of (La/Yb)n vs. Nb/Zr indicating different degrees of garnet signature and source depletion for the rocks of the Talamanca area.*

The Th/Yb vs. Ta/Yb discrimination diagram (Fig. 35) after Pearce [1983] can be used to point out source constraints in subduction zone settings. Variations of both ratios simultaneously, Th/Yb and Ta/Yb, are related to the enrichment or depletion of the mantle wedge. However, an increase in these ratios can also be recognised during the evolution of some subduction zone settings (increasing arc maturity). An increase in the Th/Yb ratio alone is predominantly related to the addition of a subduction derived sediment component to the arc wedge mantle.

The samples from the Talamanca area separate into two groups with respect of Th/Yb and Ta/Yb ratio. Precollisional arc magmas display lower ratios than the syncollisional backarc magmas. This will most probably reflect tapping of a more enriched mantle source for the backarc magmas. A within plate enrichment can be precluded since these magmas show no signs of assimilation in the arc crust by other geochemical parameter.

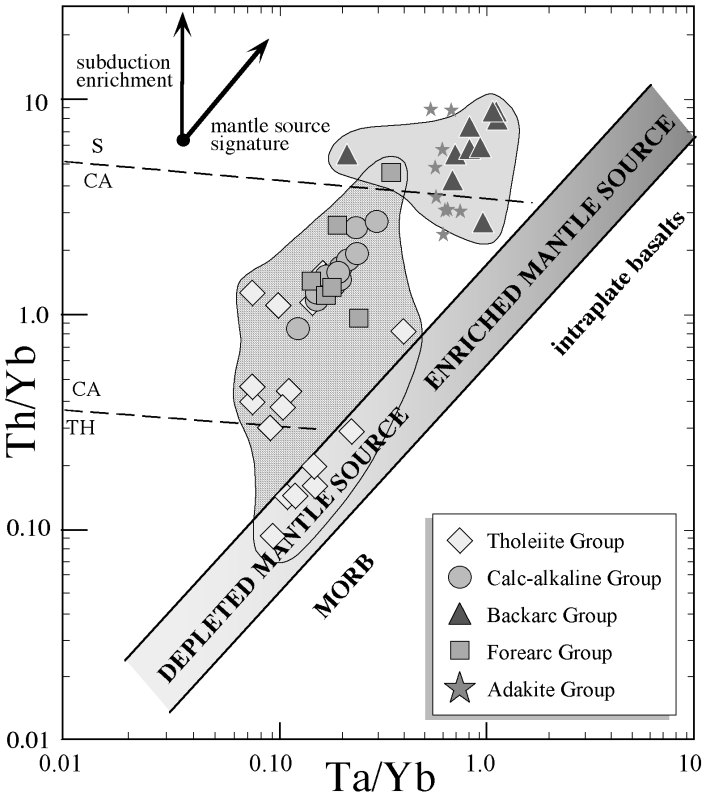

Figure 35: *Th/Yb vs. Ta/Yb discrimination diagram after Pearce [1983]. The SE Costa Rican samples separate into two groups with respect of mantle source enrichment. Backarc samples display the enriched endmember.*

Tectonomagmatic discrimination diagrams (Fig. 36) are used here to further stress the unusually enriched geochemical signature of the backarc samples. These discrimination diagrams are based on relatively immobile trace and minor elements like HFSE. The three ternary plots in figure 37are Ti/100-Zr-Yx3 after Pearce & Cann [1973], Nbx2-Zr/4-Y after Meschede [1986], and TiO2-MnOx10-P2O5x10 after Mullen [1983]. To exclude fractionation effects, the diagrams are strictly applied to basic magmatic rocks with SiO_2 <52% and Na_2O+K_2O < 5%. In the presented discrimination diagrams, the tholeiite group samples and the forearc samples plot into the fields of volcanic arc basalts, island-arc tholeiites, and calc-alkaline basalts like it is expected from their subduction-relation. The backarc samples show however signatures of within plate basalts, within plate alkalic basalts, and oceanic island alkalic basalts, respectively.

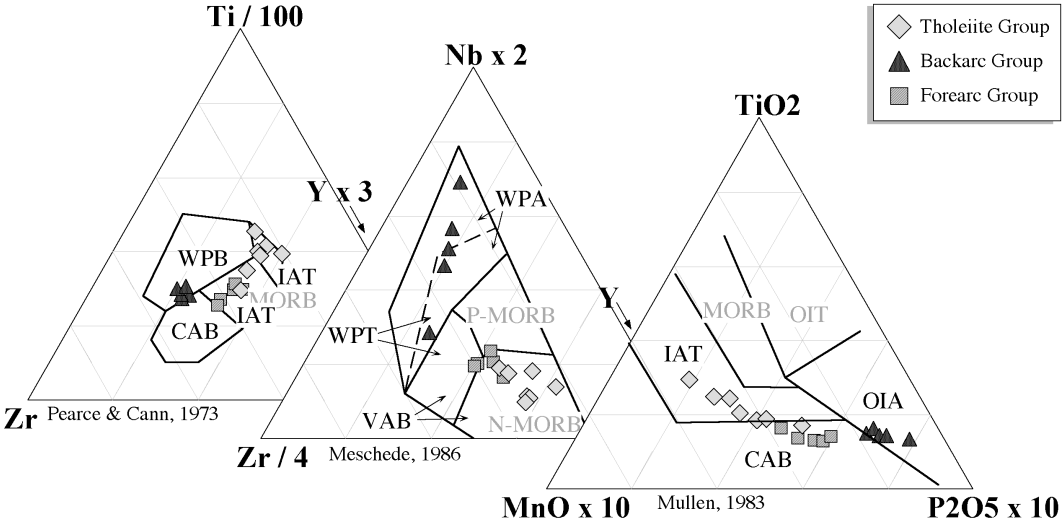

Figure 36: *Ternary tectonomagmatic discrimination diagrams after Pearce & Cann [1973], Meschede [1986], and Mullen [1983], respectively.*

4.2.4 Across-arc variations

Across arc variations in respect of the above outlined parameters for mantle source composition (Nb/Zr) and slab fluid involvement (Ba/La) are presented in Figures 37 and 38 to point to their regional distribution. Some degrees of potential displacements within the older rock series have to be taken into account.
Variations of the fluid (sediment) parameter Ba/La indicates a maximum of this slab contribution within the central arc (Fig. 37). Striking is the absence of these contributions only a few km behind the location of maximal abundance. Backarc magmatism in Costa Rica occurred unusually close to the active arc [Milionis et al., 1986] and is nevertheless virtually free from this subduction component.

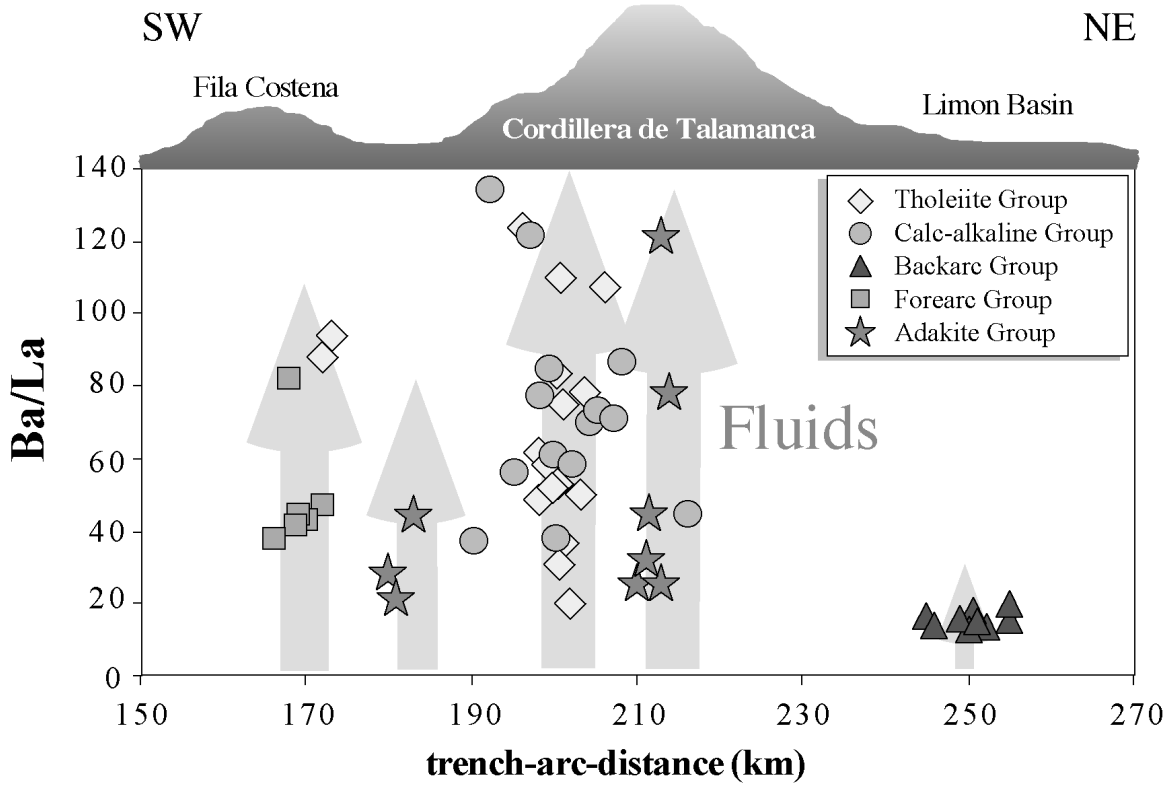

Figure 37: *Plot of Ba/La variations across the arc indicates very different contributions from slab derived fluids to the magmas.*

In a similar plot across the arc, presenting the source parameter Nb/Zr, it is obvious that the backarc rocks are derived from a considerably less depleted mantle than samples of all the remainder groups (Fig. 38). Since the central magmatic arc was active very close to the backarc sample location it is surprising that this mantle domain was obviously not affected by former melting events.

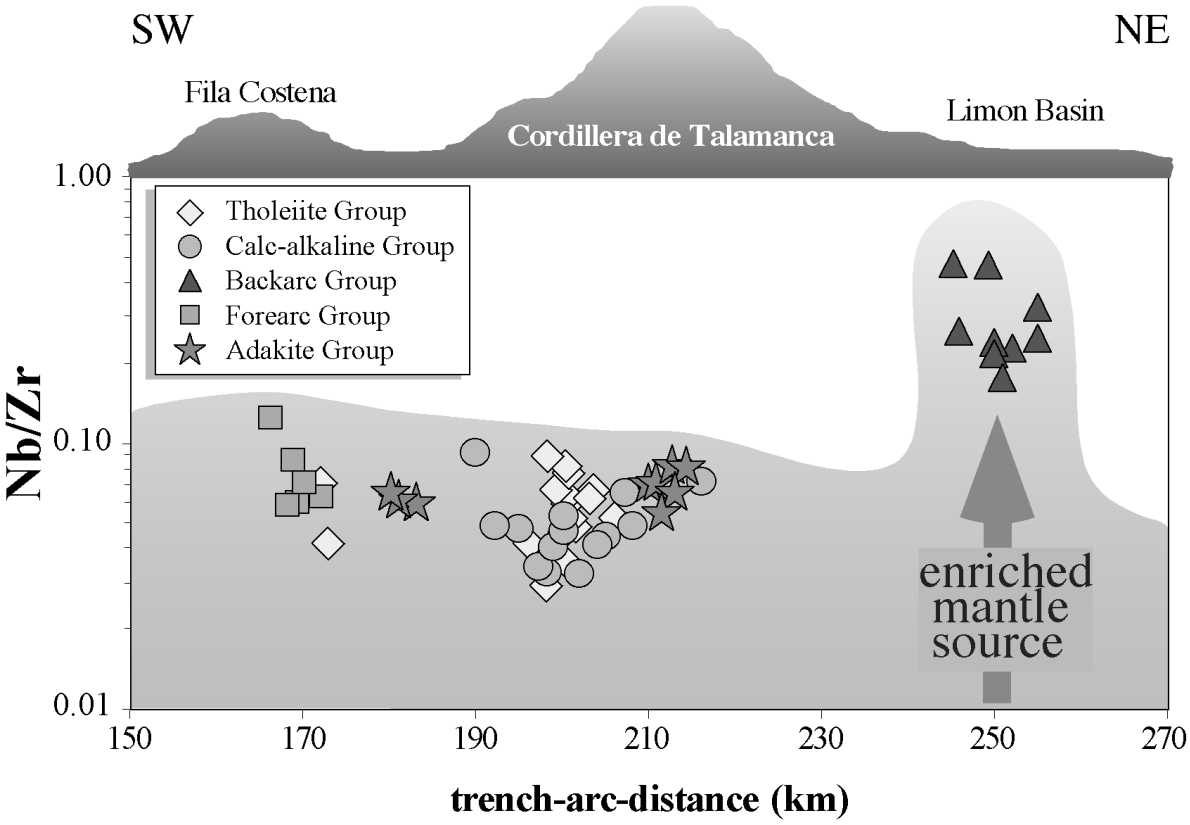

Figure 38: *Variations of the Nb/Zr ratio across the arc indicates that the backarc mantle is unusually enriched in immobile trace element concentrations. Note, that the active central arc is as close as about 10 km to the backarc locations though not probed here.*

Main results of this chapter are:

- Geochemical investigation of the magmatic rocks from the Talamanca area helped to define five distinct rock groups.
- Older rock groups (pre-collisional) are typical arc magmatics showing the trace element signature of the mantel wedge metasomatised by slab derived fluids. There are found both, arc-tholeiitic and calc-alkaline rocks. The latter are generally highly differentiated.
- Backarc rocks in the area show a geochemical tendency towards within plate magmatics or OIB with the corresponding HFSE enriched trace-element pattern.
- In modern arcs rarely occurring slab-melting products (adakites) are present in SE Costa Rica.

5 Isotopes

5.1 Radiogenic Isotopes

5.1.1 Sr- / Nd- isotopic compositions

Isotope data represent a powerful tool to substantiate the findings of considerable source compositional differences between the rock groups of the Talamanca area.
In this context, $^{87}Sr/^{86}Sr$ and $^{143}Nd/^{144}Nd$ isotope measurements were carried out on 24 selected whole rock samples.

The initial isotopic composition of the rocks provides information about the (mantle-) sources of the magmatic rocks as well as about processes by which their chemical and isotopic compositions are modified (e.g. crustal contamination, seawater interaction).
When the age of the rock is known, its initial isotopic ratios can be calculated by using the basic geochronological equations:

$$\frac{^{87}Sr}{^{86}Sr} = \left(\frac{^{87}Sr}{^{86}Sr}\right)_{initial} + \frac{^{87}Rb}{^{86}Sr}(e^{\lambda t} - 1) \qquad [5\text{-}1]$$

$$\frac{^{143}Nd}{^{144}Nd} = \left(\frac{^{143}Nd}{^{144}Nd}\right)_{initial} + \frac{^{147}Sm}{^{144}Nd}(e^{\lambda t} - 1) \qquad [5\text{-}2]$$

which are transformed to:

$$\left(\frac{^{87}Sr}{^{86}Sr}\right)_{initial} = \frac{^{87}Sr}{^{86}Sr} - \frac{^{87}Rb}{^{86}Sr}(e^{\lambda t} - 1) \qquad [5\text{-}3]$$

$$\left(\frac{^{143}Nd}{^{144}Nd}\right)_{initial} = \frac{^{143}Nd}{^{144}Nd} - \frac{^{147}Sm}{^{144}Nd}(e^{\lambda t} - 1) \qquad [5\text{-}4]$$

The overall isotopic variability of the SE Costa Rican magmatic rocks is relatively restricted with values ranging between $^{87}Sr/^{86}Sr$: 0.70332 – 0.70415 and $^{143}Nd/^{144}Nd$: 0.512953 – 0.513045. The isotopic data display an unusual trend across the mantle array (Figure 39). Furthermore, the data are not simply trending horizontally across and out of the mantle array, but describe instead a slightly upwards directed trend (a positive correlation). Thus, isotopic variations cannot be explained by a simple two-component mixing model.
The SE Costa Rican data set is consistent with general Central American isotopic variations [Feigenson & Carr, 1986, 1993]: All Central American volcanic samples display isotopic variations across the mantle array. However, an influence of old continental crust like it can be seen in Guatemalan volcanics is absent from the investigated area. Incorporation of old continental material in the source of southern Costa Rican rocks does not take place since such a process would result in a negative correlation in Sr-Nd-isotope-space. Exactly these negative trends are displayed by the majority of the arcs world-wide (Figure 39). A negative Nd-Sr correlation accounts for the incorporation of varying amounts of terrigenous sediment in the magma [Faure, 1986].
However, in contrast to MORB, the source of SE Costa Rican magmas is isotopically slightly enriched as evidenced by an offset towards bulk earth composition. This fact demands for an enrichment process that could either be related to an earlier (>200 Ma) stage of melting in this region [Feigenson & Carr, 1993] or that could be related to a process of mantle wedge modification by subducted sediments [Faure, 1986].

Figure 39 displays the epsilon notations [DePaolo & Wasserburg, 1976] which are calculated by using the following equations:

$$\varepsilon_{Nd} = \left[\frac{(^{143}Nd/^{144}Nd)_{initial}}{I^{t}_{CHUR}} - 1 \right] * 10^{4} \qquad [5\text{-}1]$$

$$\varepsilon_{Sr} = \left[\frac{(^{87}Sr/^{86}Sr)_{initial}}{(^{87}Sr/^{86}Sr)^{t}_{UR}} - 1 \right] * 10^{4} \qquad [5\text{-}2]$$

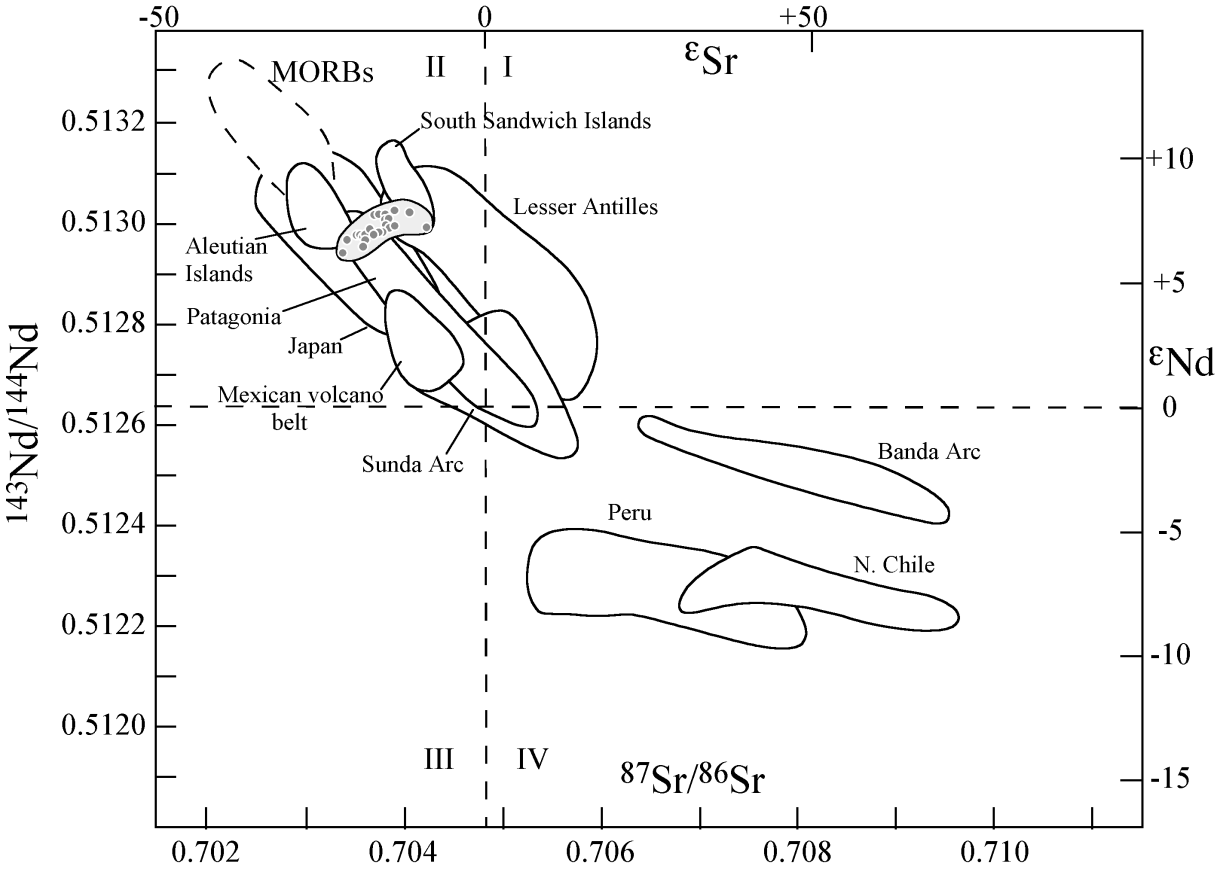

Figure 39: *Diagram of $^{143}Nd/^{144}Nd$ vs. $^{87}Sr/^{86}Sr$ presenting the data set from the Talamanca area in comparison to data fields from island arcs, continental margins and MORBs as compiled by Faure [1986]. The trend of the Talamanca data is unusual across the mantle array.*

Figure 40 presents the Nd-Sr isotopic compositions of the SE Costa Rican samples. In this close-up view it is evident that the isotopic compositions of the rocks are considerably offset from local MORB and OIB compositions towards higher Sr-isotopic ratios. Offset is largest within the Tholeiitic and Calc-alkaline Groups, it is small for samples of the Backarc Group. Adakite Group samples display a simple, almost horizontal trend across the mantle array, varying virtually only in Sr isotopic composition.

The evolutionary trend of the SE Costa Rican magmatics within this isotope diagram goes from higher Nd isotopic values to steadily increasing Sr values and thereafter sharply bending towards low Sr- and low Nd-isotopic compositions.
Additionally presented are fields from local magmatic systems like the East Pacific Rise (EPR), Galapagos Spreading Centre (GSC), and Galapagos Islands (GI) as well as ridges and seamounts on the Cocos Plate which were produced by the Galapagos hot spot. Adakite Group samples clearly reach into the field of ridges which also includes the subducted Cocos Ridge.

The offset of the arc magmatic samples to higher $^{87}Sr/^{86}Sr$ isotopic values is related to slab derived contributions to their magma source like subducted seawater and marine sediments. A second variation vector in this diagram describes the compositional variations between a depleted MORB source, represented by the EPR and GSC, and an enriched mantle part, displayed by the GI and seamounts. These different mantle compositions are also reflected in the SE Costa Rican samples. Their generation will be discussed in Chapter 6.

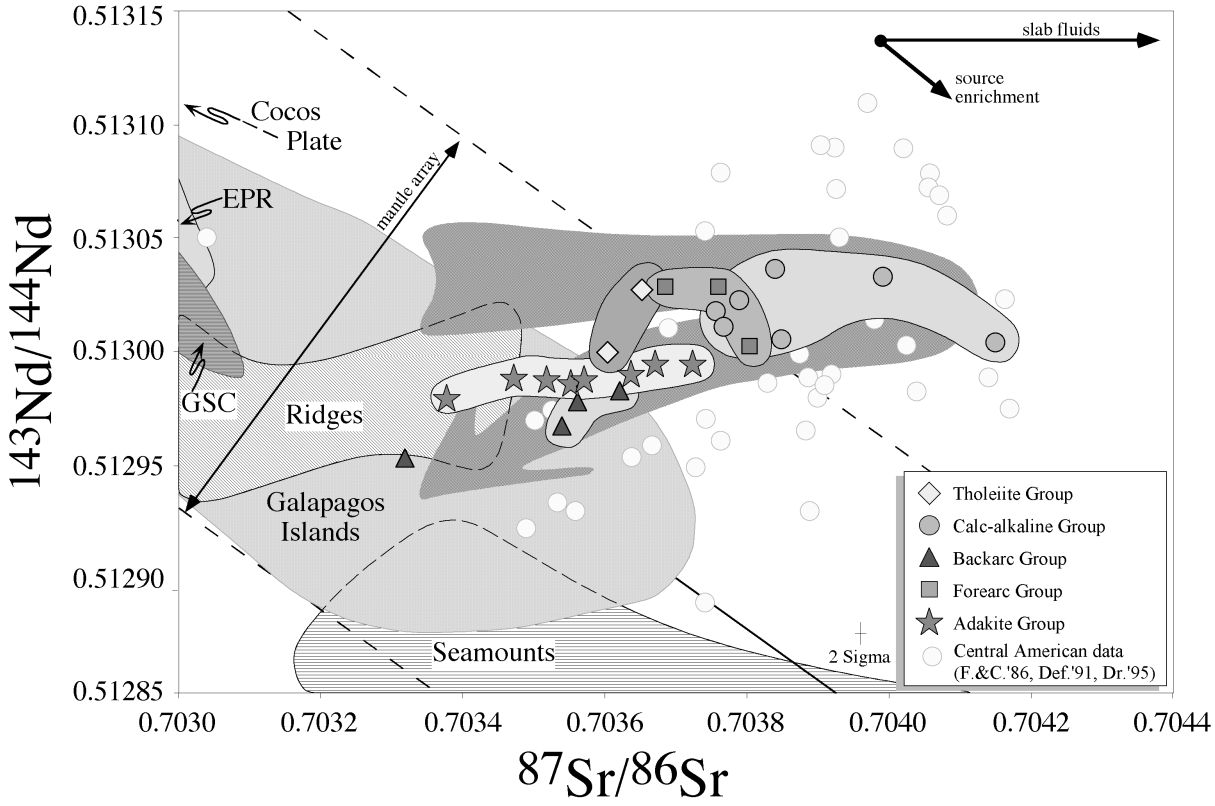

Figure 40: *Samples from the Talamanca area in a diagram of $^{143}Nd/^{144}Nd$ vs. $^{87}Sr/^{86}Sr$. The trend across the mantle array evolves with time back to the array (indicated by broad arrow). Abbreviations for literature data of Central American volcanics mean: F. & C.'86: Feigenson & Carr [1986], Def.'91: Defant et al. [1991], Dr.'95: Drummond et al. [1995]. The Fields of EPR, GSC, and GI are from White et al. [1990], the fields of Ridges and Seamounts are from v. d. Bogaard & Werner [1998].*

5.1.2 Pb- isotopic compositions

Lead isotopic compositions were determined on carefully selected whole rock samples.
The values
Figure 41 displays the compositional variability of the south Costa Rican samples in comparison with local magmatic systems (EPR, GSC, GI) and pelagic pacific sediments.

SE Costa Rican samples show a clear grouping into two suites that are distinct in their $^{206}Pb/^{204}Pb$ ratios (Fig. 41). The low-$^{206}Pb/^{204}Pb$ group consists of the Tholeiitic Group, Calc-alkaline Group, and Forearc Group. The high-$^{206}Pb/^{204}Pb$ assemblage comprises the Backarc Group and Adakite Group. Low-$^{206}Pb/^{204}Pb$ members plot near or within the fields of local depleted mantle sources (EPR, GSC) and in the field of magmas from active volcanoes in Guatemala [Carr et al., 1996]. High-$^{206}Pb/^{204}Pb$ samples plot within the field of the Galapagos Islands, which also characterises the present day volcanism in northern Costa Rica [Carr, pers. comm.].

This grouping clearly reflects the presence of two different mantle sources underneath SE Costa Rica. The mantle source of pre-collisional magmatics is more depleted and uniform with the northern end of the Central American arc system. The other source, showing HIMU tendencies (high $^{206}Pb/^{204}Pb$) is clearly influenced by the Galapagos hot spot. Since the adakites seem to be partial melting products of the Cocos Ridge, it is not surprising that they adopted the Galapagos isotope signature.
Variations of the magmatic rock compositions in $^{207}Pb/^{204}Pb$ and $^{208}Pb/^{204}Pb$ towards the sediment field are low, which means only small amounts of sediment derived lead admixed to their sources.

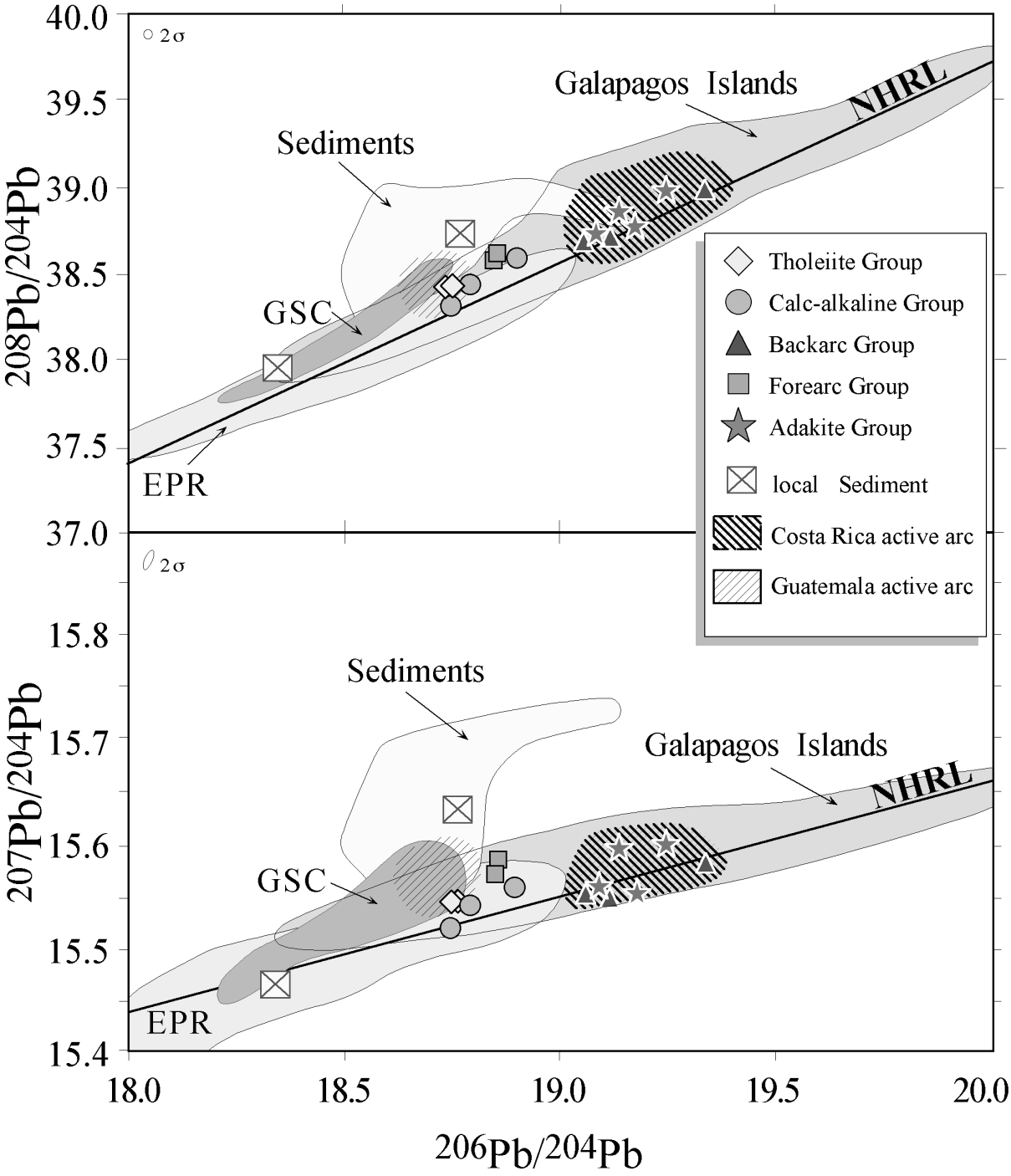

Figure 41: *Lead isotope diagrams show the Talamanca data in comparison with locally active magmatic centres (EPR, GSC, GI [White et al., 1993]) and pelagic pacific sediments [Ben Othmann]. Two data points for end-member compositions of sediments drilled off Guatemala are from GERM [1997]. The carbonaceous sediment plots outside the sediment data field. Shaded fields are active Guatemalan volcanoes [Carr et al., 1996], and active Costa Rican volcanoes [Carr, pers. comm.].*

5.2 Stable Isotopes

Oxygen isotopic compositions are determined on phenocrysts (Ol, Cpx, Hbl, Qz) from the volcanic rocks. This technique bears the advantage that secondary alteration effects are virtually excluded. All data are fractionation corrected to olivine compositions.

Calculation of the $\delta^{18}O$ values in per mil relative to the standard V-SMOW is done according to the equation:

$$\delta^{18}O = \left[\frac{(^{18}O/^{16}O)_{sample}}{(^{18}O/^{16}O)_{standard}} - 1 \right] * 10^3 \qquad [5\text{-}3]$$

$\delta^{18}O$ values of the samples vary between 5.1 and 6.9 ‰. Variations of the oxygen isotopic composition with strontium isotopic compositions are displayed in Figure 42. The majority of samples lie above the 5.2 ‰ value of upper mantle olivine [Eiler et al., 1997]. This is a common feature for arc volcanics that are easily subdued to source contamination and/or crustal contamination with a high $\delta^{18}O$ component [Taylor, 1986].

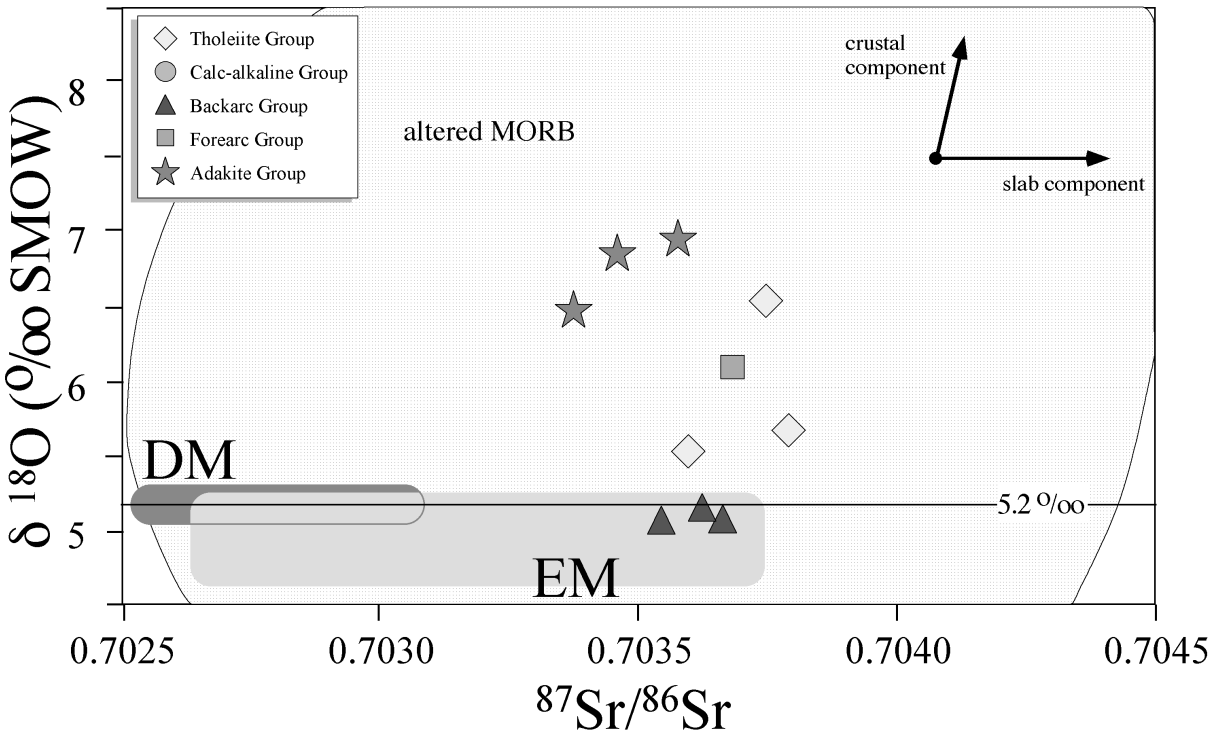

Figure 42: *Generalised fields depicting the co-variation of oxygen$_{(Ol)}$ and strontium isotope compositions of the SE Costa Rican samples and oceanic basic lavas. The field for altered MORB is from Taylor [1986].*

The adakites plot right into the field of altered MORB. From Figure 43 it is obvious that they must be derived from the upper, low temperature altered oceanic crust.
Phenocrysts of the backarc volcanic rocks fall below the 5.2 ‰ value of upper mantle olivine but within the field of the Galapagos mantle source. Values below 5.2 ‰ are indicative for a HIMU OIB source [Eiler et al., 1997]. High temperature altered oceanic crust is a further potential source for low $\delta^{18}O$ values (see Figure 43). However these backarc samples are

compositionally almost identical to primary mantle melts with high MgO, Ni, and Cr which precludes considerable contamination processes.

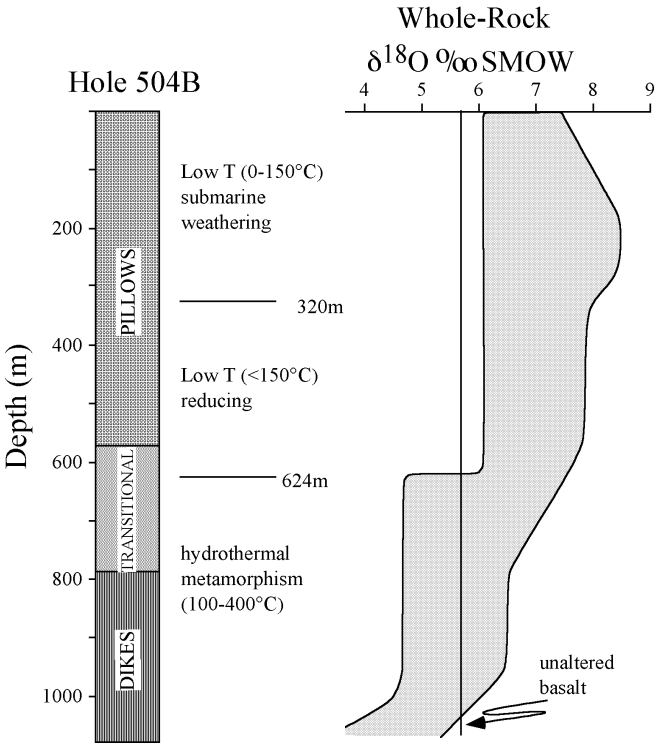

Figure 43: *Profiles of lithologic units and oxygen isotope variations in ODP drilling Hole 504B near the Galapagos Spreading Centre (GSC) from Alt et al. [1986].*

Main results of this chapter:

- Older rock groups (arc-tholeiitic and calc-alkaline) show Nd- and Pb-isotopic signatures of a relatively more depleted mantle source. Their O- and Sr-isotopic signature points to modification of their source by slab derived fluids and crustal assimilation.
- Backarc rocks in the area show isotopic ratios that are closer to the HIMU endmember composition of the Galapagos plume and show no direct fluid or sediment involvement in their mantle source.
- Adakites show isotopic variations which may reflect different portions of the melted oceanic crust that was variably altered at low temperatures.

6 Geochemical Modelling

It is now generally accepted that most magmas at subduction zones are generated in the mantle wedge above the subducting plate [Gill, 1981; Green, 1982; Wyllie, 1982; Arculus & Powell, 1986].
This mantle wedge is significantly modified by the addition of fluids and melts derived from the subducting oceanic crust and its sediment cover [White & Patchett, 1984; Tera et al., 1986; Ellam & Hawkesworth, 1988; von Huene & Scholl, 1993; Miller et al., 1994; Ishikawa & Nakamura 1994].
The transfer of elements from the subducting plate to the sub-arc mantle takes place via dehydration of the subducting basaltic crust and related sediments or by melting of the sediment cover [Nichols et al., 1994; Elliot et al., 1997; Hawkesworth et al., 1997].
Melting of the basaltic crust itself occurs relatively seldom at modern arcs and is confined to locations with unusually 'hot' slab geotherms and young subducting crust [Peacock, 1990; Defant & Drummond, 1990a,b; Peacock et al., 1994; Yodgodzinski et al., 1995; Stern & Kilian, 1996].
Further modification of the arc magmas can be expected during their ascent through the mantle wedge and overlying crust [DePaolo, 1981; Hildreth & Moorbath, 1988; Kelemen et al., 1990, 1993; Navon & Stolper, 1987; Aitcheson & Forrest, 1994].

In the preceding chapters I have documented that these processes are reflected in the geochemistry and isotopic composition of the Talamanca rocks. Aim of the present chapter is to use geochemical modelling as a means of hypothesis testing in order to verify the above constrained models.

As a prerequisite to modelling, the samples have to be recalculated to their primary, fractionation free status. 8 wt% MgO were taken to represent the primitive compositions as proposed by Klein and Langmuir [1987]. The backarc samples were recalculated to 10 wt% MgO since they are very primitive rocks and some of them already contain that amount of MgO. For the correction procedure, a correlation of each element versus MgO was plotted for each sample suite. Regressions through co-genetic series gave the recalculated concentration of each element (e.g. La_8) at 8wt% MgO.
Co-genetic series are in some instances well defined like for the backarc group: a rock suite from Bribri (BRI) and a rock suite from Guayacan (GUA). However, for other suites no clear trends exist. For the forearc group only a few samples define a poor correlation, for the tholeiitic group only those samples displaying definitive tholeiitic chemistry were selected, and for the calc-alkaline group, the entire sample set was taken as co-genetic.
With respect to the calc-alkaline group, this method is only a crude approach because all rocks from this group contain less than 4 wt% MgO. Klein & Langmuir [1987] originally applied this calculation to rock compositions between 8.5 and 5 wt% MgO.
Rocks with strong fractionations, deviating from the general trend (e.g. Eu fractionations in two samples of the calc-alkaline group) were excluded.

6.1 Partial melting

Mantle source compositions of the different Talamanca rocks were calculated by a forward batch partial melting process using REE concentrations of the assumed source types. Source REE pattern were adjusted to fit the fractionation corrected pattern of each rock group by varying source composition, source mineralogy, and melting degree.

The basic equation for modal batch melting is [after Shaw, 1970]:

$$C^i = \frac{C_0^i}{D_{RS}^i + F(1 - D_{RS}^i)} \qquad [6\text{-}1]$$

Where C_0^i is the initial source concentration of element *i*, D_{RS}^i is the bulk partition coefficient of the residual solid, and F is the melt fraction.

The REE concentrations for depleted mantle (DM) and primitive mantle (PM) as well as those for the sediments are taken from GERM [1998].

Modelling calculations reveal that not only melting degrees are different for the four mantle derived rock groups, but also mineralogy and composition.
Mantle source compositions of the four groups vary between strongly depleted and strongly enriched in LREE. Tholeiite group samples have a slightly depleted source, as have some of the forearc rocks suggesting the absence of a sedimentary contribution. The second suite of forearc rocks is instead derived from an enriched mantle, or alternatively, from a source contaminated by considerable amounts of sediment. The source of the calc-alkaline rocks can be modelled by a mantle that contains up to 1-2 % of marine sediment. The amount of sediment contribution depends on the primary degree of mantle depletion. The source of the alkalic backarc rocks is highly enriched in LREE by intra-mantle enrichment since sediment assimilation could be ruled out in the preceding chapter.

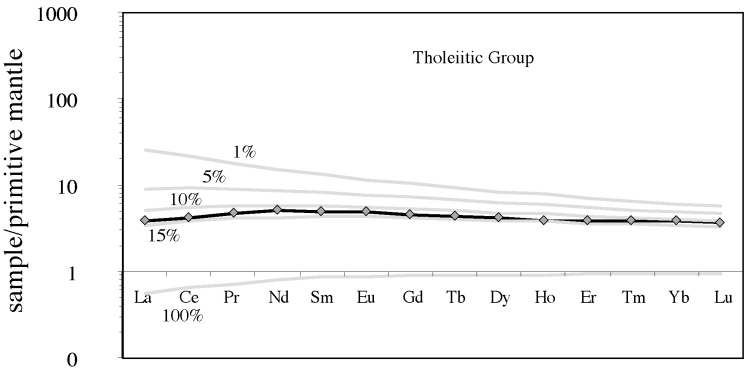

Figure 44: *Batch melting models calculated to the REE pattern of the rocks point to different source mineralogy, geochemistry and melting degrees necessary to fit the curves.*
Fig. 44a: Model for the tholeiitic group

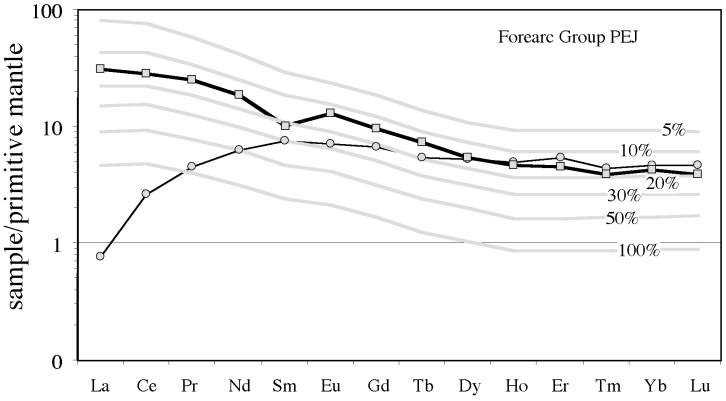

Figure 44b: Batch melting model for the forearc group, suite PEJ.

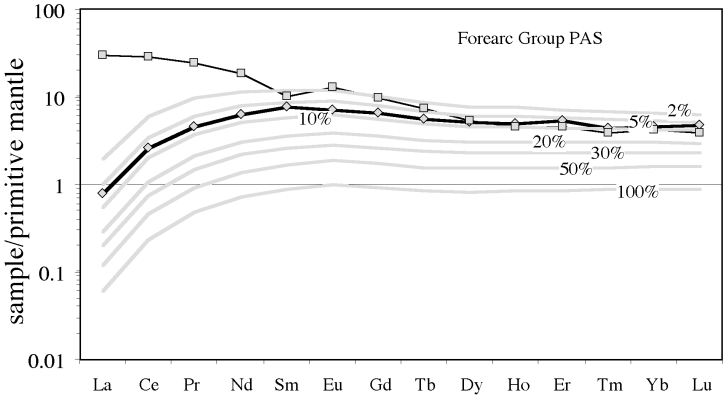

Figure 44c: Batch melting model for the forearc group, suite PAS.

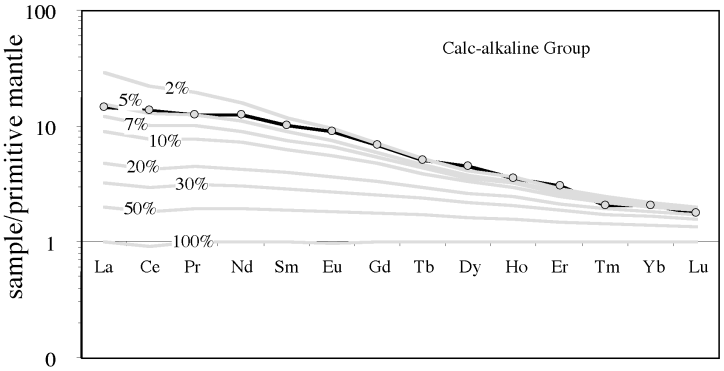

Figure 44d: Batch melting model for the calc-alkaline group.

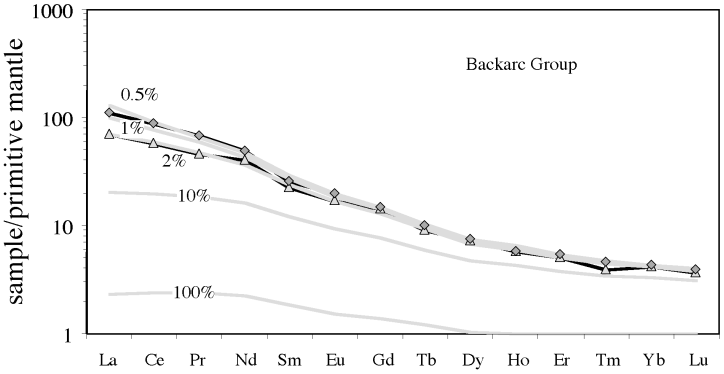

Figure 44e: Batch melting model for the backarc group.

Calculation show that the source mineralogy is also variable, but garnet is present throughout. The mantle melting products are derived from a peridotitic mantle, which contains minor amounts of garnet.
The least garnet contents in mantle mineralogy are found for the tholeiites (1.5 %) and the forearc rocks (1-2 %). The latter could also be modelled with a spinel-peridotite (3 % spinel), when assuming a more depleted source and subsequent assimilation of higher amounts of arc sediment.
The Garnet content in the source of the alkalic backarc rocks has to be higher (6 %), meaning a deeper source location.
The applied method of fractionation correction (to 8wt% MgO) obviously failed for the highly evolved, fractionated and assimilated calc-alkaline rocks since the results point to too high garnet contents in the hypothetical mantle source.

Melting degrees for batch partial melting of peridotite vary from 0.5-2% for the alkalic backarc samples to as high as 10-15% for the tholeiitic samples. For the calc-alkaline forearc samples, the melting degree was calculated to 5-10%, or in an alternative model with higher degrees of melting between 10 to 20% of a depleted mantle source and subsequent voluminous assimilation of arc sediments.
Calc-alkaline magmas in the central arc are derived from comparatively lower degrees of melting (2-5 %).

Table 6-1: *Parameters for melting models on the five rock groups*

Group	Suite	Source	Mineralogy	Melting degree
Tholeiite	flat pattern suite	slightly depleted (DM-PM 1:1)	grt-peridotite (grt 1.5%)	10-15%
Backarc	BRI+GUA	enriched in LREE (EM)	grt-peridotite (grt 3%)	0.5-2%
Forearc	PEJ	enriched in LREE (PM+ ass. arc SED)	grt-peridotite (grt 2%)	5-10%
		enriched in LREE (DM++ ass. arc SED)	sp-peridotite (sp 3%)	10-20%
	PAS	highly depleted (DM, no SED)	grt-peridotite (grt 1%)	5-10%
Calc-alkaline	entire group	slightly enriched (PM)	grt-peridotite (grt 7%)	2-5%
		slightly enriched (1/3DM+2/3PM+1%SED)	grt-peridotite (grt 7%)	5%
		slightly enriched (DM+2%marine SED)	grt-peridotite (grt 7%)	2-5%
Adakite	flat pattern suite	basalt (MORB+1/4OIB+1/5SED)	hbl-eclogite (grt 20%)	50%
	steep pattern suite	slightly evolved tholeiite (E 152)	hbl-eclogite (grt 15%)	20-30%

6.2 Mantle source – constraints from isotopes

The $^{87}Sr/^{86}Sr$ ratios of magmatic rocks in island arcs are primarily determined by the isotopic characteristic of the mantle wedge [Faure, 1986]. However, it is further modified by the subducted hydrothermally altered oceanic crust, the terrigeneous sediment of the oceanic crust, the country rocks in the overriding crust, and seawater that could interact with the hot volcanic rocks during their submarine eruption.

These effects can be quantified for the Talamanca rocks by modeling their isotopic compositions. Calculations in the Sr-Nd-isotope system point to different primary mantle source compositions and different degrees of sediment involvement (Fig. 45). Mantle source compositions vary along an array between a more depleted end-member (DM) on the one hand and a more enriched one (EM) on the other hand (Fig. 45, negative trend on the left). The depleted end-member displays isotopic compositions that are currently probed by the EPR or GSC. Older rocks in the Talamanca area, i.e. samples from the tholeiitic group and from the calc-alkaline group, own characteristics that derive from such mantle compositions.
The enriched end-member is represented by the Galapagos plume material. Galapagos plume derived rocks themselves display intermingling of enriched and depleted source components. The enriched end-member source composition is present in the Talamanca rocks within the samples of the backarc group. Except for one sample (NEI 18), the enriched source of these backarc rocks seems to document some degree of intermingling with the local arc wedge mantle (Fig. 45, positive trend in the centre).
Incorporation of sediment (or sediment derived fluids) in the magma supplied by the subducting oceanic plate shifted the mantle wedge composition to higher Sr isotopic ratios, away from the mantle array (Fig. 45, horizontal trend). The resulting, sediment enriched sub-arc mantle may be called a modified mantle (MM). The effect is clearly displayed in samples of both older rock groups, the tholeiitic and the calc-alkaline group. The more pronounced displacement of the relatively younger calc-alkaline samples points out that the source enrichment process is time related.

The adakite samples show a remarkably linear arrangement in the diagram with almost exclusively variations in the Sr-isotopic composition. The non-radiogenic end of this trend plots into the field of Galapagos basalts, the radiogenic end reaches out of that field. This linear arrangement of the adakite samples can be interpreted as a mixing array between differing relative proportions of low temperature seawater altered and unaltered basalt from the oceanic crust pile that was melted to form the adakites (Fig. 45, short horizontal trend). The higher the degree of melting of the oceanic slab, the more will the adakite isotopic composition be governed by the composition of the (unaltered) basaltic source rock. The lower the degree of melting, the higher will be the relative proportion of altered material (and marine sediments) in the composition of the newly formed adakite.

Binary mixtures of the two elements Sr and Nd with different isotope ratios are calculated with the equation (Faure, 1986):

$$R_M^X = \frac{R_A^X X_A f + R_B^X X_B (1-f)}{X_A f + X_B (1-f)} \qquad [6\text{-}2]$$

Where *A* and *B* are the two mixing endmembers, *X* is the element of interest, R^X is the isotope ratio of *X* and *f* is the weight fraction of A. $R^X{}_M$ is the isotope ratio of the mixture.

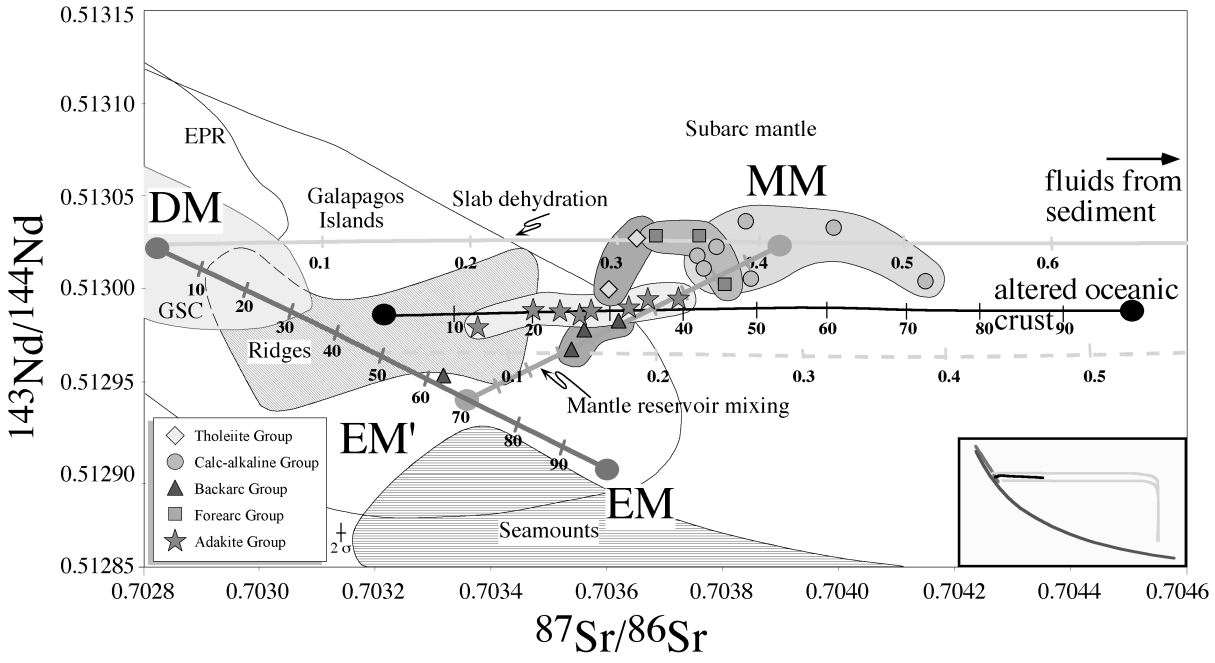

Figure 45: *Modelling in the Nd-Sr-space shows different primary mantle enrichments in Nd isotopic ratios and addition of slab-fluids to the mantle source.*

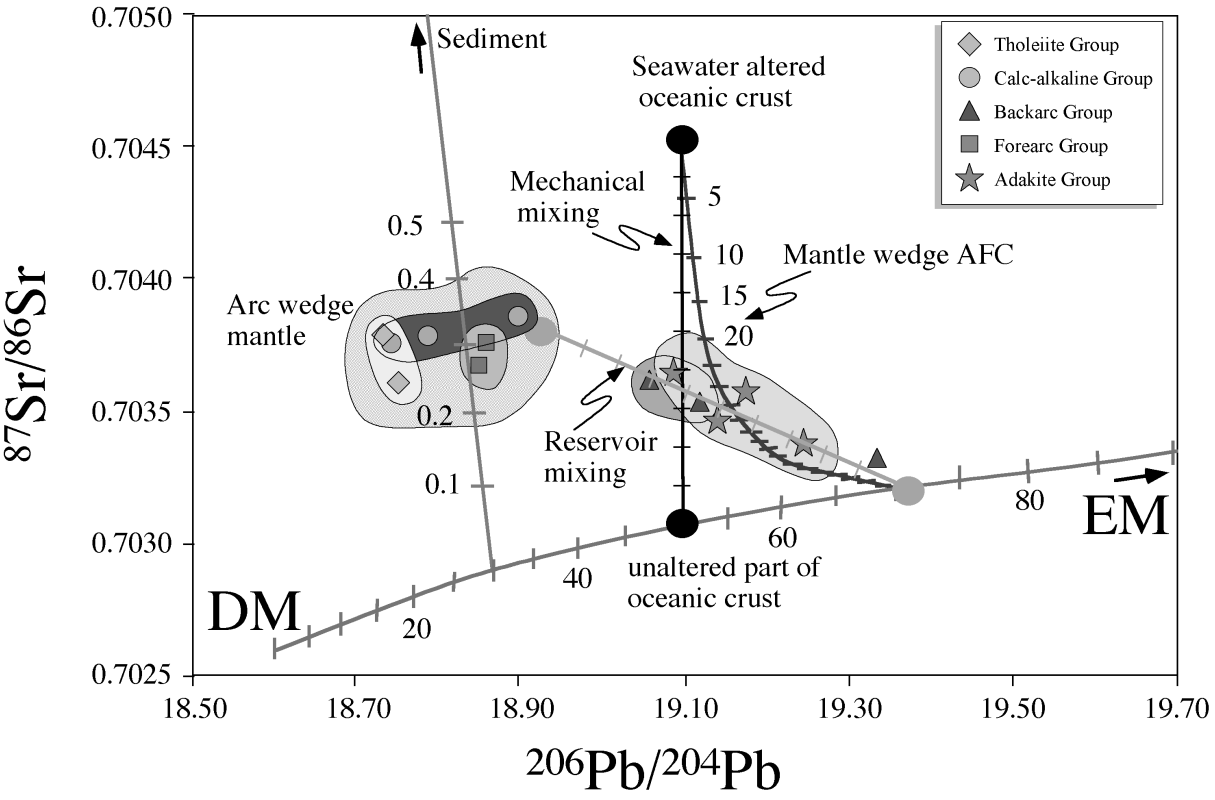

Figure 46: *Sr vs. Pb isotopic ratios and the models of slab fluid addition to different mantle sources and the adakite generation by slab melting*

In the $\delta^{18}O$ vs. Sr isotopic space (Fig. 47), forearc and arc-tholeiitic samples display evidence for source contamination as well as crustal contamination. Free from these effects are obviously the backarc samples. They may be derived from unmetasomatised plume mantle material. The adakitic samples show about 15 to 25 % of highly altered basalts in their parental source rocks.

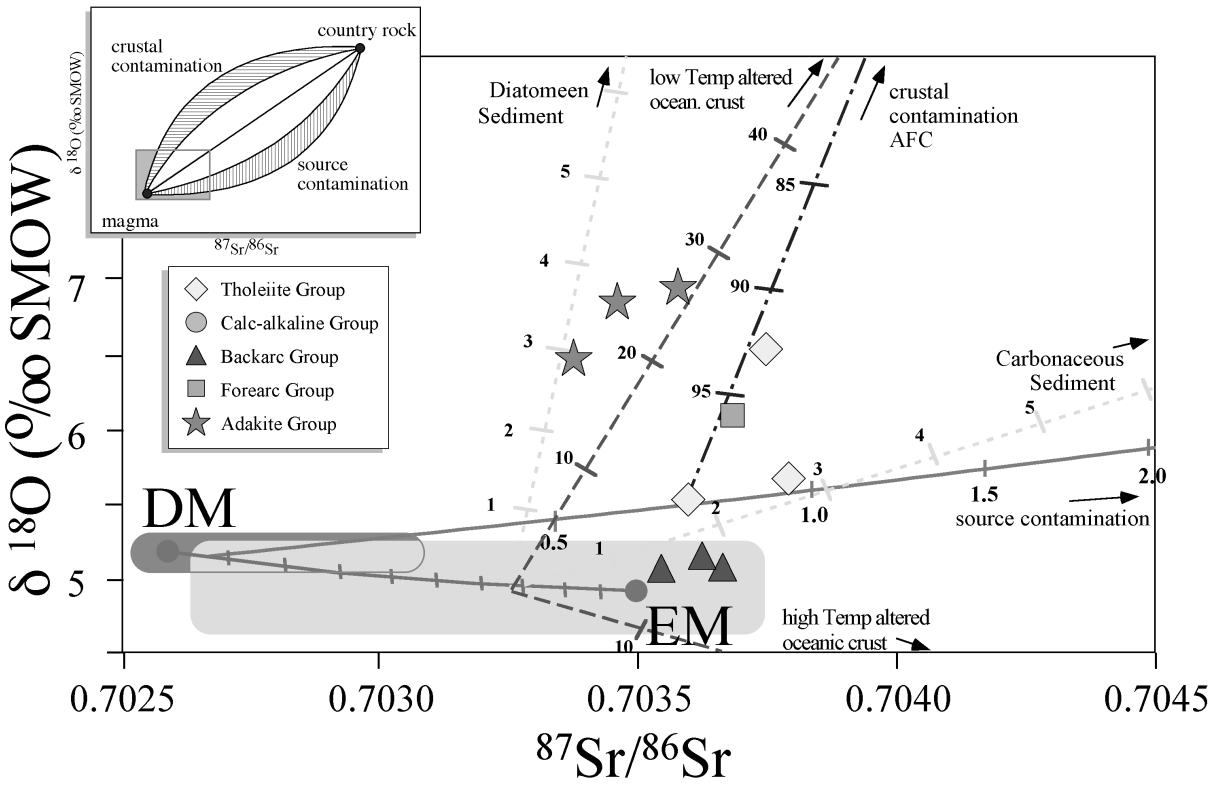

Figure 47: *$\delta^{18}O$ variations with $^{87}Sr/^{86}Sr$ and models of source contamination, crustal assimilation for the tholeiites and forearc rocks. Melting of altered basalt is favoured for the adakites, backarc rocks show no variations with these components.*

6.3 Mantle source – constraints from trace elements

A plot of $(La/Yb)_n$ versus Ba/La can be used to outline the compositional variability of magmatic rocks in the Talamanca area and to obtain melting and source constraints (Fig. 48). In addition to the samples of the five rocks groups, fractionation corrected average compositions of each rock group are displayed by the dark coloured symbols. Large circles mark mantle source compositions and contaminating marine sediments after GERM [1998].
The spread of the data in respect of the Ba/La ratio that is observed for samples of the tholeiitic group, calc-alkaline group, and forearc group can be explained by an admixture of a small amount of sediment (up to 1%) to the mantle source of those magmatic rocks (Fig. 48, lower curve).
Subsequent melting of this modified source is responsible for the variations in $(La/Yb)_n$ of this data array (Fig. 48, curve in the centre). The higher the melting degrees are, the lower is the $(La/Yb)_n$ ratio. This fact is displayed by the relative differences in the ratio of samples from the tholeiitic group and samples from the calc-alkaline group. In chapter 6.1 it was shown, that the tholeiites are essentially products of higher degrees of melting than the calc-alkaline rocks.
Modelling of the backarc rocks which are characterised by high $(La/Yb)_n$ ratios and low Ba/La ratios show that these rocks can only be derived from an enriched source that is essentially free of sedimentary contribution (Fig. 48, curve on the left). Otherwise, the modelled curve would not pass through the backarc data and would instead bend with a flat angle to higher Ba/La ratios. It is also obvious, that melting degrees have to be low (0.5 to 2%), to obtain the prominent $(La/Yb)_n$ ratio of the backarc samples. By plotting the corrected concentrations it can be shown that fractionation affects the $(La/Yb)_n$ ratio only to minor degrees, and could not obscure the effect of low degree melting of an enriched source.

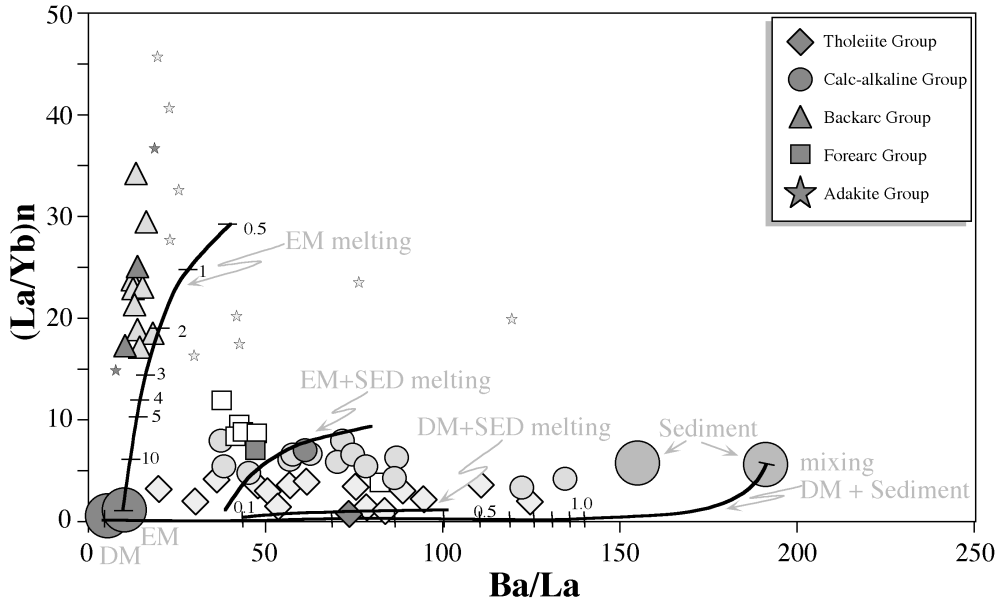

Figure 48: *(La/Yb)n vs Ba/La with the outlined melting models, showing different melting degrees, source enrichment and sediment content.*

Adakites could successfully be modelled in respect of these trace element variations by partial melting of a basaltic rock with some additional percentages of marine sediment (Fig. 48, negative curve). Derived melting degrees point to 25% and 55%, respectively for the fractionation corrected average compositions. These suggested high degrees could however

also be displayed due to the offset of the data points as a consequence of mantle AFC processes (Fig. 48, curve F). Mantle AFC processes lower the $(La/Yb)_n$ ratio, and depending on the type of assimilated mantle material (DM/EM or MM including the sediment contribution), a slight shift of the data may occur towards higher or lower Ba/La ratios.

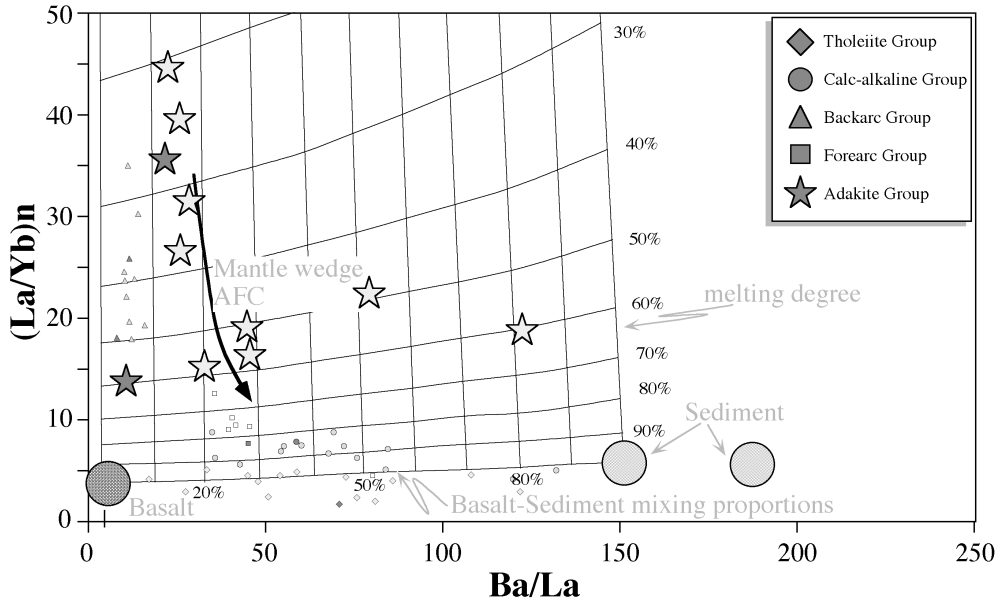

Figure 49: *(La/Yb)n vs Ba/La shows melting degrees for the adakites, which are however simultaneously covered by the effect of mantle wedge assimilation.*

Table 6-2: *Modelling parameters for mixing models. Data are from GERM [1998]*

	DM	**EM**	**SED** Diat Mud	**SED** Carb
Sr	13.2	17.9	336	1504
Ba	1.2	4.77	3941	2145
La	0.31	0.66	20.66	14.22
Nd	0.86	1.11	19.00	10.13
Yb	0.4	0.3	2.68	1.57
$^{87}Sr/^{86}Sr$	0.70261	0.70338	0.70763	0.70858
$^{143}Nd/^{144}Nd$	0.513115	0.512931	0.51274	0.51242
$^{206}Pb/^{204}Pb$	18.54	19.65	18.783	18.314
$^{207}Pb/^{204}Pb$	15.51	15.64	15.631	15.463
$^{208}Pb/^{204}Pb$	38.06	39.43	38.673	37.940

6.4 Adakites- Eclogite partial melting and mantle wedge assimilation

Since adakites are partial melts of subducted oceanic crust, batch melting calculations started with a basaltic parental material in the garnet stability field.
Modelling calculations were done on the REE (Fig. 50), like before for the mantle melt products, and additionally for Sr and Y (Fig. 51). Fitting of the model to the REE curve of the adakites showed that the basaltic parent was melted to 20 to 30 %. Results for the Sr/Y ratio pointed to 10 to 30%.
Calculations showed that the present adakites have a basaltic parental rock derived from a MORB or OIB source. Up to 20% marine sediment can be compound of the molten rock column. Taking Galapagos Island rock compositions [White et al., 1993] for the modelling process exactly matches the REE curve of the partial melting product.

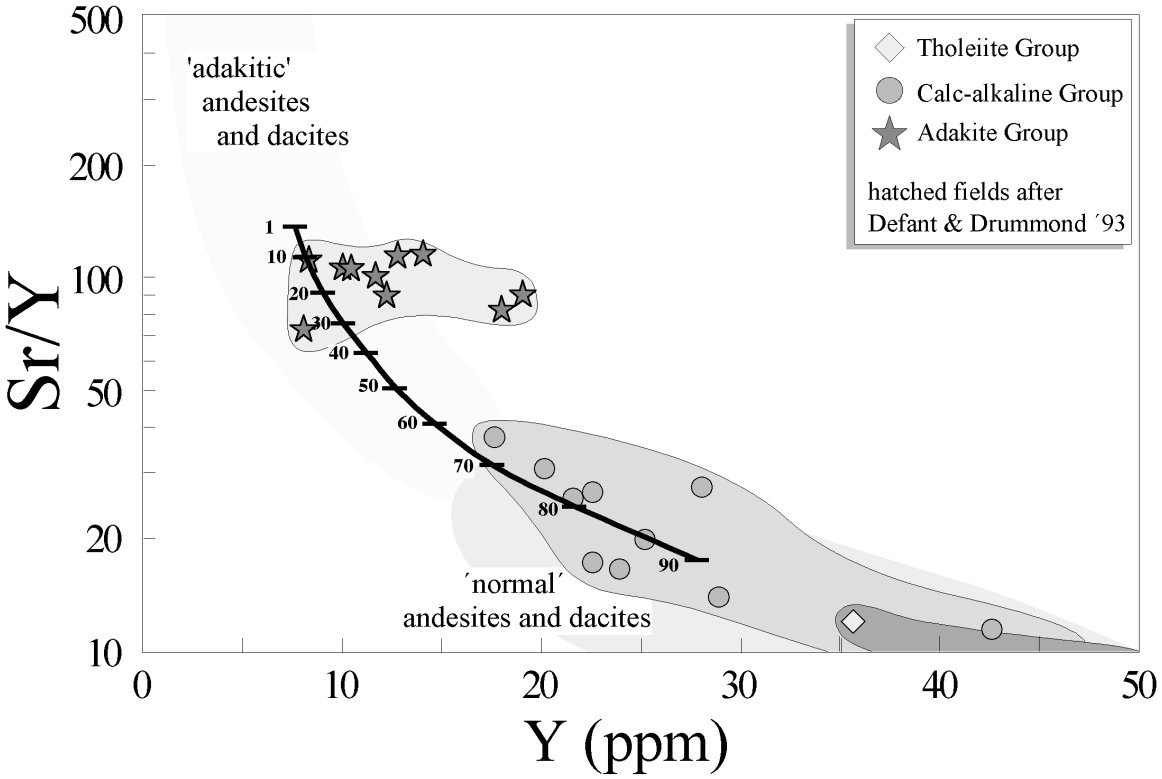

Figure 50: *Sr/Y vs Y is a discrimination plot for adakites. The melting curve for an eclogite points to 10 to 20% in the degree of melting for the generation of these adakites.*

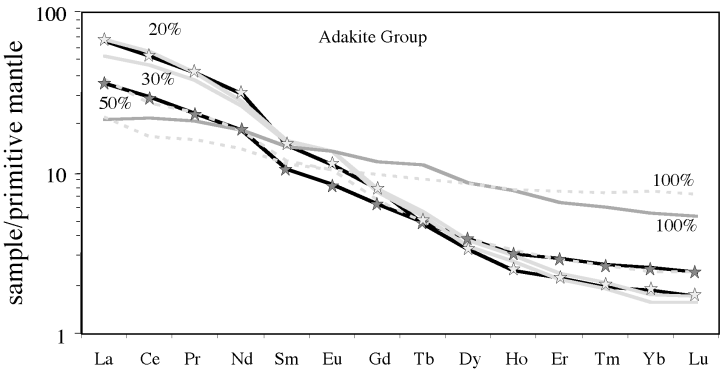

Figure 51: *The batch melting model on the REE results in 20 to 30% melting of garnet amphibolite or eclogite.*

Some of the adakites have suffered considerable interaction with the mantle material during their ascent through the mantle wedge. This fact is documented by their high MgO contents of up to 6 wt% and Mg# up to about 70 (Fig. 52). It is also conspicuous in form of mixing trends displayed by samples of the adakite group in various element correlation diagrams presented above (Figs. 28, 29).

Modelling calculations of AFC processes point to as high as 20% assimilation of mantle material for some adakite samples (Fig. 52). In this diagram of Mg# versus SiO2, mantle melts and their differentiates delineate a hyperbolic, decreasing trend from high Mg#/low SiO2 to low Mg#/high SiO2. This trend of chemical evolution is related to fractionation of the mineral assemblage as outlined in Chapter 4, and assimilation of crustal rocks. Samples of the calc-alkline group obviously follow this trend.
The almost perpendicular trend formed by the adakites is primarily related to assimilation of mantle material. This assimilation process affects more the Mg# than the SiO2 content of the slab melting products. Mixing of adakitic melts and mantle melts lowers instead simultaneously the SiO2 content. Fractionation of plagioclase and amphibole shifts the adakite composition into the opposite direction.
The mantle-AFC process severely affects the chemical composition of these rocks. Contents of compatible elements like Ni, Cr, and Co and Mg increase in the rock, whereas for example the REE contents are less affected. At least, the adakite characteristics of HREE depletion in respect to “normal” mantle melting products is still preserved.

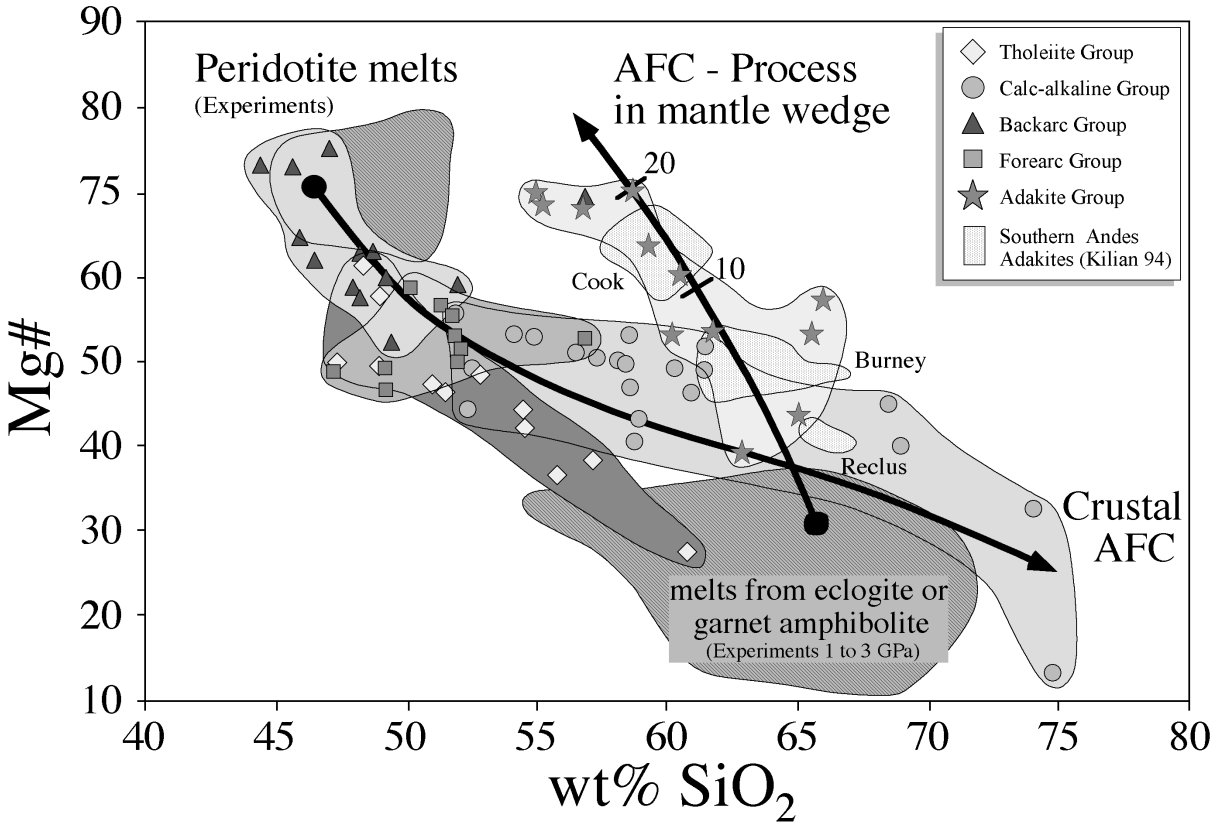

Figure 52: *Plot of Mg# vs. SiO_2 shows the assimilation trend of the adakitic melts in the mantle wedge.*

7 Discussion

The above described diversity of magma-types in south-east Costa Rica cannot be derived from a single, homogeneous magma source. Thus, a more complex arc evolution has to be expected in southern Central America with variations in major subduction parameters compared with northern Central America. Since the magmatic changes coincide approximately with the event of ridge-arc collision, a causal relationship is very likely.

A geodynamic model for the evolution of the subduction zone in south-east Costa Rica has to account for:

1. extinction of calc-alkaline volcanism in the main magmatic arc
2. occurrence of localised backarc magmatic activity
3. tapping of a mineralogically and geochemically distinct mantle source region (for backarc magmatism)
4. generation of slab melts

7.1 Geodynamic models

Potential models for the geochemical characteristics of Costa Rican magmas:

7.1.1 Locally enriched mantle

Some published models invoke an early generated more enriched mantle composition underneath Costa Rica in comparison with northern Central America. The mantle wedge is thought to be locally heterogeneous like a plum pudding [Herrstrom et al., 1995] or contains veins of frozen melt from a preceding melting event [Feigenson & Carr, 1993]. The enrichment could be derived from the Galapagos hot spot tracing its way from the former Caribbean position to its present Pacific position [Carr, pers. comm.]. An alternative to this is the enrichment of the mantle wedge by a flow of asthenosphere originating in South America [Herrstrom et al., 1995]. These enrichment models account for the geochemistry of recent northern Costa Rican lavas but cannot account for the trace-element pattern and isotopic values of pre-collisional magmas in south-eastern Costa Rica. Pre-collisional magmas were derived from a mantle source similar to that of the currently active northern Central American arc. Furthermore, the enormous transport path (~4000 km) makes the proposed asthenosphere migration model doubtful.

7.1.2 Slab angle variations

A slab roll back could induce changes in the mantle wedge counter flow and create an extensional regime resulting in decompressional melting of the deeper mantle to produce the backarc magmas. In this model the roll back would be a consequence of ridge-arc collision and temporarily reduced convergence rates. However, slab angle variations are rather slow and wide-ranging processes as long as the subducting slab is a coherent plate. A slowly adjusting, coherent plate could be expected for the Cocos Plate since it is stretching as far down into the mantle as to the core mantle boundary [van der Hilst et al., 1997].
Shallowing of the subduction angle with Cocos Ridge subduction would equally take a long time and would be evolved to only limited degrees in case that the respective slab segment is not fault bounded.
Variations in the slab angle normally result in shifts of the volcanic chain simultaneously with shifts of the slab dehydration zone. Carr [1984] documented the relationship between subduction angle and the location of the volcanic chain for Central America. Such continuous shifts in the location of the volcanic arc are not observed in south-eastern Costa Rica.

7.1.3 Slab window

My preferred model implies a slab break-off or the formation of a slab window, respectively. In this case, areas along the convergent margin evolve that are not underlain by subducted oceanic lithosphere. Such windows into the asthenosphere were first described by Dickinson & Snyder [1979] and are found at various convergent margins [Thorkelson, 1996].
This model is able to explain the cessation of normal arc volcanism, the time related signal of the enriched mantle source and provides favourable conditions for the generation of adakites.

The geodynamic evolution within the south-eastern Costa Rican arc segment can be envisaged as follows (Fig. 53):

1. Pre-collisional stage

Fluids are released during prograde metamorphism of the subducting oceanic lithosphere and enter the overlying mantle wedge. Consequently, melt generation takes place upon the fluid induced solidus lowering.
Magmas within the young convergence zone are arc tholeiitic. With time and increasing crustal thickness, the melting column reduces which leads to reduced melting degrees [Plank & Langmuir, 1988]. These magmas assimilate increasingly more crust during their ascent through the thickened crust, fractionate extensively during storage in magma chambers and erupt or intrude as calc-alkaline magmas.

2. Collision stage

A slab window (i.e. a slab free space) forms, either upon Cocos Ridge collision and slab break-off or by subduction of a spreading ridge (see below).
Above the slab window, arc volcanism ceases as a response to decreasing hydration of the upper mantle. With decreasing fluid saturation the solidus temperatures rise and melting within the mantle wedge stops.
An upflow of asthenospheric material occurs through the slab window underneath the Cordillera de Talamanca. It is either driven by the mantle material deficit due to the uplift of the Cordillera or more probably, resulting from the considerably hotter and less dense sub-slab mantle, itself increasing the Cordillera uplift. Asthenospheric upwelling through a slab window may generally also take place simply as a response to the incipient void left by extending or separating of the subducting slab [Hole et al., 1991]. In case that the adiabatic ascent was great enough, melting of the mantle material would occur [cf. Ormerod et al., 1988].
Low degree mantle melts generated by decompression melting of the upwelling sub-slab asthenosphere extrude in the backarc area where the overriding plate is sufficiently thinned or fractured in the extensional regime.
These melts display an OIB signature derived from the sub-slab mantle reservoir. The sub-slab asthenosphere between the Galapagos Islands and the Central American convergence zone may be interspersed by Galapagos plume material like a marble cake. The omnipresence of the Galapagos plume influence in this area is substantiated for example by recent volcanic activity on the Cocos Islands. Transport of the plume material through the slab window into the mantle wedge realm takes place with the general mass flux. Low degree melts are obviously preferentially generated from this plume derived mantle material.
A temporal and spatial association of mafic alkaline volcanism with slab window formation was also found in the Antarctic Peninsula, British Columbia, and northern Baja California [Hole et al., 1991].

The presence of a slab window may be substantiated by the observed lack of seismicity in that specific area: Protti et al. [1995] found that deep earthquakes associated with a subducting slab disappear entirely east of Turrialba volcano. This zone of seismic inactivity below the Cordillera de Talamanca could also result from a subducting plate that is either too young to produce earthquakes or, from one that has broken up [e.g., Reagan et al., 1986].

3. Post-collisional stage

Buoyant forces, resulting from lower density of the crustal material, young age and therefore higher thermal structure (high heat flow), lead to a relatively shallow subduction of the Cocos Ridge. Since dehydration depths are not achieved, the oceanic crust does not loose its water to the mantle wedge. Formation of the slab window brings inevitably hot, anhydrous sub-slab asthenosphere in contact with the still hydrated oceanic crust. The consequence is thermal erosion of the window margins which means partial melting of the hydrated oceanic crust resulting in the generation of adakites. At the Costa Rican convergent margin the generation of adakitic melts is only possible as a consequence of slab window formation providing an additional heat source. Otherwise, the very high convergence rates of about 90 mm/a, would have dragged the isotherms deep into the mantle so that heating of the subducted crust to supra-solidus temperatures would not have occurred prior to dehydration of the slab. Melting reactions during amphibole breakdown in the subducting plate depend on the relationship of the basalt solidus with the slab geotherm, which itself depends on promoting factors like the convergence rate [Rapp & Watson, 1995]. Experiments by Peacock et al. [1994] showed that slab melting is favoured at subduction zones with very low convergence rates.
A slab window is a very likely location for the formation of adakites. Adakites (high-Mg andesites and dacites) related to window-margin melting are also described in other places of slab window formation like Baja California and southern Chile [Kay et al., 1993; Rogers & Saunders, 1989; Stern & Kilian, 1996].

Fore arc volcanism occurs, probably related to local dehydration of the leading edge of the subducting slab and triggered by additional shear heating. Post-collisional calc-alkaline fore arc magmatism in southern Costa Rica may also be related to the influence of the slab window. Asthenospheric upwelling from the sub-slab mantle to the mantle wedge may have induced melting with the production of mafic magmatism in the fore arc region. Voluminous assimilation or anatexis of the (wet, sediment rich) fore arc wedge could have resulted in the formation of the more intermediate rocks of the Costa Rican fore arc volcanics. The OIB signal of the intruding mantle material may be hidden due to the larger melting degrees in the marble cake mantle material or as a consequence of insufficient dissemination of that mantle material in the arc wedge.
Granitoitic rocks found in the fore arc, about 30 km away from the magmatic arc, were initially interpreted as tectonically and glacially displaced from their original emplacement locality in the Cordillera de Talamanca. Now they could well be interpreted as in situ generated by anatectic melts of the wet fore arc sediments, induced by the slab window concomitant magmatism.
Intermediate to granitic fore arc magmatism resulting from slab window formation was described from various places like the Solomon Islands [Johnson et al., 1987], Japan [Hibbard & Karig, 1990], California [Johnson et al., 1987], southern Alaska [Sisson & Pavlis, 1993; Haeussler et al., 1995], and Chile [Forsythe et al., 1986].
Cocos Ridge subduction is going on with a very shallow angle upon the fault bounded slab slice. A present cessation of volcanism may either be due to displacement of the asthenospheric mantle wedge or due to a lack of fluids in the mantle wedge provided by the subducting plate which does not reach depths of dehydration.

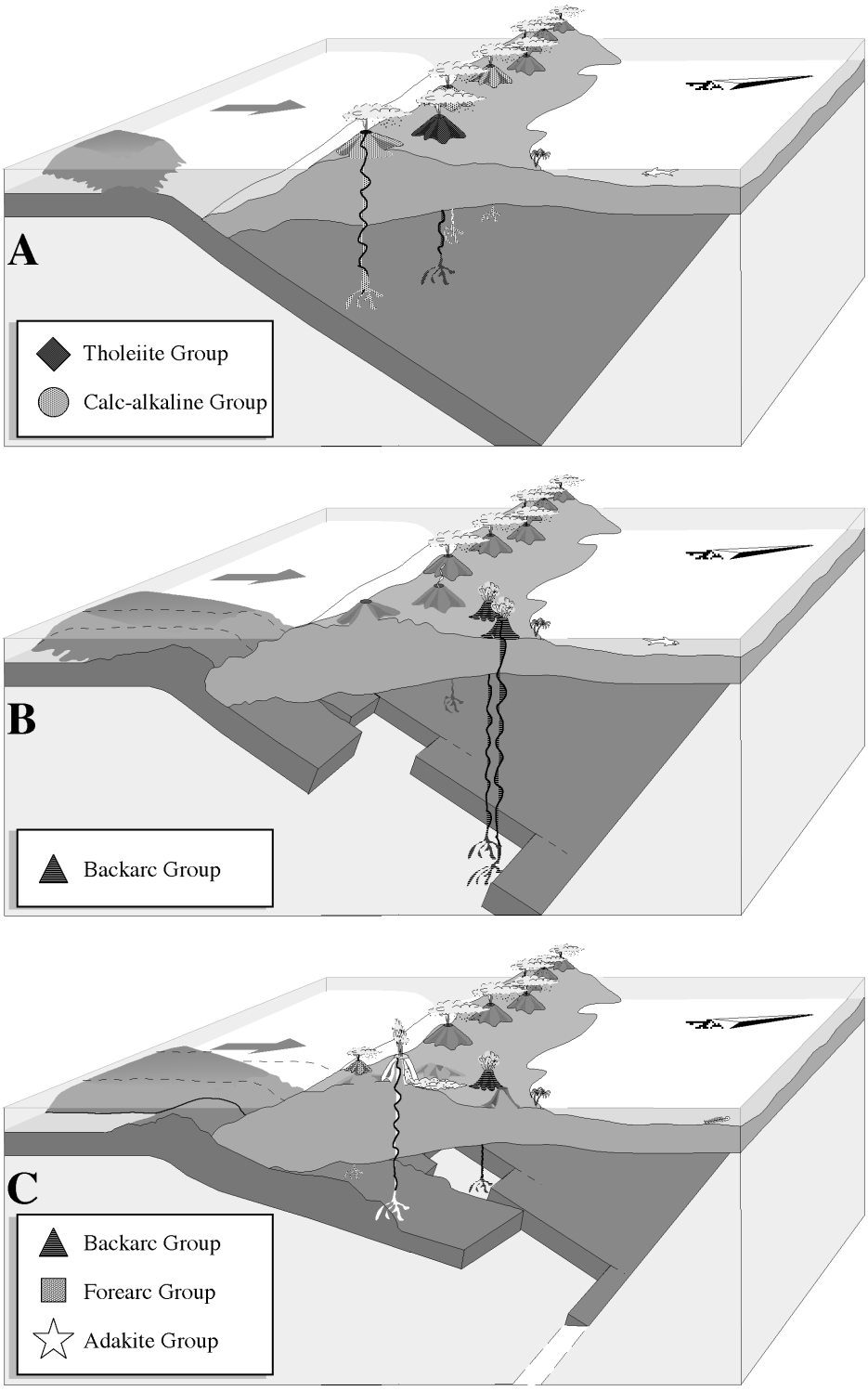

Figure 53: *Three stage evolution model in a profile through the subduction zone. A: Intact slab, production of arc-tholeiitic and calc-alkaline magmas. B: Ridge collision and slab disruption, production of backarc magmatics. C: Shallow subduction of the Cocos Ridge, production of adakites and forearc volcanism.*

The volcanic and geochemical evolution in SE Costa Rica is best explained by the formation of a slab window underneath that arc segment. However, the exact mechanism of formation of this window may be a matter of debate.
Two modes of slab window formation may be possible for the subducting plate beneath the Cordillera de Talamanca:

7.1.3.1 Slab window opening by subduction of an active rift

A slab window develops when a spreading ridge is subducted in a convergence zone. The window forms due to suppression of crustal growth on the spreading plate edges of the active rift segment [Thorkelson, 1996]. Shape and dimensions of slab windows are dependent on relative plate motions, angle of subduction, and plate geometry prior to and at the time of ridge crest-trench interaction [Hole et al., 1991].
Slab window formation as a consequence of rift subduction were described for Northern Baja California [Dickinson & Snyder, 1979; Thorkelson & Taylor, 1989], Southern Chile [Cande & Leslie, 1986; Forsythe et al., 1986] British Columbia [Thorkelson & Taylor, 1989] and the Antarctic Peninsula [Hole et al., 1991; Hole & Larter, 1993].

For Costa Rica, Johnston and Thorkelson [1997] suggest the possibility of slab window formation resulting from subduction of a series of segments of the Cocos-Nazca spreading centre. In that model, the Panama Fracture Zone (PFZ) is separating the currently subducted ridge segments from the Ecuador Rift, a segment of the Cocos-Nazca spreading centre which is still far from the trench. The slab window opened from SW to NE in accordance with general plate motions. Currently, the window will be below western Panama with the PFZ bordering it to the west. Adakitic volcanism in Panama at La Yeguada [Defant et al., 1991, Defant et al., 1992] and El Valle [Defant et al., 1991; Defant et al., 1992] which could result from melting of the plate edges would then have followed adakitic volcanism in Costa Rica and may give the latest constraints on timing and shape of the slab window formation. Since convergence rates along Panama are very low, the slab window is now relatively stationary compared to the subducting Cocos Plate. However, the leading edge of the Nazca Plate has to be that far subducted below the arc that recent volcanism could occur at El Baru in W Panama. The Cocos Ridge is delimited by the PFZ so that on geometric reasons it can be concluded that only about 100 km of the ridge are currently subducted. This in turn implies that in this case the Cocos Ridge collided with the arc since little more than about 1 Ma as it was proposed by Lonsdale and Klitgord [1978] and Corrigan et al. [1990]. The earlier beginning exhumation of the Cordillera de Talamanca which is ascribed to collision and shallow subduction would then result from subduction of a precursor of the Cocos Ridge. The model proposed by Johnston and Thorkelson [1997] does not account for the formation of alkaline volcanism in the Costa Rican back arc as a direct result of slab window opening. The observed sequential occurrence of these magmas would only be related to NW migration of sub slab asthenospheric material opposite to the direction of slab window movement. The model could also not account correctly for the formation of the Costa Rican adakites which would require subduction of the Cocos Ridge for at least 3 Ma.

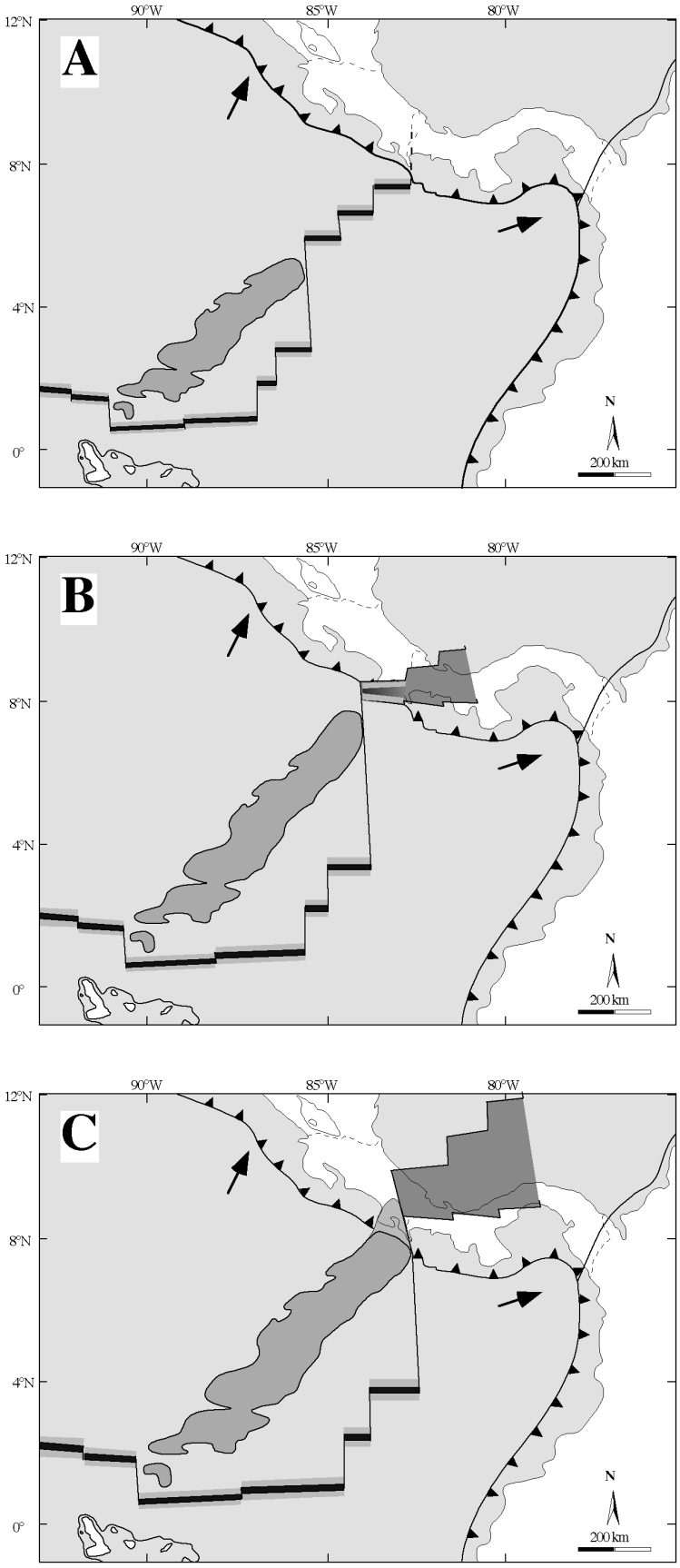

Figure 54: *Three stage model of slab window generation by subduction of rift segments from the active Cocos-Nazca spreading centre (after Johnston and Thorkelson, 1997).*

7.1.3.2 Slab break off induced by aseismic ridge collision

Disruption of the subducting slab may result from collision of an aseismic ridge with a convergence zone [e.g., McGeary et al., 1985]. This slab break off will lead to the formation of a slab window by subsequent slab roll back. An example of slab window formation upon collision of an aseismic ridge or plateau is described for the Lesser Antilles [Bouysse & Westercamp, 1990]. The aseismic ridge is acting as a buttress, temporarily resisting to subduction, while the slab is constantly pulling down into the mantle. Slab pull forces acting on the Cocos Plate seem to be large if they are reflected in the high convergence rates measured along Central America [e.g., DeMets et al., 1990]. On physical reasons, it should be valid that the longer the slab, the greater the slab pull. A correlation between slab length and convergence rate was for example found by Isacks et al. [1968]. Subduction as deep as the core-mantle boundary was attested for Central America by seismic tomography [van der Hilst et al., 1997].
As the resistant forces are superseded, the ridge is finally subducting. These fault bounded slices of the oceanic plate are subducting unusually shallow due to buoyancy of the aseismic ridge and lack of slab pull forces on the leading plate edge. Therefore, in a vertical projection to the arc, the slab window becomes rapidly covered by this shallow subducting slice of the down-going plate. Assuming an (initially) oblique subduction of the ridge or a large angle between ridge front and trench, several slab windows could be formed en echelon. In this model, the Cocos Ridge is subducting in a sequence of several fault bounded slices from east to west. The easternmost slices, which represent the leading end of the Cocos Ridge, are already subducted below Panama. They may be bordered by faults like the Balboa Fracture Zone and the Coiba Fracture Zone which parallel the PFZ to the east and are believed to be related to the currently active PFZ [Moore & Sender, 1995]. The PFZ is obviously delimiting the actually subducting part of the Cocos Ridge to the east. This model of slab-window formation and propagation following Cocos Ridge collision accounts for the observed north-westward younging of back arc alkalic volcanism marking the margin of the evolving slab window.
Bathymetric structures and magnetic anomaly pattern of the Panama basin are still enigmatic. Some authors [e.g., de Boer et al., 1995] assume spreading ridges (e.g., Sandra Rift, Fig. 2) south of Panama. If these ridges were once part of the Cocos-Nazca spreading system [e.g. Lonsdale & Klitgord, 1978], they would argue against the slab window model proposed by Johnston & Thorkelson [1997].

Slab rupturing and finally slab window formation upon aseismic ridge collision could be facilitated in southern Central America due to the strong segmentation of the plates by transform faults like the PFZ. Driving forces for the separation of the Cocos and the Nazca Plates or their segments within the subduction zone are differences in subduction direction, angles, and rates. Therefore, the slab window along the Cocos - Nazca plate boundary is passively developing by slab pull.

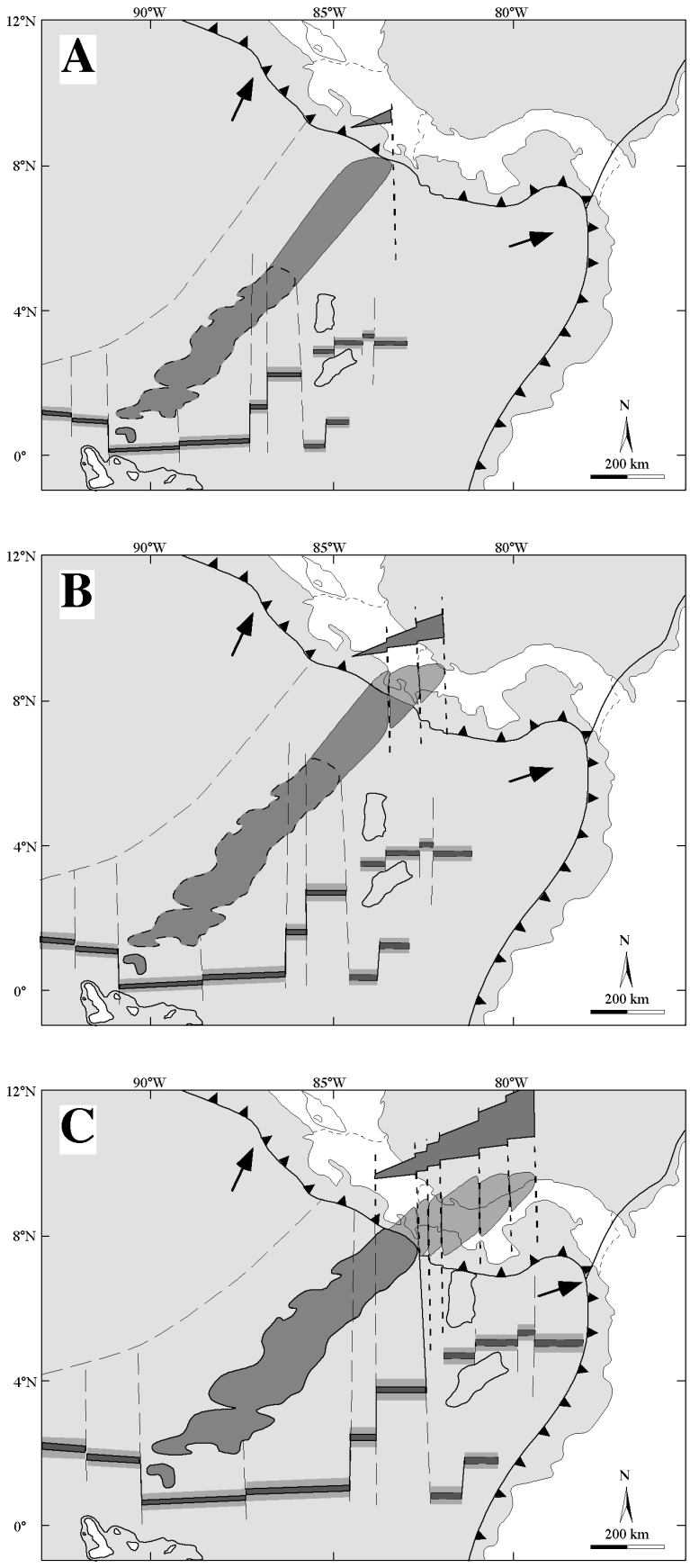

Figure 55: *Three stage model of slab window generation by slab break-off upon Cocos Ridge collision*

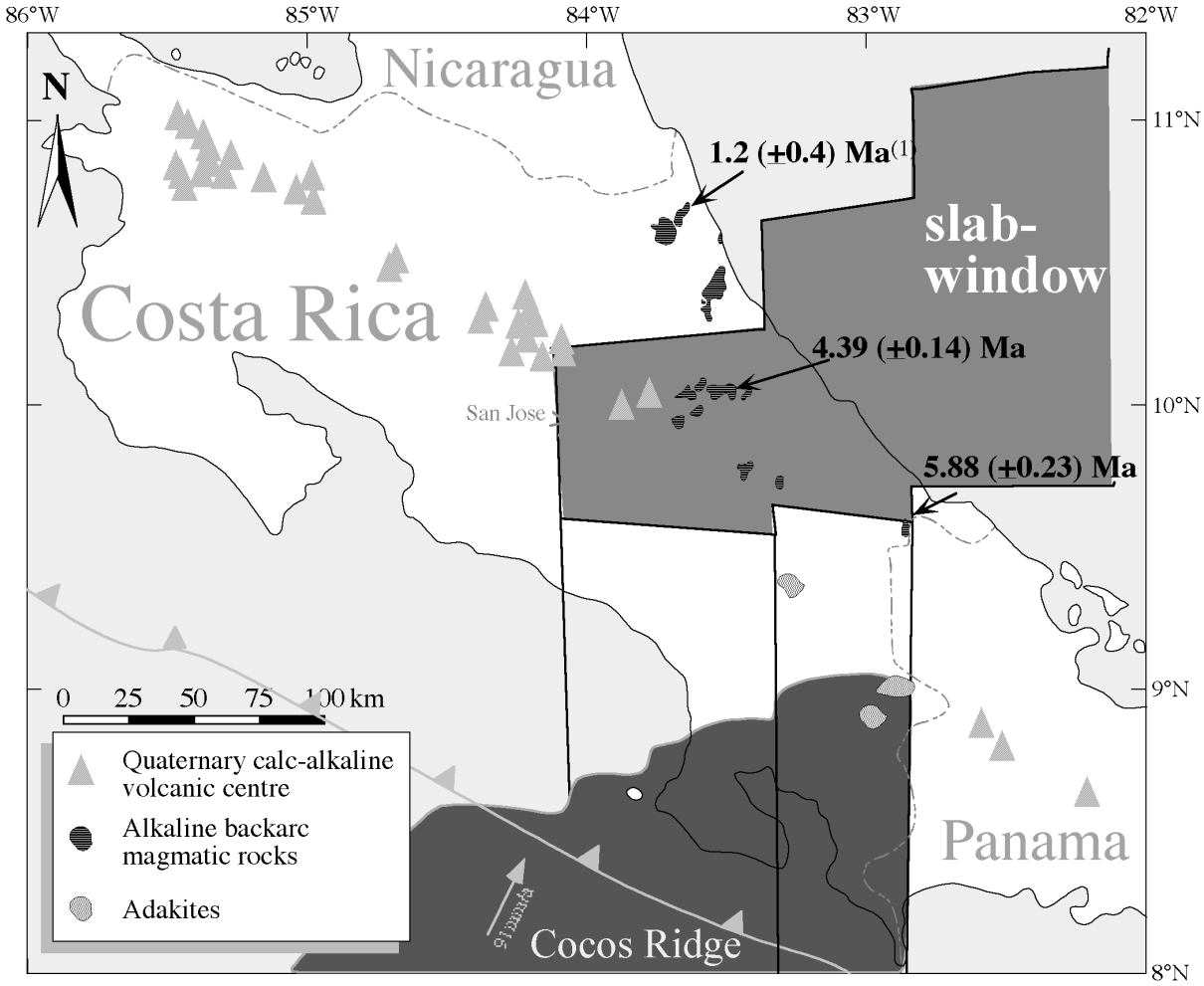

Figure 56: *Slab window presence behind the location of Cocos Ridge collision and window opening in a north-western direction is documented by the eruption sequence in backarc magmatics. Radiometric ages measured in this study are indicated,* $^{(1)}$ *is from Tournon [1984].*

7.2 Regional effects

The formation of a slab window, whether it formed as a consequence of active rift subduction or Cocos Ridge collision or a combination of both, doubtlessly means anomalous thermal, physical and chemical effects within the respective arc section. This generally results in anomalous magmatism from fore arc to back arc, sometimes fore arc metamorphism, strike slip faulting, uplift and extension [e.g., Hole et al., 1991]. Magmatic-geochemical effects induced by the slab window formation in SE Costa Rica were discussed above. In addition to this, the slab window has also appreciable effects on the regional arc volcanic evolution of Central America up to southern Nicaragua and Panama.

Figure 57 of the Central American volcanic arc demonstrates the distinct geochemical evolution of south-eastern Costa Rica and points out that probably slab window related adakites are also present in Panama. Figure 58 presents the evolution of the Central American volcanic arc with its decreasing activity in the southern end of the Central American arc system.

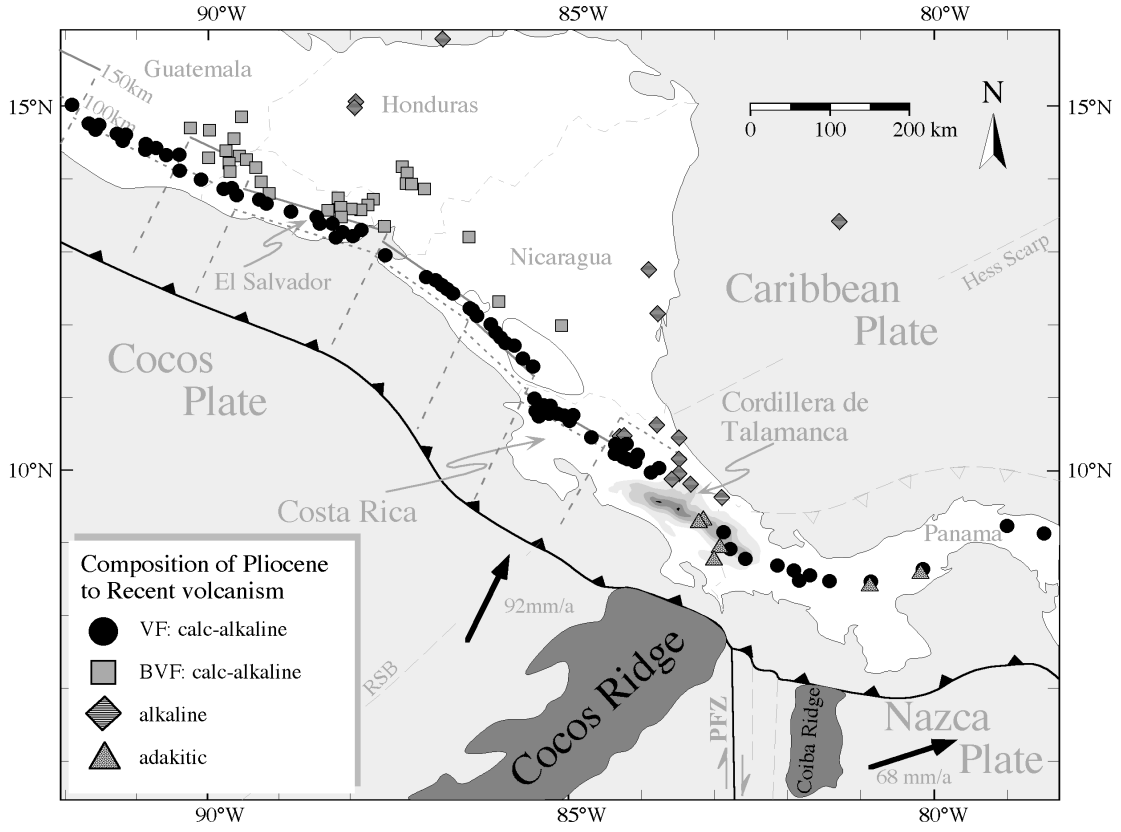

Figure 57: *Geochemical composition of volcanoes in Central America.*

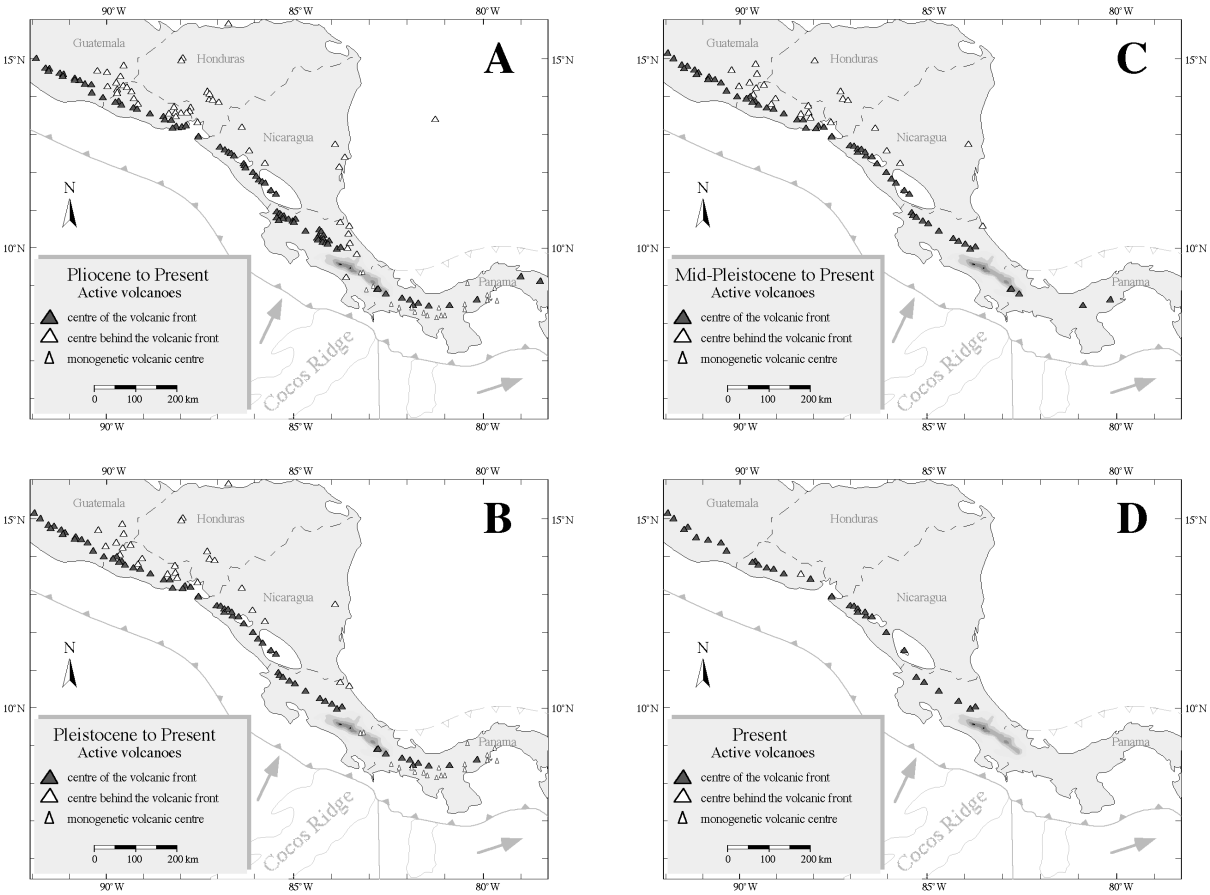

Figure 58: *Evolution of active volcanism along the Central American arc system. Shown is the cumulative activity during the respective time interval.*

Opening of a slab window gives potential pathway for an asthenospheric flow between the two mantle reservoirs that were formerly effectively isolated.
The OIB-like geochemical and isotopic signature of the back arc magmas in SE Costa Rica directly points to the sudden accessibility of sub-slab mantle after Cocos Ridge collision and subsequent slab window formation.
Present-day along-arc geochemical variations in Central America suggest a more enriched mantle source but also minor input of subducted material for Costa Rica than elsewhere in the arc [Carr et al., 1990; Leeman et al., 1994]. Variations from central Costa Rica to central Nicaragua are for example increasing $^{87}Sr/^{86}Sr$ and decreasing $^{143}Nd/^{144}Nd$ [Feigenson & Carr, 1986], increasing $^{10}Be/^{9}Be$ ratios [Leeman et al., 1994], increasing $^{230}Th/^{232}Th$ [Herrstrom et al., 1995], decreasing $^{206}Pb/^{204}Pb$ [Carr, pers. comm.], increasing Ba/La and decreasing La/Yb [Carr et al., 1990].
This geochemically and isotopically enriched mantle signature can be explained by an upwelling flow of asthenosphere through the window leading to an irreversible and increasing contamination of the Central American mantle wedge by the Galapagos plume component. North-westward propagation of this slab-window enhances lateral migration of this contaminant over time.
The slab window could also have caused the enhanced volcanic productivity observed in northern Costa Rica as compared with the rest of the Central American arc [Carr, 1984].

The present study shows that the enriched mantle source or plume signal in the Central American arc source is time dependent and its evolution is recorded by the magmatic rocks of the Talamanca area.

8 Conclusion

The Cordillera de Talamanca in SE Costa Rica, its related forearc (Fila Costena) and backarc area (Limon basin) constitute a segment of the Central American arc system which is active since about the Eocene/Oligocene [de Boer et al., 1995]. However, samples of this study date only back to the Miocene when volcanism increased considerably [de Boer et al., 1995]. Early magmatic products until mid-Miocene times are generally arc-tholeiitic in this area.
Later (mid- to upper Miocene) volcanic and intrusive activity produces calc-alkaline magmatics. This change correlates with decreased melting degrees, increased subduction contribution and increased degrees of fractionation and assimilation of the magmas within an increasingly thickened arc crust. This evolution from arc-tholeiitic to calc-alkaline magmatism is in accordance with general observations of increasing arc maturity at subduction zones world-wide [Wilson, 1989] and with findings in northern Costa Rica in the Montes del Aguacate [Tournon & Alvarado, 1997].
'Normal' arc volcanism ends when a slab window forms underneath this segment of the Central American arc system. This slab window may be a result of supposed subduction of a rift segment of the active Galapagos spreading centre (GSC) preceding the Cocos Ridge arrival at the Central American arc [Johnston & Thorkelson, 1997], or a consequence of Cocos Ridge-arc collision and subsequent slab break-off. The former model is substantiated by an apparent hiatus between the cessation of 'normal' arc volcanism and the assumed time of Cocos Ridge-arc collision, whereas the latter model is substantiated by the location and direction of opening of the slab window. A combination of both models with a slab window initiated by subduction of an active rift and extension due to ridge-arc collision may be most likely.
Coincidentally with the Cocos Ridge-arc collision, magmatics erupt and intrude in the Costa Rican backarc. An age sequence from SE to NW displayed by these rocks traces the direction of slab window widening. Compositional signatures of those backarc magmatics point to their derivation from the Galapagos plume infiltrated sub-slab asthenosphere and mark thus the beginning asthenospheric flow that increasingly contaminates the Central American arc wedge.
The generation of adakite magmas in SE Costa Rica is likely related to window margin melting when the young, hydrated, basaltic Cocos Ridge crust is subducted to depths and comes in contact with the hotter upwelling sub-slab asthenosphere.
Forearc calc-alkaline volcanics are formed where raised temperatures favour melting above the leading edge of the advancing, subducting plate. This forearc volcanic activity in the Fila Costena and the volcanic activity in western Panama producing El Baru may indicate that volcanic activity will resume in this segment of the Central American arc after displacement of the slab window. However, very shallow subduction of the Cocos Ridge will inhibit melt generation in the area for several million years.

Tasks remaining for future investigations in the area of SE Costa Rica and W Panama are:

- Testing the two different slab window models by structural and seismic investigations and by plate-tectonic reconstruction.
- Determination of the direction of slab window opening by determining the extinction sequence in calc-alkaline volcanism and by more high-precision dating of the window-margin related adakites in Costa Rica and Panama.
- Geochemical investigation of El Baru volcanics to test if this volcano is related to resuming (propagating slab) or fading (slab window) volcanic activity, e.g. by determining if the volcanic sequence contains the plume mantle signature from slab window opening.

- Substantiation of the apparently SE – NW directed exhumation of the Cordillera de Talamanca which would indicate oblique subduction of the Cocos Ridge.
- Final determination of the time of Cocos Ridge collision to test the model of slab window formation upon ridge collision.
- Search for alkalic backarc magmatics in Panama and dating of these rocks series to substantiate the observation of a directed eruption sequence.
- Geochemical investigation and dating of the forearc granitoitic complex in the Fila Costeña for a detailed test of the hypothesis of forearc magmatism induced by slab window formation.

9 References

Adamek S., Tajima F., and Wiens D.-A. (1987) Seismic rupture associated with subduction of the Cocos Ridge. *Tectonics* **6**(6), Pages 757-774.

Ahmedali S. T. (1989) X-ray fluorescence analysis in the geological sciences; advances in methodology. *Min. Assoc. Canada, Montreal, Short Course* **7**, 252 pp.

Aitcheson S. J. a. F., A.H. (1994) Quantification of Crustal Contamination in Open Magmatic Systems. *Journal of Petrology* **35,** Part **2**, 461-488.

Alt J. C., Muehlenbachs K., and Honnorez J. (1986) An oxygen isotopic profile through the upper kilometer of the oceanic crust, DSDP Hole 504B. *Earth Planet. Sci. Lett.* **80**, 217-229.

Alvarado G. E., Kussmaul S., Chiesa S., Gillot P. Y., Appel H., Woerner G., and Rundle C. (1992) Resumen cronoestratigrafico de las rocas igneas de Costa Rica basado en dataciones radiometricas Translated Title: Chronostratigraphic review of igneous rocks of Costa Rica based on radiometric dates. *Journal of South American Earth Sciences* **6**(3), Pages 151-168.

Alvarado G.-E., Denyer P., and Sinton C.-W. (1997) The 89 Ma Tortugal komatiitic suite, Costa Rica; implications for a common geological origin of the Caribbean and eastern Pacific region from a mantle plume. *Geology (Boulder)* **25**(5), Pages 439-442.

Appel H., Wörner G., Alvarado G., Rundle C., and Kussmaul S. (1994) Age relations in igneous rocks from Costa Rica. In *Geology of an Evolving Island Arc. The Isthmus of Southern Nicaragua, Costa Rica, and Western Panama*, Vol. 7 (ed. H. Seyfried and W. Hellmann), pp. 63-69. Profil.

Arculus R.-J. and Powell R. (1986) Source component mixing in the regions of arc magma generation. *Jgr* Journal of Geophysical Research. B. **91**(6), Pages 5913-5926.

Asahara Y., Tanaka T., Kamioka H., and Nishimura A. (1995) Asian continental nature of 87Sr / 86Sr ratios in north central Pacific sediments. *Earth and Planetary Science Letters* **133**, 105-116.

Astorga A. (1987) El Cretácio Superior y el Paleógeno de la vertiente Pacifica de Nicaragua meridional y Costa Rica septenreional: orígen, evolutión y dinámica de las cuencas profundas relacionadas con el margen convergente de Centroamérica. Thesis de Licenciatura (unpublished), Universidad de Costa Rica.

Azambre B. and Tournon J. (1977) Les intrusions basiques alcalines du Rio Reventazon (Costa Rica). *Société géologique de France* **2**, 104 - 107.

Ballmann P. (1976) Eine geologische Traverse des Ostteils der Cordillera de Talamanca, Costa Rica (Mittelamerika) Translated Title: A geological traverse of the eastern part of the Cordillera de Talamanca, Costa Rica, Central America. *Neues Jahrbuch fuer Geologie und Palaeontologie. Monatshefte.* **8**, 502-512.

Bellon H. and Tournon J. (1978) Contribution de la géochronométrie K-Ar à l'étude du magmatisme de Costa Rica, Amérique Centrale / Contribution of K-Ar geochronology to the study of magmatism in Costa Rica, Central America. *Bulletin de la Société Géologique de France* **20**(6), Pages 955-959.

Ben Othman D., White W. M., and Patchett J. (1989) The geochemistry of marine sediments, island arc magma genesis, and crust-mantle recycling. *Earth and Planetary Science Letters* **94**, 1-21.

Bentley L. R. (1974) Crustal structure of the Carnegie Ridge, Panama Basin, and Cocos Ridge. M.S. thesis, University of Hawaii.

Bergoeing G. P., Mora C., and Jimenez R. R. (1978) Evidencias de vulcanismo Plio-Cuaternario en la fila Costena, Terraba, Costa Rica Translated Title: Evidence of Plio-Quaternary volcanism in the coastal chain near Terraba, Costa Rica. *Informe Semestral Instituto Geografico Nacional. Julio a Diciembre.*

Bergoeing J.-P. (1982) Dataciones radiometricas en algunas muestras de Costa Rica Translated Title: Radiometric dating of some samples in Costa Rica. *Informe Semestral Instituto Geografico Nacional. Enero a junio.*

Bogaard v. d. P. and Werner R. (1998) GEOMAR Annual Report 1997.

Bouysse P. and Westercamp D. (1990): Subduction of Atlantic aseismic ridges and late Cenozoic evolution of the Lesser Antilles island arc. *Tectonophysics*. 175; 4, 349-380.

Bowin C. O. (1976) The Caribbean: Gravity field and plate tectonics. *Geological Society of America Special Paper* **169**, 79p.

Burbach G.-V., Frohlich C., Pennington W.-D., and Matumoto T. (1984) Seismicity and tectonics of the subducted Cocos Plate. *Jgr* Journal of Geophysical Research. B. **89**(9), Pages 7719-7735.

Calvo C. and Bolz A. (1994) Der älteste kalkalkaline Inselbogen-Vulkanismus in Cota Rica. Marine Pyroklastika der Formation Loma Chumico (Alb bis Campan) / The oldest calcalkaline island island arc volcanism in Costa Rica. Marine tephra deposits from the Loma Chumico Formation (Albian to Campanian). In *Geology of an Evolving Islnad Arc. The Isthmus of Southern Nicaragua, Costa Rica, and Western Panama*, Vol. 7 (ed. H. Seyfried and W. Hellmann), pp. 235-264. Profil.

Cande S. C. and Leslie R. B. (1986) Late Cenozoic tectonics of the southern Chile trench. *Journal of Geophysical Research* **91**, 471 - 496.

Carr M.-J. (1984) Symmetrical and segmented variation of physical and geochemical characteristics of the Central American volcanic front. *Journal of Volcanology and Geothermal Research* **20**(3-4), Pages 231-252.

Carr M. J., Feigenson M. D., and Bennett E. A. (1990) Incompatible element and isotopic evidence for tectonic control of source mixing and melt extraction along the Central American arc. *Contributions to Mineralogy and Petrology* **105**(4), Pages 369-380.

Carr M. J., Rose W. I., and Mayfield D. G. (1979) Potassium content of lavas and depth to the seismic zone in Central America. *Journal of Volcanology and Geothermal Research* **5**(3-4), Pages 387-401.

Carr M. J. and Stoiber R. E. (1990) Volcanism. In *The Caribbean Region*, Vol. The Geology of North America, Vol. H (ed. G. Dengo and J. E. Case), pp. 375-391. Geological Society of America.

Case J. E., MacDonald W. D., and Fox P. J. (1990) Caribbean crustal provinces; Seismic and gravity evidence. In *The Caribbean Region*, Vol. The Geology of North America, Vol. H (ed. G. Dengo and J. E. Case), pp. 15-36. Geological Society of America.

Cassel D. T. and Sen Gupta B. K. S. (1989) Foraminiferal stratigraphy and paleoenvironments of the Tertiary Uscari formation, Limon basin, Costa Rica. *Journal of Foraminiferal Research* **19**, 52-71.

Castillo P., Batiza R., Vanko D., Malavassi E., Barquero J., and Fernandez E. (1988) Anomalously young volcanoes on old hot-spot traces; I, Geology and petrology of Cocos Island; with Suppl. Data 88-18. *Geological Society of America Bulletin* **100**(9), Pages 1400-1414.

Castillo P. R. (1984) Geology and geochemistry of Cocos Island, Costa Rica: Implications for the evolution of the aseismic Cocos Ridge. Ph.D. thesis, Washington University.

Chen J. H. and Wasserburg G. J. (1985) U, Th and Pb isotopes in hydrothermal fluids from the Juan de Fuca Ridge. *Eos, Transactions, American Geophysical Union* **66**(46), Pages 929.

Chung W. Y. and Kanamori H. (1978) A mechanical model for plate deformation associated with aseismic ridge subduction in the New Hebrides Arc. *Tectonophysics* **50**(1), 29-40.

Collins L.-S., Coates A.-G., Jackson J.-B. C., and Obando J.-A. (1995a) Timing and rates of emergence of the Limon and Bocas del Torro basins; Caribbean effects of Cocos Ridge subduction? *Special Paper Geological Society of America* **295**, 263-289.

Collins L.-S., Geary D.-H., and Lohmann K. C. (1995b) A test of the prediction of decreased Caribbean coastal upwelling caused by emergence of the Isthmus of Panama, using stable isotopes of neritic foraminifera. *Abstracts with Programs - Geological Society of America* **27**(6), Pages 156.

Corrigan J., Mann P., and Ingle J.-C. r. (1990) Forearc response to subduction of the Cocos Ridge, Panama-Costa Rica. *Geological Society of America Bulletin* **102**(5), Pages 628-652.

Cox K. G., Bell J. D., and Pankhurst R. J. (1979) *The interpretation of igneous rocks*. Chapman & Hall.

Dalrymple G. B. and Duffield W. A. (1988): High precision (super 40) Ar/ (super 39) Ar dating of Oligocene rhyolites from the Mogollon-Datil volcanic field using a continuous laser system. *Geophysical Research Letters*. 15; 5, 463-466.

de Boer J. Z., Defant M. J., Stewart R. H., Restrepo J. F., Clark L. F., and Ramirez A. H. (1988) Quaternary calc- alkaline volcanism in western Panama. regional variation and

implication for the plate tectonic framework. *Journal of South American Earth Sciences* **1**(3), 275-293.

de Boer J. Z., Drummond M.-S., Bordelon M. J., Defant M.-J., Bellon H., and Maury R.-C. (1995b) Cenozoic magmatic phases of the Costa Rican island arc (Cordillera de Talamanca). *Special Paper Geological Society of America* **295**, 35-55.

de Boer J. Z., Drummond M.-S., Bordelon M. J., Defant M.-J., Bellon H., and Maury R.-C. (1995a) Cenozoic magmatic phases of the Costa Rican island arc (Cordillera de Talamanca). In *Geologic and Tectonic Development of the Caribbean Plate Boundary in the Southern Central America*, Vol. Special Paper. Vol. 295 (ed. P. Mann), pp. 35-55. Geological Society of America.

de Boer J.-Z., Defant M.-J., Stewart R.-H., and Bellon H. (1991) Evidence for active subduction below western Panama. *Geology (Boulder)* **19**(6), Pages 649-652.

Deer, W.A., Howie, R.A. and Zussmann, J. (1966): An introduction to rock forming minerals. Longman, Harlow. 528 p.

Defant M. J. and Drummond M. S. (1990a) Derivation of some modern magmas through melting of young subducted lithosphere. *Eos, Transactions, American Geophysical Union* **71**(43), Pages 1715.

Defant M.-J. and Drummond M.-S. (1990b) Derivation of some modern arc magmas by melting of young subducted lithosphere. *Nature (London)* **347**(6294), Pages 662-665.

Defant M. J., Richerson P. M., De Boer J. Z., Stewart R. H., Maury R. C., Bellon H., Drummond M. S., Feigenson M. D., and Jackson T. E. (1991a) Dacite genesis via both slab melting and differentiation: petrogenisi of La Yeguada volcanic complex, Panama. *Journal of Petrology* **32**(6), 1101-1142.

Defant M.-J., Clark L.-F., Stewart R.-H., Drummond M.-S., de B.-J. -. Z., Maury R.-C., Bellon H., Jackson T.-E., and Restrepo J.-F. (1991b) Andesite and dacite genesis via contrasting processes; the geology and geochemistry of El Valle Volcano, Panama. *Contributions to Mineralogy and Petrology* **106**(3), Pages 309-324.

Defant M. J., Jackson T. E., Drummond M. S., De Boer J. Z., Bellon H., Feigenson M. D., Maury R. C., and Stewart R. H. (1992) The geochemistry of young volcanism throughout western Panama and southeastern Costa Rica. *Journal of the Geological Society , London* **149**, 569-579.

Defant M. J. and Drummond M. S. (1993): Subducted lithosphere-derived andesitic and dacitic rocks in young volcanic arc setting. *Nature* 347: 662-665.

DeMetz C., Gordon R. G., Argus D. F., and Stein S. (1990) Current plate motions. *Geophysical Journal International* **101**, 425-478.

Dengo G. (1962) Tectonic- Igneous Sequence in Costa Rica. *Geological Society of America Special Paper*, 133-161.

DePaolo D. J. (1981) Trace element and isotopic effects of combined wallrock assimilation and fractional crystallization. *Earth and Planetary Science Letters **53**, 189-202.*

DePaolo D. J. and Wasserburg G. J. (1976) Nd isotopic variations and petrogenetic models. *Geophys. Res. Lett.* **3**, 249-252.

Dickinson W. R. and Snyder W. S. (1979) Geometry of subducted slabs related to San Andeas transform. *Journal of Geology* **87**, 609 - 627.

Diebold J. B., Stoffa P. L., Buhl P. and Truchan. M. (1981): Venezuela Basin crustal structure. JGR. *Journal of Geophysical Research*. B. 86; 7901-7923.

Donnelly T. W., Beets D., Carr M. J., Jackson T., Klaver G., Lewis J., Maury R., Schellenkens H., Smith A. L., Wadge G., and Westercamp D. (1990) History and tectonic setting of Caribbean magmatism. In *The Caribbean Region*, Vol. The Geology of North America, Vol. H (ed. G. Dengo and J. E. Case), pp. 339-374. Geological Society of America.

Draper G. and Dengo G. (1990) History of geological inverstigation in the Caribbean region. In *The Caribbean Region*, Vol. The Geology of North America, Vol. H (ed. G. Dengo and J. E. Case), pp. 1-14. Geological Society of America.

Drummond M. S., Bordelon M., de B.-J. Z., Defant M. J., Bellon H., and Feigenson M. D. (1994) Igneous petrogenesis and tectonic setting of the Cordillera de Talamanca, Costa Rica-Panama, Central American arc. *Abstracts with Programs - Geological Society of America* **26**(7), Pages 331.

Drummond M.-S., Bordelon M., de B.-J. -. Z., Defant M.-J., Bellon H., and Feigenson M.-D. (1995) Igneous petrogenesis and tectonic setting of plutonic and volcanic rocks of the Cordillera de Talamanca, Costa Rica-Panama, Central American arc. *American Journal of Science* **295**(7), Pages 875-919.

Duncan R. A. and Hargraves R. B. (1984) Plate tectonic evolution of the Caribbean region in the mantle reference frame. *Geol. Soc. America, Memoir* **162**, 81-93.

Eiler J. M., Farley K. A., Valley J. W., Hauri E., Craig H., Hart S. R., and Stolper E. M. (1997) Oxygen isotope variations in ocean island basalt phenocrysts. *Geochimica et Cosmochimica Acta* **6**(11), 2281-2293.

Ellam R. M. and Hawkesworth C. J. (1988) Elemental and isotopic variations in subduction related basalts; evidence for a three-component model. *Contributions to Mineralogy and Petrology* **98**(1), Pages 72-80.

Elliot T., Planck T., Zindler A., White W., and Bourdon B. (1997) Element transport from slab to volcanic front at the Mariana arc. *Journal of Geophysical Research* **102**(7), 14,991-15,019.

Escalante G. (1990) The geology of southern Central America and western Colombia. In *The Caribbean Region*, Vol. The Geology of North America, Vol. H (ed. G. Dengo and J. E. Case), pp. 201-230. Geological Society of America.

Faure G. (1986) *Principles of isotope geology*. John Wiley & Sons, New York, 2nd edition, 589pp.

Feigenson M.-D. and Carr M.-J. (1986) Positively correlated Nd and Sr isotope ratios of lavas from the Central American volcanic front. *Geology (Boulder)* **14**(1), Pages 79-82.

Feigenson M.-D. and Carr M.-J. (1993) The source of Central American lavas; inferences from geochemical inverse modeling. *Contributions to Mineralogy and Petrology* **113**(2), Pages 226-235.

Fisher S. P. and Pessagno E. A. (1965) Upper Cretaceous strata of north-western Panama. *American Association of petroleum Geologists Bulletin* **49**, 433-444.

Forsythe R. D., Nelson E. P., Carr M. J., Kaeding M. E., Herve M., Mpodozis C., Soffia J. M., and Harambour S. (1986) Pliocene near- trench magmatism in southern Chile: A possible manifestation of ridge collision. *Geology* **14**, 23 - 27.

Gabb W. M. (1874a) Note on the Geology of Costa Rica. *American Journal of Science* **7**, 438-439.

Gabb W. M. (1874b) Notes on the geology of Costa Rica. *American Journal of Science* **8**, 388-390.

Gabb W. M. (1875) Notes on the geology of Costa Rica. *American Journal of Science* **9**, 198-204.

Gaber L. J., Foland K. A. and Corbato C. E. (1988): On the significance of argon release from biotite and amphibole during 40Ar/39Ar vacuum heating. *Geochim. Cosmochim. Acta*. 52; 2457-2465

Gardner T. W. and others a. (1987) *Central America and Caribbean*. Geological Society of America Centennial Special Volume.

Gardner T.-W., Verdonck D., Pinter N.-M., Slingerland R.-L., Furlong K.-P., Bullard T.-F., and Wells S.-G. (1992) Quaternary uplift astride the aseismic Cocos Ridge, Pacific Coast, Costa Rica. *Geological Society of America Bulletin* **104**(2), Pages 219-232.

Gargantini M. (1993) Analisi petrologica em geochimica di un sill differenziato della formazione alcalina di Guyacan, Squirres, Costa Rica. Tesi di Laurea, Universita´degli studi di Milano.

GERM. (1998) Global Earth Reference Model - online data bank: F. Albarede, W. McDonough, H. Shaw, H. Staudigel, W. White, A. Zindler (eds.). http://www.-ep.es.llnl.gov/germ/germ-home.html .

Ghosh N., Hall S. A. and Casey J. F. (1984): Seafloor spreading magnetic anomalies in the Venezuelan Basin. In: Bonini W. E., Hargraves R. B. and Shagam R. (eds.) The Caribbean-South American plate boundary and regional tectonics. *Memoir - Geological Society of America*. 162; 65-80.

Gill, J.B. (1981): Orogenic andesites and plate tectonics. Springer Verlag, Berlin. 358 pp.

Goedde H. (1998) Study results presented on annual TICOSECT meeting Göttingen.

Graefe K. (1998) Study results presented on annual TICOSECT meeting Göttingen.

Green, T.H. (1982): Anatexis of mafic crust and high pressure crystallisation of andesite. In Thorpe, R.S. (Ed.): *Andesites: orogenic andesites and related rocks*. Wiley, Chichester: 465-487.

Guendel F. D. (1986) Seismotectonics of Costa Rica: An analytical view of the southern terminus of the Middle American trench. Ph.D. thesis, University of California.

Haeussler P.-J., Bradley D.-C., Goldfarb R.-J., Snee L.-W., and Taylor C.-D. (1995) Link between ridge subduction and gold mineralization in Southern Alaska. *Geology (Boulder)* **23**(11), Pages 995-998.

Handschuhmacher D. W. (1976) Post-Eocene plate tectonics of the Eastern Pacific. *In: Sutton, G.H.; Manghnani, M.H. & Moberly, R. (ed.): The Geophysics of the Pacific Ocean and its margins; American Geophys Union*, 177-202.

Hart S. R. and Dodd R. T. Jr (1962): Excess radiogenic argon in pyroxenes. *J. Geophys. Res*. 67; 2998-2999.

Hauff F. (1998) Study results presented on annual TICOSECT meeting Göttingen.

Hauff F., Hoernle K., Schminke H.-U., and Werner R. (1997) A Mid Cretaceaous Origin for the Galápagos Hotspot: Volcanological, Petrological and Geochemical Evidence from Costa Rican Oceanic Crustal Segments. *Geologische Rundschau*, **86**, 141-155

Hawkesworth C. J., Turner S. P., McDermott F., Peate D. W., and Van Calsteren P. (1997) U-Th Isotopes in Arc Magmas: Implications for Element Transfer from the Subducted Crust. *Science* **276**, 551-555.

Heezen B. C. and Rawson M. (1977) Visual observations of contemporary current erosion and tectonic deformation on the Cocos Ridge crest. *Marine Geology* **23**, 173-196.

Heinrichs H. and Herrmann A. G. (1990) *Praktikum der Analytischen Geochemie*. Springer-Verlag, 669pp.

Henningsen D. (1966a) Die pazifische Küstenkordillere (Cordillera Costena) Costas Ricas und ihre Stellung innerhalb des süd-zentralamerikanischen Gebirges. *Geotektonische Forschungen* **23**, 3-66.

Henningsen D. (1966b) Estratigrafia y paleogeografia de los sedimentos del Cretacico . . .-Terciario en el sector sureste de Costa Rica. *Inst. Centroamericano Inv. y Tecnologia Indus. Pub. Geol. ICAITI* **1**, 53-57.

Herrstrom E. A., Reagan M. K., and Morris J. D. (1995) Variations in lava composition associated with flow of asthenosphere beneath southern Central America. *Geology (Boulder)* **23**(7), Pages 617-620.

Hey R. (1977) Tectonic evolution of the Cocos-Nazca spreading center. *Geological Society of America Bulletin* **88**, 1404-1420.

Hey R., Johnson G. L., and Lowrie A. (1977) Recent plate motions in the Galapagos area. *Geological Society of America Bulletin* **88**, 1385-1403.

Heywood C. E. (1984) Forearc deformation in southern Costa Rica: A consequence of the collision of the aseismic Cocos Ridge. M.S. thesis, University of California.

Hibbard J. P. and Karig D. E. (1990) Structural and magmatic responses to spreading ridge subduction; an example from Southwest Japan. *Tectonics* **9**(2), Pages 207-230.

Hildreth W. and Moorbath S. (1988) Crustal contributions to arc magmatism in the Andes of central Chile. *Contributions to Mineralogy and Petrology* **98**(4), Pages 455-489.

Hole M. J. and Larter R. D. (1993) Trench- proximal volcanism following ridge crest- trench collision along the antartic peninsula. *Tectonics* **12**(4), 897 - 910.

Hole M. J., Rogers G., Saunders A. D., and Storey M. (1991) Relation between alkalic volcanism and slab-window formation. *Geology (Boulder)* **19**(6), Pages 657-660.

Irvine T. N. and Baragar W. R. A. (1971) A guide to the chemical classification of common volcanic rocks. *Canadian Journal of Earth Sciences* **8**, 523-548.

Ishikawa T. and Nakamura E. (1994) Origin of the slab component in arc lavas from across-arc variation of B and Pb isotopes. *Nature (London)* **370**(6486), Pages 205-208.

Johnson R. W., Jaques A. L., Langmuir C. H., Perfit M. R., Staudigel H., Dunkley P. N., Chappell B. W., Taylor S. R., and Baekisapa M. (1987) Ridge subduction and forearc volcanism; petrology and geochemistry of rocks dredged from the western Solomon Arc and Woodlark Basin. *Circum Pacific Council for Energy and Mineral Resources, Earth Science Series* **7**, 155-226.

Johnston S.-T. and Thorkelson D.-J. (1997) Cocos-Nazca slab window beneath Central America. *Earth and Planetary Science Letters* **146**(3-4), Pages 465-474.

Kay R. W. (1978) Aleutian magnesian andesites; melts from subducted Pacific Ocean crust. *Journal of Volcanology and Geothermal Research* **4**(1-2), Pages 117-132.

Kay S. M., Ramos V. A., and Marquez M. (1993) Evidence in Cerro Pampa volcanic rocks for slab-melting prior to ridge-trench collision in southern South America. *Journal of Geology* **101**(6), Pages 703-714.

Keigwin L. D., Jr. (1982) Late Cenozoic isotope stratigraphy of DSDP Site 157 (Panama Basin); onset of Northern Hemisphere glaciation. *Eos, Transactions, American Geophysical Union* **63**(45), Pages 1143.

Kelemen P.-B., Johnson K. T. M., Kinzler R. J., and Irving A. J. (1990) High-field-strength element depletions in arc basalts due to mantle-magma interaction. *Nature (London)* **345**(6275), Pages 521-524.

Kelemen P.-B., Shimizu N., and Dunn T. (1993) Relative depletion of niobium in some arc magmas and the continental crust; partitioning of K, Nb, La and Ce during melt/ rock reaction in the upper mantle. *Earth and Planet. Sci. Lett.* **120**(3-4), Pages 111-133.

Kelleher J. and McCann W. (1976): Buoyant zones, great earthquakes, and unstable boundaries of subduction. *J. Geophys. Res.* 81; 4885-4896.

Kelleher J. and McCann W. (1977) Bathymetric highs and the development of convergent plate boundaries. In *Island Arcs, Deep Sea Trenches and Back-Arc Basins*, Vol. 1 (ed. M. Talwani and W. C. Pitman III), pp. 115-122. Am. Geophys. Union, Maurice Ewing Ser.

Kepezhinskas P., McDermott F., Defant M.-J., Hochstaedter A., Drummond M.-S., Hawkesworth C.-J., Koloskov A., Maury R.-C., and Bellon H. (1997) Trace element

and Sr-Nd-Pb isotopic constraints on a three-component model of Kamchatka Arc petrogenesis. *Geochimica et Cosmochimica Acta* **61**(3), Pages 577-600.

Kesel R.-H. (1983) Quaternary history of the Rio General Valley, Costa Rica. *Research Reports National Geographic Society* **15**, 339-358.

Kilian R. and Stern C. (1994) New trace element and isotopic constraints on the genesis of andesites and dacites of the Quaternary Austral Volcanic Zone of the Andes. *Mineralogical Magazine* **58A**(A-K), Pages 477-478.

Kimura G., Silver E. A., Blum P., and al. e. (1997) Proccedings of the Ocean Drilling Program, Initial Reports. **170**(College Station, Texas), 7-17.

Klein E. M. and Langmuir C. H. (1987) Global correlations of ocean ridge basalt chemistry with axial depth and crustal thickness. *J. Geophys. Res.* **92**, 8089-8115.

Kolarsky R.-A., Mann P., and Montero W. (1995a) Island arc response to shallow subduction of the Cocos Ridge, Costa Rica. In *Geologic and Tectonic Development of the Caribbean Plate Boundary in Southern Central America*, Vol. Special Paper. Vol.295 (ed. P. Mann), pp. 235-262. Geological Society of America.

Kolarsky R.-A., Mann P., and Montero W. (1995b) Island arc response to shallow subduction of the Cocos Ridge, Costa Rica. *Special Paper Geol. Society of America* **295**, 235-262.

Kruckow T. (1974) Landhebung im Valle Central und Wachstum der Küstenebenen in Costa Rica (Mittelamerika). *Jahrbuch Wittheit zu Bremen* **18**, 247-263.

Kuijpers E. P. (1979) Analisis sedimentológico de la Formación Punta Caballo (Mioceno), Costa Rica. *Geogr. Nac., Informe Semest.* **1979/2**, 77-94.

Kussmaul S. (1987) Petrologia de las rocas intrusivas Neogenas de Costa Rica Translated Title: Petrology of the Neogene intrusive rocks of Costa Rica. *Revista Geologica de America Central* **7**, 83-111.

Kussmaul S., Tournon J., and Alvarado G. (1994) Evolution of the Neogene to Quaternary igneous rocks of Costa Rica. In *Geology of an Evolving Island Arc. The Isthmus of Southern Nicaragua, Costa Rica, and Western Panama*, Vol. 7 (ed. H. Seyfried and W. Hellmann), pp. 97-123. Profil.

Lanphere M. A. and Dalrymple G. B. (1971) A test of the 40Ar/39 Ar age spectrum technique on some terrestrial materials. *Earth Planet. Sci. Lett.* **12**, 359-372.

Lanphere M. A. and Dalrymple G. B. (1976) Identification of excess 40Ar by the 40Ar/39Ar age spectrum technique. *Eart Planet. Sci. Lett.* **32**, 141-148.

Le Maitre, R.W. (1989): A classification of igneous rocks and glossary of terms. Recommendations of the International Union of Geological Sciences, subcommission on the systematics of igneous rocks. Blackwell Scientific Publications, Oxford, London, Edinburgh, Boston, Melbourne.

Leake, B.E., Woolley, A.R., Arps, C.E.S., Birch, W.D., Gilbert, M.C., Grice, J.D., Hawthorne, F.C., Kato, A., Kisch, H.J., Krivovichev, V.G., Linthout, K., Laird, J., Mandarino, J., Maresch, W.V., Nickel, E.H., Rock, N.M.S., Schumacher, J.C., Smith,

D.C., Stephenson, N.C.N., Ungaretti, L., Whittaker, E.J.W. and Youzhi, G. (1997): Nomenclature of amphiboles. Report on the subcommittee on amphiboles of the international mineralogical association commision on new minerals and mineral names. *European Journal of Mineralogy* 9: 623-651.

Leeman W.-P. and Carr M.-J. (1995) Geochemical constraints on subduction processes in the Central American volcanic arc; implications of boron geochemistry. In *Geologic and Tectonic Development of the Caribbean Plate Boundary in the Southern Central America*, Vol. Special Paper. Vol. 295 (ed. P. Mann), pp. 57-73. Geological Society of America.

Leeman W.-P., Carr M.-J., and Morris J.-D. (1994) Boron geochemistry of the Central American volcanic arc; constraints on the genesis of subduction-related magmas. *Geochimica et Cosmochimica Acta* **58**(1), Pages 149-168.

Lundberg N. (1991) Detrital record of the early Central American magmatic arc; petrography of intraoceanic forearc sandstones, Nicoya Peninsula, Costa Rica. *Geological Society of America Bulletin* **103**(7), Pages 905-915.

Luoni F. (1993) Petrologica e geochemica dei prodotti effusivi e subvulcanici della Formazione alcalina di Guayacan, Squirres (Costa Rica). Tesi di Laurea, Universita ´Degli Studi di Milano.

Longerich, H.P. (1993): Oxychlorine ions in inductively coupled plasma-mass spectrometry: effect of chlorine speciation as Cl^- and ClO_4. *Journal of Analytical Atomic Spectrometry* 8: 439-444.

Lonsdale P. and Klitgord K. D. (1978) Structure and tectonic history of the eastern Panama Basin. *Geological Society of America Bulletin* **89**, 981-999.

Malfait B. T. and Dinkelman M. G. (1972) Circum-Caribbean Tectonic and Igneous Activity and the Evolution of the Caribbean Plate. *Geological Society of America Bulletin* **83**, 251-272.

Mann P. and Burke K. (1984) Neotectonics of the Caribbean. *Reviews of Geophysics and Space Physics* **22**, 309-362.

Mann P., Schubert C., and Burke K. (1990) Review of Caribbean neotectonics. In *The Caribbean Region*, Vol. The Geology of North America, Vol. H (ed. G. Dengo and J. E. Case), pp. 307-338. Geological Society of America.

McCulloch M.-T. and Gamble A. J. (1991) Geochemical and geodynamical constraints on subduction zone magmatism. *Earth and Planetary Science Letters* **102**(3-4), 358-374.

McDougall I. and Harrison T. M. (1988) *Geochronology and Thermochronology by the 40Ar/39Ar method*. Oxford University Press.

McGeary S., Nur A., and Ben Avraham Z. (1985) Spatial gaps in arc volcanism: the effect of collision or subduction of oceanic plateaus. *Tectonophysics* **119**, 195-221.

McIntyre G. A., Brooks C., Compston W., and Turek A. (1966) The statistical assessment of Rb-Sr isochrons. *J. Geophys. Res.* **71**, 5459-5468.

Meschede M. (1986) A method of discriminating between different types of mid-ocean ridge basalts and continental tholeiites with the Nb-Zr-Yb diagram. *Chem. Geol.* **56**, 207-218.

Meschede M. (1998) Neue Erkenntnisse zur plattentektonischen Entwicklung der Cocos-Platte als Ergebnis einer multidisziplinären Studie. *Ocean Drilling Programm- Deep Sea Drilling, 4.-6. March 1998, Abstract Volume*, 38-39.

Milionis P. N., Feigenson M. D., Carr M. J., and Alvarado G. E. (1986) Constraints on the Source of Central Costa Rica Alkalic Lavas. *EOS*.

Miller D.-M., Goldstein S.-L., and Langmuir C.-H. (1994) Cerium/ lead and lead isotope ratios in arc magmas and the enrichment of lead in the continents. *Nature (London)* **368**(6471), Pages 514-520.

Miyamura S. (1975) Recent crustal movements in Costa Rica disclosed by relevelling surveys. *Tectonophysics* **29**, 191-198.

Montero W. (1994) Neotectonics and related stress distribution in a subduction-collisional zone: Costa Rica. In *Geology of an Evolving Island Arc. The Isthmus of Soutern Nicaragua, Costa Rica, and Western Panama*, Vol. 7 (ed. H. Seyfried and W. Hellmann), pp. 125-141. Profil.

Moore G. F. and Sender K. L. (1995) Fracture zone collision along the South Panama margin. In *Geologic and Tectonic Development of the Caribbean Plate Boundary in the Southern Central America*, Vol. Special Paper. Vol. 295 (ed. P. Mann), pp. 201-212. Geological Society of America.

Morgan W. J. (1971) Convecting plumes in the lower mantle. *Nature* **230**, 42-43.

Morris J. D., Leeman W. P., and Tera F. (1990) The subducted component in island arc lavas; constraints from B-Be isotopes and Be systematics. *Nature (London)* **344**(6261), Pages 31-36.

Mullen E. D. (1983) MnO/TiO2/P2O5: a minor element discriminant for basaltic rocks of oceanic environments and its implications for petrogenesis. *Earth Planet. Sci. Lett.* **62**, 53-62.

Navon, O. and Stolper, E. (1987): Geochemical consequences of melt percolation: the upper mantle as a chromatographic column. *Journal of Geology* 95: 285-307.

Nesbitt H. W., Markovics G., and Price R. C. (1980) Chemical processes affecting alkalis and alkaline earths during continental weathering. *Geochimica et Cosmochimica Acta* **44**, 1659 - 1666.

Nichols G.-T., Wyllie P.-J., and Stern C.-R. (1994) Subduction zone melting of pelagic sediments constrained by melting experiments. *Nature (London)* **371**(6500), Pages 785-788.

Ormerod D.-S., Hawkesworth C.-J., Rogers N.-W., Leeman W.-P., and Menzies M.-A. (1988) Tectonic and magmatic transitions in the western Great Basin, USA. *Nature (London)* **333**(6171), Pages 349-353.

Peacock S. M. (1990): Numerical simulation of metamorphic pressure-temperature-time paths and fluid production in subducting slabs. *Tectonics*. 9; 5

Peacock S.-M., Rushmer T., and Thompson A.-B. (1994) Partial melting of subducting oceanic crust. *Earth and Planetary Science Letters* **121**(1-2), Pages 227-244.

Pearce J. A. (1983) Role of the sub-continental lithosphere in magma genesis at active continental margins. In *Continental basalts and mantle xenoliths* (ed. Hawkesworth and Norry), pp. 230-272. Shiva.

Pearce J. A. and Cann J. R. (1973) Tectonic setting of basic volcanic rocks determined using trace element analysis. *Earth Planet. Sci. Lett.* **19**, 290-300.

Pearce J. A. and Norry M. J. (1979): Petrogenetic implications of Ti, Zr, Y, and Nb variations in volcanic rocks. *Contrib. Min. Pet.* 69, 33-47.

Peccerillo, A. and Taylor, S.R. (1976): Geochemistry of Eocene calc-alkaline volcanic rocks from the Kastamonu area, Northern Turkey. *Contributions to Mineralogy and Petrology* 58: 63-81.

Pichler H. and Schmitt-Riegraf C. (eds) (1987): Gesteinsbildende Minerale im Dünnschliff, Translated Title: Rock-forming minerals in thin-section. Enke Verlag. Stuttgart, 230 pp.

Pindell J. L. and Barrett S. F. (1990) Geological evolution of the Caribbean region; a plate-tectonic perspective. In *The Caribbean Region*, Vol. The Geology of North America, Vol. H (ed. G. Dengo and J. E. Case), pp. 405-432. Geological Society of America.

Plank T. and Langmuir C.-H. (1988) An evaluation of the global variations in the major element chemistry of arc basalts. *Earth and Planetary Science Letters* **90**(4), 349-370.

Potts P. J. (1987) *A handbook of silicate rock analysis*. Blackie, London, 669p.

Protti M., Güendel F., and McNally K. (1995) Correlation between the age of the subducting Cocos plate and the geometry of the Wadati- Benioff zone under Nicaragua and Costa Rica. In *Geologic and Tectonic Development of the Caribbean Plate Boundary in Southern America*, Vol. Special Paper. No. 295 (ed. P. Mann), pp. 309-326. Geological Society of America.

Rapp R. P. (1994) Partial melting of metabasalts at 2-7 GPa: Experimental results and implications for lower crustal and subduction zone processes. *Mineral. Mag.* **58A**, 760-761.

Rapp, R.P. and Watson, E.B. (1995): Dehydration melting of metabasalt at 8-32 kbar: implications for continental growth and crust-mantle recycling. *Journal of Petrology* 35: 891-931.

Rea D. K. and Malfait B. T. (1974) Geologic Evolution of the Northern Nazca Plate. *Geology*, 317-320.

Reagan M.-K., Gill J.-B., and Mattinson J.-M. (1986) The origin of "intraplate" basalt in an arc setting at Turrialba Volcano, Costa Rica. *Eos, Transactions, American Geophysical Union* **67**(44), Pages 1280.

Rickwood P. C. (1989) Boundary lines within petrologic diagrams which use oxides of major and minor elements. *Lithos* **22**, 247-263.

Rivier S.-F. (1985) Seccion geologica del Pacifico al Atlantico a traves de Costa Rica Translated Title: Geologic section across Costa Rica from the Pacific to the Atlantic. *Revista Geologica de America Central* **2**, 23-32.

Robin C. and Tournon J. (1978) Spatial relations of andesitic and alkaline provinces in Mexico and Central America. *Can. J. Earth Sci.* **15**, 1633 - 1641.

Rogers G. and Saunders D. (1989) Magnesian andesites from Mexico, Chile and the Aleutian Islands: implications for magmatism associated with ridge- trench collision. In *Boninites and related Rocks* (ed. A. J. Crawford), pp. 416-445.

Roddick J. C., Cliff R. A., and Rex D. C. (1980) The evolution of excess argon in alpine biotites - A 40Ar-39Ar analysis. *Earth Planet. Sci. Lett.* **48**, 185-208.

Saenz R.-R. (1982) Edades radiometricas de algunas rocas en Costa Rica Translated Title: Radiometric ages of some rocks in Costa Rica. *Boletin de Vulcanologia* **12**, 8-10.

Sapper K. (1937) *Mittelamerika*. Steinmann and Wikkens.

Schumacher J. C. (1997) The estimation of ferric iron in electron microprobe analysis of amphiboles. *Eur. J. Mineral.* **9**, 643-651.

Seebach K. v. (1892) *Über Vulkane Zentralamerikas*. Dieterische Verlags-Buchhandlung.

Shaw D. M. (1970) Trace element fractionation during anatexis. *Geochim. Cosmochim. Acta* **34**, 237-243.

Shi Y. (1992) Induced mantle flow and back-arc opening due to roll-back subduction. *International Geological Congress, Abstracts Congres Geologique Internationale, Resumes* **29**(131).

Shi Y. and Wang Y.-c. (1979) Roll-back subduction and back-arc opening. *Diqiu Wulixue Bao = Acta Geophysica Sinica* **36**(1), Pages 37-43.

Shipboard Sci. Party; Kimura G., Silver E. A., Blum P., et al.. (1997) *Proccedings of the Ocean Drilling Program, Initial Reports*. Vol 170, 458 pp.

Sisson V.-B. and Pavlis T.-L. (1993) Geologic consequences of plate reorganization; an example from the Eocene Southern Alaska fore arc. *Geology (Boulder)* **21**(10), Pages 913-916.

Stack C. M. (1991) Inverse modeling of alkaline lavas from Guyacan, Costa Rica. Master of Science, Rutgers, University of New Jersey.

Stern C. R. and Kilian R. (1996) Role of the subducted slab, mantle wedge and continental crust in the generation of adakites from the Andean Austral Volcanic Zone. *Contrib. Mineral. Petrol.* **123**, 263-281.

Stoiber R. E. and Carr M. J. (1973) Quaternary Volcanic and Tectonic Segmentation of Central America. *Bulletin Volcanologique* **37**, 304-325.

Streckeisen A. (1976) To each plutonic rock its proper name. *Earth Sci. Rev.* **12**, 1-33.

Sun, S.S. and Mc Donough, W.F. (1989): Chemical and isotopic systematics of oceanic basalts. In Saunders, A.D. and Norry, M.J. (Eds.): Magmatism in the Ocean basins. *Geological Society of London Special Publication* 42: 313-345.

Tajima F. and Kikuchi M. (1995) Tectonic implications of the seismic ruptures associated with the 1983 and 1991 Costa Rica earthquakes. In *Geologic and Tectonic Development of the Caribbean Plate Boundary in the Southern Central America*, Vol. Special Paper. Vol. 295 (ed. P. Mann), pp. 327-340. Geological Society of America.

Taylor H. P., Jr. (1986) Igneous Rocks II: Isotopic case studies of circumpacific magmatism. In *Stable Isotopes in high temperature geological processes*, Vol. 16 (ed. J. W. Valley, H. P. Taylor, Jr., and J. R. O'Neil).

Tera F., Brown L., Morris J., Sacks I. S., Klein J., and Middleton R. (1986) Sediment incorporation in island-arc magmas: Inferences from ^{10}Be. *Geochim. Cosmochim. Acta* **50**, 535-550.

Thorkelson D.-J. (1996) Subduction of diverging plates and the principles of slab window formation. *Tectonophysics* **255**(1-2), Pages 47-63.

Thorkelson D. J. and Taylor R. P. (1989) Cordilleran slab windows. *Geology* **17**, 833-836.

Thorpe R. S., Francis P. W., and Moorbath S. (1979) Strontium isotope evidence for petrogenesis of Central American andesites. *Nature (London)* **277**(5691), Pages 44-45.

TICOSECT. (1998) Annual meeting, unpub. meeting report.

Tiedemann R., Franz S. O., Haug G., and Zahn R. (1998) Pliocene closure of the Central American Isthmus and its impact on the formation of North Atlantic deep and intermediate water. *Ocean Drilling Programm- Deep Sea Drilling Project*, 61-62.

Tournon J. (1972) Présence de Basaltes Alcalins Récents au Costa Rica (Amérique Centrale). *Bulletin volcanologique* **36**, 140 - 147.

Tournon J. (1984) Magmatismes du mésozoique à l´actuel en Amérique Centrale. L´exemple de Costa Rica, des ophiolites aux andesites. Ph.D. thesis, Université Pierre et Marie Curie. 335p

Tournon J. and Alvarado G. (1997) *Carte géologique du Costa Rica / Mapa geológico de Costa Rica. Notice explicative / Folleto explicativo.* Instituto tecnológico de Costa Rica, 80p.

Turner G. (1971) 40Ar-39Ar ages from the lunar maria. *Earth. Planet. Sci. Lett.* **11**, 169-191.

Turner S., Hawkesworth C., van C.-P., Heath E., Macdonald R., and Black S. (1996) U-series isotopes and destructive plate margin magma genesis in the Lesser Antilles. *Earth and Planetary Science Letters* **142**(1-2), Pages 191-207.

Van Andel T. H., Heath G. R., Malfait B. T., Heinrichs D. F., and Ewing J. I. (1971) Tectonics of the Panama Basin, Eastern Equatorial Pacific. *Geological Society of America Bulletin* **82**, 1489-1508.

Van der Hilst R. D., Widiyantoro S., and Engdahl E. R. (1997) Evidence for deep mantle circulation from global tomography. *Nature* **386**, 578-584.

Vogt P. R., Lowrie A., Bracey D. R., and Hey R. N. (1976) Subduction of Aseismic Oceanic Ridges: Effects on Shape, Seismicity, and Other Characteristics of Consuming Plate Boundaries. *The Geological Society of America* Special Paper **172**, 1 - 59.

Von Huene R. and Scholl D. W. (1993) The return of sialic material to the mantle indicated by terrigeneous material subducted at convergent margins. *Tectonophys.* **219**, 163-175.

Wartho J. A., Rex D. C. and Guise P. G. (1996): Excess argon in amphiboles linked to greenschist facies alteration in the Kamila amphibolite belt, Kohistan island arc system, northern Pakistan; insights from (super 40) Ar/ (super 39) Ar step-heating and acid leaching experiments. *Geolog. Mag*. 133, 595-609.

Werner R. (1998) Report on study results, annual TICOSECT meeting Göttingen.

Weyl R. (1957) Beitraege zur Geologie der Cordillera de Talamanca Costa Ricas (Mittelamerika). *Neues Jahrbuch fuer Geologie und Palaeontologie. Abhandlungen. Pages*.

Weyl R. (1961) Volcanoes and Volcanic Landscapes in Central America. *Germany- the Magazine of the Federal Republic* **6**(25), 1-5.

Weyl R. (1980) *Geology of Central America*. Gebrüder Bornträger, Berlin, 410p.

White, W.M. and Patchett, P.J. (1984): Hf-Nd-Sr isotopes and incompatible element abundances in island arcs: implications for magma origin and crust mantle evolution. *Earth and Planetary Science Letters* 67: 167-185.

White W.-M., McBirney A.-R., and Duncan R.-A. (1993) Petrology and geochemistry of the Galapagos Islands; portrait of a pathological mantle plume. *Journal of Geophysical Research, B, Solid Earth and Planets* **98**(11), Pages 19,533-19,563.

Wiechert U. and Hoefs. J. (1995): An excimer laser-based micro analytical preparation technique for in-situ oxygen isotope analysis of silicate and oxide minerals. In: Vanko and Brown (eds) Papers presented at PACROFI V; 5th biennial Pan-American Conf. on Research on fluid inclusions. *Geochim. Cosmochim. Acta*. 59, 4093-4101.

Wilson J. T. (1963): Age and location of islands and aseismic ridges as a key to behavior of the upper mantle. *Transactions, American Geophysical Union*. 44; 97pp.

Wilson M. (1989) *Igneous Petrogenesis*. Unwin Hyman, London, 466p.

Wyllie P. J. (1982) Subduction products according to experimental prediction-. *Geological Society of America Bulletin* **93**, 468 - 476.

Yogodzinski G. M., Kay R. W., Volynets O. N., Koloskov A. V., and Kay S. M. (1995) Magnesian andesite in the western Aleutian Komandorsky region; implications for slab melting and processes in the mantle wedge. *Geol. Soc. America Bull.* **107**(5), 505-519.

10 Appendix

10.1 Analytical Methods

110 igneous rock samples were collected in Costa Rica for the present study. After a first revision, 80 of these rocks were analysed by XRF. Based on the acquired geochemical data, a number of 60 samples was chosen for ICP-MS analysis, and a subset of 30 of these was additionally selected for isotope analyses.
All analyses were carried out at the Geochemisches Institut and the Institut für Geologie und Dynamik der Lithosphäre, University of Göttingen except for the $^{40}Ar/^{39}Ar$ dating which was done in co-operation with the German Geological Survey, BGR, at Hanover.

10.1.1 Sample Preparation

The sample size varies from about 500 g to 20 kg, depending on availability, grain size, and analytical processing (e.g. mineral separation). To minimise secondary contamination of the samples, removal of alteration rims and splitting up into suitable chips was done directly at their sampling location.
Remaining alteration rims were cut off with a diamond saw, sawmarks were raped off with Si-carbide grinding paper and the samples were all carefully cleaned.
Hand-specimen were kept from all samples and thin sections were made from those samples which were selected to be analysed. The entire rest of the sample material was crushed in Fe-Mn-steel-jaw crushers. About 250 g of that material was separated using a rotation-separator. These aliquots of each sample were grinded in agate ball mills until grain-sizes were <65 µm.

Sample preparation for those analytical procedures not using the powder fraction (e.g. mineral separation) are described in the respective chapters.

10.1.2 Analysis of Ferrous Iron (Fe^{2+})

Since ferrous iron could not be distinguished from ferric iron by XRF analysis, it had to be determined separately by titration of the HF-H_2SO_4 dissolved sample powder against $KMnO_4$ (method after Pratt). For details refer to Heinrichs and Herrmann 1990.

10.1.3 Determination of Loss On Ignition (LOI)

The volatile content of the samples (mainly H_2O, CO_2) was determined by heating of about 1g of rock powder to more than 1000°C in a muffle oven for about 4 hours. The resulting weight loss in percent is called loss on ignition.

10.1.4 X-Ray Fluorescence Spectroscopy (XRF)

XRF spectroscopy uses characteristic x-rays (secondary fluorescence), generated by excitation of inner shell electrons with primary x-rays to specify elements and concentration. For details of the method refer to Potts [1987]- This analytical method was used to determine major- and minor elements (Si, Ti, Al, Fe, Mn, Mg, Ca, Na, K, P) of the rocks as well as some trace elements (Rb, Sr, Ba, Sc, V, Cr, Ni, Zn, Ga, Y, Zr, Nb, Pb). The analysis was done on glass tablets [Ahmedali, 1989], prepared by melting of 1g of sample powder with 5.5g spectroflux ($Li_2B_4O_7$) and 0.5g LiF at 1100°C using a semi-automated melting apparatus. Measurements were carried out on a Philips PW 1408 with calibration against multiple

international standards and internal correction for matrix effects. A check for correctness and reproducibility was provided by simultaneous measurement of standards.

10.1.5 Inductively Coupled Plasma Mass Spectrometry (ICPMS)

10.1.5.1 Whole Rock Analysis

The ICPMS technique provides the advantage of simultaneous determination of a wide range of trace elements from Li to U, low detection limits and good analytical precision especially for masses >80. Fundamentals of this method are described in Potts 1987, Garbe-Schönberg 1993. For the present purpose, trace elements like REE (La – Lu), HFSE (Nb, Ta, Zr, Hf), LILE (Rb, Sr, Ba, Tl, Cs), and others (Li, Be, Cu, Y, Pb, Th, U, Sc, V, Cr, Co, Ni, Zn) of 78 selected samples were analysed on an ICPMS VG-PlasmaQuad STE. Selection of respective isotopes was done on criteria of abundance and exclusion of isobaric interference. Calibration of the intensities against concentration values for each element is provided by measuring multi-element calibration solutions prior to sample acquisition. These calibration solutions were prepared from stock solutions by aiming to span the total range of expected concentrations and by the attempt to keep the elemental ratios close to natural conditions. A control for contaminations due to dissolution processes is obtained by measurement of simultaneously prepared blank solutions, a correction for the machine drift is provided by repeated measurement of one of the calibration solutions and by the internal standards of Rh, Re, In. Co-processed lab-internal and international standards provided an external check for accuracy and reproducibility.

Sample preparation: About 100 mg of sample powder was weighed into Teflon beakers after Heinrichs and Herrmann [1990] and dissolved under pressure in a mixture of acids composed of 3 ml HF, 3ml $HClO_4$, and 1 ml HNO_3. After cessation of gas formation, the beakers were tightly closed and heated in a muffle oven at 200°C for 14 hours. After cooling to ambient temperatures, the beakers were opened and placed on a hot plate for evaporation at 180°C. The dried sample was re-dissolved in 2 ml HNO_3 and once again put onto the hot plate. After the second stage of evaporation, 2 ml HNO_3, 5 ml de-ionised water and the internal standard were added to the sample. This solution was rinsed into a 100ml quartz-glass flask and the remaining volume was filled with de-ionised water. The resulting solution contained the sample in a dilution 1:1000 in 2 % HNO_3 with 20 ppb Rh, Re, In as internal standard. It was kept in polyethylene bottles and measured within two days to minimise the risk of precipitation or interchange with the container. For each batch of fifteen samples a blank solution and a lab-intern or international standard were prepared. All reagents used were three times distilled to suppress blank values.

10.1.5.2 Mineral Analysis (LA-ICPMS)

To obtain in-situ trace element analysis of single minerals, ICPMS analysis in combination with laser ablation technique was applied.

The Nd:YAG-laser of type Fisons VG UV-Microprobe is operating at 266 nm wavelength in pulsating mode. Ablated particles from polished mineral surfaces in thick sections are transported by an argon gas stream into the Fisons VG PlasmaQuad 2+ (with S-option) ICPMS. Trace elements (REE and Ba) of amphibole, plagioclase and biotite were measured in three samples. Calibration was done against the international standard glass NIST 612. Ba was measured as internal standard but turned out as not suitable. Operating parameters were: large aperture, full energy of 3 mJ, beam frequency 5 Hz, acquisition time 40 sec., uptake delay 20 sec. Sensitivity is around 5000 cps/ppm for ^{140}Ce, background is at about 10 – 20 counts/sec (Simon, pers. comm.). A detailed descriptions of the method can be found in Longerich et al., 1996.

10.1.6 Isotope Analysis

10.1.6.1 Radiogenic Isotopes (TIMS)

Rb-, Sr-, Sm-, Nd- isotope ratios were determined on 24 whole rock samples.

Prior to dissolution, the sample powder (~100 mg) has been leached for half an hour at 60°C in 2.5 N HCl to remove surface alteration and radiogenic ^{87}Sr derived from seawater-interaction during submarine eruption. Leaching experiments with 6 N HCl have been made for comparison but showed no further improvements. The leaching method is described by Asahara et al. [1995]

After rinsing and drying, the leaching residue was dissolved in 6 ml HF:HNO_3 (1:1) for 16 hours at 110°C within Savillex© vials on a hot plate. The solution was evaporated to complete dryness and baked at 180°C. After dissolution of the cake in 1 ml HNO_3, following evaporation, dissolution in 2 ml HCl 6 N, and evaporation for the last time, it was re-dissolved in 3.2 ml 2.6 N HCl and stored in PE vials. For separation, the sample solution was rinsed with 2.6 N HCl through columns containing ion-exchange resin BIORAD AG 50W-X8 Resin, 200-400 mesh. The strontium rich eluation fraction was caught in a vial, evaporated to dryness and stored until measuring.

For Nd separation, the REE rich fraction gained from the above separation sequence was separated in a second set of columns containing Teflon powder which is impregnated with ion-exchanging HDEHP Bis-(2-etylhexyl)-Phosphate. Eluation of Nd was done with 0.18 N HCl, after that eluation of Sm with 0.5 N HCl.

For measurement, Sr was dissolved in 0.5 N H_3PO_4 and mounted on Ta-single filaments (~2 µg), Sm and Nd were dissolved in 2 N HCl and mounted on Re-double-filaments (~1 µg).

The strontium isotopic ratios were corrected to $^{86}Sr/^{88}Sr=0.1194$, according to the recommendations of the IUGS Subcommission. Sr-Standard NBS 987 gave an average value of $^{87}Sr/^{86}Sr=0.71025\pm1$. Measurement of a single sample was carried on until 2σ $^{87}Sr/^{86}Sr$ was less than $2*10^{-5}$. Reproducibility (n=105) of $^{87}Sr/^{86}Sr=0.71024\pm4(1\sigma)$. Total procedural blanks: 2-4 ng.

$^{143}Nd/^{144}Nd$ ratios have been corrected for isotope fractionation to $^{146}Nd/^{144}Nd=0.7219$. The Nd-standard La Jolla had an ideal value of $^{143}Nd/^{144}Nd=0.51185\pm1$. Measurement of a Nd sample was done until 2σ $^{143}Nd/^{144}Nd$ was less than $6*10^{-6}$. Reproducibility (n=42) of $^{143}Nd/^{144}Nd=0.511851\pm1(1\sigma)$. Total procedural blanks: 0.7-1 ng.

For lead isotopic determination about 100 mg rock chips were used for each dissolution process. These chips of about 1 to 2 mm diameter were received by hand-picking from the crushed rock in order to exclude admixture of altered material. To remove contaminations, the sample was leached in 6 N HCl for ½ hour.

Lead separation was done according to the HBr-HCl method (e.g. Chen and Wasserburg, 1981) on anion exchange columns containing 100 µl resin (Biorad AG1-X8, 200-400 mesh). The samples were dissolved in 1 ml 2N HCl and washed into the columns, afterwards rinsed with 2 ml 0.6N HBr and finally eluated with 1ml 6N HCl. To get rid of alkalis and earth-alkalis, the separation process was repeated. The entire processing was carried out within a laminar flow box to exclude contamination by lead which is bound to dust particles. Total blanks were 50-100 pg. Pb was mounted on Re-single-filaments using 0.5N H_3PO_4 + silica-gel.

Measurements of Sr-, Nd-, Sm-, and Pb-isotopes were carried out on a MAT 262 RPQ+ TIMS in static mode. Ionisation temperature for Pb measurement was held constant at 1180°C. Correction of sample measurements according to multiple measurement of standard NBS 981 yielding fractionation factors of 0.451, 0.465, 0.478 $*amu^{-1}$ ($^{206}Pb/^{204}Pb$, $^{207}Pb/^{204}Pb$, $^{208}Pb/^{204}Pb$)

10.1.7 Stable Isotopes (LA-SIRMS)

Oxygen isotope measurements were done with the laser probe on mineral separates. Suitable separates consisted of hand-picked olivine, clinopyroxene, amphibole, or quartz grains of at least 1 mm size. Measurements were carried out on a SIRMS type Finigan MAT 251 fitted with a KrF-excimer laser (COMPex, 193nm). With help of the pulsating laser beam the mineral separate is vaporised in a stainless steel reaction chamber. The chamber is filled with gaseous fluorine (ClF_3) which prevents recombination of released oxygen atoms. Within the preparation line, oxygen is converted into CO_2 which can be measured in the gas source mass spectrometer. For a detailed description of this method refer to Wiechert and Hoefs [1995].

10.1.8 $^{40}Ar/^{39}Ar$ Dating (LA-Noble-Gas-MS)

Mineral separation:

Datable rocks of the suites of interest were selected by checking for datable amphiboles in thin-sections and hand-specimen. In this case, biotites were not suitable for dating since they were either absent or suspected to be altered. K-feldspar was also not present or not fresh in the rocks of interest. The pre-crushed material of the selected rocks was repeatedly crushed and sieved to gain the appropriate grain sizes. Depending on the size of the amphiboles, material between 500 and 125 µm was kept. This material, comprising between 2 and 10 kg, was pre-enriched on a Wilfrey-table. Mineral separation was done in a processing sequence consisting of gravity precipitation in bromoform and diiodmethane, separation in a magnetic-separator and finally handpicking.

Irradiation:

Placed in a vacuum sealed quartz vial, alternating with the biotite standard HD-B1 (K-Ar age 24.21 Ma) as irradiation monitor to obtain the J-curve [Dalrymple and Duffield, 1988], irradiation of the samples was done in the FRG-2 GKSS Geesthacht reactor.

Analytical procedure:

$^{40}Ar/^{39}Ar$ analysis were carried out at the BGR, Hannover with the laser probe consisting of a Fisons VG 3600 mass spectrometer fitted with a 12 W Nd:YAG IR-laser system (Baasel Lasertech), a low volume ultra high vacuum inlet line, and a Johnston secondary electron multiplier. The IR laser (λ= 1064nm) was operated in continuous mode with a beam diameter of 200 µm. Argon gas was released by total fusion of amphibole separates, and by stepwise heating with de-focussed laser in one instance. Due to low Ar contents of certain samples it was necessary to fuse three grains at once. Sample gas purification was achieved by letting the gas pass a cold trap (dry ice/alcohol) and two Zr-Al getter elements (350°C, SAES).
Analyses of amphibole separates were also done in a conventional step-heating apparatus with resistance furnace. Gas cleaning stage and measurement in the mass spectrometer (VG 1200) are comparable to the above described technique, the only major difference is the argon extraction technique. In a resistance furnace, the sample is degassed in discrete intervals of 30 min duration at successively higher temperatures between 600° and 1550°C.

Method:

An excellent description of the $^{40}Ar/^{39}Ar$ method can be found in McDougall and Harrison [1988].
Here is only a brief outline of the method:
The $^{40}Ar/^{39}Ar$ technique is a variant of the K-Ar dating method, using the basic equation in geochronology:

$$t = \frac{1}{\lambda} \ln\left(1 + \frac{D}{N}\right)$$

Of principal necessity is the measurement of:

$^{40}Ar^*$ produced by natural decay of ^{40}K

$^{39}Ar_K$ produced by bombardment of ^{39}K with fast neutrons.

Simultaneous measurement of ^{36}Ar and ^{37}Ar is indispensable to correct for atmospheric and interfering Ar from K and Ca, respectively.

Mineral standards of known age, irradiated together with the samples are used to obtain a J-curve where J is a function of the neutron dose received by the samples. The above equation rearranges to:

$$t = \frac{1}{\lambda} \ln\left(1 + J \frac{^{40}Ar^*}{^{39}Ar_K}\right)$$

Data presentation:

Results obtained from the resistance furnace technique are displayed as $^{40}Ar/^{39}Ar$ release spectra, where the plateau statistically defines an age. The shape of the release spectrum may signal argon loss or inheritance (metamorphism/contamination). Simultaneous presentation of the Ca/K ratio provides control of the degassing phases.

An inverse isochron correlation diagram used for multiple crystal analyses by the laser fusion method gives an age by its lower intercept. The upper intercept gives the pure trapped, non-radiogenic component, i.e. initial Ar. Initial Ar values deviating from the atmospheric value of 295.5 indicates extraneous Ar, i.e. excess or inherited Ar.

A sphenochron is displayed by a wedge shaped distribution of the data in the isotope correlation diagram, confined by an upper isochron that corresponds to the eruption age and a lower isochron that corresponds to the age of inherited xenocrysts [Chen et al., 1996]. The intercept of initial $^{40}Ar/^{36}Ar$ is defined to pass through the atmospheric value.

10.1.9 Electron Microprobe Analysis (EMP)

Microprobe analysis is typically applied for quantitative chemical analysis with demand for high local resolution as for example for the analysis of single minerals.

Here, this method was used mainly to determine the K-content of amphiboles from samples selected for Ar/Ar dating. (For the dating technique the K-content is as important to know as the assumed ages to estimate the necessary amount of mineral separate for a successful procedure.) Three single grains from each sample were taken from the mineral separates which were ready for the dating procedure. The grains were mounted in epoxy resin and the surface of sample-holder and grains was polished and graphite coated.

Measurements were carried out on the newly acquired JEOL 8900 RL under the following operating conditions:

Acceleration Voltage: 15kV, Probe Current: 12nA, Probe Diameter: 2µm, Take-off Angle: 40°, Absorption Correction: $\phi\rho z$; Background Correction: Off-Peak

sample		group	lithology	locality	map	right	high	kg	thin-s	XRF	ICP-M	Sr/Nd	Pb
ALT-01	◇	Tholeiite	basalt	Cerro Irkibi	Uniòn 3642-IV	592 975	324 950						
ALT-02	◇	Tholeiite	basalt	Cerro Chai	Uniòn 3642-IV	592 250	324 540	1	x	x	x	x	x
ALT-03	◇	Tholeiite	basalt	Cerro Chai	Uniòn 3642-IV	592 145	324 400	4.5	x	x	x		
ALT-04	◇	Tholeiite	andesite	Cerro Chai	Uniòn 3642-IV	592 300	324 115	1.4	x	x	x		
ALT-05	◇	Tholeiite	bas.trachyand.	Cerro Bellavista	Uniòn 3642-IV	595 510	322 580	1.5	x	x	x		
ALT-06	◇	Tholeiite	trachyandesite	Cerro Bellavista	Uniòn 3642-IV	595 540	323 420	1.7	x	x	x		
ALT-07	◇	Tholeiite	andesite	Cerro Bellavista	Uniòn 3642-IV	595 545	323 095						
ALT-08	◇	Tholeiite	andesite	Cerro Bellavista	Uniòn 3642-IV	595 545	323 095						
ALT-09	◇	Tholeiite	bas.andesite	Cerro Bellavista	Uniòn 3642-IV	595 490	322 925	1	x	x	x		
ALT-10	◇	Tholeiite	basalt	Cerro Bellavista	Uniòn 3642-IV	595 465	322 785	1.8	x	x	x		
ALT-11	◇	Tholeiite	bas.andesite	Brus	Uniòn 3642-IV	594 350	322 570	2.5	x	x			
ALT-12	◇	Tholeiite	basalt	Brus	Uniòn 3642-IV	594 350	322 570	3	x	x	x	x	x
ALT-13	◇	Tholeiite	basalt	Brus	Uniòn 3642-IV	594 285	322 510						
ALT-14	◇	Tholeiite	basalt	Brus	Uniòn 3642-IV	594 285	322 510	3	x	x	x	x	
ALT-15	◇	Tholeiite	basalt	Brus	Uniòn 3642-IV	593 870	322 500	3.6	x	x	x		
ALT-16	◇	Tholeiite	bas.andesite	Brus	Uniòn 3642-IV	593 870	322 500	3	x	x	x		
UVI-19	◇	Tholeiite	gabbro	Punta Uvita	Coronado 3443-II	495 250	342 500	4	x	x			
NUE-76	◇	Tholeiite	gabbro	Alto Correviento	Changuena 3542-IV	540 300	326 620	5.9	x	x	x		
NUE-77	◇	Tholeiite	gabbro	Interamericana	Changuena 3542-IV	540 775	325 510						
INA-82	◇	Tholeiite	bas.andesite	General Viejo	San Isidro 3444-II	503 260	369 190	3	x	x			
INA-83	◇	Tholeiite	gabbro	Division	San Isidro 3444-II	496 725	382 350						
INA-84	◇	Tholeiite	gabbro	Alto Macho Mora	Cuerici 3444-I	495 800	386 400	2.5	x	x	x	x	
INA-88	◇	Tholeiite	gabbro	Int.am. Km 90	Vueltas 3444-IV	490 825	391 225	3.9	x	x			
NUE-92	◇	Tholeiite	gabbro	Quebr. Boruca	Changuena 3542-IV	539 510	325 550	5.3	x	x	x	x	
DOT-99	◇	Tholeiite	basalt	San Jeronimo	Dota 3344-I	450 650	398 000						
DOT-102	◇	Tholeiite	gabbro	San Josecito	Dota 3344-I	448 500	397 450						
CHI-113	◇	Tholeiite	bas.andesite	Cerro Pyramida	Durika 3544-III	519 500	381 075	3	x	x	x	x	
CHI-117	◇	Tholeiite	bas.andesite	Cerro Sin Fe	San Isidro 3444-II	515 105	377 185	6	x	x	x	x	x
CHI-118	◇	Tholeiite	andesite	Fila C.d.l.Maquina	San Isidro 3444-II	514 350	377 200						
TAL-79	○	Calc-alkal	tonalite	Ujarraz	Buenos Aires 3543-IV	540 450	354 400	3.3	x	x	x	x	x
TAL-80	○	Calc-alkal	tonalite	Quebr. Tirgra	Buenos Aires 3543-IV	541 050	355 900	3	x	x	x		
TAL-81	○	Calc-alkal	monzogranite	Rio Skra	Buenos Aires 3543-IV	539 300	357 040	3.6	x	x	x		
INA-67	○	Calc-alkal	dacite	Cerro Jaboncillo	Vueltas 3444-IV	486 575	394 925	5.3	x	x	x		
INA-85	○	Calc-alkal	alkali granite	Siberia	Cuerici 3444-I	494 825	388 175	5.6	x	x	x	x	
INA-86	○	Calc-alkal	andesite	La Ese	San Isidro 3444-II	494 560	375 480						
INA-87	○	Calc-alkal	andesite	Cerr. de la Muerte	Vueltas 3444-IV	490 075	390 175	2.5	x	x	x		
INA-89	○	Calc-alkal	granite	Division-Piedra	Cuerici 3444-I	497 175	384 350						
INA-90	○	Calc-alkal	granite	Division-Piedra	Cuerici 3444-I	498 950	384 400						
INA-91	○	Calc-alkal	tonalite	Piedra	Cuerici 3444-I	499 575	384 300						
ALT-95	○	Calc-alkal	monzodiorite	Sitio Coto Brus	Uniòn 3642-IV	599 540	325 725	7.2	x	x	x	x	
INA-96	○	Calc-alkal	andesite	Rivas	San Isidro 3444-II	500 900	375 900						
DOT-97	○	Calc-alkal	alkali granite	Copey	Vueltas 3444-IV	469 350	400 300	2.5	x	x	x		
DOT-98	○	Calc-alkal	monzodiorite	Santa Maria	Vueltas 3444-IV	469 250	400 525	7	x	x	x		
TAL-103	○	Calc-alkal	trachyandesite	Rio Lori	Siola 3544-II	550 000	366 700	2.5	x	x	x	x	
TAL-108	○	Calc-alkal	trachyandesite	Rio Lori	Siola 3544-II	548 750	367 850	4.8	x	x			
TAL-109	○	Calc-alkal	monzonite	Rio Lori	Siola 3544-II	549 850	367 775	0.5	x	x	x		
CHI-110	○	Calc-alkal	diorite	Alaska	Cuerici 3444-I	500 875	386 200	6.5	x	x			
CHI-111	○	Calc-alkal	diorite	San Juan Norte	San Isidro 3444-II	500 350	381 750	4.7	x	x	x		
CHI-112	○	Calc-alkal	diorite	San Juan Norte	San Isidro 3444-II	500 390	381 700	4	x	x			
CHI-114	○	Calc-alkal	diorite	Cerro Pyramida	Durika 3544-III	519 300	381 350						
CHI-115	○	Calc-alkal	tonalite	Cerro Chirripo	Durika 3544-III	519 300	381 725	5.5	x	x	x		
CHI-116	○	Calc-alkal	tonalite	Cerro Uran	Cuerici 3444-I	514 625	384 350	4.5	x	x	x	x	x
CHI-119	○	Calc-alkal	diorite	Fila C.d.l.Maquina	San Isidro 3444-II	510 485	379 400	4.5	x	x	x		
CHI-120	○	Calc-alkal	diorite	San Gerardo	San Isidro 3444-II	506 650	379 010	3	x	x	x		
NEI-18	△	Backarc	CA-lamprophyr	Cerro Bola, Neily	Canoas 3641-IV	582 350	286 850	12.2	x	x	x	x	x
BRI-20	△	Backarc	trachybasalt	s. Piedra Grande	Amubri 3644-IV	586 200	393 275	5.2	x	x			
BRI-21	△	Backarc	basalt	s. Piedra Grande	Amubri 3644-IV	586 200	393 275	16.2	x	x	x	x	x
BRI-22	△	Backarc	basalt	Shiroles	Amubri 3644-IV	574 100	393 400		x				
BRI-23	△	Backarc	basalt	s. Piedra Grande	Amubri 3644-IV	586 200	393 275	16.5	x	x	x	x	
BRI-24	△	Backarc	trachybasalt	s. Piedra Grande	Amubri 3644-IV	586 250	393 475	9.8	x	x	x		
BRI-25	△	Backarc	bas.trachyand.	Piedra Grande	Amubri 3644-IV	586 300	393 775	5.6	x	x	x		
GUA-26	△	Backarc	teschenite	Linda Vista	Bonilla 3446-II	583 050	220 990	4.7	x	x	x		
GUA-27	△	Backarc	teschenite	Bajo Tigre	Bonilla 3446-II	585 750	221 825	7	x	x	x	x	
GUA-28	△	Backarc	teschenite	Bajo Tigre	Bonilla 3446-II	585 750	221 825	8	x	x	x		
GUA-29	△	Backarc	teschenite	Bajo Tigre	Bonilla 3446-II	585 650	222 800						
GUA-30	△	Backarc	bas.andesite	Bajo Tigre	Bonilla 3446-II	585 650	222 800	2	x	x			
GUA-31	△	Backarc	teschenite	Bajo Tigre	Bonilla 3446-II	585 725	222 700			x			
GUA-32	△	Backarc	alkali basalt	Guayacan	Bonilla 3446-II	585 750	225 060						
GUA-34	△	Backarc	teschenite	Petroleo	Bonilla 3446-II	582 485	224 075						

sample		group	lithology	locality	map	right	high	kg	thin-s	XRF	ICP-M	Sr/Nd	Pb
GUA-35	△	Backarc	teschenite	Petroleo	Bonilla 3446-II	582 735	223 250						
GUA-36	△	Backarc	teschenite	Petroleo	Bonilla 3446-II	582 760	223 600						
GUA-37	△	Backarc	alkali basalt	Petroleo	Bonilla 3446-II	583 045	223 500						
GUA-38	△	Backarc	teschenite	Petroleo	Bonilla 3446-II	583 760	223 450	2.6	x	x			
GUA-39	△	Backarc	teschenite	Petroleo	Bonilla 3446-II	584 700	223 700						
GUA-40	△	Backarc	alkali basalt	Moravia	Bonilla 3446-II	585 250	227 860						
GUA-41	△	Backarc	teschenite	Fila Tunel	Bonilla 3446-II	579 890	224 960	5	x	x	x		
GUA-42	△	Backarc	teschenite	Rio Blanco	Bonilla 3446-II	578 210	225 750	3	x	x	x	x	x
GUA-43	△	Backarc	alkali basalt	Rio Blanco	Bonilla 3446-II	578 400	225 600						
GUA-44	△	Backarc	teschenite	Fila Tunel	Bonilla 3446-II	579 890	224 960						
GUA-45	△	Backarc	alkali basalt	Moravia	Bonilla 3446-II	585 850	229 000						
GUA-46	△	Backarc	alkali basalt	Moravia	Bonilla 3446-II	585 700	228 910						
GUA-47	△	Backarc	alkali basalt	Moravia	Bonilla 3446-II	585 380	228 665						
GUA-49	△	Backarc	alkali basalt	Moravia	Bonilla 3446-II	585 565	228 230						
GUA-50	△	Backarc	alkali basalt	Rio Siquirres	Bonilla 3446-II	585 500	227 550		x				
GUA-51	△	Backarc	alkali basalt	Rio Siquirres	Bonilla 3446-II	585 500	227 550						
ALT-17	☆	Adakite	andesite	Alturas	Uniòn 3642-IV	591 260	321 950						
ALT-56	☆	Adakite	andesite	Cerro Chivo	Uniòn 3642-IV	599 840	321 300						
ALT-57	☆	Adakite	andesite	Cerro Chivo	Uniòn 3642-IV	599 760	321 350						
ALT-58	☆	Adakite	andesite	Cerro Chivo	Uniòn 3642-IV	599 800	321 500	9	x	x	x		
ALT-59	☆	Adakite	bas.andesite	Tajo Cerro Pelon	Uniòn 3642-IV	596 690	319 000	7	x	x			
ALT-60	☆	Adakite	bas.andesite	Tajo Cerro Pelon	Uniòn 3642-IV	596 690	319 000	4	x	x	x	x	x
ALT-61	☆	Adakite	andesite	Tajo Cerro Pelon	Uniòn 3642-IV	596 745	319 060	3	x	x			
ALT-62	☆	Adakite	andesite	Tajo Cerro Pelon	Uniòn 3642-IV	596 585	319 020	16.6	x	x	x	x	
ALT-63	☆	Adakite	andesite	Fila Coton	Uniòn 3642-IV	599 380	320 400	8	x	x	x	x	x
ALT-94	☆	Adakite	andesite	Tajo Cerro Pelon	Uniòn 3642-IV	596 585	319 020						
VIT-52	☆	Adakite	andesite	north of San Vito	Uniòn 3642-IV	579 300	312 175	2	x	x	x	x	
VIT-53	☆	Adakite	andesite	north of San Vito	Uniòn 3642-IV	578 595	312 110						
VIT-54	☆	Adakite	bas.andesite	San Bosco	Canas Gordas 3642-III	580 450	304 500	5	x	x	x	x	x
VIT-55	☆	Adakite	andesite	San Bosco	Canas Gordas 3642-III	580 450	304 575	14	x	x	x		
VIT-93	☆	Adakite	andesite	San Bosco	Canas Gordas 3642-III	580 550	305 100						
TAL-104	☆	Adakite	dacite	northern Dome	Siola 3544-II	546 900	368 450	8	x	x	x	x	x
TAL-105	☆	Adakite	dacite	southern Dome	Siola 3544-II	546 650	367 800	3.5	x	x	x	x	
TAL-106	☆	Adakite	bas.trachyand.	southern Dome	Siola 3544-II	546 950	367 925	6	x	x	x	x	
TAL-107	☆	Adakite	dacite	Rio Lori	Siola 3544-II	547 600	367 875	5	x	x			
PAS-74	□	Forearc	bas.trachyand.	Mano de Tigre	General 3543-III	540 390	333 380	5.1	x	x	x		
PAS-75	□	Forearc	basalt	San Antonio	General 3543-III	540 895	331 870	2.5	x	x	x	x	x
PAS-78	□	Forearc	basalt	Paso Real	Cabagra 3543-II	548 225	328 750	3.2	x	x	x		
PEJ-68	□	Forearc	basalt	Ojo de Agua	General 3543-III	524 650	340 210	6	x	x	x		
PEJ-69	□	Forearc	basalt	Alto de Agua	General 3543-III	524 980	329 440	3.4	x	x	x	x	x
PEJ-70	□	Forearc	basalt	Pejibaye	General 3543-III	524 330	341 020	2.9	x	x	x	x	
PEJ-71	□	Forearc	basalt	Pejibaye	General 3543-III	524 330	341 020						
PEJ-72	□	Forearc	basalt	Cerro las Bolas	General 3543-III	521 080	341 820	3.5	x	x			
PEJ-73	□	Forearc	granite	China Kicha	Repunta 3443-I	516 300	349 650						
GUA-33	active arc		basalt	Guayacan	Bonilla 3446-II	582 900	224 830	3	x	x	x		
GUA-48	active arc		basalt	Moravia	Bonilla 3446-II	585 470	228 440	2	x	x			
TUR-64	active arc		trachyandesite	Rio Reventazon	Tucurrique 3445-I	574 825	207 250	5.1	x	x	x		
TUR-65	active arc		andesite	Rio Reventazon	Tucurrique 3445-I	574 850	208 550						
TUR-66	active arc		bas.trachyand.	Rio Reventazon	Tucurrique 3445-I	575 175	208 350	5	x	x	x		
TUR-100	active arc		andesite	Rio Guayabo	Tucurrique 3445-I	569 075	217 575	8	x	x	x		
TUR-101	active arc		bas.andesite	Rio Guayabo	Tucurrique 3445-I	569 500	217 700	8	x	x			

Sample		ALT02	ALT03	ALT04	ALT05	ALT06	ALT09	ALT10	ALT12	ALT14	ALT15	ALT16	CHI113	CHI117	INA82	INA84	NUE76	NUE92
SiO2		47.38	50.70	56.27	59.42	53.55	53.62	48.13	48.50	45.95	50.07	51.82	53.86	51.43	51.17	53.60	47.34	49.44
TiO2		1.07	1.03	1.07	1.20	1.18	1.13	1.02	1.08	1.10	1.01	1.16	0.91	0.81	0.90	0.80	0.83	0.95
Al2O3		18.82	19.40	15.16	14.76	15.47	14.86	20.46	19.40	19.54	18.74	18.36	16.81	18.17	20.09	16.25	19.75	14.99
FeO		5.83	6.35	6.65	4.33	6.40	7.09	7.16	4.85	5.84	5.81	5.89	6.64	5.70	5.75	6.55	5.96	7.60
Fe2O3		5.12	2.85	3.75	4.90	3.93	4.58	3.35	5.84	5.99	4.18	3.99	2.77	4.56	2.94	3.07	3.58	3.77
MnO		0.20	0.18	0.25	0.27	0.25	0.26	0.21	0.21	0.19	0.19	0.23	0.15	0.23	0.19	0.19	0.19	0.21
MgO		6.73	3.40	2.82	1.55	3.51	3.68	4.30	5.74	4.85	3.75	3.87	4.35	4.13	2.95	4.50	3.53	6.45
CaO		9.02	10.12	7.23	4.51	6.65	9.67	10.32	10.48	9.63	9.83	8.57	7.74	9.33	9.34	8.82	10.67	10.51
Na2O		2.85	2.33	3.20	4.01	3.89	2.17	2.15	1.96	3.22	2.55	2.90	2.83	2.36	3.19	2.81	2.89	2.47
K2O		0.12	1.20	0.95	1.88	2.43	0.30	0.08	0.16	0.08	1.12	0.56	1.18	0.44	0.44	1.53	0.68	1.12
P2O5		0.13	0.30	0.35	0.46	0.42	0.27	0.23	0.12	0.07	0.31	0.17	0.19	0.13	0.15	0.20	0.18	0.27
LOI		2.11	1.18	1.22	1.50	1.21	1.11	1.20	1.34	2.37	1.30	1.88	1.35	1.56	1.46	0.62	3.52	1.33
Sum		99.38	99.04	98.93	98.78	98.88	98.75	98.61	99.67	98.83	98.86	99.40	98.77	98.84	98.56	98.92	99.11	99.11
FeOt		10.66	9.05	10.18	8.93	10.10	11.39	10.36	10.21	11.56	9.75	9.66	9.30	10.02	8.59	9.40	9.53	9.42
Na2O+K2O		3.04	3.58	4.22	6.02	6.42	2.51	2.27	2.17	3.40	3.74	3.52	4.08	2.86	3.71	4.38	3.70	3.15
Mg#		57	44	40	29	45	43	47	54	48	45	48	52	49	44	52	45	47
Li	ICP	12.14	6.51	5.95	3.58	5.94	1.85	3.44	9.38	12.47	8.59	6.28	17.01	4.70	3.88	7.18	7.83	3.22
Be	ICP	0.38	0.88	1.12	1.26	0.89	0.61	0.38	0.37	0.20	1.04	0.42	1.34	0.53	0.35	0.85	0.36	0.40
Sc	ICP	36.55	19.69	27.36	22.52	23.76	28.21	20.78	23.92	25.86	25.52	19.60	34.76	30.57	17.19	23.78	21.55	21.30
V	XRF	341.00	246.00	166.00	16.33	251.00	351.00	267.00	344.00	393.00	273.00	216.00	235.00	276.00	188.00	269.00	310.00	299.00
Cr	XRF	235.00	247.00	203.00	79.00	89.00	156.00	236.00	101.00	138.00	258.00	181.00	312.50	237.50	67.00	63.00	69.00	33.50
Co	XRF	47.00	27.00	24.00	8.67	29.00	31.00	34.00	29.67	35.00	29.00	24.00	27.00	32.00	19.00	31.00	30.00	28.00
Ni	XRF	126.00	120.00	97.00	33.67	45.00	71.00	121.00	49.00	66.00	137.00	84.00	142.50	116.50	34.00	30.00	33.00	16.00
Cu	ICP	46.68	260.70	28.39	23.93	153.01	231.29	144.31	110.11	130.41	220.17	53.83	61.27	111.86	702.22	160.97	244.24	138.46
Zn	XRF	78.00	85.00	122.00	143.00	116.00	122.00	76.00	78.33	68.00	71.00	83.00	98.00	86.50	68.00	82.00	78.00	76.00
Ga	XRF	17.00	17.00	17.00	16.00	15.00	18.00	15.00	18.00	17.00	<5	16.00	18.00	16.50	16.00	15.00	17.00	22.00
Rb	ICP	2.25	20.43	13.70	27.27	48.06	4.77	1.72	2.30	1.42	17.41	5.69	24.03	6.50	3.86	34.47	9.14	4.79
Sr	XRF	388.00	548.00	422.00	431.33	322.00	726.00	456.00	400.33	381.00	588.00	415.00	430.50	440.00	631.00	494.00	1007.00	526.00
Y	ICP	18.56	27.53	35.73	59.21	32.18	27.49	20.37	18.66	15.41	25.05	23.83	24.57	19.12	17.24	24.31	17.50	16.09
Zr	XRF	37.00	99.00	92.00	150.67	99.00	67.00	55.00	42.00	36.00	75.00	53.00	81.00	33.00	32.00	109.00	27.00	35.50
Nb	ICP	3.08	7.63	5.69	8.07	5.95	3.32	3.58	1.92	1.30	5.15	3.52	7.11	1.72	1.35	3.21	1.94	1.49
Cs	ICP	0.11	0.10	0.10	0.32	0.92	0.05	0.36	0.17	0.14	0.32	0.25	0.22	0.07	0.03	0.84	0.25	0.02
Ba	XRF	193.00	508.00	698.00	1606.33	1607.00	217.00	191.00	202.67	164.00	703.00	416.00	620.50	414.50	566.00	745.00	563.00	458.50
La	ICP	3.64	13.93	13.93	21.28	14.61	10.92	6.29	3.82	1.97	12.15	5.33	12.78	3.86	4.56	12.12	6.38	4.88
Ce*	ICP	9.70	33.14	32.70	51.06	34.88	25.96	16.21	10.10	5.81	29.22	14.29	29.07	10.28	11.70	27.93	15.23	12.06
Pr	ICP	1.51	4.58	4.45	7.13	4.84	3.59	2.45	1.57	0.99	4.09	2.24	3.80	1.60	1.76	3.71	2.12	1.74
Nd	ICP	7.86	19.49	20.63	32.71	22.26	16.94	11.93	7.84	5.33	18.71	11.53	17.18	7.76	8.75	16.25	9.84	8.37
Sm	ICP	2.34	4.92	5.40	8.36	5.71	4.56	3.40	2.42	1.80	4.61	3.54	4.02	2.36	2.49	4.11	2.98	2.38
Eu	ICP	0.89	1.53	1.66	2.45	1.55	1.42	1.06	0.89	0.69	1.44	1.22	1.32	0.93	1.01	1.03	1.08	0.87
Gd	ICP	2.62	4.70	5.52	8.47	5.33	4.53	3.34	2.61	2.08	4.36	3.67	3.77	2.69	2.54	3.86	3.00	2.38
Tb	ICP	0.45	0.74	0.90	1.33	0.83	0.71	0.54	0.45	0.36	0.70	0.62	0.63	0.48	0.42	0.60	0.45	0.40
Dy	ICP	2.93	3.92	5.47	8.19	5.06	4.58	3.39	2.89	2.30	4.25	3.99	4.25	3.04	2.65	3.74	2.61	2.47
Ho	ICP	0.59	0.81	1.13	1.65	0.98	0.89	0.68	0.58	0.48	0.81	0.81	0.78	0.58	0.53	0.74	0.54	0.51
Er	ICP	1.72	2.50	3.37	4.66	2.91	2.61	2.01	1.78	1.43	2.37	2.39	2.12	1.82	1.56	2.22	1.62	1.48
Tm	ICP	0.25	0.37	0.51	0.64	0.41	0.37	0.29	0.27	0.21	0.36	0.34	0.36	0.29	0.22	0.34	0.22	0.22
Yb	ICP	1.73	2.18	3.29	3.95	2.70	2.33	1.83	1.65	1.36	2.33	2.23	2.50	1.85	1.49	2.13	1.45	1.42
Lu	ICP	0.25	0.34	0.51	0.57	0.39	0.35	0.27	0.25	0.20	0.33	0.33	0.34	0.27	0.22	0.31	0.22	0.21
Hf	ICP	0.84	2.26	2.51	2.73	1.76	1.21	1.03	0.88	0.63	1.95	1.39	2.08	0.92	0.85	0.77	0.82	0.86
Ta	ICP	0.42	0.38	0.27	0.48	0.31	0.19	0.29	0.16	0.18	0.36	0.26	0.44	0.15	0.24	0.23	0.61	0.14
Tl	ICP	0.00	0.05	0.07	0.15	0.18	0.02	0.01	0.02	0.00	0.08	0.04	0.11	0.02	0.02	0.11	0.01	0.02
Pb	ICP	1.26	14.43	4.59	9.62	3.83	3.55	1.77	0.77	1.22	2.51	2.38	3.65	2.21	2.56	2.67	2.21	2.72
Th	ICP	0.48	3.29	3.92	1.64	0.96	0.89	0.34	0.15	0.18	2.54	0.30	3.54	0.82	0.22	2.22	1.17	0.40
U	ICP	0.08	0.77	0.88	1.02	0.60	0.53	0.27	0.10	0.04	0.62	0.17	0.88	0.21	0.20	1.38	0.27	0.27

Sample		ALT95	CHI111	CHI115	CHI116	CHI119	CHI120	DOT97	DOT98	INA67	INA85	INA87	TAL79	TAL80	BRI21	BRI23	BRI24
		○	○	○	○	○	○	○	○	○	○	○	○	○	△	△	△
SiO2		57.91	55.94	60.85	60.49	58.08	57.16	73.56	57.61	65.85	74.02	56.80	59.20	59.63	47.29	47.18	46.35
TiO2		0.76	0.72	0.62	0.62	0.77	0.72	0.28	0.79	0.43	0.26	0.69	0.67	0.62	1.44	1.58	1.73
Al2O3		16.98	16.62	16.59	16.43	16.50	16.73	13.46	16.24	14.39	13.29	16.93	15.66	16.13	16.14	16.48	16.89
FeO		4.51	4.51	2.97	3.11	3.43	4.33	0.95	4.22	2.36	0.64	5.02	4.44	3.05	6.57	5.79	6.36
Fe2O3		2.28	3.81	3.31	3.23	3.62	3.31	1.00	3.33	1.37	1.29	2.26	2.30	3.47	3.10	3.99	3.05
MnO		0.15	0.20	0.16	0.12	0.13	0.19	0.04	0.18	0.10	0.13	0.16	0.15	0.10	0.17	0.17	0.16
MgO		2.24	3.58	2.50	2.81	3.11	3.37	0.41	2.80	1.08	0.13	2.17	2.75	2.36	6.32	6.37	5.42
CaO		5.94	7.65	5.65	6.06	6.89	7.16	0.99	6.04	3.15	0.21	6.48	5.60	5.00	9.86	10.12	10.03
Na2O		3.38	2.91	3.78	3.19	3.54	3.07	2.96	3.75	4.05	3.12	3.37	3.04	3.21	2.97	2.79	3.06
K2O		3.46	2.43	2.28	1.97	2.12	2.74	5.61	2.93	2.43	5.90	2.16	3.74	3.99	1.85	1.84	1.83
P2O5		0.28	0.20	0.18	0.16	0.18	0.17	0.05	0.18	0.11	0.04	0.29	0.19	0.18	0.65	0.80	0.74
LOI		0.68	0.89	0.79	1.61	0.60	0.18	0.68	1.00	3.91	0.65	2.56	0.64	0.73	1.89	1.85	2.45
Sum		98.55	99.46	99.68	99.78	99.40	99.82	99.98	99.07	99.22	99.67	98.87	98.39	98.47	98.26	98.94	98.09
FeOt		6.67	8.01	6.00	6.11	7.33	7.67	1.86	7.32	3.76	1.82	7.28	6.63	6.29	9.64	9.59	9.52
Na2O+K2O		6.96	5.39	6.10	5.23	5.69	5.82	8.62	6.78	6.78	9.10	5.70	6.90	7.34	4.97	4.74	5.06
Mg#		45	50	50	52	47	48	36	48	42	16	42	51	48	59	59	56
Li	ICP	14.10	3.86	12.62	6.51	4.56	8.26	6.09	3.93	1.71	2.59	1.69	18.61	7.17	9.03	4.20	8.86
Be	ICP	1.77	0.82	1.09	0.91	0.88	0.87	1.47	1.20	1.06	1.90	0.97	1.38	1.19	2.30	2.32	2.20
Sc	ICP	14.95	19.51	14.39	15.60	20.00	19.23	3.99	19.27	7.90	4.19	14.28	16.54	15.59	22.87	20.23	13.41
V	XRF	128.50	214.00	145.00	165.00	201.50	211.50	25.00	200.00	59.60	16.00	133.00	149.00	140.00	261.40	247.00	261.00
Cr	XRF	69.00	91.00	105.50	59.00	60.00	41.00	118.00	46.00	69.00	113.00	57.50	77.00	57.00	166.20	190.00	80.00
Co	XRF	17.00	28.00	18.00	15.50	18.50	23.50	*3.14*	23.00	8.60	*1.87*	21.00	21.00	11.00	38.40	34.00	33.50
Ni	XRF	29.50	48.00	50.00	27.50	29.00	19.00	42.00	19.00	26.20	41.00	30.50	29.00	24.00	74.40	89.00	61.00
Cu	ICP	65.42	143.13	59.64	18.25	257.54	125.99	12.77	111.17	39.73	7.14	74.46	96.36	74.68	76.10	103.03	111.70
Zn	XRF	60.00	96.00	106.50	40.00	51.50	104.00	23.00	58.00	51.40	50.00	90.50	96.00	43.00	81.60	88.00	96.50
Ga	XRF	16.00	17.00	20.50	24.00	15.50	16.50	23.00	13.00	13.40	12.00	16.00	15.00	15.00	17.20	18.00	18.50
Rb	ICP	109.71	54.42	44.47	38.06	43.64	66.92	125.53	56.84	82.14	141.60	34.76	104.53	150.56	42.52	42.66	34.79
Sr	XRF	496.50	530.00	623.50	662.50	601.00	555.00	165.00	503.00	280.40	83.00	771.50	397.00	396.00	988.00	1101.00	1195.00
Y	ICP	42.81	22.41	20.13	17.68	22.62	21.69	19.01	25.35	28.26	38.97	28.27	29.05	23.98	25.34	25.78	24.68
Zr	XRF	212.00	121.00	97.00	75.50	138.00	206.00	149.00	151.00	184.60	275.00	117.50	198.00	263.00	166.00	174.50	181.50
Nb	ICP	15.34	5.49	4.78	4.89	5.65	6.70	13.91	7.42	6.41	12.90	4.83	9.47	8.75	34.79	30.03	13.80
Cs	ICP	2.52	1.44	1.28	0.64	0.71	2.17	1.77	0.55	2.92	0.77	3.96	3.51	1.13	0.39	2.83	0.56
Ba	XRF	1234.00	1280.00	1328.50	1171.50	1123.00	1045.50	713.00	1969.00	1806.40	1026.00	1314.50	1324.00	1321.00	680.20	663.50	809.50
La	ICP	27.71	17.32	15.34	16.40	15.90	17.91	19.14	14.65	14.83	27.12	15.48	23.29	17.25	47.19	47.48	48.35
Ce*	ICP	64.10	38.14	33.79	35.61	35.38	39.18	40.84	32.98	33.47	59.76	36.04	51.23	38.50	100.37	101.43	102.39
Pr	ICP	8.56	4.77	4.22	4.36	4.49	4.85	4.87	4.25	4.33	7.48	4.85	6.39	4.91	11.92	12.12	12.07
Nd	ICP	35.12	19.51	17.48	17.79	18.61	19.37	17.72	17.81	17.71	28.78	20.63	25.37	19.59	45.20	47.26	46.58
Sm	ICP	7.97	4.33	3.79	3.80	4.34	4.31	3.40	4.20	4.14	6.18	5.06	5.53	4.39	8.45	8.58	8.61
Eu	ICP	1.46	1.12	1.07	1.06	1.17	1.06	0.57	1.30	0.97	0.63	1.38	1.20	1.06	2.42	2.43	2.56
Gd	ICP	6.88	3.89	3.41	3.30	3.79	3.71	2.86	3.89	3.78	5.47	4.55	4.88	3.89	6.66	6.98	6.98
Tb	ICP	1.05	0.59	0.52	0.47	0.56	0.55	0.43	0.61	0.63	0.86	0.70	0.75	0.59	0.89	0.89	0.91
Dy	ICP	6.22	3.45	2.98	2.75	3.47	3.32	2.52	3.79	3.87	5.09	4.18	4.29	3.56	4.51	4.54	4.55
Ho	ICP	1.24	0.68	0.59	0.52	0.68	0.66	0.52	0.74	0.81	1.04	0.85	0.86	0.69	0.80	0.78	0.81
Er	ICP	3.78	1.97	1.73	1.53	1.99	1.93	1.61	2.22	2.58	3.25	2.55	2.60	2.06	2.19	2.16	2.21
Tm	ICP	0.58	0.28	0.26	0.22	0.28	0.28	0.26	0.34	0.41	0.51	0.37	0.39	0.31	0.30	0.29	0.29
Yb	ICP	3.78	1.83	1.66	1.37	1.84	1.83	1.66	2.19	2.74	3.25	2.47	2.46	2.02	1.88	1.75	1.81
Lu	ICP	0.54	0.27	0.24	0.19	0.27	0.27	0.25	0.33	0.42	0.46	0.37	0.36	0.29	0.27	0.25	0.25
Hf	ICP	0.78	0.40	0.30	0.43	0.53	0.73	0.78	0.81	4.90	2.09	3.11	0.77	0.87	3.63	3.58	3.80
Ta	ICP	0.81	0.33	0.28	0.28	0.38	0.39	1.03	0.41	0.45	0.82	0.33	0.57	0.51	1.64	1.77	0.42
Tl	ICP	0.38	0.23	0.09	0.15	0.15	0.27	0.43	0.17	0.42	0.47	0.13	0.34	0.27	0.04	0.02	0.09
Pb	ICP	6.06	11.03	7.16	3.76	4.49	8.51	7.24	4.82	7.92	8.58	6.81	7.67	6.60	3.57	6.51	3.49
Th	ICP	6.04	2.62	1.90	2.07	2.35	2.58	9.50	2.93	3.25	7.83	2.04	4.19	3.74	13.33	4.35	9.45
U	ICP	2.78	1.41	0.80	0.80	1.11	1.43	3.95	1.46	2.52	2.98	1.54	2.20	1.87	2.44	2.08	1.78

Sample		BRI25	GUA26	GUA27	GUA28	GUA33	GUA41	GUA42	NEI18	ALT58	ALT60	ALT62	ALT63	TAL104	TAL105	TAL106	VIT52	VIT54
SiO2		50.00	43.81	42.57	46.72	44.35	46.88	44.59	55.61	57.40	53.77	60.69	57.74	62.04	61.19	52.74	59.32	55.37
TiO2		1.24	1.75	1.70	2.02	1.82	2.01	1.75	1.18	0.79	1.01	0.63	0.77	0.52	0.51	0.80	0.72	0.74
Al2O3		16.83	16.49	13.13	17.15	13.91	16.49	13.54	14.07	15.87	15.97	17.51	16.04	17.63	17.47	17.50	16.45	15.76
FeO		4.52	4.34	4.50	4.15	5.11	4.21	4.64	1.97	2.71	4.33	1.35	1.84	1.16	1.03	4.33	2.03	1.60
Fe2O3		3.56	4.13	5.43	3.59	4.46	3.64	4.56	4.45	3.03	2.93	4.05	3.97	2.95	3.13	3.56	3.77	4.97
MnO		0.17	0.17	0.14	0.19	0.15	0.13	0.14	0.08	0.09	0.11	0.09	0.10	0.06	0.07	0.18	0.09	0.11
MgO		4.59	5.28	9.25	3.48	8.91	4.59	9.34	5.08	4.81	6.05	1.44	3.75	1.30	1.86	3.90	3.35	4.96
CaO		7.45	10.30	14.73	7.64	12.38	8.34	9.96	8.09	6.95	7.94	5.00	6.96	3.56	2.64	7.50	6.64	7.97
Na2O		4.48	4.21	2.29	5.47	3.17	4.95	3.35	2.99	3.25	3.25	3.49	3.32	3.66	3.15	3.37	3.56	3.43
K2O		2.33	1.90	0.84	2.66	1.36	2.31	1.47	3.69	2.35	1.67	2.03	2.53	2.15	2.21	2.50	1.73	2.02
P2O5		0.56	1.53	0.81	1.05	1.06	1.19	0.90	0.52	0.24	0.27	0.21	0.31	0.21	0.14	0.29	0.20	0.35
LOI		2.36	4.64	2.84	3.82	1.80	3.84	4.51	0.91	0.98	0.81	2.22	0.78	2.88	4.85	1.49	0.52	0.72
Sum		98.08	98.54	98.22	97.95	98.49	98.59	98.75	98.62	98.44	98.12	98.69	98.10	98.11	98.22	98.15	98.37	97.99
FeOt		8.02	8.53	9.79	7.81	9.39	7.86	9.23	6.10	5.55	7.13	5.17	5.55	4.00	4.11	7.76	5.52	6.22
Na2O+K2O		7.07	6.48	3.26	8.59	4.66	7.63	5.09	6.82	5.72	5.09	5.71	6.00	6.09	5.73	6.04	5.39	5.57
Mg#		58	60	67	52	67	59	71	67	67	65	40	62	45	54	55	59	64
Li	ICP	19.42	9.25	4.42	11.86	6.60	7.98	9.56	7.99	3.09	3.34	3.19	3.54	5.91	6.49	4.29	3.38	4.59
Be	ICP	2.94	2.28	1.05	2.91	1.54	2.49	1.63	2.57	1.19	0.96	1.37	1.88	1.40	1.68	1.50	1.10	1.54
Sc	ICP	15.20	13.62	34.13	8.11	24.33	13.83	21.32	19.96	14.99	14.36	11.20	12.85	7.24	7.93	22.57	12.24	14.78
V	XRF	193.00	319.00	223.00	370.00	256.50	264.00	220.00	194.50	173.00	216.00	142.50	165.00	116.50	108.00	248.50	179.00	197.50
Cr	XRF	108.00	51.00	259.00	27.00	336.00	60.00	332.00	126.50	192.50	185.00	57.50	104.00	31.50	72.00	109.00	70.00	236.50
Co	XRF	29.00	33.00	39.00	22.00	43.00	31.00	42.00	27.00	21.50	31.50	18.50	23.00	13.00	15.50	23.50	20.00	26.00
Ni	XRF	45.00	35.00	121.00	14.00	183.00	74.00	211.50	89.50	105.50	124.00	43.00	69.00	19.50	51.50	59.50	35.00	114.00
Cu	ICP	55.49	203.13	95.41	391.78	135.49	140.02	92.71	87.56	105.16	110.91	84.96	159.24	105.11	88.35	143.15	90.56	91.24
Zn	XRF	85.00	99.00	76.00	115.00	89.00	86.00	86.00	69.00	63.00	74.50	58.00	68.00	58.50	55.00	80.50	66.00	78.00
Ga	XRF	17.00	18.00	17.00	19.00	16.00	16.00	16.50	19.00	18.00	19.50	18.00	18.00	18.50	18.50	17.00	18.00	19.00
Rb	ICP	59.49	29.18	14.40	40.09	22.87	36.20	22.73	87.12	43.30	23.52	34.43	43.13	43.18	38.95	38.11	24.95	35.05
Sr	XRF	838.00	2594.00	1634.00	2584.00	1836.50	2010.00	1730.50	2046.00	1225.00	1132.50	1118.00	1635.00	927.50	598.00	949.50	1077.00	1497.00
Y	ICP	24.69	29.46	24.01	36.74	26.03	30.79	25.31	18.42	11.63	12.26	10.27	14.12	8.29	8.16	18.84	10.06	12.89
Zr	XRF	189.00	155.00	119.00	221.00	139.50	200.00	151.50	238.50	113.50	124.00	94.50	129.00	67.00	62.50	90.50	86.00	120.50
Nb	ICP	46.11	71.04	27.81	100.80	44.60	52.16	33.49	18.75	8.11	9.03	5.33	8.54	5.51	5.22	9.21	5.27	7.90
Cs	ICP	1.60	0.52	0.24	0.81	0.35	0.36	0.27	0.25	0.28	0.17	0.50	0.42	0.48	0.60	0.48	0.37	0.38
Ba	XRF	914.00	1451.00	635.00	1963.00	896.50	1029.00	787.50	1956.00	809.50	718.50	1029.50	1273.00	1471.00	1949.50	1030.50	867.00	1161.00
La	ICP	48.72	91.32	48.60	143.82	60.50	78.47	59.94	72.31	31.22	21.80	23.16	49.63	18.51	15.98	25.36	19.06	40.51
Ce*	ICP	104.67	187.30	104.64	272.00	127.79	165.12	127.39	153.63	63.92	46.83	48.34	103.80	39.32	35.63	53.92	39.92	85.61
Pr	ICP	12.62	20.95	12.66	26.03	15.01	19.27	15.11	18.21	7.13	5.64	5.57	12.00	4.66	4.53	6.40	4.62	10.06
Nd	ICP	41.32	74.46	50.36	89.99	57.37	70.73	56.66	66.77	27.26	22.28	20.96	45.39	18.20	18.00	25.08	17.89	37.59
Sm	ICP	7.62	11.73	9.17	14.01	9.84	11.77	9.66	10.56	4.52	4.11	3.75	6.84	3.22	3.21	4.88	3.30	6.16
Eu	ICP	2.36	3.30	2.65	4.03	2.87	3.30	2.75	2.78	1.29	1.25	1.17	1.92	1.05	1.02	1.47	1.00	1.70
Gd	ICP	5.91	8.79	7.20	10.29	7.77	8.86	7.49	6.77	3.29	3.20	2.75	4.73	2.30	2.18	3.99	2.46	4.24
Tb	ICP	0.88	1.08	0.91	1.32	0.97	1.14	0.95	0.76	0.39	0.44	0.34	0.51	0.28	0.26	0.55	0.33	0.49
Dy	ICP	4.13	5.24	4.43	6.52	4.84	5.60	4.61	3.36	1.91	2.26	1.74	2.35	1.37	1.28	2.91	1.69	2.24
Ho	ICP	0.71	0.92	0.78	1.15	0.83	0.96	0.82	0.55	0.34	0.41	0.32	0.39	0.23	0.23	0.55	0.30	0.38
Er	ICP	2.12	2.51	2.02	3.26	2.26	2.68	2.18	1.49	0.92	1.11	0.86	1.06	0.67	0.67	1.60	0.87	1.00
Tm	ICP	0.32	0.34	0.26	0.45	0.29	0.35	0.29	0.20	0.13	0.16	0.13	0.14	0.09	0.09	0.23	0.12	0.14
Yb	ICP	1.81	2.10	1.56	2.84	1.81	2.25	1.78	1.25	0.80	0.96	0.82	0.85	0.56	0.57	1.44	0.79	0.88
Lu	ICP	0.27	0.30	0.22	0.41	0.25	0.29	0.25	0.17	0.11	0.14	0.12	0.13	0.09	0.08	0.21	0.12	0.13
Hf	ICP	4.42	3.83	3.36	5.06	3.62	4.81	3.82	7.48	2.48	2.80	1.84	3.45	1.61	1.39	1.99	1.88	2.63
Ta	ICP	2.05	2.49	1.13	3.31	1.57	2.20	1.31	0.82	0.48	0.75	0.50	0.61	0.39	0.38	0.45	0.53	0.58
Tl	ICP	0.16	0.05	0.02	0.09	0.05	0.04	0.01	0.17	0.08	0.06	0.08	0.10	0.10	0.13	0.11	0.08	0.07
Pb	ICP	3.80	7.61	3.00	11.79	4.69	6.09	4.03	11.11	6.71	4.14	6.95	9.60	7.22	8.38	6.58	5.58	8.49
Th	ICP	15.23	17.45	6.46	23.08	10.76	13.23	9.79	31.80	3.77	2.92	2.88	7.59	1.66	1.33	4.81	2.38	5.29
U	ICP	3.09	2.85	1.15	3.76	1.57	2.30	1.52	5.73	1.65	1.27	1.43	3.07	1.25	1.05	1.27	1.21	2.55

Sample		VIT55	PAS74	PAS75	PAS78	PEJ68	PEJ69	PEJ70	TAL103	TAL109	TUR100	TUR64	TUR66
SiO2		58.48	55.79	48.30	50.32	49.99	51.77	51.08	55.56	54.05	58.52	55.46	55.41
TiO2		0.76	0.73	0.86	0.67	0.99	1.05	1.01	0.56	0.69	1.14	1.10	1.07
Al2O3		16.97	17.50	20.69	18.61	17.46	17.37	17.84	20.34	18.09	15.71	17.27	17.06
FeO		1.11	3.72	5.83	4.96	5.83	5.63	5.40	2.47	3.68	4.02	3.24	4.46
Fe2O3		4.69	3.45	3.83	3.95	3.60	4.10	3.96	1.95	3.10	2.12	3.95	2.50
MnO		0.10	0.14	0.19	0.17	0.18	0.25	0.18	0.10	0.16	0.10	0.11	0.12
MgO		2.59	3.26	3.94	4.46	4.94	4.78	5.05	1.42	2.73	4.07	3.25	3.95
CaO		6.04	6.99	10.91	9.63	8.90	8.47	9.09	6.38	6.17	6.33	6.44	7.06
Na2O		3.42	3.43	2.53	2.61	2.72	2.86	2.78	3.73	3.26	3.79	3.69	3.52
K2O		2.65	2.44	0.57	1.06	1.68	1.88	1.72	4.11	4.12	2.20	2.35	2.47
P2O5		0.30	0.35	0.15	0.25	0.41	0.45	0.41	0.33	0.41	0.49	0.42	0.41
LOI		1.21	0.77	1.45	1.82	1.36	0.10	0.52	0.98	2.20	0.35	1.16	0.89
Sum		98.29	98.58	99.25	98.52	98.06	99.90	99.48	97.91	98.67	98.85	98.44	98.91
FeOt		5.48	6.95	11.15	8.76	9.72	9.91	9.32	4.35	6.68	5.99	6.96	6.81
Na2O+K2O		6.24	5.98	3.64	3.78	4.73	4.75	4.52	8.06	7.62	6.06	6.19	6.08
Mg#		53	53	55	52	49	50	53	45	51	62	54	58
Li	ICP	3.81	8.59	10.49	2.34	6.08	3.13	7.51	5.63	3.74	4.55	5.46	8.02
Be	ICP	2.20	1.47	0.58	0.77	1.14	1.44	1.40	3.86	3.09	1.34	1.43	1.39
Sc	ICP	12.68	15.50	32.38	21.95	21.35	22.56	23.37	9.54	14.00	11.96	16.10	17.65
V	XRF	166.00	201.00	346.00	260.00	273.00	296.50	273.00	99.00	178.00	140.00	190.00	196.00
Cr	XRF	56.50	194.00	143.00	83.00	62.00	84.50	89.00	102.00	56.00	190.00	75.00	110.00
Co	XRF	18.50	22.00	43.00	35.00	27.00	33.50	32.00	10.50	20.00	20.00	23.00	23.00
Ni	XRF	44.00	84.00	62.00	41.00	40.00	51.00	41.00	44.50	19.00	92.00	35.00	56.00
Cu	ICP	137.22	132.73	239.05	148.74	270.74	294.79	267.06	65.15	173.25	61.04	119.36	158.49
Zn	XRF	66.00	79.00	99.00	75.00	100.00	105.50	91.00	61.00	89.00	76.00	77.00	79.00
Ga	XRF	21.00	17.00	16.00	17.00	17.00	16.50	15.00	17.50	17.00	17.00	19.00	18.00
Rb	ICP	45.01	45.20	19.73	18.05	42.50	37.30	36.33	86.56	99.07	52.23	59.45	59.71
Sr	XRF	1520.50	1103.00	565.00	848.00	990.00	927.50	975.00	1751.00	1252.00	822.00	861.00	878.00
Y	ICP	18.02	21.47	23.34	14.72	24.06	26.10	23.70	19.12	19.32	19.45	21.42	20.43
Zr	XRF	134.50	93.00	67.00	47.00	93.00	105.50	77.00	155.00	184.00	214.00	199.00	197.00
Nb	ICP	8.19	11.39	3.95	3.39	6.01	6.33	6.64	18.94	15.46	30.61	19.79	24.51
Cs	ICP	0.44	0.33	0.67	0.26	1.22	1.00	0.55	0.42	0.70	0.53	0.81	0.75
Ba	XRF	1471.50	1107.00	834.00	705.00	1229.00	1200.50	1038.00	1482.50	1242.00	957.00	1023.00	964.00
La	ICP	66.41	29.11	10.15	16.28	25.78	27.15	24.47	47.97	45.36	48.15	44.46	42.17
Ce*	ICP	138.27	61.41	23.58	36.11	56.41	59.73	54.33	98.90	96.05	100.30	94.28	84.75
Pr	ICP	15.87	7.20	3.17	4.56	6.99	7.46	6.78	11.16	11.33	11.52	11.14	9.15
Nd	ICP	60.47	27.99	14.57	19.23	29.43	30.58	28.08	40.70	41.97	42.31	41.14	37.61
Sm	ICP	9.32	5.33	3.90	4.07	6.20	6.37	5.79	6.95	7.88	7.13	7.18	6.76
Eu	ICP	2.44	1.59	1.26	1.20	1.66	1.75	1.71	2.04	1.88	1.85	1.76	1.63
Gd	ICP	6.45	4.29	3.92	3.23	4.92	5.33	4.93	5.13	5.59	5.29	5.33	5.09
Tb	ICP	0.67	0.58	0.58	0.45	0.69	0.75	0.69	0.64	0.68	0.67	0.69	0.61
Dy	ICP	2.92	3.03	3.47	2.49	3.87	4.17	3.78	3.16	3.33	3.40	3.62	3.43
Ho	ICP	0.47	0.58	0.72	0.46	0.73	0.80	0.72	0.55	0.56	0.59	0.65	0.67
Er	ICP	1.32	1.70	2.24	1.32	2.13	2.30	2.09	1.55	1.55	1.60	1.85	1.80
Tm	ICP	0.17	0.25	0.30	0.18	0.31	0.33	0.30	0.23	0.20	0.22	0.25	0.23
Yb	ICP	1.00	1.65	1.99	1.17	1.95	2.10	1.92	1.46	1.29	1.39	1.64	1.68
Lu	ICP	0.15	0.26	0.31	0.18	0.29	0.31	0.29	0.22	0.18	0.20	0.24	0.26
Hf	ICP	3.37	2.38	1.24	1.32	2.19	2.31	2.02	3.67	1.36	4.43	4.46	3.90
Ta	ICP	0.58	0.57	0.34	0.28	0.34	0.34	0.38	0.89	0.70	1.71	1.06	1.20
Tl	ICP	0.18	0.06	0.02	0.05	0.06	0.07	0.05	0.13	0.29	0.11	0.10	0.08
Pb	ICP	12.05	4.97	3.45	4.09	8.87	7.74	7.47	10.88	14.15	6.15	7.36	6.34
Th	ICP	9.09	7.64	2.34	1.13	2.45	2.93	5.13	16.65	7.76	5.60	6.73	18.11
U	ICP	3.22	1.42	0.56	0.67	1.46	1.58	1.32	5.07	3.54	3.24	3.70	3.21

Sample name		$^{87}Sr/^{86}Sr_{ul}$	2σ	Rb (ppm)	Sr (ppm)	$^{87}Sr/^{86}Sr_{i}$	$^{143}Nd/^{144}Nd$	2σ	Sm (ppm)	Nd (ppm)	$^{143}Nd/^{144}Nd_{i}$	εNd	Pb (ppm)	$^{206}Pb/^{204}Pb$	$^{207}Pb/^{204}Pb$	$^{208}Pb/^{204}Pb$
ALT-02	◇	0.70380	6.0E-06	3	388	**0.70378**							1.3	18.734	15.547	38.411
ALT-12	◇	0.70373	1.1E-05	3	400	**0.70360**	0.512999	4.9E-06	3	8	**0.512999**	7.10	0.8	18.751	15.546	38.420
ALT-14	◇	0.70369	1.9E-05	2	381	**0.70365**	0.513027	6.0E-06	2	6	**0.513027**	7.65				
CHI-113	◇	0.70429	1.4E-05	25	431	**0.70415**	0.513012	2.9E-06	4	18	**0.513004**	7.36				
CHI-117	◇	0.70382	2.3E-05	7	440	**0.70379**	0.513032	5.0E-06	3	9	**0.513022**	7.70	2.6	18.789	15.542	38.442
INA-84	◇	0.70390	2.0E-05	51	494	**0.70384**	0.513045	9.4E-06	4	17	**0.513036**	8.01				
NUE-92	◇	0.70383	1.6E-05	24	565	**0.70380**	0.513015	5.0E-06	4	15	**0.513002**	7.43				
ALT-95	○	0.70389	1.5E-05	160	497	**0.70377**	0.513019	5.4E-06	8	36	**0.513010**	7.50				
CHI-116	○	0.70390	4.9E-06	55	663	**0.70385**	0.513013	4.7E-06	4	18	**0.513005**	7.40	3.7	18.899	15.560	38.593
INA-85	○	0.70473	2.1E-05	202	83	**0.70399**	0.513042	5.8E-06	7	30	**0.513034**	7.97				
TAL-79	○	0.70390	1.1E-05	154	397	**0.70376**	0.513025	5.5E-06	6	26	**0.513017**	7.64	7.4	18.745	15.520	38.328
BRI-21	△	0.70363	1.2E-05	47	988	**0.70354**	0.512967	2.9E-06	9	48	**0.512967**	6.54	3.7	19.12	15.548	38.725
BRI-23	△	0.70381	1.1E-05	63	1101	**0.70356**	0.512977	5.4E-06	9	48	**0.512977**	6.75				
GUA-27	△	0.70367	1.4E-05	21	1634	**0.70366**	0.513022	1.2E-05	10	54	**0.513022**	7.61				
GUA-42	△	0.70379	8.3E-06	27	1731	**0.70362**	0.512982	6.4E-06	11	63	**0.512982**	6.83	4.5	19.058	15.555	38.692
NEI-18	△	0.70341	1.5E-05	110	2046	**0.70332**	0.512953	5.0E-06	12	73	**0.512953**	6.14	12.2	19.335	15.578	38.981
ALT-60	☆	0.70352	1.5E-05	35	1133	**0.70347**	0.512988	5.4E-06	5	23	**0.512988**	6.90	4.2	19.137	15.594	38.852
ALT-62	☆	0.70354	1.0E-05	51	1118	**0.70352**	0.512988	4.4E-06	4	22	**0.512988**	6.89				
ALT-63	☆	0.70340	2.0E-05	64	1635	**0.70338**	0.512979	5.2E-06	7	46	**0.512979**	6.72	9.6	19.245	15.600	38.971
TAL-103	☆	0.70379	1.7E-05	87	1751	**0.70377**	0.513000	9.0E-06	7	41	**0.512995**	7.16				
TAL-104	☆	0.70371	1.4E-05	63	928	**0.70364**	0.512990	6.3E-06	4	19	**0.512990**	6.92	7.0	19.085	15.555	38.731
TAL-105	☆	0.70370	1.8E-05	56	598	**0.70367**	0.512995	6.9E-06	4	18	**0.512995**	7.02				
TAL-106	☆	0.70370	1.6E-05	38	950	**0.70368**	0.512976	3.2E-06	5	25	**0.512970**	6.69				
VIT-52	☆	0.70356	1.8E-05	36	1077	**0.70355**	0.512985	6.3E-06	4	19	**0.512985**	6.84				
VIT-54	☆	0.70357	1.3E-05	51	1497	**0.70357**	0.512987	5.7E-06	7	39	**0.512987**	6.87	8.4	19.174	15.552	38.781
PAS-75	□	0.70378	1.6E-05	7	526	**0.70376**	0.513034	6.1E-06	3	9	**0.513029**	7.75	2.6	18.859	15.584	38.615
PEJ-69	□						0.512998	3.7E-06	6	31	**0.512994**	7.06		18.852	15.730	38.583
PEJ-70	□	0.70428	1.9E-05	49	975	**0.70368**	0.513033	9.2E-06	6	29	**0.513028**	7.74	7.2			

subscript ul indicates unleached values
subscript i indicates initial values

Sample	$\delta^{18}O_{Ol}$	$\delta^{18}O_{Ol}$	$\delta^{18}O_{Ol}$	$\delta^{18}O_{Ol}$ mean	$\delta^{18}O_{Px}$	$\delta^{18}O_{Px}$	$\delta^{18}O_{Px}$ mean	$\delta^{18}O_{Amph}$	$\delta^{18}O_{Amph}$	$\delta^{18}O_{Amph}$	$\delta^{18}O_{Amph}$	$\delta^{18}O_{Amph}$ mean	$\delta^{18}O_{Ol}$ calc	$\delta^{18}O_{WR}$ calc
ALT-02					6.88	6.63	6.76						6.36	6.86
ALT-12					5.8		5.80						5.40	5.90
CHI-117					5.94		5.94						5.54	6.04
PEJ-69	5.79			5.79									5.79	6.29
BRI-21	5.14	4.79	5.25	5.06	5.69		5.69						5.06	5.56
GUA-27	5.06			5.06									5.06	5.56
GUA-42	5.01	5.2		5.11	5.69		5.69						5.11	5.61
ALT-62									7.11	6.84		6.98	6.68	7.18
ALT-63								5.94	7.07	7.16	6.09	6.57	6.27	6.77
TAL-104									5.99	7.6	7.5	7.03	6.73	7.23
NEI-18								5.58				5.58	5.28	5.78

"$\delta^{18}O_{Ol}$ calc" and "$\delta^{18}O_{WR}$ calc" is calculated from the measured values and the appropriate mineral-mineral and mineral-whole rock fractionation coefficients after Bottinga & Javoy [1975]; Chiba et al. [1989]

	CORR. INTENSITIES (errors: 2SD/abs.)						RESULTS (errors: 2SD/abs.)								
Sample	**40Ar***	**+/-**	**39Ar**	**+/-**	**37Ar**	**+/-**	**40K/ 40Ar**	**+/-**	**36/ 40Ar**	**+/-**	**37Ar 39Ar**	**+/-**	**R/ R+A**	**+/-**	**Date Ma**
AMPH "ALT" - - - Sample ALT-16 - - -															
ALT001	19.93	0.27	2.53	0.03	44.56	0.20	**17.62**	0.22	**2.58E-03**	2.2E-04	**17.62**	0.22	**23.75**	5.81	**18.33**
ALT002	87.58	0.34	12.32	0.04	229.75	0.29	**18.65**	0.06	**1.93E-03**	1.0E-04	**18.65**	0.06	**42.97**	2.49	**16.54**
ALT003	101.27	0.93	13.44	0.06	258.38	0.54	**19.23**	0.10	**2.76E-03**	7.2E-05	**19.23**	0.10	**18.58**	1.33	**17.53**
ALT004	71.79	0.26	9.12	0.05	168.64	0.21	**18.49**	0.11	**2.14E-03**	8.6E-05	**18.49**	0.11	**36.68**	1.93	**18.30**
ALT005	86.96	0.38	10.81	0.04	199.04	0.31	**18.41**	0.08	**2.03E-03**	9.2E-05	**18.41**	0.08	**40.06**	2.20	**18.70**
ALT006	54.81	0.26	7.32	0.04	133.96	0.27	**18.29**	0.10	**2.04E-03**	1.3E-04	**18.29**	0.10	**39.62**	3.32	**17.40**
ALT007	62.39	0.27	9.09	0.06	170.69	0.37	**18.77**	0.12	**1.94E-03**	1.6E-04	**18.77**	0.12	**42.67**	4.26	**15.96**
ALT008	80.43	0.45	11.66	0.04	217.18	0.53	**18.63**	0.08	**2.05E-03**	8.5E-05	**18.63**	0.08	**39.41**	1.92	**16.05**
ALT009	107.04	0.56	13.57	0.03	258.20	0.34	**19.02**	0.05	**2.06E-03**	7.5E-05	**19.02**	0.05	**39.07**	1.66	**18.34**
Total-Gas	672.19	1.39	89.87	0.13	1680.40	1.08	**18.70**	0.03	**2.25E-03**	5.3E-05	**18.70**	0.03	**33.47**	0.76	**17.40**
Weight. MEAN															**17.36**
MEAN ± 1SD											**18.57**	0.46	**35.87**	8.64	**17.46**
Minimum											**17.62**		**18.58**		**15.96**
Maximum											**19.23**		**42.97**		**18.70**
AMPH "GUA" - - - Sample GUA-28 - - -															
GUA001	65.45	0.17	34.68	0.05	167.74	0.32	**4.84**	0.01	**1.75E-03**	1.4E-04	**4.84**	0.01	**48.21**	3.37	**4.44**
GUA002	54.75	0.26	32.85	0.05	156.49	0.23	**4.76**	0.01	**2.28E-03**	1.0E-04	**4.76**	0.01	**32.76**	2.44	**3.92**
GUA003	58.48	0.11	32.50	0.06	159.77	0.33	**4.92**	0.01	**1.16E-03**	2.1E-04	**4.92**	0.01	**65.85**	4.62	**4.24**
GUA004	53.70	0.27	34.34	0.08	164.91	0.31	**4.80**	0.01	**2.62E-03**	9.1E-05	**4.80**	0.01	**22.68**	2.10	**3.68**
GUA005	61.60	0.15	37.18	0.05	184.59	0.23	**4.96**	0.01	**1.79E-03**	1.3E-04	**4.96**	0.01	**47.21**	3.04	**3.90**
GUA006	68.90	0.41	41.93	0.08	210.08	0.17	**5.01**	0.01	**2.86E-03**	6.6E-05	**5.01**	0.01	**15.35**	0.95	**3.87**
GUA007	70.48	0.24	44.46	0.08	224.16	0.46	**5.04**	0.01	**1.73E-03**	1.2E-04	**5.04**	0.01	**48.98**	2.92	**3.73**
single crystal															
GUA008	24.54	0.23	12.96	0.05	62.20	0.18	**4.80**	0.02	**1.75E-03**	3.2E-04	**4.80**	0.02	**48.25**	7.85	**4.46**
GUA009	8.86	0.11	8.03	0.05	42.85	0.15	**5.34**	0.04	**2.09E-03**	6.0E-04	**5.34**	0.04	**38.23**	14.53	**2.60**
GUA010	37.18	0.24	20.70	0.06	110.15	0.26	**5.32**	0.02	**1.63E-03**	2.3E-04	**5.32**	0.02	**51.96**	5.45	**4.23**
GUA011	11.31	0.13	11.33	0.03	58.06	0.13	**5.12**	0.02	**2.50E-03**	2.7E-04	**5.12**	0.02	**25.99**	6.80	**2.35**
GUA012	16.36	0.09	10.56	0.04	52.22	0.10	**4.94**	0.02	**1.41E-03**	5.9E-04	**4.94**	0.02	**58.19**	13.11	**3.65**
GUA013	36.30	0.25	20.11	0.06	94.69	0.23	**4.71**	0.02	**1.47E-03**	2.9E-04	**4.71**	0.02	**56.64**	6.81	**4.25**
GUA014	19.46	0.22	11.10	0.07	55.16	0.15	**4.97**	0.03	**1.67E-03**	4.5E-04	**4.97**	0.03	**50.51**	10.46	**4.13**
GUA015	17.98	0.23	10.97	0.06	54.22	0.18	**4.94**	0.03	**1.78E-03**	4.3E-04	**4.94**	0.03	**47.53**	10.06	**3.86**
GUA016	16.76	0.22	12.81	0.05	63.45	0.14	**4.95**	0.02	**1.73E-03**	4.8E-04	**4.95**	0.02	**48.81**	10.92	**3.08**
Total-Gas	622.11	0.88	376.54	0.24	1860.73	0.96	**4.94**	0.00	**2.18E-03**	5.5E-05	**4.94**	0.00	**35.68**	0.92	**3.89**
Weight. MEAN															**3.92**
MEAN ± 1SD											**4.96**	0.18	**44.20**	13.69	**3.77**
Minimum											**4.71**		**15.35**		**2.35**
Maximum											**5.34**		**65.85**		**4.46**

	CORR. INTENSITIES (errors: 2SD/abs.)						RESULTS (errors: 2SD/abs.)								
Sample	**40Ar***	+/-	**39Ar**	+/-	**37Ar**	+/-	**40K/ 40Ar**	+/-	**36/ 40Ar**	+/-	**37Ar 39Ar**	+/-	**R/ R+A**	+/-	**Date Ma**
AMPH "TAL" - - - Sample TAL-104 - - -															
TAL_01	1.89	0.14	11.83	0.04	100.55	0.19	**5203.3**	55.2	**2.99E-03**	8.5E-04	**8.50**	0.04	**11.70**	24.39	**0.39**
TAL_02	9.42	0.24	17.17	0.06	174.73	0.37	**1158.2**	7.5	**3.08E-03**	2.3E-04	**10.18**	0.04	**8.96**	6.64	**1.33**
TAL_03	19.55	0.34	29.97	0.20	241.35	0.48	**5057.1**	58.5	**1.81E-03**	5.3E-04	**8.05**	0.06	**46.53**	15.29	**1.58**
TAL_04	60.31	0.95	47.75	0.39	405.46	1.66	**1682.6**	18.0	**2.37E-03**	1.7E-04	**8.49**	0.08	**29.98**	4.90	**3.06**
Tal_05	26.67	1.00	23.95	0.17	302.40	1.17	**915.6**	9.4	**2.90E-03**	1.1E-04	**12.62**	0.10	**14.37**	3.25	**2.70**
TAL_06	46.03	1.92	26.02	0.17	231.37	0.95	**557.9**	5.7	**2.91E-03**	9.2E-05	**8.89**	0.07	**13.92**	2.64	**4.29**
TAL_07															
TAL_08	15.91	1.03	21.37	0.19	289.30	0.95	**1010.3**	12.3	**3.03E-03**	1.9E-04	**13.54**	0.13	**10.61**	5.36	**1.81**
TAL_09	10.71	0.31	15.92	0.11	123.88	0.22	**2517.6**	27.4	**2.58E-03**	4.3E-04	**7.78**	0.05	**23.88**	12.30	**1.63**
TAL_10	5.85	0.34	11.79	0.08	114.33	0.33	**1871.8**	21.3	**2.94E-03**	3.8E-04	**9.70**	0.07	**13.10**	10.86	**1.20**
TAL_11	4.87	0.32	12.70	0.08	112.58	0.22	**1939.7**	20.9	**3.03E-03**	3.5E-04	**8.87**	0.06	**10.49**	10.14	**0.93**
TAL_12	12.96	0.32	10.85	0.10	103.99	0.39	**1789.1**	23.7	**2.36E-03**	4.3E-04	**9.58**	0.10	**30.14**	12.42	**2.90**
TAL_13	16.03	0.34	24.42	0.19	199.44	0.63	**2867.8**	30.7	**2.49E-03**	3.1E-04	**8.17**	0.07	**26.54**	8.76	**1.59**
TAL_14	9.71	0.26	17.14	0.15	163.22	0.30	**2011.7**	21.8	**2.84E-03**	3.3E-04	**9.52**	0.08	**16.07**	9.43	**1.37**
TAL_15	23.70	0.34	33.77	0.15	253.11	0.66	**4209.9**	37.7	**1.97E-03**	3.8E-04	**7.50**	0.04	**41.67**	10.95	**1.70**
TAL_16	26.52	0.45	26.64	0.18	192.77	0.73	**3335.6**	38.8	**1.80E-03**	4.3E-04	**7.24**	0.06	**46.83**	12.33	**2.41**
TAL_17	2.85	0.34	11.78	0.09	138.91	0.32	**1812.6**	21.6	**3.17E-03**	4.6E-04	**11.79**	0.10	**6.19**	13.23	**0.59**
TAL_18	10.85	0.20	17.27	0.13	142.28	0.27	**2022.0**	19.3	**2.78E-03**	3.5E-04	**8.24**	0.06	**17.91**	9.90	**1.52**
TAL_19															
TAL_20	9.90	0.29	10.93	0.07	190.04	0.50	**611.9**	5.1	**3.12E-03**	1.9E-04	**17.38**	0.12	**7.82**	5.55	**2.20**
TAL_21	3.67	0.27	11.39	0.06	91.28	0.18	**2631.3**	29.8	**2.98E-03**	6.5E-04	**8.01**	0.04	**11.97**	18.73	**0.78**
TAL_22	8.08	0.29	12.58	0.06	98.16	0.28	**2644.2**	29.0	**2.57E-03**	5.5E-04	**7.80**	0.04	**23.96**	15.84	**1.56**
TAL_23a															
TAL_23b															
TAL_24															
TAL_25	13.59	0.23	24.25	0.14	145.63	0.34	**2475.8**	20.3	**2.72E-03**	2.3E-04	**6.01**	0.04	**19.56**	6.64	**1.36**
TAL_26a	13.35	0.28	12.20	0.07	104.12	0.22	**965.3**	8.2	**2.88E-03**	2.6E-04	**8.53**	0.05	**14.90**	7.39	**2.65**
TAL_26b	21.37	0.32	18.66	0.08	162.30	0.31	**1868.4**	15.1	**2.36E-03**	2.5E-04	**8.70**	0.04	**30.17**	7.31	**2.78**
TAL_26c	26.24	0.37	21.16	0.13	183.34	0.33	**2212.7**	21.2	**2.07E-03**	3.9E-04	**8.67**	0.05	**38.70**	11.30	**3.01**
Total-Gas	400.01	2.92	471.50	0.72	4264.54	3.01	**1452.4**	7.8	**2.83E-03**	4.7E-05	**9.04**	0.02	**16.38**	1.35	**1.94**
Weight. MEAN															**1.90**
MEAN ± 2SD											**9.32**	2.41	**21.50**	12.34	**1.89**
Minimum											**6.01**		**6.19**		**0.39**
Maximum											**17.38**		**46.83**		**4.29**

	CORR. INTENSITIES (errors: 2SD/abs.)						RESULTS (errors: 2SD/abs.)								
Sample	**40Ar***	**+/-**	**39Ar**	**+/-**	**37Ar**	**+/-**	**40K/ 40Ar**	**+/-**	**36/ 40Ar**	**+/-**	**37Ar 39Ar**	**+/-**	**R/ R+A**	**+/-**	**Date Ma**
AMPH "BRI" - - - Sample BRI-25 - - -															
BRI25_2	55.88	0.88	24.17	0.25	77.96	0.52	**511.6**	5.9	**2.82E-03**	1.2E-04	**3.23**	0.04	**16.68**	3.48	**5.60**
BRI25_02b	12.26	0.13	5.70	0.09	19.19	0.11	**1868.7**	33.3	**1.47E-03**	5.9E-04	**3.37**	0.06	**56.69**	17.06	**5.21**
BRI25_03	20.95	0.19	9.17	0.05	49.19	0.15	**1323.5**	11.3	**1.94E-03**	4.6E-04	**5.36**	0.03	**42.64**	13.24	**5.54**
BRI25_04	19.43	0.24	9.55	0.06	37.87	0.15	**1602.2**	15.5	**1.83E-03**	4.0E-04	**3.97**	0.03	**45.99**	11.44	**4.93**
BRI25_4b	9.65	0.17	4.69	0.07	19.61	0.13	**1527.2**	25.7	**1.88E-03**	1.1E-03	**4.18**	0.07	**44.33**	30.37	**4.99**
BRI25_06	30.36	0.37	15.36	0.09	75.66	0.29	**656.3**	5.3	**2.76E-03**	1.1E-04	**4.93**	0.04	**18.30**	3.19	**4.79**
BRI25_07	26.26	0.32	11.71	0.09	51.73	0.26	**1172.7**	12.3	**2.13E-03**	2.6E-04	**4.42**	0.04	**37.08**	7.59	**5.43**
Br25_08	28.95	0.26	12.00	0.07	60.65	0.15	**1391.6**	12.5	**1.78E-03**	2.5E-04	**5.05**	0.03	**47.35**	7.27	**5.85**
BRI_09	31.54	0.27	14.68	0.09	73.52	0.23	**1032.4**	8.4	**2.33E-03**	1.6E-04	**5.01**	0.03	**31.28**	4.55	**5.21**
BRI_10	78.29	1.82	30.62	0.19	151.14	0.62	**568.9**	5.3	**2.69E-03**	7.6E-05	**4.94**	0.04	**20.51**	2.18	**6.19**
BRI_11	41.61	0.41	16.17	0.09	85.72	0.26	**1044.3**	8.9	**2.10E-03**	1.7E-04	**5.30**	0.03	**37.90**	4.81	**6.24**
BRI_12	52.58	0.56	20.30	0.12	95.87	0.36	**628.1**	5.1	**2.61E-03**	1.0E-04	**4.72**	0.03	**22.94**	2.92	**6.28**
BRI_13	57.75	0.19	25.52	0.10	103.04	0.17	**1353.6**	8.7	**1.92E-03**	1.1E-04	**4.04**	0.02	**43.20**	3.26	**5.48**
BRI_14	41.54	0.26	16.09	0.10	74.06	0.17	**1386.3**	11.9	**1.68E-03**	2.2E-04	**4.60**	0.03	**50.46**	6.38	**6.25**
BRI_15	25.81	0.25	11.48	0.07	61.14	0.32	**1105.1**	9.6	**2.20E-03**	2.9E-04	**5.33**	0.04	**35.04**	8.47	**5.45**
BRI_16	27.71	0.42	11.17	0.09	50.11	0.20	**654.4**	6.6	**2.61E-03**	1.9E-04	**4.49**	0.04	**22.89**	5.48	**6.01**
BR_18(b)	58.66	0.27	24.25	0.13	98.70	0.29	**1743.5**	13.5	**1.37E-03**	1.8E-04	**4.07**	0.02	**59.49**	5.21	**5.86**
BRI_19	13.52	0.20	5.69	0.08	25.83	0.11	**985.5**	14.8	**2.27E-03**	3.4E-04	**4.54**	0.06	**33.00**	9.65	**5.75**
BRI_20	65.98	0.30	26.02	0.12	96.84	0.23	**1809.0**	13.6	**1.19E-03**	1.7E-04	**3.72**	0.02	**64.70**	4.93	**6.15**
BRI_21	44.97	0.25	18.88	0.06	83.78	0.29	**1935.5**	13.5	**1.18E-03**	2.3E-04	**4.44**	0.02	**65.01**	6.72	**5.77**
BRI_22	24.54	0.29	9.56	0.11	43.92	0.16	**427.0**	5.2	**2.86E-03**	1.1E-04	**4.59**	0.05	**15.45**	3.06	**6.22**
BRI_23	35.59	0.33	13.04	0.08	64.57	0.15	**1120.3**	9.9	**1.93E-03**	2.2E-04	**4.95**	0.03	**43.11**	6.29	**6.61**
BRI_24	19.63	0.24	8.56	0.06	38.50	0.15	**1219.4**	12.3	**2.05E-03**	3.9E-04	**4.50**	0.04	**39.45**	11.07	**5.56**
BRI_25a	8.68	0.24	4.55	0.04	21.66	0.16	**605.0**	6.7	**2.83E-03**	3.1E-04	**4.76**	0.05	**16.25**	8.90	**4.62**
BRI_25b	35.81	0.27	17.48	0.10	84.48	0.18	**2002.8**	17.4	**1.43E-03**	3.1E-04	**4.83**	0.03	**57.85**	8.89	**4.96**
BRI_26	54.81	0.28	20.41	0.09	89.27	0.26	**1623.0**	12.2	**1.30E-03**	1.7E-04	**4.37**	0.02	**61.47**	4.88	**6.51**
BRI_27	32.02	0.56	15.69	0.11	74.68	0.29	**411.8**	3.7	**2.98E-03**	8.2E-05	**4.76**	0.04	**11.85**	2.34	**4.95**
BRI_28	26.82	0.72	12.08	0.10	54.03	0.17	**200.1**	1.9	**3.17E-03**	9.2E-05	**4.47**	0.04	**6.26**	2.63	**5.38**
BRI_29	38.73	0.45	13.96	0.11	63.18	0.17	**727.8**	7.3	**2.42E-03**	1.5E-04	**4.53**	0.04	**28.47**	4.43	**6.72**
BRI_30a	12.91	0.43	6.80	0.08	34.53	0.18	**358.9**	4.8	**3.06E-03**	2.1E-04	**5.07**	0.07	**9.60**	6.05	**4.60**
BRI_30b	13.49	0.26	5.56	0.05	30.11	0.11	**1708.4**	25.7	**1.41E-03**	8.6E-04	**5.41**	0.05	**58.41**	24.92	**5.87**
BRI_31	36.08	0.33	16.18	0.08	76.54	0.25	**1001.6**	7.4	**2.32E-03**	2.9E-04	**4.73**	0.03	**31.51**	8.47	**5.41**
Total-Gas	1082.80	2.74	457.12	0.58	2067.09	1.43	**836.5**	4.3	**2.45E-03**	3.2E-05	**4.52**	0.01	**27.46**	0.91	**5.64**
Weight. MEAN															**5.82**
MEAN ± 2SD											**4.58**	0.53	**36.72**	17.30	**5.64**
Minimum											**3.23**		**6.26**		**4.60**
Maximum											**5.41**		**65.01**		**6.72**

	CORR. INTENSITIES						RESULTS										
Sample	**40Ar***	**+/-**	**39Ar**	**+/-**	**37Ar**	**+/-**	**40K/ 40Ar**	**+/-**	**36/ 40Ar**	**+/-**	**37Ar 39Ar**	**+/-**	**R/ R+A**	**+/-**	**Date Ma**	**+/-int.**	**+/-ext.**
AMPH ALT																	
600°	1.92	1.68	1.26	0.06	8.54	0.13	**33.0**	1.6	**3.36E-03**	2.0E-04	**6.79**	0.35	**0.69**	5.93	**3.58**	**30.52**	**30.52**
1000°	199.41	4.13	13.28	0.06	211.79	0.57	**84.6**	0.5	**2.80E-03**	4.0E-05	**15.94**	0.08	**17.29**	1.20	**34.84**	**2.46**	**2.47**
1200°	1389.92	9.91	192.13	0.74	3469.11	8.69	**505.1**	2.7	**1.70E-03**	2.2E-05	**18.06**	0.08	**49.75**	0.65	**16.87**	**0.26**	**0.27**
1550°	117.31	6.56	10.60	0.09	55.07	0.21	**480.0**	19.8	**9.38E-04**	3.7E-04	**5.19**	0.05	**72.29**	10.94	**25.74**	**4.07**	**4.07**
1550°																	
total gas	1708.57	12.70	217.28	0.75	3744.51	8.71	**363.6**	1.7	**2.07E-03**	2.6E-05	**17.23**	0.07	**38.92**	0.77	**18.33**	**0.39**	**0.40**
AMPH BRI																	
1550°	2286.26	18.72	745.15	2.66	3497.54	7.78	**1080.1**	5.7	**1.81E-03**	7.0E-05	**4.69**	0.02	**46.65**	2.09	**7.42**	**0.33**	**0.34**
1550°																	
total gas	2286.26	18.72	745.15	2.66	3497.54	7.78	**1080.1**	5.7	**1.81E-03**	7.0E-05	**4.69**	0.02	**46.65**	2.09	**7.42**	**0.33**	**0.34**
AMPH GUA																	
600°	7.67	1.61	7.68	0.06	4.01	0.14	**222.3**	2.3	**3.28E-03**	2.1E-04	**0.52**	0.02	**3.06**	6.15	**2.37**	**4.70**	**4.70**
1200°	1328.25	9.14	716.14	2.55	3444.28	8.81	**2092.6**	10.7	**1.57E-03**	5.4E-05	**4.81**	0.02	**53.47**	1.63	**4.39**	**0.14**	**0.14**
1550°	113.87	6.48	32.85	0.14	182.49	0.48	**943.8**	24.5	**1.86E-03**	2.1E-04	**5.56**	0.03	**45.07**	6.20	**8.20**	**1.18**	**1.18**
1550°																	
1550°																	
total gas	1449.79	11.32	756.67	2.56	3630.78	8.83	**1838.4**	9.4	**1.74E-03**	5.2E-05	**4.80**	0.02	**48.53**	1.54	**4.54**	**0.15**	**0.15**
AMPH TAL																	
1550°	1059.02	17.28	1338.17	5.03	12883.89	28.55	**2459.7**	13.6	**2.45E-03**	4.6E-05	**9.63**	0.04	**27.48**	1.38	**1.92**	**0.10**	**0.10**
1550°																	
1550°																	
1550°																	
total gas	1059.02	17.28	1338.17	5.03	12883.89	28.55	**2459.7**	13.6	**2.45E-03**	4.6E-05	**9.63**	0.04	**27.48**	1.38	**1.92**	**0.10**	**0.10**

Name	TAL 104_1	TAL 104_2	TAL 104_3_1	TAL 104_3_2	TAL 104_1_R1	TAL 104_1_R2	TAL 104_1_M1
SiO2	43.16	40.66	42.95	42.70	43.52	43.41	43.65
TiO2	1.81	1.68	1.77	1.78	1.79	1.64	1.77
Al2O3	11.67	13.69	12.45	12.32	11.89	11.78	11.71
Cr2O3	0.22	0.01	0.03	0.09	0.04	0.05	0.18
FeO	8.46	14.15	10.57	10.37	8.67	8.50	8.55
MnO	0.07	0.25	0.11	0.08	0.13	0.11	0.08
MgO	16.49	11.85	14.72	14.96	16.27	16.62	16.84
CaO	11.67	11.86	11.29	11.45	11.53	11.55	11.61
BaO	0.01	0.01	0.03	0.00	0.00	0.10	0.01
Na2O	2.46	2.64	2.65	2.65	2.37	2.35	2.48
K2O	0.63	0.30	0.59	0.59	0.63	0.64	0.66
Total	96.65	97.10	97.17	96.99	96.85	96.74	97.54

cations on basis of 23 oxygen

Si	6.325	6.103	6.310	6.287	6.356	6.349	6.335
Al	2.016	2.422	2.155	2.137	2.047	2.030	2.004
Ti	0.199	0.190	0.196	0.198	0.197	0.180	0.193
Cr	0.026	0.001	0.004	0.011	0.005	0.006	0.020
Mg	3.603	2.652	3.225	3.284	3.542	3.624	3.643
X (Zn,Ni,Li)	0.000	0.000	0.000	0.000	0.000	0.000	0.000
Fe	1.037	1.776	1.299	1.276	1.059	1.040	1.038
Mn	0.009	0.032	0.014	0.010	0.017	0.013	0.010
Ca	1.832	1.907	1.776	1.806	1.805	1.811	1.805
Na	0.699	0.768	0.754	0.758	0.670	0.668	0.698
K	0.117	0.057	0.111	0.110	0.117	0.119	0.122
Ba	0.001	0.001	0.002	0.000	0.000	0.006	0.000
Total	15.863	15.909	15.846	15.877	15.815	15.845	15.869

ideal site formular

Si	6.26	6.05	6.26	6.24	6.30	6.28	6.27
Al^{IV}	1.74	1.95	1.74	1.76	1.70	1.72	1.73
Ti^{IV}							
sum T	8.000	8.000	8.000	8.000	8.000	8.000	8.000
Al^{VI}	0.26	0.44	0.40	0.36	0.32	0.29	0.25
Ti	0.20	0.19	0.19	0.20	0.20	0.18	0.19
Fe^{3+}	0.44	0.43	0.36	0.36	0.43	0.50	0.50
Cr	0.03	0.00	0.00	0.01	0.00	0.01	0.02
Mg	3.57	2.63	3.20	3.26	3.51	3.58	3.60
X (Zn,Ni,Li)							
Fe^{2+}	0.50	1.29	0.84	0.81	0.53	0.43	0.43
Mn	0.00	0.02	0.01	0.00	0.01	0.01	0.01
sum C	5.000	5.000	5.000	5.000	5.000	5.000	5.000
Fe^{2+}	0.08	0.04	0.09	0.09	0.09	0.09	0.10
Mn	0.00	0.02	0.01	0.00	0.01	0.01	0.01
Ca	1.81	1.89	1.76	1.79	1.79	1.79	1.79
Na	0.10	0.059	0.136	0.111	0.113	0.111	0.114
sum B	2.000	2.000	2.000	2.000	2.000	2.000	2.000
Na	0.59	0.70	0.61	0.64	0.55	0.55	0.58
K	0.12	0.06	0.11	0.11	0.12	0.12	0.12
Ba	0.00	0.00	0.00	0.00	0.00	0.01	0.00
sum A	0.710	0.759	0.724	0.751	0.667	0.673	0.698
total	15.71	15.76	15.72	15.75	15.67	15.67	15.70

Ca_B	1.81	1.89	1.76	1.79	1.79	1.79	1.79
$(Na+K)_A$	0.71	0.76	0.72	0.75	0.67	0.67	0.70
Ti	0.199	0.190	0.196	0.198	0.197	0.180	0.193
Si(formular)	6.26	6.05	6.26	6.24	6.30	6.28	6.27
Mg/(Mg+Fe2+)	0.86	0.66	0.77	0.78	0.85	0.87	0.87
AlVI/Fe3+	0.59	1.03	1.12	0.98	0.76	0.57	0.50
name	magnesiohasting	pargasite	pargasite	magnesiohasting	magnesiohasting	magnesiohasting	magnesiohasting

Name	TAL 104_2_M1	TAL 104_2_M2	TAL 104_2_M3	TAL 104_2_R1	TAL 104_2_R2	TAL 104_3_M1	TAL 104_3_R1
SiO2	40.96	40.88	40.95	40.82	40.63	42.85	42.64
TiO2	1.74	1.71	1.64	1.54	1.65	1.76	1.86
Al2O3	14.00	13.82	13.72	14.29	13.67	12.49	12.49
Cr2O3	0.00	0.00	0.00	0.00	0.01	0.04	0.03
FeO	14.29	14.22	14.60	14.11	14.06	10.69	10.85
MnO	0.23	0.32	0.31	0.18	0.28	0.10	0.05
MgO	11.88	12.06	11.75	11.33	11.70	14.70	15.01
CaO	11.77	11.90	11.68	11.75	11.85	11.35	11.43
BaO	0.02	0.07	0.05	0.06	0.04	0.04	0.06
Na2O	2.65	2.72	2.74	2.52	2.70	2.56	2.63
K2O	0.29	0.31	0.34	0.35	0.31	0.62	0.59
Total	97.83	98.01	97.78	96.95	96.91	97.19	97.64

cations on basis of 23 oxygen

Si	6.096	6.085	6.116	6.122	6.113	6.300	6.251
Al	2.456	2.424	2.415	2.527	2.424	2.163	2.159
Ti	0.195	0.192	0.184	0.174	0.186	0.195	0.205
Cr	0.000	0.000	0.000	0.000	0.002	0.004	0.003
Mg	2.636	2.675	2.615	2.534	2.623	3.220	3.280
X (Zn,Ni,Li)	0.000	0.000	0.000	0.000	0.000	0.000	0.000
Fe	1.779	1.770	1.823	1.770	1.769	1.315	1.330
Mn	0.029	0.040	0.039	0.023	0.036	0.012	0.006
Ca	1.877	1.898	1.869	1.889	1.910	1.787	1.796
Na	0.764	0.784	0.794	0.734	0.787	0.731	0.747
K	0.055	0.059	0.064	0.067	0.060	0.117	0.111
Ba	0.001	0.004	0.003	0.003	0.002	0.002	0.003
Total	15.889	15.932	15.923	15.843	15.912	15.846	15.892

ideal site formular

Si	6.04	6.02	6.06	6.08	6.06	6.25	6.19
Al^{IV}	1.96	1.98	1.94	1.92	1.94	1.75	1.81
Ti^{IV}							
sum T	8.000	8.000	8.000	8.000	8.000	8.000	8.000
Al^{VI}	0.47	0.43	0.45	0.59	0.47	0.40	0.33
Ti	0.19	0.19	0.18	0.17	0.18	0.19	0.20
Fe^{3+}	0.44	0.46	0.43	0.32	0.36	0.36	0.45
Cr	0.00	0.00	0.00	0.00	0.00	0.00	0.00
Mg	2.61	2.65	2.59	2.52	2.60	3.19	3.25
X (Zn,Ni,Li)							
Fe^{2+}	1.27	1.26	1.33	1.39	1.36	0.84	0.76
Mn	0.01	0.02	0.02	0.01	0.02	0.01	0.00
sum C	5.000	5.000	5.000	5.000	5.000	5.000	5.000
Fe^{2+}	0.05	0.04	0.05	0.05	0.03	0.10	0.10
Mn	0.01	0.02	0.02	0.01	0.02	0.01	0.00
Ca	1.86	1.88	1.85	1.88	1.89	1.77	1.78
Na	0.075	0.064	0.079	0.066	0.056	0.123	0.118
sum B	2.000	2.000	2.000	2.000	2.000	2.000	2.000
Na	0.68	0.71	0.71	0.66	0.72	0.60	0.62
K	0.05	0.06	0.06	0.07	0.06	0.12	0.11
Ba	0.00	0.00	0.00	0.00	0.00	0.00	0.00
sum A	0.738	0.774	0.774	0.732	0.787	0.721	0.735
total	15.74	15.77	15.77	15.73	15.79	15.72	15.73

Ca_B	1.86	1.88	1.85	1.88	1.89	1.77	1.78
$(Na+K)_A$	0.74	0.77	0.77	0.73	0.78	0.72	0.73
Ti	0.195	0.192	0.184	0.174	0.186	0.195	0.205
Si(formular)	6.04	6.02	6.06	6.08	6.06	6.25	6.19
Mg/(Mg+Fe2+	0.66	0.67	0.65	0.64	0.65	0.77	0.79
AlVI/Fe3+	1.07	0.93	1.06	1.85	1.30	1.09	0.72
name	pargasite	magnesiohasting	pargasite	pargasite	pargasite	pargasite	magnesiohasting

Name	TAL 104_3_R2	TAL 104_3_M2	BRI 25_1_M1	BRI 25_1_R2	BRI 25_2_M1	BRI 25_2_R1	BRI 25_3_M1
SiO2	42.78	42.95	39.44	40.33	40.05	40.34	40.39
TiO2	1.77	1.77	2.69	3.13	3.19	3.10	3.38
Al2O3	12.43	12.45	15.00	14.07	13.31	13.16	13.05
Cr2O3	0.00	0.05	0.00	0.02	0.00	0.02	0.00
FeO	10.57	10.38	10.93	10.02	10.59	10.76	11.75
MnO	0.01	0.11	0.11	0.11	0.13	0.08	0.14
MgO	14.62	14.83	13.62	13.96	14.11	13.93	13.39
CaO	11.34	11.52	12.14	12.10	11.78	11.97	12.01
BaO	0.05	0.00	0.10	0.08	0.06	0.02	0.05
Na2O	2.64	2.64	2.25	2.59	2.52	2.40	2.66
K2O	0.57	0.58	1.40	1.06	0.95	0.98	0.99
Total	96.78	97.29	97.68	97.47	96.69	96.76	97.81
cations on basis of 23 oxygen							
Si	6.310	6.300	5.848	5.956	5.977	6.015	5.996
Al	2.161	2.152	2.621	2.450	2.340	2.313	2.284
Ti	0.197	0.195	0.300	0.347	0.358	0.347	0.377
Cr	0.000	0.006	0.000	0.002	0.000	0.002	0.000
Mg	3.214	3.244	3.011	3.073	3.140	3.097	2.962
X (Zn,Ni,Li)	0.000	0.000	0.000	0.000	0.000	0.000	0.000
Fe	1.303	1.273	1.356	1.238	1.322	1.342	1.458
Mn	0.001	0.014	0.014	0.014	0.017	0.010	0.018
Ca	1.792	1.811	1.929	1.915	1.884	1.913	1.910
Na	0.755	0.750	0.647	0.742	0.730	0.694	0.765
K	0.106	0.109	0.265	0.199	0.180	0.186	0.188
Ba	0.003	0.000	0.006	0.004	0.003	0.001	0.003
Total	15.842	15.854	15.996	15.941	15.952	15.920	15.960
ideal site formular							
Si	6.27	6.26	5.80	5.94	5.93	5.98	5.97
Al^{IV}	1.73	1.74	2.20	2.06	2.07	2.02	2.03
Ti^{IV}							
sum T	8.000	8.000	8.000	8.000	8.000	8.000	8.000
Al^{VI}	0.41	0.39	0.40	0.38	0.26	0.28	0.25
Ti	0.20	0.19	0.30	0.35	0.36	0.34	0.38
Fe^{3+}	0.33	0.32	0.38	0.14	0.32	0.28	0.18
Cr	0.00	0.01	0.00	0.00	0.00	0.00	0.00
Mg	3.19	3.22	2.99	3.06	3.12	3.08	2.95
X (Zn,Ni,Li)							
Fe^{2+}	0.88	0.86	0.93	1.06	0.94	1.01	1.24
Mn	0.00	0.01	0.01	0.01	0.01	0.00	0.01
sum C	5.000	5.000	5.000	5.000	5.000	5.000	5.000
Fe^{2+}	0.09	0.09	0.03	0.03	0.05	0.04	0.04
Mn	0.00	0.01	0.01	0.01	0.01	0.00	0.01
Ca	1.78	1.80	1.91	1.91	1.87	1.90	1.90
Na	0.128	0.110	0.046	0.051	0.069	0.053	0.052
sum B	2.000	2.000	2.000	2.000	2.000	2.000	2.000
Na	0.62	0.64	0.60	0.69	0.66	0.64	0.71
K	0.11	0.11	0.26	0.20	0.18	0.18	0.19
Ba	0.00	0.00	0.01	0.00	0.00	0.00	0.00
sum A	0.731	0.743	0.864	0.892	0.838	0.823	0.900
total	15.73	15.74	15.86	15.89	15.84	15.82	15.90
Ca_B	1.78	1.80	1.91	1.91	1.87	1.90	1.90
$(Na+K)_A$	0.73	0.74	0.86	0.89	0.83	0.82	0.90
Ti	0.197	0.195	0.300	0.347	0.358	0.347	0.377
Si(formular)	6.27	6.26	5.80	5.94	5.93	5.98	5.97
Mg/(Mg+Fe2+	0.77	0.77	0.76	0.74	0.76	0.75	0.70
AlVI/Fe3+	1.26	1.21	1.04	2.67	0.80	0.98	1.41
name	pargasite	pargasite	pargasite	pargasite	magnesiohasting	magnesiohasting	pargasite

Name	BRI 25_3_R1	ALT 16_1_M1	ALT 16_1_R1	ALT 16_2_M1	ALT 16_2_R1	ALT 16_3_M1	ALT 16_3_R1
SiO2	39.52	42.28	42.19	42.73	42.91	42.50	43.06
TiO2	3.65	2.57	2.56	2.56	2.66	2.58	2.39
Al2O3	14.01	11.65	11.47	11.69	11.83	10.93	10.81
Cr2O3	0.00	0.00	0.00	0.01	0.00	0.00	0.02
FeO	11.11	13.16	13.35	13.15	12.94	16.83	16.64
MnO	0.05	0.36	0.39	0.29	0.29	0.52	0.68
MgO	13.45	13.71	13.57	13.62	13.46	11.33	11.57
CaO	11.74	11.13	11.17	11.09	11.10	10.26	10.25
BaO	0.00	0.01	0.02	0.05	0.02	0.06	0.00
Na2O	2.68	2.60	2.68	2.47	2.44	2.40	2.57
K2O	0.95	0.28	0.27	0.25	0.27	0.23	0.22
Total	97.16	97.75	97.67	97.91	97.92	97.64	98.22
cations on basis of 23 oxygen							
Si	5.884	6.258	6.261	6.299	6.315	6.385	6.422
Al	2.459	2.032	2.007	2.032	2.051	1.936	1.901
Ti	0.409	0.286	0.285	0.284	0.294	0.291	0.268
Cr	0.000	0.000	0.000	0.001	0.000	0.000	0.002
Mg	2.986	3.026	3.001	2.994	2.952	2.536	2.572
X (Zn,Ni,Li)	0.000	0.000	0.000	0.000	0.000	0.000	0.000
Fe	1.383	1.629	1.657	1.621	1.593	2.114	2.076
Mn	0.006	0.045	0.049	0.036	0.036	0.066	0.086
Ca	1.873	1.765	1.776	1.752	1.751	1.652	1.639
Na	0.773	0.747	0.772	0.707	0.695	0.700	0.742
K	0.180	0.052	0.052	0.047	0.050	0.045	0.043
Ba	0.000	0.001	0.001	0.003	0.001	0.003	0.000
Total	15.953	15.842	15.861	15.776	15.738	15.729	15.751
ideal site formular							
Si	5.86	6.18	6.19	6.23	6.26	6.31	6.34
Al^{IV}	2.14	1.82	1.81	1.77	1.74	1.69	1.66
Ti^{IV}							
sum T	8.000	8.000	8.000	8.000	8.000	8.000	8.000
Al^{VI}	0.30	0.19	0.18	0.24	0.29	0.22	0.22
Ti	0.41	0.28	0.28	0.28	0.29	0.29	0.26
Fe^{3+}	0.22	0.54	0.51	0.50	0.42	0.57	0.56
Cr	0.00	0.00	0.00	0.00	0.00	0.00	0.00
Mg	2.97	2.99	2.97	2.96	2.93	2.50	2.54
X (Zn,Ni,Li)							
Fe^{2+}	1.09	0.97	1.04	1.00	1.06	1.39	1.37
Mn	0.00	0.02	0.02	0.02	0.02	0.03	0.04
sum C	5.000	5.000	5.000	5.000	5.000	5.000	5.000
Fe^{2+}	0.06	0.10	0.09	0.11	0.10	0.13	0.12
Mn	0.00	0.02	0.02	0.02	0.02	0.03	0.04
Ca	1.86	1.74	1.76	1.73	1.74	1.63	1.62
Na	0.073	0.136	0.129	0.142	0.145	0.204	0.217
sum B	2.000	2.000	2.000	2.000	2.000	2.000	2.000
Na	0.70	0.60	0.63	0.56	0.54	0.49	0.52
K	0.18	0.05	0.05	0.05	0.05	0.04	0.04
Ba	0.00	0.00	0.00	0.00	0.00	0.00	0.00
sum A	0.876	0.655	0.686	0.607	0.595	0.535	0.558
total	15.88	15.65	15.69	15.61	15.60	15.53	15.56
Ca_B	1.86	1.74	1.76	1.73	1.74	1.63	1.62
$(Na+K)_A$	0.88	0.65	0.69	0.60	0.59	0.53	0.56
Ti	0.409	0.286	0.285	0.284	0.294	0.291	0.268
Si(formular)	5.86	6.18	6.19	6.23	6.26	6.31	6.34
Mg/(Mg+Fe2+	0.72	0.74	0.72	0.73	0.72	0.62	0.63
AlVI/Fe3+	1.34	0.36	0.35	0.49	0.69	0.39	0.39
name	pargasite	magnesiohasting:	magnesiohasting:	magnesiohasting:	magnesiohasting:	magnesiohasting:	magnesiohasting:

Name	GUA 28_1_M1	GUA 28_1_R1	GUA 28_2_M1	GUA 28_2_R1	GUA 28_2_incl	GUA 28_3_M1	GUA 28_3_R1	GUA 28_3_M2
SiO2	39.73	40.19	39.85	40.14	39.33	40.11	39.91	40.20
TiO2	6.52	6.26	6.41	6.25	6.14	6.17	6.04	6.11
Al2O3	12.15	11.91	11.95	11.78	12.02	12.06	11.37	12.04
Cr2O3	0.04	0.00	0.00	0.00	0.00	0.00	0.00	0.03
FeO	10.05	10.25	10.21	10.67	9.88	9.77	9.99	10.32
MnO	0.23	0.28	0.25	0.28	0.22	0.18	0.34	0.26
MgO	13.32	13.08	13.13	13.07	13.02	13.13	13.24	13.17
CaO	11.95	11.88	11.76	11.76	11.55	11.83	11.63	11.73
BaO	0.29	0.30	0.32	0.31	0.28	0.30	0.27	0.35
Na2O	2.75	2.76	2.85	2.90	2.64	2.85	3.03	2.88
K2O	0.99	1.07	1.06	1.07	1.02	1.01	1.07	1.06
Total	98.02	97.97	97.80	98.22	96.10	97.41	96.89	98.14

cations on basis of 23 oxygen

Si	5.862	5.930	5.895	5.927	5.912	5.936	5.961	5.928
Al	2.113	2.071	2.084	2.050	2.130	2.104	2.002	2.093
Ti	0.724	0.695	0.713	0.694	0.694	0.687	0.679	0.678
Cr	0.004	0.000	0.000	0.000	0.000	0.000	0.000	0.003
Mg	2.931	2.878	2.896	2.878	2.918	2.897	2.949	2.896
X (Zn,Ni,Li)	0.119	0.148	0.149	0.119	0.091	0.149	0.120	0.119
Fe	1.240	1.265	1.263	1.318	1.242	1.209	1.248	1.273
Mn	0.029	0.035	0.032	0.034	0.028	0.022	0.043	0.032
Ca	1.889	1.878	1.864	1.861	1.860	1.876	1.861	1.853
Na	0.787	0.790	0.818	0.830	0.769	0.818	0.878	0.823
K	0.186	0.201	0.200	0.201	0.196	0.191	0.203	0.199
Ba	0.017	0.017	0.019	0.018	0.016	0.017	0.016	0.020
Total	15.901	15.909	15.933	15.929	15.857	15.905	15.960	15.917

ideal site formular

Si	5.86	5.93	5.89	5.92	5.91	5.93	5.96	5.92
Al^{IV}	2.11	2.07	2.08	2.05	2.09	2.07	2.00	2.08
Ti^{IV}	0.03		0.03	0.03			0.04	
sum T	8.000	8.000	8.000	8.000	8.000	8.000	8.000	8.000
Al^{VI}	0.00	0.00	0.00	0.00	0.04	0.04	0.00	0.01
Ti	0.69	0.69	0.68	0.66	0.69	0.69	0.64	0.68
Fe^{3+}	0.04	0.01	0.06	0.03	0.03	0.00	0.00	0.04
Cr	0.00	0.00	0.00	0.00	0.00	0.00	0.00	0.00
Mg	2.93	2.88	2.89	2.88	2.92	2.90	2.95	2.89
X (Zn,Ni,Li)	0.12	0.15	0.15	0.12	0.09	0.15	0.12	0.12
Fe^{2+}	1.20	1.26	1.20	1.28	1.22	1.20	1.24	1.23
Mn	0.02	0.01	0.02	0.02	0.02	0.02	0.04	0.02
sum C	5.000	5.000	5.000	5.000	5.000	5.000	5.000	5.000
Fe^{2+}	0.00	0.00	0.00	0.00	0.00	0.00	0.00	0.00
Mn	0.01	0.02	0.02	0.01	0.01	0.00	0.00	0.01
Ca	1.89	1.88	1.86	1.86	1.86	1.88	1.86	1.85
Na	0.101	0.101	0.122	0.131	0.133	0.123	0.138	0.138
sum B	2.000	2.000	2.000	2.000	2.000	2.000	2.000	2.000
Na	0.68	0.69	0.69	0.70	0.64	0.69	0.74	0.69
K	0.19	0.20	0.20	0.20	0.20	0.19	0.20	0.20
Ba	0.02	0.02	0.02	0.02	0.02	0.02	0.02	0.02
sum A	0.887	0.907	0.913	0.917	0.848	0.903	0.958	0.904
total	15.89	15.91	15.91	15.92	15.85	15.90	15.96	15.90

Ca_B	1.89	1.88	1.86	1.86	1.86	1.88	1.86	1.85
$(Na+K)_A$	0.87	0.89	0.89	0.90	0.83	0.89	0.94	0.88
Ti	0.724	0.695	0.713	0.694	0.694	0.687	0.679	0.678
Si(formular)	5.86	5.93	5.89	5.92	5.91	5.93	5.96	5.92
Mg/(Mg+Fe2	0.71	0.70	0.71	0.69	0.71	0.71	0.70	0.70
AlVI/Fe3+	0.00	0.17	0.00	0.00	1.44	7.67	0.00	0.39
name	kaersutite	kaersutite	kaersutite	kaersutite	kaersutite	kaersutite	kaersutite	kaersutite

Group	Sample locality	Sample	Lithology	Source	Isotopic Age (Ma)		
Tholeiitic	La Ese	C4-47-88	Basalt	de Boer et al 1995	**21.61**	+/-	1.08
	Division	CR27	tholeiitic Gabbro	de Boer et al 1995	**31.65**	+/-	2.00
	Division (5-10km S)	CR-88-73	Gabbro	Berrange & Whittaker 1977	**11.4**	+/-	0.60
	C. Kamuk (near Sukut)	KAM-052	Gabbro	Appel 1990	**18.8**	+/-	1.60
					(amph 22,7	+/-	3,6)
	F. Costena (Boruca)		Gabbro	Heywood, 1984	**11.1**		
	F. Costena (Boruca)		Gabbro	and	**11.6**		
	F. Costena (Boruca)		Gabbro	Woodward-Clyde 1990	**13.1**		
	F. Costena (Boruca)		Gabbro	--"--	**14.8**		
Calc-Alkaline	Escazu (C. La Cruz)	72	Monzogabbro-M.Diorite	Bergoeing, 1982	**5.33**	+/-	0.61
	Escazu	CR34	Granodiorite	de Boer et al 1995	**6.3**	+/-	0.24
	Cerros de Escazu		Granodiorite	Saenz, 1982	**7.2**		
	near Empalme	PA 4	Andesite with Px	Bellon & Tournon 1978	**8.3**	+/-	0.40
	El Empalme	CR1	Andesite	de Boer et al 1995	**3.37**	+/-	0.08
	Santa Maria de Dota	B-4	Qz Monzogabbro w/ Amph	Bergoeing, 1982	**9.13**	+/-	0.33
	Tapanti		intrusive rock	Tournon 1984	**9.3**		
	Tapanti	CR-86-73	Plag-Diorite	Berrange & Whittaker 1977	**11.5**	+/-	0.50
	Tajo Jaboncillo	PA 12	Andesite/Dacite	Bellon & Tournon 1978	**16.9**	+/-	2.50
	Division	CR-87-73	Diorite with Amph	Berrange & Whittaker 1977	**9.6**	+/-	0.40
	Division (0.5km S)	CR-87A-73	Fsp-plutonic rock	Berrange & Whittaker 1977	**9.3**	+/-	0.30
	Division	49	Quartz-Diorite	Bellon & Tournon 1978	**8.5**	+/-	0.40
	Division	TA 1	Granophyr	Bellon & Tournon 1978	**10.1**	+/-	0.50
	near Division		intrusive rock	de Boer 1981, unpublished	**9.3**	+/-	0.34
	near Division		intrusive rock	de Boer 1981, unpublished	**9.4**	+/-	0.28
	near Division		intrusive rock	de Boer 1981, unpublished	**10.3**	+/-	0.21
	near Division		intrusive rock	de Boer 1981, unpublished	**10.7**	+/-	0.25
	near Division		intrusive rock	de Boer 1981, unpublished	**11.2**	+/-	0.27
	near Division		intrusive rock	de Boer 1981, unpublished	**12.4**	+/-	0.40
	south of Division	CR-87B-73	Plag-plutonic rock	Berrange & Whittaker 1977	**9.8**	+/-	0.40
	C. Chirripo	C4-1-88	Dacite	de Boer et al 1995	**9.4**	+/-	0.47
	San Isidro (S)	C4-6-88	Dacite	de Boer et al 1995	**11.79**	+/-	0.59
	C. Chirripo	14-3-90	Diorite	de Boer et al 1995	**9.3**	+/-	0.18
	C. Chirripo	18-3-90	Diorite	de Boer et al 1995	**7.81**	+/-	0.31
	Buenos Aires	CR10	Quartz Monzonite	de Boer et al 1995	**10.22**	+/-	0.20
	Buenos Aires	CR9	Granodiorite	de Boer et al 1995	**10.37**	+/-	0.21
	south of C. Durika	CR8B	Gabbro	de Boer et al 1995	**9.83**	+/-	0.23
	south of C. Durika		plutonic rock	Ballmann 1976	**10.3**	+/-	0.50
	C. Kamuk (3000m asl)	KAM-066	Granodiorite	Appel 1990	**7.9**	+/-	0.90
					(Bio 9,2	+/-	1,2)
					(Plag 30,1	+/-	0,9)
	C. Aka	CR13M	Quartz Monzonite	de Boer et al 1995	**11.05**	+/-	0.31
	El Baru	P40	Diorite	de Boer et al 1995	**31.15**	+/-	2.25
Fore Arc	Terraba	C4-39-88	Andesite	de Boer et al 1995	**3.56**	+/-	0.08
	Mano de Tigre	C3-16-89	Andesite	de Boer et al 1995	**4.31**	+/-	0.07
	Cerro Mano de Tigre	R-3969	Basalt	Kesel 1983	**5.0**	+/-	0.4
	Paso Real	C4-37-88	Basalt	de Boer et al 1995	**1.25**	+/-	0.03
Alkaline	C. Coronel, Caribbean	C 14 a	Basanite	Bellon & Tournon 1978	**1.2**	+/-	0.40
	Qda. Guayabo, Turrialb	TU13	Alkali Basalt	Bellon & Tournon 1978	**5.1**	+/-	0.75
	Guayacan, Siquirres	S25	Basanite	Bellon & Tournon 1978	**4.6**	+/-	0.25
	Qda. Terciopelo		Teschenite	Cassel 1986	**4.5**	+/-	0.50
	Rio Chirripo	CH-14	Nephelinite	Tournon 1984	**5.2**		
Adakite	Rio Xikiaria, F. Matama	Pc 2c	Andesite with Amph	Bellon & Tournon 1978	**2.4**		
	Durika Area			de Boer 85 unpublished	**0.95**	+/-	0.01
	Durika Area			de Boer 85 unpublished	**2.8**	+/-	0.05
	San Vito (NW)	CR 17A	Andesite	de Boer et al 1995	**1.07**	+/-	0.04
	San Vito (NW)	C4-62-88	Andesite	de Boer et al 1995	**1.1**	+/-	0.06
	San Vito (N)	Pc 2c	Andesite with Amph	Bellon & Tournon 1978	**2.6**	+/-	0.40
	San Vito (SE)	C4-4-88	Andesite	de Boer et al 1995	**1.71**	+/-	0.09

Acknowledgements

The present study was sponsored by the German Science Foundation (DFG) under the project number Wo 362/10 and is part of the multidisciplinary TICOSECT research program.

Foremost I am greatly indebted to Prof. Dr. G. Wörner, who initiated this fascinating project, supported me with constructive discussions and prepared a fertile ground for high quality scientific work. - During our field campaign in 1995 he introduced me to Costa Rican rocks, plants and beaches and gave lessons in white-water rafting and -swimming.

Prof. Dr. B. Hansen has to be thanked for doing the co-referate for my thesis.

I particularly thank Dr. G. I. Alvarado for his intense aid and interest in my field work and fruitful discussions. I want to thank Prof. Dr. S. Kussmaul for his support during my stay in Costa Rica, and for sure I will not forget Luis, Jose, Miguel, Raquel, Adolfo and Mayela who helped me much during my field work or gave me friendly lodging.

This work profited much from discussions and exchange with Dr. M. Meschede, Prof. M. J. Carr, F. Hauff, Dr. R. Werner, F. Dorendorf.

Dr. B. Bock and P. Bogaard are especially thanked for doing a hard job with criticism of the earlier versions of this thesis.

Many colleges from the Geochemisches Institut Göttingen have to be thanked for supporting me during my lab work and for introducing me to the instruments, among them P.D. Dr. A. Eisenhauer, Dr. K. Simon, Dr. G. Hartmann, Dr. A. Kronz, Dr. E. Gohn, Dr. U. Wiechert, E. Schiffczyk, A. Reitz, L. Reese, R. Przybilla, A. Gerdes, T. Agemar, H. Ehrig.

The geochronological work was made possible thanks to good co-operation with Dr. F. Henjes-Kunst, BGR. I want to thank him and H. Klappert very much for having made my stay successful and comfortable.

Finally, I want to thank Catherine, my wife, for her continual encouragement, patience and moral support.

LEBENSLAUF

Am 06.11.1966 wurde ich als erstes Kind von Harald Abratis (Diplom-Ingenieur) und Gretel Abratis, geb. Müller (Erzieherin) in Oldenburg in Holstein geboren.
Seit 1997 bin ich mit der Historikerin Catherine Abratis, geb. Fauconnier verheiratet.

Nach dem Besuch der Grundschule und des Carl-Maria-von-Weber Gymnasiums in Eutin, erwarb ich 1986 meine Allgemeine Hochschulreife.

Im Anschluss an den Wehrdienst, studierte ich von 1987 bis 1988 Chemie an der Christian-Albrechts Universität zu Kiel.
Zum Wintersemester 1988/1989 immatrikulierte ich mich an der Georg-August Universität zu Göttingen für das Fach Geologie-Paläontologie. Meine Diplomarbeit mit dem Titel “Geology, Petrology and Geochemistry of Vonarskard, Central Iceland” fertigte ich unter der Betreuung von Dr. A. Schneider, Prof. Dr. H.-J. Behr und Prof. Dr. G. Sigvaldason am Institut für Geologie und Dynamik der Lithosphäre an der Universität Göttingen an. Im Februar 1994 schloss ich das Studium der Geologie mit der Diplomprüfung ab.

Bis Ende 1994 arbeitete ich in der angewandten Geologie bei der Firma Getec in Dransfeld bei Göttingen.

Seit Oktober 1994 beschäftige ich mich am Geochemischen Institut der Universität Göttingen unter Anleitung von Prof. Dr. G. Wörner mit der vorliegenden Arbeit.